BALANCED ANTENNAS FOR MOBILE HANDSET APPLICATIONS

A G ALHADDAD

PhD

UNIVERSITY OF BRADFORD

-2012-

BALANCED ANTENNAS FOR MOBILE HANDSET APPLICATIONS

Simulation and Measurement of Balanced Antennas for Mobile Handsets, investigating Specific Absorption Rate when operated near the human body, and a Coplanar Waveguide alternative to the Balanced Feed

ABDOLRAUF GAWAD ALHADDAD
B.Eng., M.Sc.

Submitted for the Degree of

Doctor of Philosophy

School of Engineering, Design and Technology

University of Bradford

-2012-

Abstract

BALANCED ANTENNAS FOR MOBILE HANDSET APPLICATIONS

Simulation and Measurement of Balanced Antennas for Mobile Handsets, investigating Specific Absorption Rate when operated near the human body, and a Coplanar Waveguide alternative to the Balanced Feed

Keywords

Balanced Antennas; Planar Antennas; Digital Cellular System (DCS); Personal Communication Service (PCS); Universal Mobile Telecommunication System (UMTS); Wireless Local Area Network (WLAN); Ultra-Wide Bandwidth (UWB); Specific Absorption Rate (SAR); Coplanar Waveguide; Hybrid Method.

The main objectives of this research are to investigate and design low profile antennas for mobile handsets applications using the balanced concept. These antennas are considered to cover a wide range of wireless standards such as: DCS (1710–1880 MHz), PCS (1850–1990 MHz), UMTS (1920–2170 MHz), WLAN (2400–2500 MHz and 5000 – 5800 MHz) and UWB frequency bands. Various antennas are implemented based on built-in planar dipole with a folded arm structure.

The performance of several designed antennas in terms of input return loss, radiation patterns, radiation efficiency and power gain are presented and several remarkable results are obtained. The measurements confirm the theoretical design concept and show reasonable agreement with computations. The stability performance of the proposed antenna is also evaluated by analysing the current distribution on the mobile phone ground plane. The specific absorption rate (SAR) performance of the antenna is also studied experimentally by measuring antenna near field exposure. The measurement results are correlated with the calculated ones.

A new dual-band balanced antenna using coplanar waveguide structure is also proposed, discussed and tested; this is intended to eliminate the balanced feed network. The predicted and measured results show good agreement, confirming good impedance bandwidth characteristics and excellent dual-band performance.

In addition, a hybrid method to model the human body interaction with a dual band balanced antenna structure covering the 2.4 GHz and 5.2 GHz bands is presented. Results for several test cases of antenna locations on the body are presented and discussed. The near and far fields were incorporated to provide a full understanding of the impact on human tissue. The cumulative distribution function of the radiation efficiency and absorbed power are also evaluated.

Table of Contents

Acknowledgment

I wish to express my gratitude to my supervisors, ***Prof. Raed A. Abd-Alhameed*** and ***Prof. Peter S. Excell***. I am most grateful to them for advice, assistance, support and their continuous encouragement during the difficult starting times, sharing with me the exciting times and for being consistently supportive throughout this work. I will never forget the many opportunities that they gave me in facilities, publications, teaching and travel during the years of my PhD study.

I am gratefully acknowledged the financial support from the UK Engineering and Physical Sciences Research Council (EPSRC) under grant EP/E022936/1, in supporting the measurements facilities.

I would like also express my special thanks to Dr D. Zhou for his continuous help and kindness through the time of this research work. My appreciation is also to extend to Dr N. J. McEwan, Mr M. B. Child and Dr C. H. See for their generous assistances.

My thanks are also extended to all the other people in the antenna and electromagnetic research group; Dr K.N.B Ramli, Mr M. M. Musa, I.E.T. Elfergani, and, Y. Dama, T. Sadeghpour; in addition to Mr. A. Mistry, M. Cribb and Mr D Chavda whose co-operation in connection with the practical aspect of this work cannot be underestimated.

In addition, thanks to all members of the antenna lab, workshop and computer officers of the school of Engineering, Design and Technology, Bradford University, for their great support and help.

I am indebted to all my family for their support and encouragement that I always I am given.

Acronyms

3D	Three Dimension
ABC	Absorbing Boundary Condition
ADC	Analogue to Digital Convertor
ADS	Advance Design System
AUT	Antenna Under Test
Balun	Balanced Unbalanced
CDF	Cumulative Distribution Function
CPW	Coplanar Waveguide
CST	Computer Simulation Technology
DCS	Digital Cellular System
EBG	Electromagnetic Band Gap
EM	Electro Magnetic
FCC	Federal Communications Commission
FDTD	Finite Difference Time Domain
FEM	Finite Element Method
GA	Genetic Algorithm
GSM	Global System Mobile
GPS	Global Position System
HFSS	High Frequency Structure Simulator
HOR	Horizontal
MoM	Method of Moment
NEC	Numerical Electromagnetics Code
PC	Personal Computers
PCS	Personal Communication System
PIFA	Planar Inverted F Antenna
PML	Perfectly Matched Layer
RF	Radio Frequency
RF4CE	Radio Frequency for Consumer Electronics
SAR	Specific Absorption Rate
SDR	Software Defined Radio
WLAN	Wireless Local Area Network
UMTS	Universal Mobile Telecommunication System

WIMAX	Worldwide Interoperability for Microwave Access
WPAN	Wireless Personal Area Networking
UWB	Ultra Wide Band
VER	Vertical
VNA	Vector Network Analyser
VSWR	Voltage Standing Wave Ratio

List of Tables

List of Figures

CHAPTER ONE

Introduction

1.1 Background and Motivations

The contemporary demands of the mobile communications industry place a variety of demanding long term design challenges, particularly to the antenna engineer. Small antennas always pose problems to designers, partly due to the existence of fundamental physical limits, and partly due to the dynamically changing market demands and consumer expectations. One constant feature is the need to design antennas which meet these various constraints, and whose basic performance is not degraded by the adjacent coupling to the user

Throughout the course of this research, a number of concerns have been identified from the needs and requirements of the mobile communications industry, to provide a well-defined subset of goals to guide the design strategy. Consequently the motivations for these studies have matured as each component has been investigated. With this in mind, the direction of the work is guided by the need for a quality discussion on balanced and unbalanced antenna design techniques.

Antenna designs intended for realistic mobile handset use must have an ideal combination of the maximum possible efficiency, protection to the user and minimum cost. This is governed by market needs, and governmental regulation. The technical

factors alluded to, define a design space for optimisation, which includes the gain, the input impedance over the required frequency band(s), the minimisation of an easily violate the interaction between the radiator and the user's body, particularly regarding energy deposition to the head. These electrical criteria are further constrained by the mechanical footprint of the handset and the enclosures offered to the antenna designer within or on the handset chassis, these volumes typically fall outside the range required for the ideal performance range of the antenna.

Planar antennas have the perceived advantages of low profile, small size and light weight [1, 2]. It seems that planar antennas are natural candidates for mobile antenna designs. These antennas may be realised as a planar metal plate, which acts as the radiator, positioned over a finite ground plane. In practice a variety of shapes have been utilized, including simple monopoles, T shaped elements, L shaped elements, inverted L shaped elements, and folded inverted L shaped elements. One of the more significant such developments has been the planar inverted F antenna (PIFA) [3-16].

Many novel planar antenna designs have been devised in recent years to meet the specific requirement specifications for mobile communications services [2]. Some of the more significant services include:

- the global system for mobile communication (GSM; 890–960 MHz)
- the digital cellular system (DCS; 1710–1880 MHz)
- the personal communication system (PCS; 1850–1990 MHz)
- the universal mobile telecommunication system (UMTS; 1920–2170 MHz)

Planar antennas are also very attractive for applications in communication devices for wireless local area network (WLAN) systems in the 2.4 GHz (2400–2484 MHz) and 5.2 GHz (5150–5350 MHz) bands. Several planar antenna designs for achieving wideband applications in ultra wideband UWB (3.1-10.6 GHz) have also been demonstrated.

The wire antennas such as dipoles, monopoles and loops are the principal form of small radiators in practical use. However, the application to the future mobile handsets may not be straight forward, due to size constraints, and also the number of antennas required on within already crowded housing. The folded dipole is traditionally thought of as an alternative to a dipole for applications that require higher input impedance. For example the input impedance of the half-wave folded dipole is approximately four times that of the half-wave dipole, as demonstrated by a transmission-line model [17]. In addition, the folded dipole antenna has a wider bandwidth than the common dipole, although at the expense of a little constructional complexity. Therefore, the dipole structure is the choice of antenna design for wide band application for handset mobile.

Unbalanced antennas such as Planar Inverted-antennas (PIFAs) have been used extensively in mobile communication systems and have attracted much attention from researchers and engineers because of their advantage of compact, low profile, and low cost of manufacture. However, they have a narrow bandwidth and need a height from substrate to ground for matching [18-20]. Moreover, these antennas exhibit inferior performance when they are held by users. This can be attributed to the user holding the mobile phone, which largely covers the ground plane since the ground plane is used as part of the radiator in these antennas. Therefore, radiating currents are induced on both the ground plane and the antenna element, resulting in currents flowing on the human

body, which degrade the performance of the antenna's radiation characteristics and introduce losses and uncertainty in its matching [21].

A balanced structure is a genuine alternative to avoid the degradation of antenna performance in unbalanced antennas. In a balanced structure, currents cancel the effect of each other, the current flows only on the antenna element and not on the ground plane. Therefore when the mobile is held by its user, no coupling takes place between the antenna and the user's body, thus the performance of the antenna is not affected. A balun is one key components used to excite a balanced antenna, as it is a device which enables compatibility between systems, and is used for converting feeding mechanism between an unbalanced circuit structure and a balanced circuit structure.

Suitable balanced antenna structures remain a significant design challenge. The nature of the optimisation problem has already been outlined, to this we may also add further practical constraints arising from the overall weight of the package, and the need for multiple service bands. Several novel balanced designs has been reported [22-24] for single band operation, but these antennas have tended to be large (relative to the full design target for a handset). Therefore there exists a strong motivation to establish a systematic size reduction strategy, whilst maintaining generally good electrical performance, and maximising the number of possible service bands available to a single antenna.

This study presents the results of an investigation of several new wideband balanced antenna designs. These newly designed antennas can be used in wideband mobile handset antennas to provide balanced features, and as such are promising candidates for mobile communication systems.

1.2 State of the Art of the Present Research

The rationale behind the research presented in this thesis is to investigate and analyse the operation of balanced antenna geometries for hand-held mobile terminals. It is thought that the mutual coupling of a balanced antenna is not totally affected by the induced currents on the terminal's chassis. This results in the antenna performance being preserved when the handset is loaded, or in contact with the user's hand. These antennas are fed by two sources which carry currents of equal magnitude, but which are 180° out of phase. As a result of the symmetric geometry, the induced current appearing on the handset will mostly cancel, i.e. no current flows on the antenna ground plane. In fact, the effect of the antenna radiation next to the human head also suggests reducing the possibility of the electromagnet energy absorption by the user's head.

The early part of the thesis has two primary approaches. The first reviews the definition of balanced and unbalanced operation concepts, and how this is applied to antennas. The use of a balanced feed is investigated for practical measurements; a wide bandwidth planar balun is used to feed a wideband balanced antenna from an unbalanced source. The second aim is to develop a family of small, compact and low-profile wide-band balanced antenna suitable for integration with mobile handsets. In most designs, a planar metal plate antenna with dipole structure with folded arms is used to achieve the workable bandwidth. The capacitive coupling between the dipole arms and the chassis has been modified to maintain a sufficient impedance bandwidth at the lower frequency band. This has been done by implementing several design techniques, and optimizing the antenna characteristics. This investigation also encompasses the impact on

performance a number of other key issues, including coplanar structures, hybrid computational methods, and the specific absorption rate (SAR).

The coplanar structure as a transmission line has become an intensive topic of recent research due to its attractive characteristics, such as a possibility for a wider impedance matching bandwidth, and easy fabrication process. A new printed circuit antenna using a coplanar waveguide structure is introduced in this work. The principal attraction of this design is to eliminate the need for a balanced feed network (i.e. a balun).

The implementation of a hybrid computational method is also considered as a design tool. The rationale is to model the interaction between a balanced antenna located over several positions in close proximity to the human body. A simple statistical analysis of the results is used to provide a performance map, the data is summarised in terms of the CDF of the radiation efficiency and the location based ratio of the absorbed power to radiated power. This approach provides an enhanced understanding of the impact of electromagnetic energy on human tissue.

The SAR performance of a wide-band balanced antenna is studied empirically through measuring the near field exposure, the results show that there is a low induced current in the ground plane, and thus confirms the expected minimising performance variations, and SAR.

Several antenna prototypes have been constructed and tested using these design principles. The investigations have shown good agreement between the simulated and empirical results, and have confirmed the good wideband impedance characteristics, and multi-band functionality of these antennas.

Routine investigations into electrical structure and performance were carried out using the commercial packages HFSS [25] and CST Microwave studio [26]. HFSS was used for obtaining frequency domain responses over the working bandwidth of the proposed structure, whilst CST was used for general time domain analysis, and broadband sweeps. Occasionally, IE3D [27] has been used in place of HFSS for frequency domain analysis where the geometry is awkward for the volume mesh. The human body analysis was carried out using an in house hybrid (FDTD) (MoM) code. This last approach is described in Chapter 6.

1.3 Organization of the Report

Chapter 2 establishes the theoretical basis of balanced and unbalanced antenna structures. It explains how the use of balanced antenna structures may benefit performance in hand-held terminals, or wireless sensor tags positioned in close proximity with the human body. The use of balun feeds from unbalanced antennas is also discussed here, along with two experimental methods for determining the differential input impedance.

Chapter 3 investigates in detail the design of balanced dipole antennas for multi-band operation in a suitable generic mobile terminal. It is assumed that the antenna will be in-built within the housing of the terminal, and the target service bands are GSM 1800, GSM 1900, and UMTS. Operational extensions to this coverage are also discussed, specifically with respect to Bluetooth/WLAN (2.45 GHz) operation. The measurement of input impedance is addressed, and a wideband planar balun embedded within the chassis is discussed as a means of providing a suitable balanced feed.

The themes of chapters 2 and 3 are deepened and extended through the designs presented in Chapter 4. The target service bands are DCS (1710 MHz–1880 MHz), PCS (1850 MHz–1990 MHz), UMTS (1920 MHz–2170 MHz) and WLAN (2400 MHz – 2484 MHz). A wideband folded dipole is proposed, with the addition of a dual-arm on each monopole. The stability of the antenna performance, under realistic operating conditions, is critical to the success of such designs. In order to evaluate this stability problem, the effect of the user's hand on the terminal return loss and radiation pattern is investigated. The specific absorption rate (SAR) is also studied for the antenna empirically, by measuring near field exposure, to confirm the minimising effect on SAR performance. The relationship between induced surface currents and unit size is also investigated in this chapter.

Chapter 5 investigates the design concepts behind two new antennas operating over WLAN (2.4 GHz and 5 GHz) and WiMAX (2.5 GHz and 3.5 GHz) bands. The basic building block is a modified folded monopole is proposed, in which an additional thin strip is used to excite the second resonant mode. A long slot is also introduced to each folded arm of the dipole antenna, as a means of maintaining sufficient impedance bandwidth, whilst meeting the height constraint of the unit. This size restriction is shown to be effective, and is arrived through a semi-empirical design optimisation, using simulation and prototype measurements.

Chapter 6 discusses the implementation of a hybrid computational method in which frequency domain method of moment (MoM) for modelling the antenna and finite difference time domain FDTD for modelling the human body have been hybridised and used. It is successfully models the interaction between dual balanced antennas, placed in close proximity with the human body. This code is used to investigate the radiation

characteristics of the antenna over a variety of body locations. The near and far fields are incorporated into the study, and are used to obtain a more complete understanding of their impact on human tissue. The results are characterised in terms of the CDF of the radiation efficiency and the ratio of the absorbed power to radiated power of the various locations over the body.

Chapter 7 provides a brief overview of ultra-wideband (UWB) techniques. The principal outcome is a new antenna design for mobile terminals, in which an in-built planar metal plate, with balanced operation, is investigated. This design reduces the current flow on the conductive surface of the unit, and a parametric study is devised to reduce the overall size of the unit.

Chapter 8 provides a brief overview of microstrip and coplanar antennas. The main development to be reported here is the use of coplanar waveguide structures in implementing the balanced feed network. To this end, a new dual-band balanced antenna using a coplanar waveguide structure is introduced, from which a prototype design is fully realised. This particular design operates for the 2.4 GHz and 5 GHz WLAN service bands.

Finally chapter 9 states the overall conclusions of this thesis, and makes a series of recommendations to improve the depth of coverage of balanced antenna design, as well as its industrial relevance in mobile communications. The recommendations focus on techniques and processes to promote extended multi-band coverage, maintenance of high efficiency and optimised bandwidth.

1.4 References

[1] K.-L. Wong, *Compact and Broadband Microstrip Antennas*. New York: John Wiley & Sons, Inc, 2002.

[2] K.-L. Wong, *Planar antennas for wireless communications* Hoboken, N.J. : J. Wiley, 2003.

[3] D. M. Nashaat, H. A. Elsadek, and H. Ghali, "Single Feed Compact Quad-Band PIFA Antenna for Wireless Communication Applications," *IEEE Transactions on Antennas and Propagation*, vol. 53, pp. 2631-2635, 2005.

[4] Hoon Park, K. Chung, and J. Choi, "Design of a Planar Inverted-F Antenna With Very Wide Impedance Bandwidth," *IEEE Microwave and Wireless Components Letters*, vol. 16, pp. 113-115, 2006.

[5] S. Liw and G. A. Ellis, "Planar Inverted-F Antennas as an Inverse Class-F Termination for Wireless Applications," *IEEE Antennas and Wireless Propagation Letters*, vol. 2, pp. 250-253 2003.

[6] W.-I. Kwak, S.-O. Park, and J.-S. Kim, "A Folded Planar Inverted-F Antenna for GSM/DCS/Bluetooth Triple-Band Application," *IEEE Antennas and Wireless Propagation Letters,*, vol. 5, pp. 18-21, 2006.

[7] B.-N. Kim, S.-O. Park, Y.-S. Yoon, J.-K. Oh, K.-J. Lee, and G.-Y. Koo, "Hexaband Planar Inverted-F Antenna With Novel Feed Structure for Wireless Terminals," *IEEE Antennas and Wireless Propagation Letters*, vol. 6, pp. 66-69, 2007.

[8] Pekka Salonen, M. Keskilammi, and M. Kivikoski, "Single-Feed Dual-Band Planar Inverted-F Antenna with U-Shaped Slot," *IEEE Transactions on Antennas and Propagation*, vol. 48, pp. 1262-1264, 2000.

[9] Y.-B. Kwon, J.-I. Moon, and S.-O. Park, "An Internal Triple-Band Planar Inverted-F Antenna," *IEEE Antennas and Wireless Propagation Letters*, vol. 2, pp. 341-344, 2003.

[10] C.-W. Ling, C.-Y. Lee, C.-L. Tang, and S.-J. Chung, "Analysis and Application of an On-Package Planar Inverted-F Antenna," *IEEE Transactions on Antennas and Propagation*, vol. 55, pp. 1774-1780, 2007.

[11] Z. Du, K. Gong, J. S. Fu, B. Gao, and Z. Feng, "A Compact Planar Inverted-F Antenna With a PBG-Type Ground Plane for Mobile Communications," *IEEE Transactions on Vehicular Technology*, vol. 52, 2003.

[12] J.-S. Row, "Dual-Frequency Triangular Planar Inverted-F Antenna," *IEEE Transactions on Antennas and Propagation*, vol. 53, pp. 874-876, 2005.

[13] B. Sanz-Izquierdo, J. C. Batchelor, R. J. Langley, and M. I. Sobhy, "Single and Double Layer Planar Multiband PIFAs," *IEEE Transactions on Antennas and Propagation*, vol. 54, pp. 1416-1422, 2006.

[14] D.-U. Sim and J.-I. Choi, "A Compact Wideband Modified Planar Inverted F Antenna (PIFA) for 2.4/5-GHz WLAN Applications," *IEEE Antennas and Wireless Propagation Letters*, vol. 5, pp. 391-394, 2006.

[15] S.-H. Yeh, K.-L. Wong, T.-W. Chiou, and S.-T. Fang, "Dual-Band Planar Inverted F Antenna for GSM/DCS Mobile Phones," *IEEE Transactions on Antennas and Propagation*, vol. 51, pp. 1124-1126, 2003.

[16] P. Nepa, G. Manara, A. A. Serra, and G. Nenna, "Multiband PIFA for WLAN Mobile Terminals," *IEEE Antennas and Wireless Propagation Letters*, vol. 4, pp. 349-350, 2005.

[17] C. G. Buxton, W. L. Stutzman, R. R. Nealy, and A. M. Orndorff, "The Folded Dipole: A Self-Balancing Antenna," *Microwave and Optical Technology Letters*, vol. 29, pp. 155-160, May 2001.

[18] H. Morishita, H. Furuuchi, and K. Fujimoto, "Performance of balance-fed antenna system for handsets in the vicinity off a human head or hand," *IEE Proceeding Microwave Antennas Propagation*, vol. 149, pp. 85-91, 2002.

[19] S. Hayashida, H. Morishita, Y. KIM, Y. Koyanagi, and K. Fujimoto, "Wideband folded loop antenna for handsets," *IEEE AP-S Proc.*, vol. 3, pp. 2-5, Jun. 2002.

[20] M. J. Ammann and Z. N. Chen, "Wideband Monopole Antennas for Multi-Band Wireless Systems," *IEEE Antennas and Propagation Magazine*, vol. 45, pp. 146-150, 2003.

[21] R. A. Abd-Alhameed, P. S. Excell, R. A. K. Khalil, and J. Mustafa, "SAR and radiation performance of balanced and unbalanced mobile antennas using a hybrid computational electromagnetics formulation," *IEE Proceedings-Science, Measurement and Technology special issue on Computational Electromagnetics*, vol. 151, pp. 440-444, 2004.

[22] H. Morishita, Y. Kim, Y. Koyanagi, and K. Fujimoto,"A folded loop antenna system for handsets," *IEEE Antennas and Propagation Society International Symposium*, vol. 3, pp. 440-443, 2001.

[23] J. J. Arenas, J. Anguera, and C. Puente, "Balanced and single-ended handset antennas: free space and human loading comparison," *Microwave And Optical Technology Letters*, vol. 51, pp. 2248-2254, September 2009.

[24] U. Navsariwaln and J. Svigetj, "A reduced sized balanced antenna for 2.4 GHz WLAN," *IEEE Antennas and Propagation Society International Symposium*, vol. 2, pp. 6 - 9 2003

[25] "High Frequency Structure Simulator, Version 11, Ansoft Corporation, USA."

[26] "Computer Simulation Technology Corporation, CST Microwave Studio, Version 5.0, Germany."

[27] "IE3D User's Manual, Zeland Software Inc., Release 5, 2000."

CHAPTER TWO

Balanced and Unbalanced Antenna Concept

2.1 Introduction

Contemporary developmental trends in the mobile communications equipment industry require antenna designs which combine multi-band operation and small physical size. The mobile communications market is in part driven by extra features within these multi-band services; furthermore, there are corresponding trends in ubiquitous wireless networks in medicine and infrastructure. The main focus of this thesis will be the design of balanced antennas for hand held mobile terminals. More generally, these antennas may be unbalanced or balanced, and this chapter begins with a review of these design principles.

2.2 Unbalanced Antenna

Many handset designs utilize antennas with unbalanced terminals fed by unbalanced lines, usually for size considerations. In this type of antenna, the radiation currents are induced on the conducting surfaces of the handset chassis, as well as on the radiating element itself [1]. Therefore, it can be said that the antenna (radiator) accounts for only half the radiation mechanism, and the ground plane is the other half. The most

commonly used example of this type of antenna is the PIFA, or planar inverted F antenna. PIFA types are in widespread use due to their size advantages compared against conventional λ/2-radiators, low profile, and relative low costs in high volume manufacturing [2-8]. The generic PIFA structure comprises a ground plane, top patch, cable (or wire) feed and shorting post, which give rise to λ/4-resonator. In fact there is an approximate 50% length reduction between a PIFA and λ/2-radiator [9-11]. However, the ground plane plays a highly significant role, which can be seen through the impedance matching and radiation characteristics, which may constrain the use of PIFA types for some applications. It should also be noted, that the height and shorting post also place practical limits on the antenna size [3, 12, 13].

Unbalanced antenna units tend to be fed by coaxial cables, or occasionally microstrip lines printed over the ground plane; the current induced on the ground plane varies due to the surface currents on the radiator. These currents may contribute to improve or degrade operating performance, especially when the antenna element is small compared with one wavelength. Since these currents may be varied by their proximity to the user's hand and head, there is a significant degradation in antenna performance. The antenna gain may suffer reductions of between 6 and 10 dB [14] due to the current flow on the human body, as well as uncertainty in the antenna's matching requirement [15]. If the size of the ground plane is changed, or when components are relocated over the ground plane, the antenna detunes, and thus radiation performance may be degraded further [16].

In order to develop the concept of an unbalanced antenna further, the current distribution on the coaxial feed cable is explored. The central conductor is shielded as

shown in Figure 2.1; the current on the conductor and the inner side of the shield are equal and opposite, this is due the fact that the fields associated with both the currents are restricted to a same common place [17]. As a result of the skin effect a current flows on the outer side of the shield [18]. If the current on the outer side of the shield is high enough it will cause the coaxial cable to radiate fields like an antenna, this radiation field is proportional to the current.

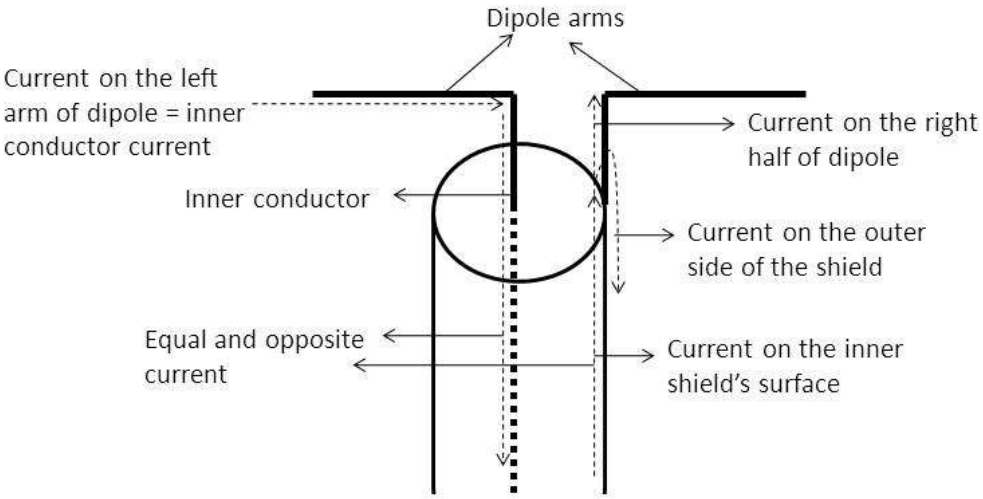

Figure 2.1: Coaxial cable current distribution

Figure 2.1 shows the current distribution on the coaxial feed and the dipole. On the right hand side of the antenna, the outer side of the shielding appears as a separate conductor connected at the feed point. The current on the left arm of the dipole is supplied by the central conductor of the coaxial cable. While the current on the inner side of the shield, which is equal and opposite to that of the central conductor current flows partly on the dipole's right arm, and also partly along the outer side of the shield. If the length of the outside path of the cable from the antenna to ground is a multiple of half wavelengths, then the current on this outer path is maximum, since the impedance presented by this undesirable path is low [18]. Therefore, if an antenna is fed by a coaxial cable this phenomenology will apply, and the currents on the outer side of the shield will flow on

the antenna ground plane because the cable is grounded. When a user holds such an antenna in his/her hand, coupling will take place between the user's hand and the ground plane thus affecting the antenna performance. The best solution to this problem is to isolate or reduce the current flow from the antenna to the ground plane. This may be simply implemented using balanced antennas, as will be discussed in the following section.

2.3 Balanced Antenna

An antenna with symmetrical structure which is fed with balanced, electrically symmetrical, currents may be termed as a balanced antenna. The input voltage/current signal of a balanced circuit comprises two signal components. These signals have same magnitude, which are 180° out of phase with one another. These signals flow on the antenna, and their resulting effects will be cancelled on the ground plane. The net result is to improve the antenna performance, and also reduce the coupling effects of the radiating element to the handset. This offers a possible improvement over unbalanced antennas. On an unbalanced antenna, the currents induced on the chassis interact strongly with the unpredictable (response) characteristics of the body [16, 19, 20]. In addition, the maximum SAR values have been shown to be substantially reduced using balanced antennas when placed next to the human head, compared with conventional unbalanced antennas [15].

Dipoles and loops are the most common balanced antennas in practice; balanced antennas may also be realized in meander-line, helix and microstrip forms. A balanced antenna requires a balanced feed. In principle, the balanced antenna with balanced feed keeps the ground plane almost free of induced current [14], hence any degradation of

the antenna performance due to the influence of the human body can be largely eliminated. As a result, balanced antennas should have good efficiency, and more importantly should maintain their performance when in use adjacent to the human body.

Balanced antennas may have some limitations, such as reduced bandwidth, and sub optimal pattern shaping, which can degrade their overall performance. Some novel techniques have been proposed for the enhancement of impedance bandwidth. For example, a genetic algorithm technique has been implemented to improve the impedance bandwidth [21]. Parametric modelling has been applied to the length and width of strip lines to obtain a wider bandwidth for the folded loop antenna system [22].

The size constraints of balanced antennas in the lower frequency bands (e.g. GSM 900) are another limiting factor for mobile phone applications. Since the antenna size is comparable to the operating wavelength at these frequencies, it might be difficult to accommodate such an antenna. On the other hand, balanced antenna designs can be more easily applied to the frequency bands above 1.5 GHz [16], these designs have been extended to multiband operations [20].

2.4 Balanced/Unbalanced Operation using a Balun Circuit.

When a balanced antenna is fed using an unbalanced voltage source (such as a coaxial cable), current flow through the antenna element in one direction at any instant, and at the same time another current flows in the opposite direction along the inside and the outer conductor of the coaxial cable. These unwanted currents flowing through the outer shield of the coaxial cable are induced into the ground plane and the antenna element. This will distort the antenna radiation pattern, and affect the performance of the system.

In order to overcome this kind of situation, a balun can be used. It eliminates the unwanted portion of the current flowing through the ground plane and antenna elements and providing a balanced currents at the input terminals of the antenna [23].

The output signals of a balanced circuit comprise two signal components with the same magnitude but 180-degree phase difference. Many analogue circuits require balanced inputs and outputs in order to reduce noise and high order harmonics as well as improve the dynamic range of the circuits at which the baluns provides the required compatibility between systems, such that used in balanced mixers [24, 25], push-pull amplifiers [26, 27], and antenna feed networks [28-34]. Baluns can be classified into two different categories either active or passive [23, 35] and they can be found with different types; as examples: LC, transmission line (TL), microstrip and mix of LC and TL.

2.5 Measuring the Impedance Bandwidth of Balanced Antennas

In this section, two methods for obtaining the differential input impedance of balanced antennas are presented. These are (i) the monopole method, and (ii) the two port scattering parameter method.

2.5.1 Equivalent Monopole Antenna:

In this method half of the balanced structure is replaced by a conducting ground plane, as shown in Figure 2.2. The size of the ground plane is a critical parameter in characterizing the impedance function of the balanced antenna. A basic experimental

result is that the size of the ground must be greater than four times the maximum optimum wavelength [36].

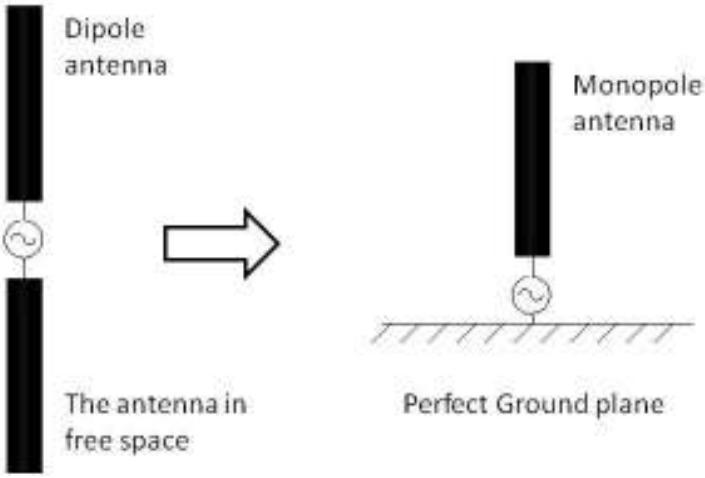

Figure 2.2**:** Converting dipole antenna to monopole antenna

The input impedance of the balanced antenna using this method can be expressed as following:

$$Z_{balanced} = 2\, Z_{monopole}$$

Where $Z_{balanced}$ and $Z_{monopole}$ are the input impedances of the equivalent balanced and monopole antenna respectively.

2.5.2 Two Ports Network Method:

To achieve a balanced antenna design, such as a dipole, the feeding currents must be equal and exactly 180° out of phase. This is conventionally realized through the use of a balun circuit, although other techniques are available (for dipoles). The quality of the balun circuit design and its actual performance is critical in this approach, as will be seen subsequently in future Chapters, e.g. Chapter 5. The difficulties associated with

the balun circuit can become notably problematic when measuring the antenna impedance function over a very wide bandwidth [37]. This is addressed as a practical issue in Chapter 7.

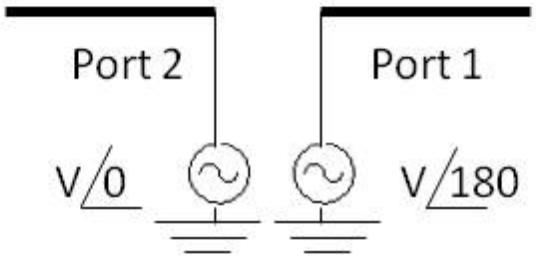

(a)

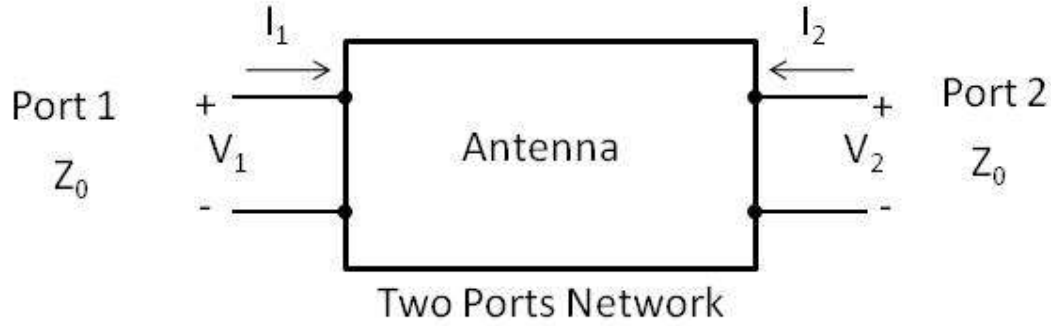

(b)

Figure 2.3: Basic representation of balanced antenna; (a) Simple balanced structure with feed sources, (b) equivalent two ports network [38].

To work around this problem, the input impedance of a balanced antenna can be measured by applying the two port network method in which the balun is completely not required. This may be achieved by connecting the two ports of the balanced antenna directly into the input ports of a calibrated VNA. The input impedance may be extracted from the S-parameters as follows.

In Figure 2.3, the equivalent input port currents and voltages can be expressed in the following impedance matrix elements [38]:

$$V_1 = Z_{11} I_1 + Z_{12} I_2 \tag{2.1}$$

$$V_2 = Z_{21} I_1 + Z_{22} I_2 \tag{2.2}$$

Where

$$Z = \begin{bmatrix} Z_{11} & Z_{12} \\ Z_{21} & Z_{22} \end{bmatrix} \tag{2.3}$$

Then, the differential input voltage V_d is given by:

$$V_d = V_1 - V_2 \tag{2.4}$$

$$V_d = (Z_{11} I_1 - Z_{21} I_1 + Z_{12} I_2 - Z_{22} I_2) \tag{2.5}$$

Now subject to the applied input voltages, one can assume the following,

$$I_1 = I \text{ and } I_2 = -I \tag{2.6}$$

It follows that equation (2.5) can be expressed as,

$$V_d = (Z_{11} - Z_{21} - Z_{12} + Z_{22})I \tag{2.7}$$

Therefore, the differential input impedance can stated as follows:

$$Z_d = Z_{11} - Z_{21} - Z_{12} + Z_{22} \tag{2.8}$$

Since the antenna is passive and symmetric it can be assumed that,

$$Z_{11} = Z_{22} \text{ and } Z_{21} = Z_{12} \tag{2.9}$$

Using the differential input impedance in (2.8), the expression can be simplified to:

$$Z_d = 2(Z_{11} - Z_{21}) \tag{2.10}$$

In terms of 2-port scattering parameters, the differential impedance in (2.10) can be given as,

$$Z_{11} = Z_o \frac{(1 + S_{11})(1 - S_{22}) + S_{12}S_{21}}{(1 - S_{11})(1 - S_{22}) - S_{12}S_{21}} \tag{2.11}$$

$$Z_{12} = Z_o \frac{2S_{12}}{(1 - S_{11})(1 - S_{22}) - S_{12}S_{21}} \tag{2.12}$$

It follows that similar values for Z_{21} and Z_{22} can be also obtained. Using (2.9), the differential input impedance can be expressed in terms the of the S-parameters as follows,

$$\mathrm{Z_d} = 2Z_o \frac{1 - S_{11}^2 + S_{12}^2 - 2S_{12}}{(1 - S_{11})^2 - S_{12}^2} \tag{2.13}$$

Where Z_0 is the characteristic impedance of the transmission line. Z_0 is usually considered to be 50 Ω for most practical measurements, this convention is adopted throughout.

2.6 Summary

This chapter has provided a brief overview of the balanced antenna concept. In particular a theoretical framework for deriving the characteristics of both balanced and unbalanced antenna types has been presented. The use of balun circuits has been introduced. Two measurement techniques for the impedance input of balanced antennas were discussed. The first is the monopole method, where a conducting ground plane with only one half of the antenna is used, and the real part of the measured impedance value is doubled. The second uses two port scattering parameters to evaluate the input impedance of the balanced antenna. This two port methodology is useful, and has been proven in the characterization of the equivalent impedance of the balanced antenna.

2.7 References

[1] K. Fujimoto and J. R. James, *Mobile antenna systems handbook*. Boston Artech House, 1994.

[2] M. F. Abedin and M. Ali, "Modifying the Ground Plane and Its Effect on Planar Inverted-F Antennas (PIFAs) for Mobile Phone Handsets," *IEEE Antennas and Wireless Propagation Letters*, vol. 2, pp. 226- 229, 2003.

[3] Y.-B. Kwon, J.-I. Moon, and S.-O. Park, "An Internal Triple-Band Planar Inverted-F Antenna," *IEEE Antennas and Wireless Propagation Letters*, vol. 2, pp. 341-344, 2003.

[4] K. R. Boyle and L. P. Ligthart, "Radiating and Balanced Mode Analysis of PIFA Antennas," *IEEE Transactions on Antennas and Propagation,* , vol. 54 pp. 231-237, 2006.

[5] K.-L. Wong, *Planar antennas for wireless communications* Hoboken, N.J. : J. Wiley, 2003.

[6] C. H. See, R. A. Abd-Alhameed, N. J. M. P.S. Excell, and J. G. Gardiner, "Internal triple-band folded planar antenna design for third generation mobile handsets," *IET Microwaves, Antennas & Prapagation*, vol. 2, pp. 718-724, October 2008.

[7] P. Nepa, G. Manara, A. A. Serra, and G. Nenna, "Multiband PIFA for WLAN Mobile Terminals," *IEEE Antennas and Wireless Propagation Letters*, vol. 4, pp. 349-350, 2005.

[8] R. A. Bhatti and S. O. Park, "Hepta-band internal antenna for personal communication handsets," *IEEE Transactions on antennas and propagation*, vol. 55, pp. 3398-3403, December 2007.

[9] W.-I. Kwak, S.-O. Park, and J.-S. Kim, "A Folded Planar Inverted-F Antenna for GSM/DCS/Bluetooth Triple-Band Application," *IEEE Antennas and Wireless Propagation Letters,*, vol. 5, pp. 18-21, 2006.

[10] B.-N. Kim, S.-O. Park, Y.-S. Yoon, J.-K. Oh, K.-J. Lee, and G.-Y. Koo, "Hexaband Planar Inverted-F Antenna With Novel Feed Structure for Wireless Terminals," *IEEE Antennas and Wireless Propagation Letters*, vol. 6, pp. 66-69, 2007.

[11] M.-C. Huynh and W. Stutzman, "Ground plane effects on planar inverted-F antenna (PIFA) performance," *IEE Proc.-Microw. Antennas Propag.,*, vol. 150, pp. 209-213, August 2003.

[12] Z. Du, K. Gong, J. S. Fu, B. Gao, and Z. Feng, "A Compact Planar Inverted-F Antenna With a PBG-Type Ground Plane for Mobile Communications," *IEEE Transactions on Vehicular Technology*, vol. 52, 2003.

[13] G. A. Ellis and S. Liw, "Active Planar Inverted-F Antennas for Wireless Applications," *IEEE Transactions on Antennas and Propagation* vol. 51, pp. 2899-2906, 2003.

[14] H. Morishita, H. Furuuchi, and K. Fujimoto, "Performance of balance-fed antenna system for handsets in the vicinity off a human head or hand," *IEE Proceeding Microwave Antennas Propagation*, vol. 149, pp. 85-91, 2002.

[15] R. A. Abd-Alhameed, P. S. Excell, R. A. K. Khalil, and J. Mustafa, "SAR and radiation performance of balanced and unbalanced mobile antennas using a hybrid computational electromagnetics formulation," *IEE Proceedings-Science, Measurement and Technology special issue on Computational Electromagnetics*, vol. 151, pp. 440-444, 2004.

[16] S. Kingsley, "Advances in handset antenna design, ," *RF Design*, May 2005.

[17] H. H. Skilling, *Electric transmission lines: distributed constants, theory, and applications* 1st ed: McGraw-Hill 1951

[18] R. W. Lewallen, "Baluns: what they do and how they do it," *ARRL Antenna Compendium*, vol. 1, pp. 157-163, 1985.

[19] K. Ogawa, H. Iwai, and Y. Koyanagi, "Balance-fed planar built-in antenna," *IEEE, Electronics Letters*, vol. 37, pp. 476 - 478, 2001.

[20] B. S. Collins, S. P. Kingsley, J. M. Ide, S. A. Saario, R. W. Schlub, and S. G. O'Keefe, "A Multi-Band Hybrid Balanced Antenna," *IEEE International Workshop, Antenna Technology Small Antennas and Novel Metamaterials*, pp. 100-103, 2006

[21] D. Zhou, R. A. Abd-Alhameed, and P. S. Excell, "Bandwidth enhancement of balanced folded loop antenna design for mobile handsets using genetic algorithms," *National URSI symposium, University of Portsmouth, Portsmouth, UK*, 2007.

[22] S. Hayashida, H. Morishita, Y. KIM, Y. Koyanagi, and K. Fujimoto, "Wideband folded loop antenna for handsets," *IEEE AP-S Proc.*, vol. 3, pp. 2-5, Jun. 2002.

[23] "Balun for an Antenna," http://www.freepatentsonline.com/7319435.pdf.

[24] M. C. Tsai, "A new compact wide-band balun," *IEEE Microwave and Millimeter-Wave Monolithic Circuits Symposium* pp. 123–125, 1993.

[25] R. Sturdivant, "Balun designs for wireless mixers, amplifiers and antennas," *Appl. Microw*, pp. 34–44, 1993.

[26] P. C. Hsu, C. Nguyen, and M. Kintis, "Uniplanar broad-band pushpull FET amplifiers," *IEEE Trans. Microwave Theory Tech*, vol. 45, pp. 2150–2152, Dec. 1997.

[27] M. N. Tutt, H. Q. Tsemg, and A. Ketterson, "A low loss, 5.5 GHz-20 GHz monolithic balun," *IEEE MTT-S Int. Microwave Symp. Dig*, pp. 933–936, 1997.

[28] Z. Y. Zhang, Y. X. Guo, L. C. Ong, and M. Y. W. Chia, "A New Wide-band Planar Balun on a Single-Layer PCB," *IEEE Microwave and wireless components letters*, vol. 15, pp. 416-418, June 2005.

[29] G. S. Hilton, C. J. Railton, C. J. Ball, M. Dean, and A. L. Hume, "Modeling a Three-element Printed Dipole Antenna Array using the FDTD Technique," *IEEE Antennas and Propagation Society International Symposium*, vol. 2, pp. 1062–1065, 1997.

[30] M. W. Nurnberger and J. L. Volakis, "A new planar feed for slot spiral antennas," *IEEE Trans. Antennas, Propagat*, vol. 44, pp. 130–131, Jan 1996.

[31] Y. X. Guo, Z. Y. Zhang, L. C. Ong, and M. Y. W. Chia, "A new balanced UWB planar antenna," *Wireless Technology, The European Conference* pp. 515 - 517, 2005.

[32] G.-Y. Chen and J.-S. Sun, "A Printed Dipole Antenna With Microstrip Tapered Balun," *Microwave and Optical Technology Letters*, vol. 40, pp. 344-346, 2004.

[33] D. Staiculescu, N. Bushyager, A. Obatoyinbo, Lara J. Martin, and M. M. Tentzeris, "Design and Optimization of 3-D Compact Stripline and Microstrip Bluetooth/WLAN Balun Architectures Using the Design of Experiments Technique," *IEEE Transactions on Antennas and Propagation* vol. 53, pp. 1805-1812, 2005.

[34] By J. Thaysen, K. B. Jakobsen, and J. Appel-Hansen, "A Wideband Balun — How Does it Work?," *Applied Microwave & Wireless*, pp. 40-50, 2002.

[35] K. W. Kobayashi, "A novel HBT active transformer balanced Schottky diode mixer," *IEEE MTT-S International Microwave Symposium Digest* vol. 2, pp. 947–950, Jun. 1996.

[36] R.A.A.Abd-Alhameed, "Simulation of The Complete Current Distribution on Wire and Dielectric-Loaded Antennas Using Integral-Equation Methods," PhD. Thesis, Department of Electronic and Electrical Engineering, University of Bradford, Bradford, UK, 1997.

[37] R. Meys and F. Janssens, "Measuring the impedance of balanced antennas by an S-Parameter method," *IEEE antennas and propagation magazine*, vol. 40, pp. 62-65, 1998.

[38] D. M. Pozar, *Microwave Engineering*, second edition: john Wiley &Sons, Inc, United State of America, 1998.

CHAPTER THREE

Wideband Balanced Folded Dipole Antenna with Dual Arm Monopole Structure for Mobile Handsets

3.1 Introduction

The need to expand the bandwidth of antennas in mobile handheld devices follows from the ever-increasing data rates, and hence spectrum requirements, of mobile devices. Antennas are a major part of the complete design in mobile device systems. Conventionally, the unbalanced planar inverted F antenna (PIFA) is one of the most popular candidates for compact internalised antennas for mobile handsets. PIFAs use the ground plane as a part of the radiator, enabling very small antennas to achieve adequate gain and bandwidth [1-5]. Because of the unbalanced feed, however, radiating currents are induced on both the ground plane and the antenna element in almost all cases. Since the currents on the ground plane couple strongly to the user's body, these antennas exhibit variable performance when the handset is held in the hand.

Balanced antennas offer a means of removing these limitations. The currents are mostly confined to the radiating elements, thus reducing the current flow to the ground plane [6]. It follows that a well designed balanced antenna will reduce the specific absorption rate (SAR) to the user's body [7]. In recent years, several mobile antennas designed

with the balanced technique have demonstrated the enhanced stability of antenna performance, compared to the unbalanced type, when the handset is placed next to the human head and/or hand [8-19].

In this chapter, the design of an inbuilt wideband balanced slotted dipole antenna is introduced. The target design includes full coverage of the GSM 1800, GSM 1900 and UMTS service bands. An improvement of the antenna impedance was achieved in order to realise multiple-band operation, including Bluetooth/WLAN (2.45 GHz). Detailed simulations models were developed using HFSS, and the performance was optimised by tracking the return loss, and calculated radiation patterns [20]. Methods for measuring input impedance of the proposed antenna are addressed, and a wideband planar balun feed is adopted for the fully realised design. Finally, the calculated and measured results for the antenna are presented, compared and discussed.

3.2 Antenna Design Concept and Structure

Planar metal-plate monopole antennas have been investigated in the past as good candidates for ultrawide-band applications [21, 22]. A pair of such wideband monopole antennas can be integrated together to configure a dipole and to maintain a wide bandwidth. Following this principle, a wideband planar dipole antenna in free space can be developed. A simple technique for enhancing antenna impedance bandwidth was employed by symmetrically trimming a triangle at the monopole edge near the feed point, to give a tapered feed [23].

The first design iteration was for a free space model, which was then systematically modified for realistic handset operations. The antenna (see Figure 3.1) is mounted on

the top of a rectangular conducting plate (120×50 mm), which can be regarded as the practical chassis or ground plane of a mobile handset.

Like most balanced antennas, the planar dipole antenna works best in free space and its operation can be degraded when placed in the vicinity of other conductors (in particular, mobile phone chassis). In order to mitigate the effects of the ground plane, a technique was applied to reduce the effects of the induced current on the ground plane by inserting a slot in each of the arms of the planar dipole. Consequently, the ground plane may have less mutual coupling on the proposed antenna. In this way, the antenna may be placed close to the ground plane of the handset (e.g. 1 mm away), without major performance degradation. In order to achieve a low profile for built-in applications, two arms of the dipole antenna were required to be folded [24-27] only but not connected at their ends, as shown in Figure 3.1.

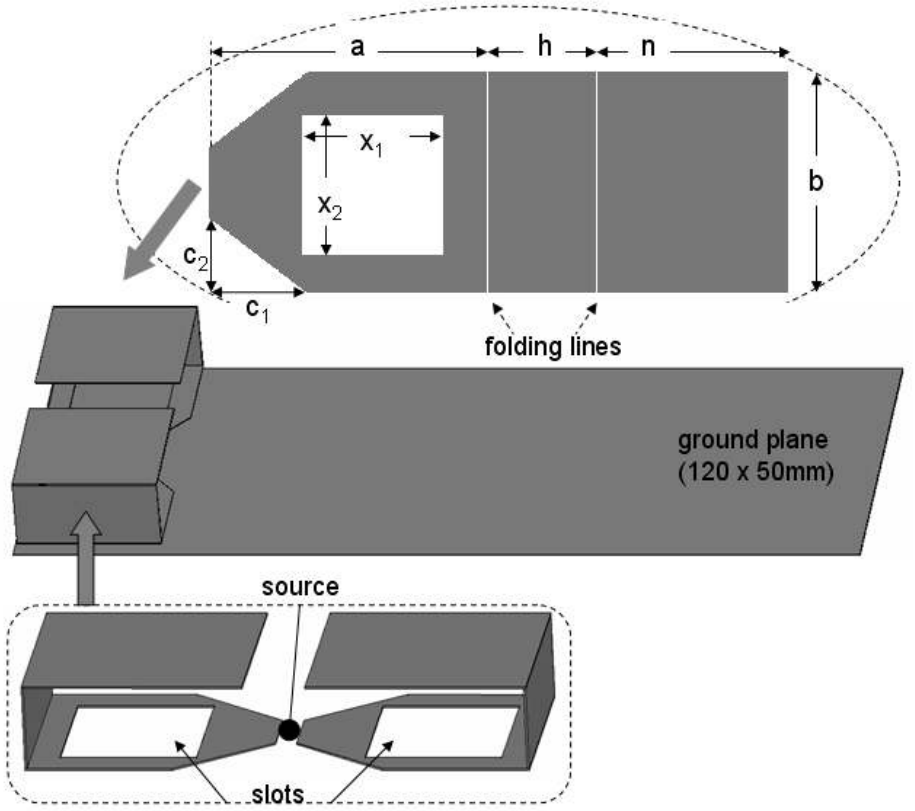

Figure 3.1: Antenna configuration studied (a=23, b=20.5, h=9.5, n=20.5, c_1=9, c_2=7, x_1=13 and x_2=14; dimensions are in mm).

The size and location of the slots in the antenna, together with other parameters, were optimised to ensure that the design entirely covered the required frequency bands 1710 to 2170 MHz at an input return loss ≤ -6 dB; as well as to minimise size of the antenna as far as possible.

3.3 Measuring Input Impedance of Balanced Antenna

Conventionally balanced antennas, such as dipoles, will use a balun feed network. The input impedance or return loss of the balanced antenna measured for such a configuration is from the antenna plus balun, rather than from the discrete antenna feed point. Therefore, the two different methods discussed in Chapter 2 were used to verify and validate the impedance of this balanced antenna. The first is the S-parameter method, in which balanced antennas are considered as two-port devices (see Figure 3.2) and the S-Parameters can be obtained from a VNA. Equations (2.11) and (2.13) are then employed to derive the differential input impedance of the balanced antennas. In addition, a monopole mirrored over the ground [28, 29] is used as the other method to compare the results obtained from the first measurement method (see Chapter 2).

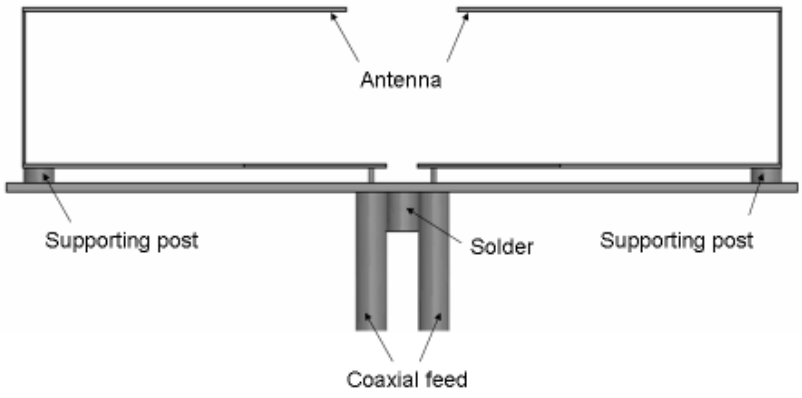

Figure 3.2: Side view of the balanced antenna with two-port S-Parameter measurement method.

3.3.1 Wideband Balun Design and Characterisation

To obtain the desired antenna stability and radiation pattern, a suitable wideband balun circuit [30], which was then modified for this design, as shown in Figure 3.3. This re-

design was carried out using ADS [31]. The final balun structure is shown in Figure 3.4, it was mounted on Duroid with a permittivity of 3.48, thickness 0.8 mm, and tan δ = 0.0019.

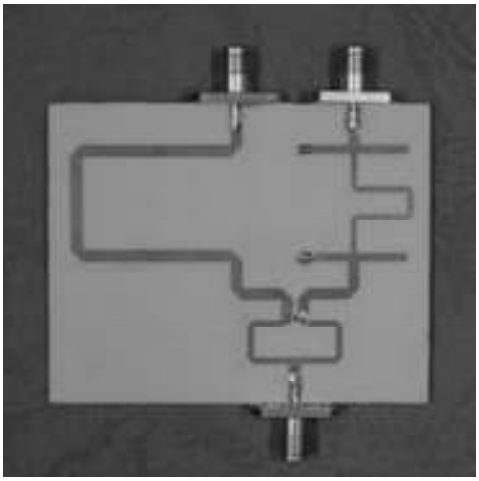

Figure 3.3: Photograph of the fabricated board for the adopted balun in [30].

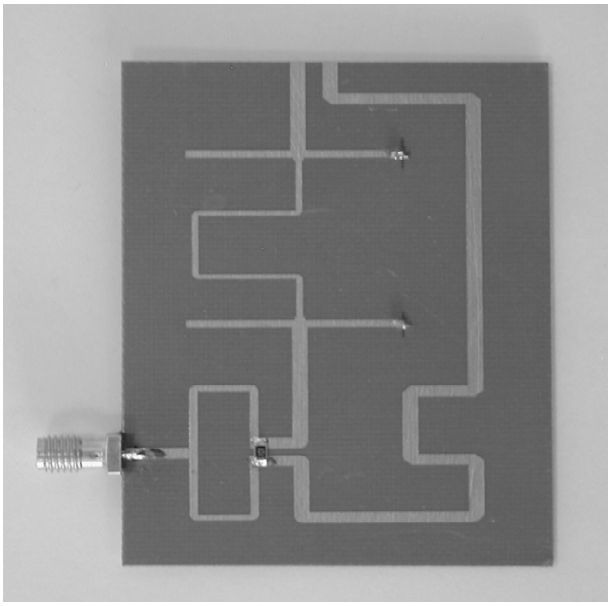

Figure 3.4: Photograph of the fabricated board for the modified balun.

Two back-to-back modified wideband planar baluns were built up and measured in order to evaluate their insertion loss and return loss in the intended frequency bands [32]. In addition, the magnitude and phase difference between the two outputs was

investigated using a single balun: an excellent balance in magnitude and phase within the intended bandwidth was found, as shown in Table 3.1.

Table 3.1: Comparison between the present design and the prior art.

Item	Frequency range (GHz)	Insertion loss max. (dB)	Relative Errors: Amplitude (dB)/ Phase (degrees)	Return loss max. (dB)
Prior art in [30]	1.7-3.3	-	± 0.3 / ± 5	10
Present Balun	1.4-2.4	1.65	± 0.1 / ± 2	10

3.3.2 Results and Discussion

A monopole representing half of the intended balanced antenna, including half of the phone chassis (ground plane), was constructed and tested in order to examine the actual input impedance at the feed point for the proposed balanced design. Copper sheeting of thickness 0.15 mm (for the ground plane) and 0.5 mm (for the antenna arms) was used, whilst a copper plate with dimensions 500 mm × 500 mm was chosen as a finite ground plane for the monopole design. Figure 3.5 compares the measured return loss for the prototype, against the simulated values. As can be seen, a fairly good agreement in return loss can be observed. A wideband characteristic with less than -6 dB return loss can also be confirmed. It should be noted that the reference plane for the antenna impedance measurement was effectively moved to the input port of the antenna by applying the equivalent delay, and using a function in the VNA (HP 8510C) to calibrate out the effect of introducing the semi-rigid coaxial cable (see Figure 3.2) in the two-port measurement.

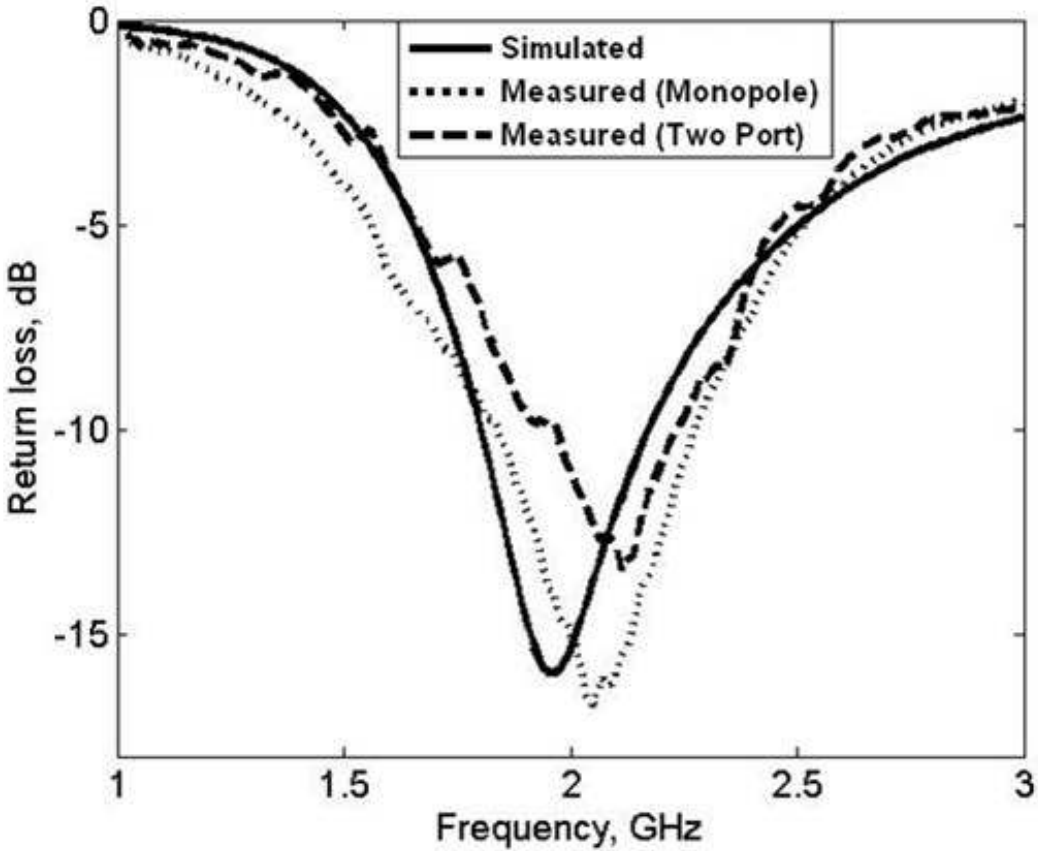

Figure 3.5: Comparison of return loss among the two different measurement methods and simulation.

To investigate the stability and radiation performance of this concept, another version of the antenna, integrating a planar balun, was designed and constructed, as illustrated in Figure 3.6. The ground plane of this variant was printed on one side of the dielectric substrate and the balun was printed on the other side. The positions of the two balanced outputs from the balun were carefully located directly beneath the feed points of the balanced antenna. Two thin wires were used to connect the antenna feed point with the balun through holes. In this way, the antenna and its feed network were closely integrated and could be regarded as a single system. The calculated radiation patterns in the xz plane and yz plane for the balanced dipole with and without the balun at 1780,

1900 and 2150 MHz were presented in Figure 3.7. The results found to be quite similar to each other at all three designated centre frequencies.

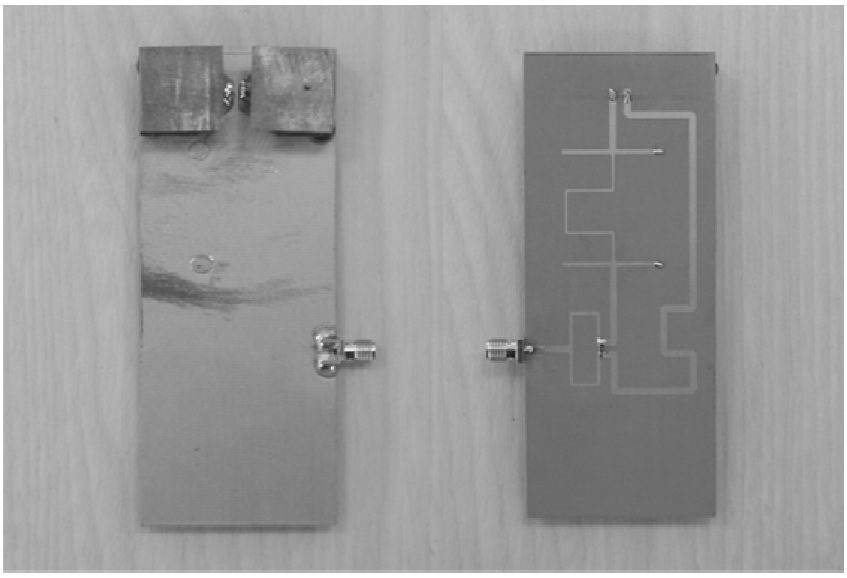

Figure 3.6: The fabricated prototype balanced antenna, together with its feeding network, where left is top view and right is underside view.

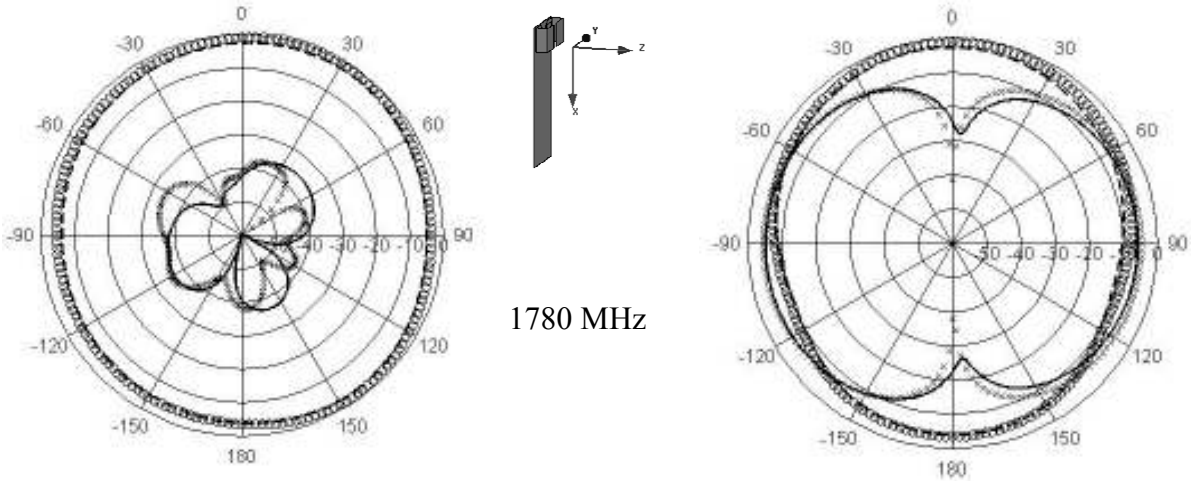

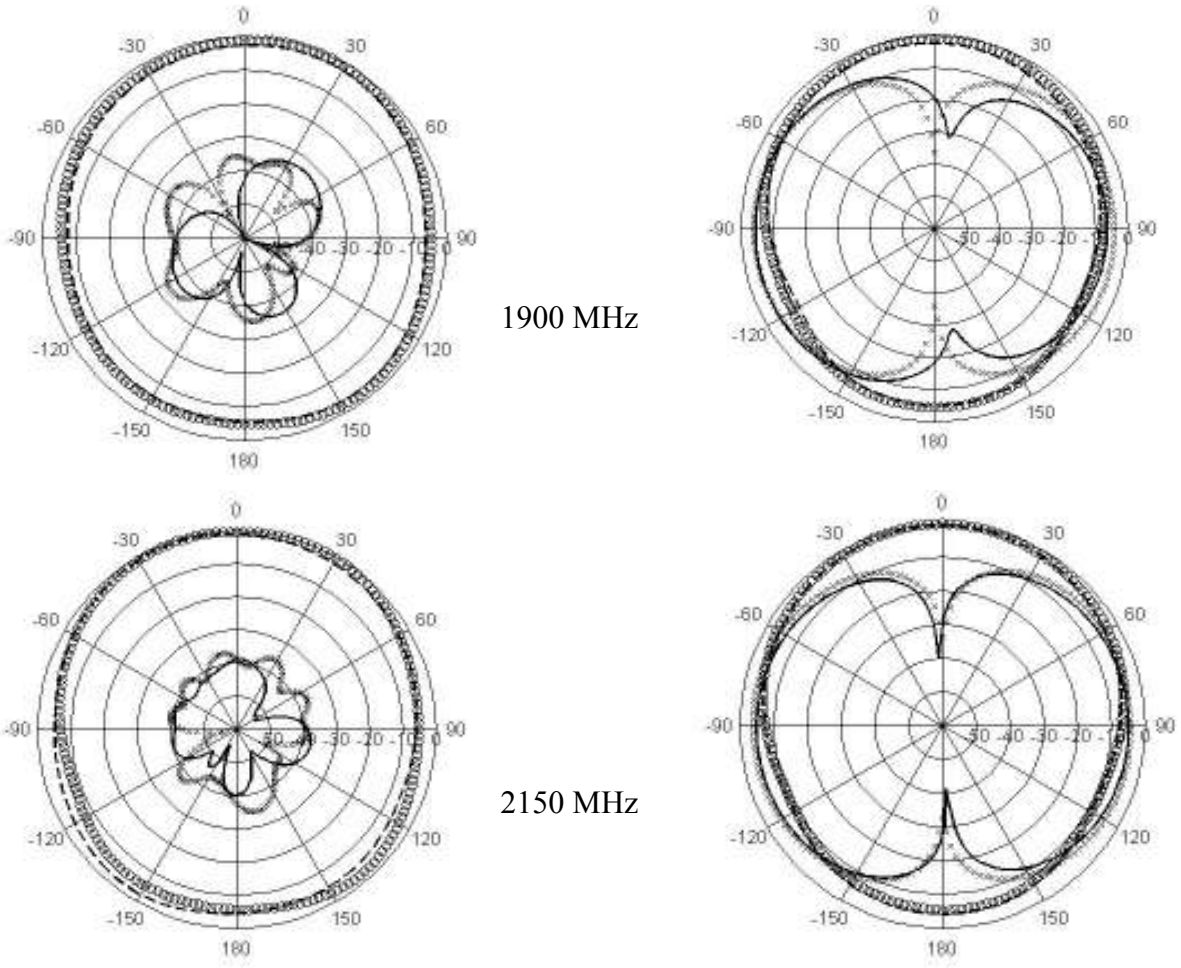

Figure 3.7: Radiation patterns for the proposed antenna at 1780 MHz, 1900 MHz and 2150 MHz in the x-z plane (a) and y-z plane (b); 'x x x': simulated E_ϕ without balun, 'o o o' simulated E_θ without balun, '------' simulated E_ϕ with balun, '——' simulated E_θ with balun

3.4 Studying the Antenna Performance

3.4.1 Effect of Slots and Taper of the Antenna Arms on Return Loss

Techniques were applied to successfully achieve the required low profile construction and wideband characteristics in the design. These included the symmetrical tapering of each arm of the dipole near the feed point, and inserting slots in the dipole arms. The

performance of the antenna was analysed and evaluated with trimmed tapering, or the introduction of slots. The resulting return loss is shown in Figure 3.8. One may conclude that introducing these modifications into the antenna plays a vital important role in achieving good balanced design. The application of symmetrical trimming to the taper enables some freedom in antenna impedance matching, by varying the length of the trimmed laterals (c_1 and c_2).

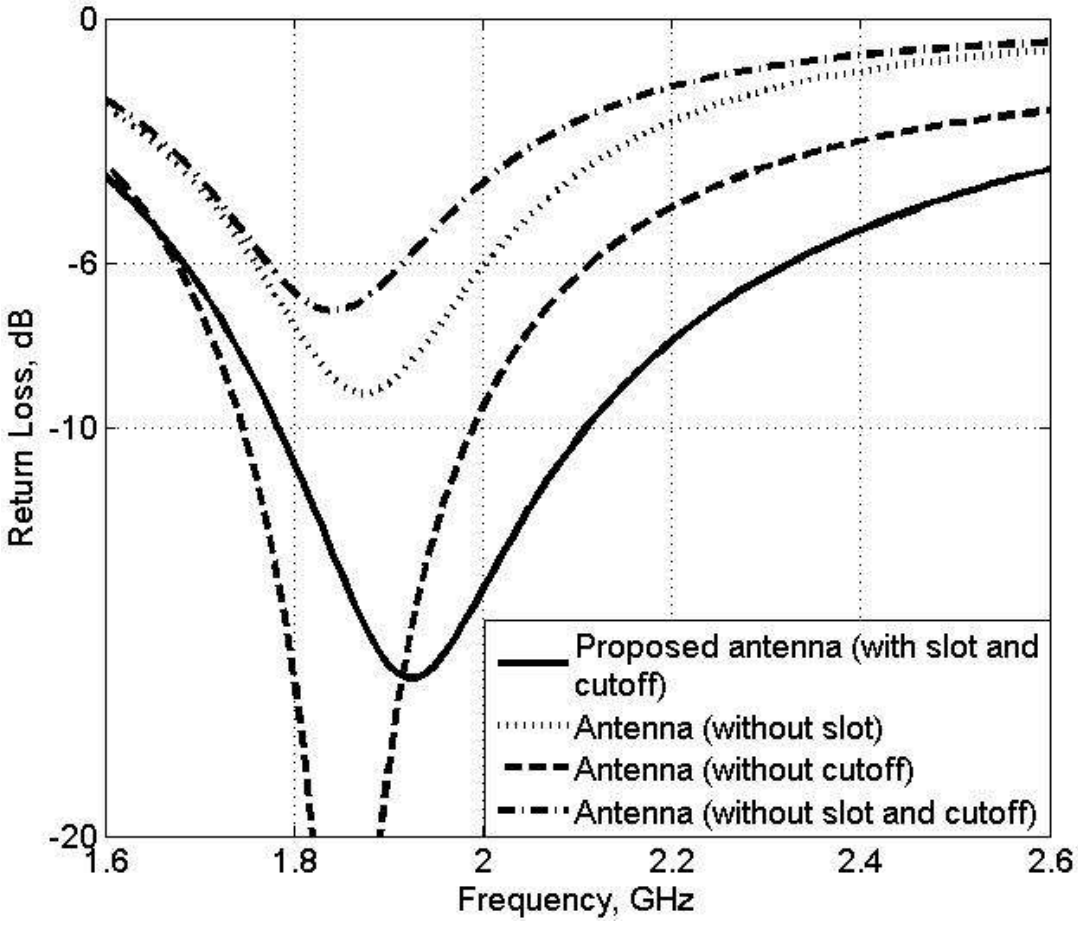

Figure 3.8: Effect on the antenna return loss by introducing slots or taper (corner cutoff) to the configuration.

3.4.2 The Effect of Head and Hand on the Antenna Return Loss

The effect of adjacent human tissue mass on the performance of the prototype antenna was evaluated firstly by having the ground plane in the user's hand (without electrical contact), and secondly by placing it in the vicinity of the user's head in a simulated 'talk' position, as in Figure 3.9. In this simulation, a simple model that includes hand and spherical head is used. This model is a realistic well known model by several published data [6,33,34], which is good enough to compare some computed result with the one achieved by other. It was found that the antenna return loss in the two different situations showed only small variations within the intended operating range, as shown in Figure 3.10. This confirmed the stability of the proposed balanced antenna when the phone is held in the vicinity of the head.

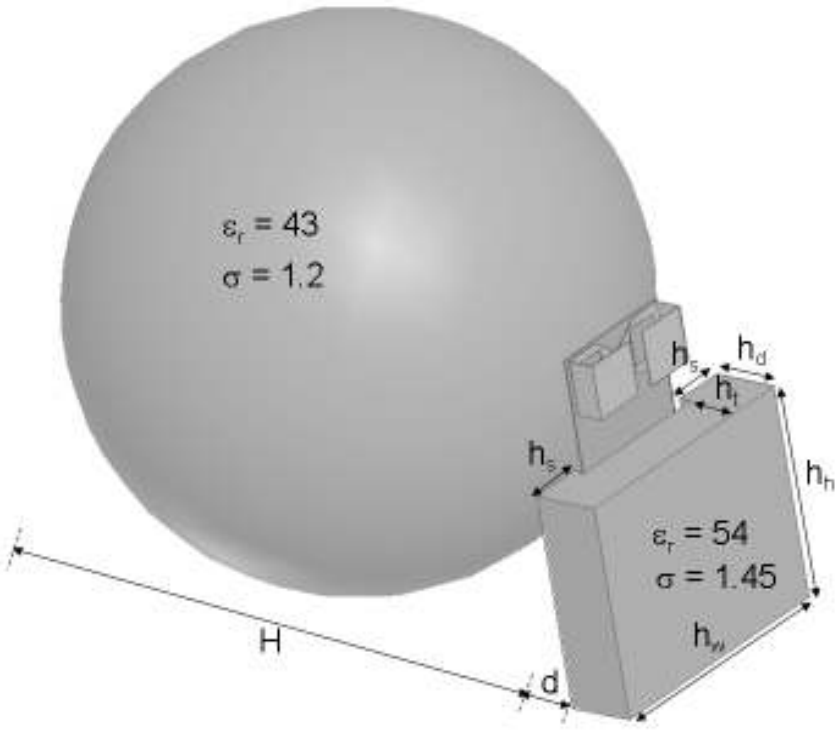

Figure 3.9: Spherical human head and hand model interaction with mobile handset (where H = 200 mm, h_w = 98 mm, h_h = 80 mm, h_d = 24.5 mm, h_t = 20 mm, d (distance from the head) = 10 mm and h_s = 20 mm).

Figure 3.10 also presents the measured and simulated return loss (i.e. of antenna and balun together) of the fabricated prototype antenna shown in Figure 3.6. The results are in close agreement, but it is necessary to take into account the effect of modifications to the physical prototype during the development process, and a further change in the inclusion of the dielectric substrate beneath the ground plane. It should be noted that an additional resonance was found in the measured at 2.4 GHz. This is believed to be due to constraints on the operating frequency range of the balun (see Table 3.1).

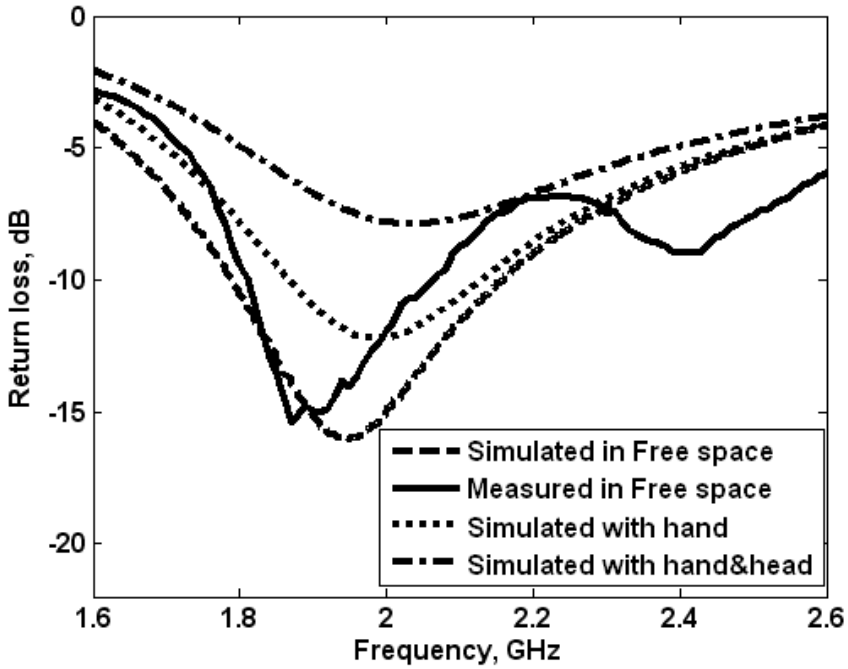

Figure 3.10: Return loss characteristics of proposed balanced antenna with integrated planar balun and head and hand models.

3.4.3 The Effect of the Ground Plane and the Current Distribution

An investigation of the effect of the ground plane length on the antenna return loss was carried out. The length of ground plane was varied from 120 mm to 60 mm in increments of 20 mm. The corresponding results are presented in Figure 3.11. For

lengths 80 mm ≤ 100 mm ≤120 mm, it can be seen that the calculated return loss shows little variation. By contrast, when the length is set at 60 mm, the impedance match was improved, whilst the resonant frequency remained unchanged. This effect is not obvious, and indicates that the proposed antenna also features a low degree of sensitivity to ground plane size, implying that the same antenna design can potentially be adopted for many other mobile devices with little modification, this has useful implications for antenna construction.

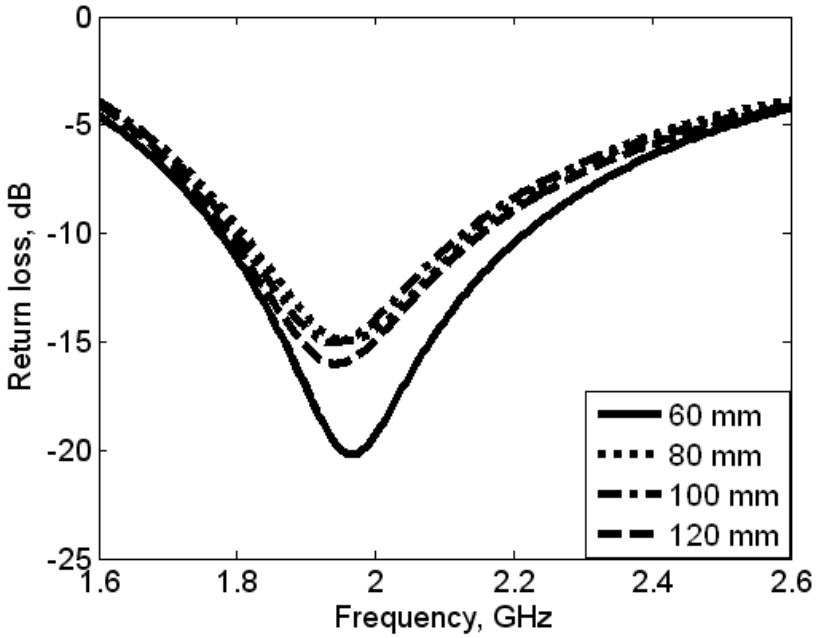

Figure 3.11: Antenna return loss characteristics for ground plane lengths of 60 mm, 80 mm, 100 mm and 120 mm.

The current distribution on the mobile phone ground plane was also determined. It was observed that most of the current induced on the ground plane was concentrated in the area beneath the antenna, and less current appeared on the rest of the ground plane, in line with expectations.

3.5 Far Field Measurement of the Wideband Balanced Antenna

Measurements of the far field radiation patterns of the antenna were carried out in an anechoic chamber. The fixed antenna (reference antenna) was a calibrated broadband EMCO horn (type 3115) and the spacing between the test antenna and the horn was held at 4 m. Two pattern cuts were taken for three selected operating frequencies that cover the target bandwidth in this study. The radiation patterns in the xz plane and yz plane for the balanced dipole at 1780, 1900 and 2150 MHz were measured. The results were plotted against predictions in Figure 3.12, where the patterns of the fabricated prototype antenna (i.e. the AUT) are seen to be quite similar to each other at all three designated centre frequencies. It is obvious for 20 dB to 30 dB down the fields magnitude is less important on the cross polar components in x-z plane; however, the differences on the lower values of the cross polar components might rise from the contribution of the feeding network. In addition, the xz plane presents a nearly omni-directional radiation pattern in all intended frequency bands. The radiation patterns for other frequencies within the intended frequency bands were also investigated and found to be similar to one or other of these and hence are not presented.

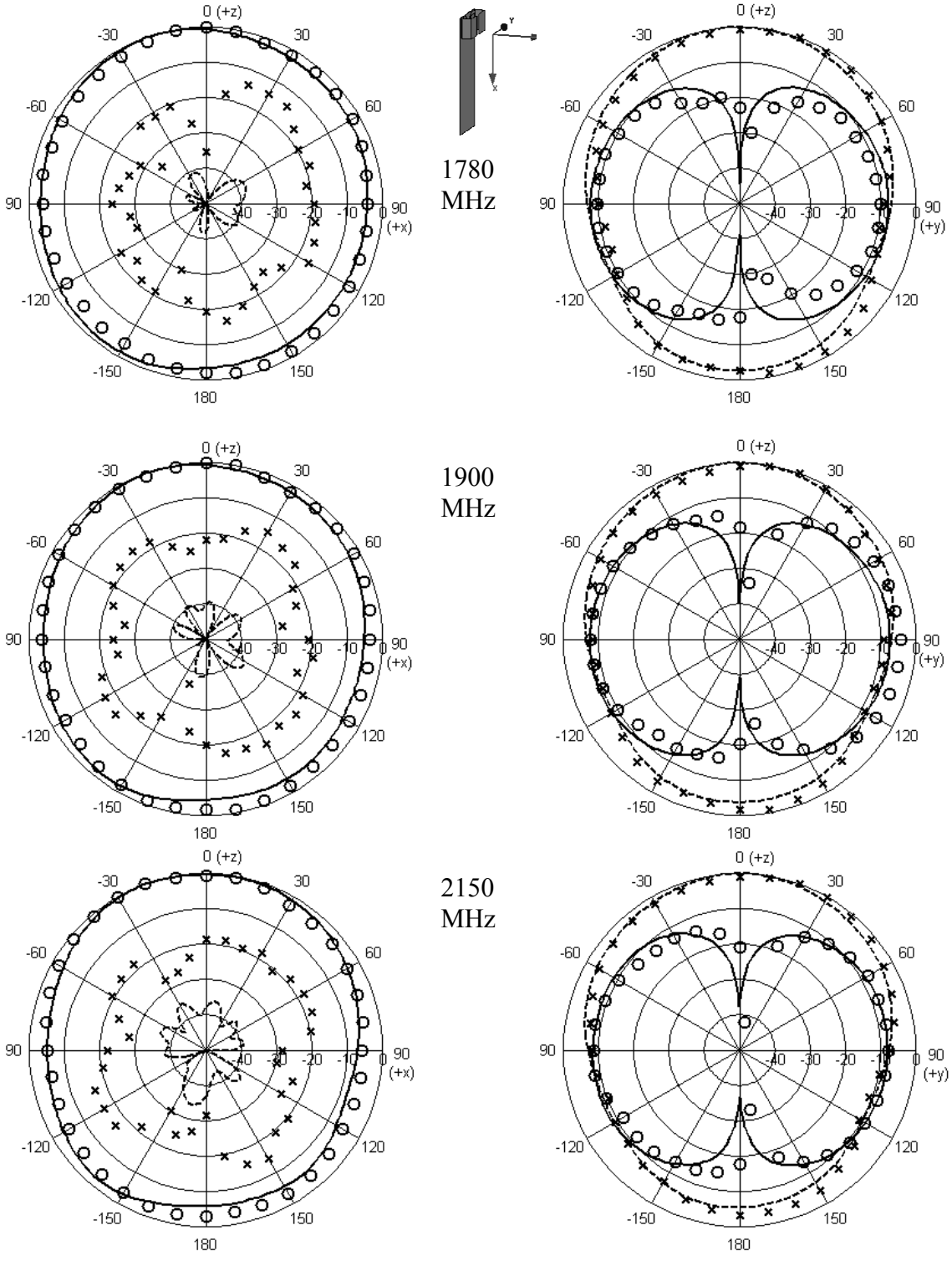

Figure 3.12: Radiation patterns for the proposed antenna at 1780 MHz, 1900 MHz and 2150 MHz in the x-z plane (a) and y-z plane (b), where: 'x x x': measured E_ϕ, 'o o o' measured E_θ, '------' simulated E_ϕ, '——' simulated E_θ.

Figure 3.13 illustrates the measured antenna gain compared to the simulations in the broadside direction for the frequencies across the GSM 1800, GSM 1900 and UMTS bands. It should be noted that the insertion loss of the feed network was subsequently added to the measured power gain at each specific frequency in the measurement plot. As can be seen in Figure 3.13, antenna gain measurements varied between approximately 2.5 dBi and 3.5 dBi over the bandwidth. Generally, this variation of the measured antenna gain was mainly caused by planar balun integrated with the handset ground, and the wire connections between the antenna and the balun. For the bandwidths of the three specific operating bands, the peak antenna gain variations are less than 0.5 dBi, as compared with the predictions.

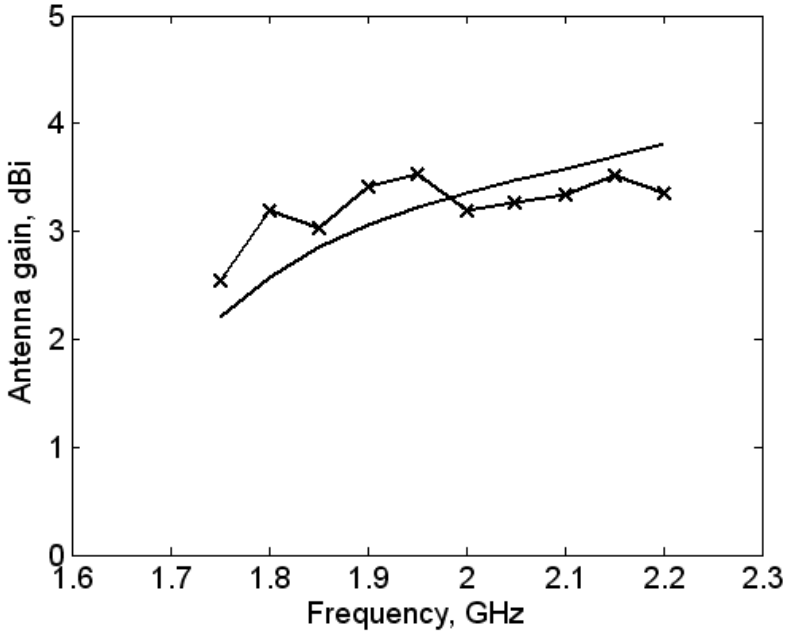

Figure 3.13: Comparison of simulated and measured antenna gain for the proposed folded balanced antenna

3.6 The Improved Version of the Wideband Balanced Antenna

In this section a further improvement in the impedance bandwidth for this antenna is introduced, in order to cover an additional band at 2.45 GHz for WLAN, since most mobile phones available in the market have such a feature.

3.6.1 New Antenna Configuration

Initially, new simulation model for the antenna operating around 2 GHz was build (‘dipole 1’: see Figure 3.14b). In addition, a new technique was applied by inserting an additional thin-strip arm (‘dipole 2’: see Figure 3.14b) for each planar dipole arm to generate another resonant frequency at 2.45 GHz. Using this technique, the balanced resonant antenna was modified and developed as a wideband dual-resonant variant for multi-band operation. A symmetrically stepped structure was used on the edges of the arms near the feed point [35], as shown in Figure 3.14c. This replaces the symmetrical triangular trimming structure used in previous design. This is because the stepped configuration has better control of the impedance bandwidth, as verified in the analysis.

Similarly, the slot size, including its location and length, and also the location of additional arms for ‘dipole 2’, together with other parameters (see Figure 3.14c), were adjusted and optimised to ensure that the design entirely covered the required frequency bands (1710-2484 MHz) with a VSWR at the input port of less than 3 (equivalent to return loss ≤ -6 dB).

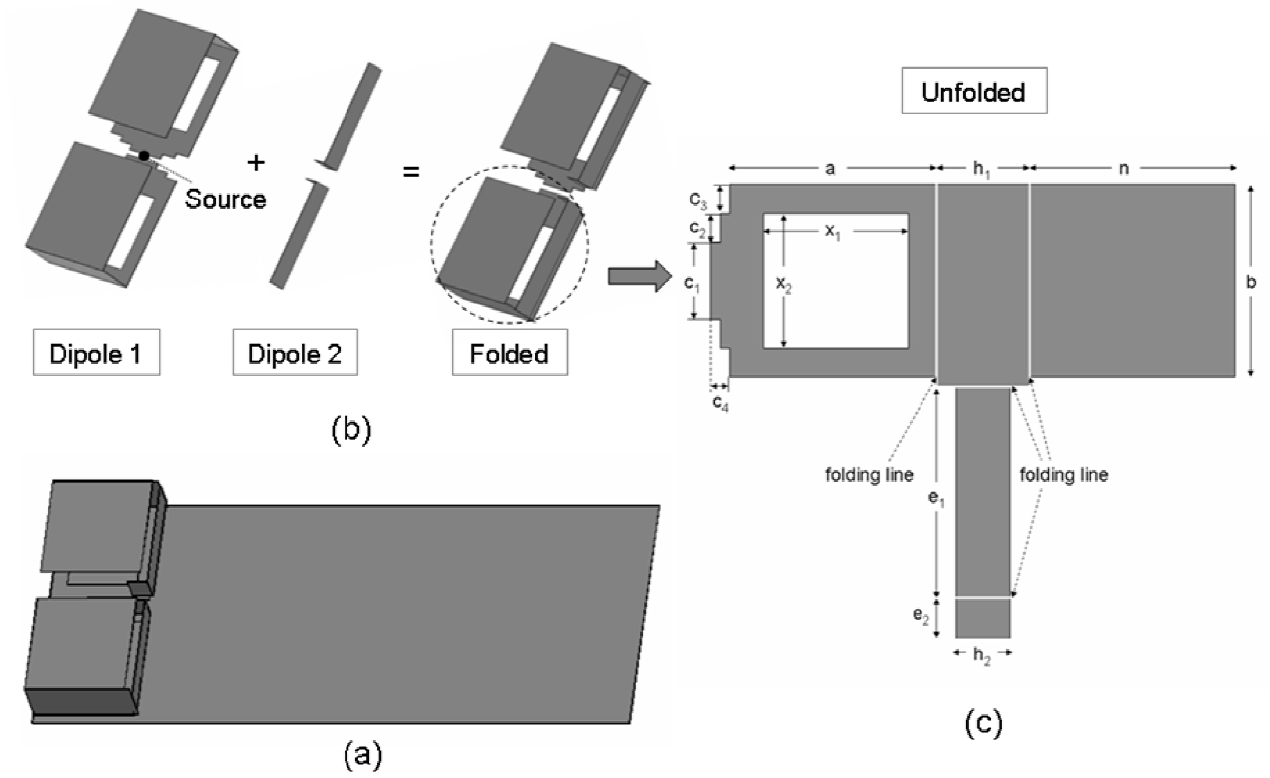

Figure 3.14: Antenna configuration studied; (a) balanced folded dipole antenna with conducting plate; (b) development of the proposed multi-band design; (c) unfolded structure of the proposed antenna.

An optimised antenna configuration was found with excellent performance in terms of return loss, radiation patterns and power gain, with aid of the EM simulator. The most important dimensions shown in Figure 3.14c were established to be as shown in Table 3.2

.

Table 3.2: Summary of important parameters of the antenna.

Parameters	Value (mm)
a	21.5
b	20
h_1	9.5
h_2	5.5
n	21
c_1	8
c_2	3
c_3	3
c_4	2
x_1	15
x_2	14
e_1	22
e_2	4

3.6.2 Parametric Study Results

In order to fully understand the influence of the antenna parameters on the impedance bandwidth and overall antenna size constraints, a parametric study was carried out by varying each parameter, while holding the remaining parameter values at the assumed optimum values. The impedance bandwidth was the main goal to be optimized throughout the parametric study in this work (i.e., return loss < -6 dB).

3.6.2.1 Effect of the Length of the Antenna Arm (n) and Length of The Slot (x_1)

It was found the length of the antenna arm (n) and the length of the slot x_1 control the resonant mode of this antenna. As can be seen from the Figure 3.15 and Figure 3.16, the

optimum values of n and x_1 were found to be 21 mm and 15 mm, respectively. This gave the best performance for the antenna in the mobile frequency bands of interest.

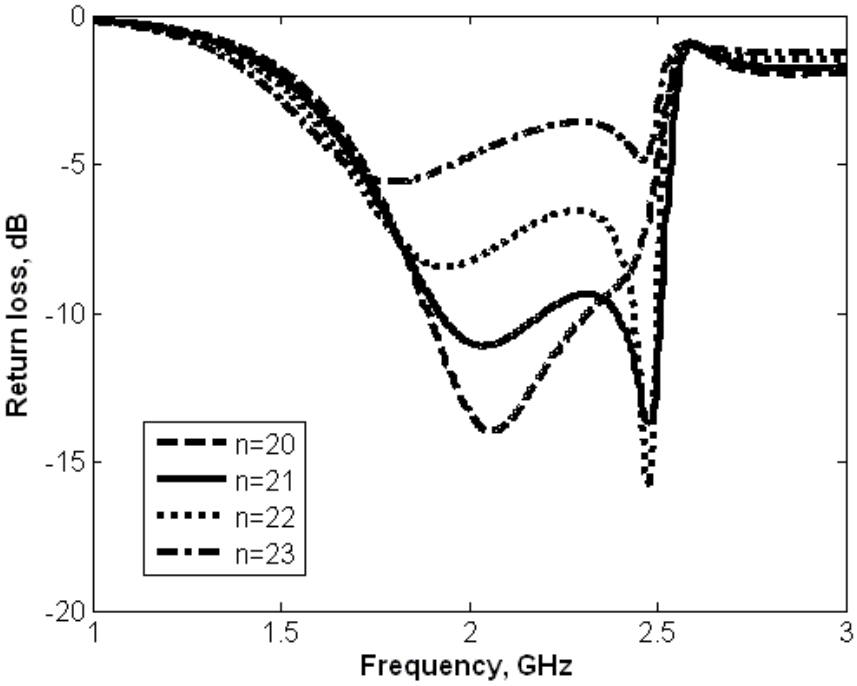

Figure 3.15: Parametric study of parameter n (in mm) against operating frequency.

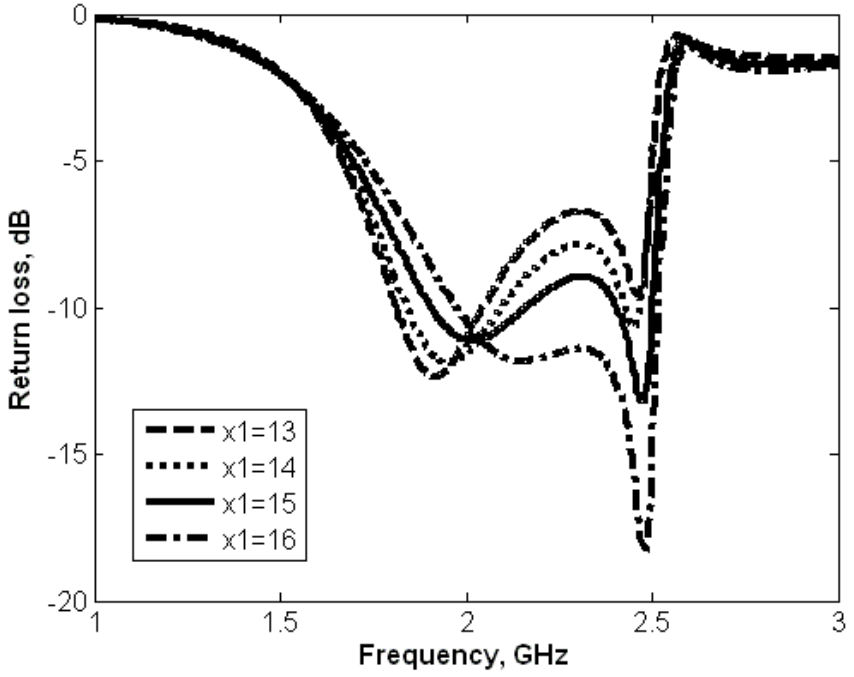

Figure 3.16: Parametric study of parameter x_1 (in mm) against operating frequency.

3.6.2.2 Effect of the Length of the Thin-Strip (e_1 and e_2)

The purpose of introducing the thin-strip 'dipole 2' was to introduce another resonance, thus creating a further variant to the existing multiple-band antenna. A parametric study on the thin-strip dimensions e_1 and e_2 was performed. Figure 3.17 presents the resulting variations of antenna return loss against the operating frequency, for e_1 and e_2. It is observed that the additional resonant frequency next to the existing one is at about 2.4 GHz and gradually decreases as the length of the strips on 'dipole 2' are increased.

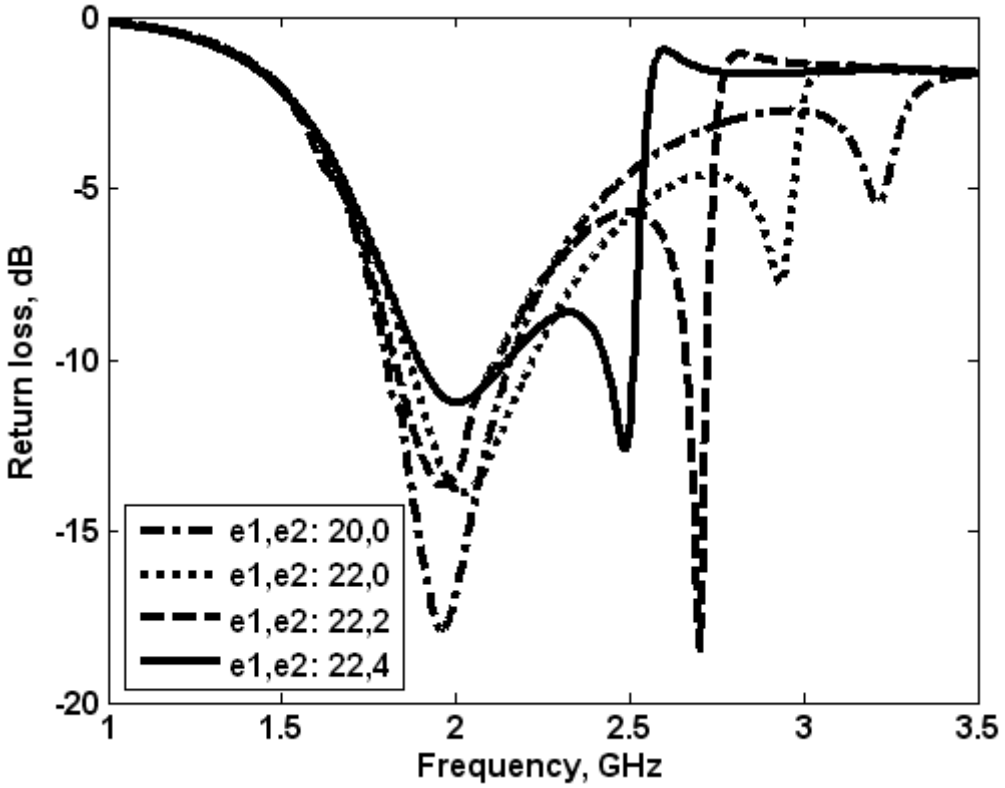

Figure 3.17: Parametric study of parameters e_1 and e_2 (in mm) against operating frequency.

3.6.2.3 The Effect of the Ground Plane Length

The influence of the ground plane on the antenna's performance was investigated in terms of the return loss, and is illustrated in Figure 3.18. The length of ground plane was reduced from the end opposite the antenna, from 60 mm to 120 mm in increments of 20 mm. As can be seen in the figure, there was a small variation in calculated return loss observed for all design cases. Similarly, the radiation patterns were examined for each length and found to vary by no more than 2% (the full-length results are discussed below). These results suggest that the antenna is fulfilling its intended function of inducing very little current into the ground plane. As a check, the computed surface currents for different ground plane lengths were also simulated, and are shown in Figure 3.19, in which it is seen that they are negligible except in the region underneath the antenna. These results indicate that the antenna does feature a low degree of sensitivity with respect to the ground plane size. This implies that the same antenna design has the capability to be adapted for many other mobile devices.

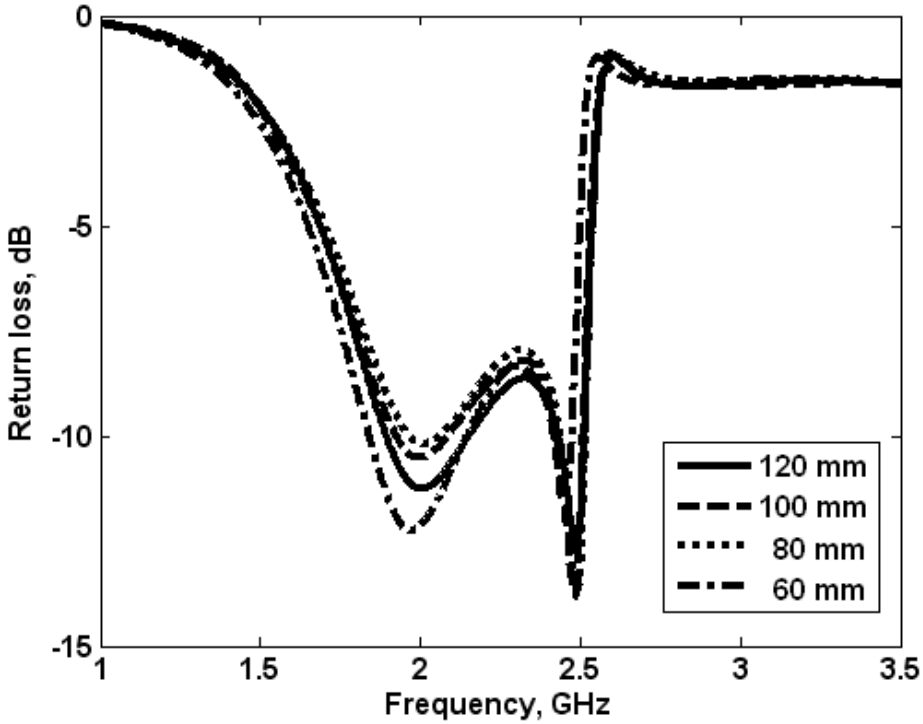

Figure 3.18: Variations of antenna return loss against ground length of 60 mm, 80 mm, 100 mm and 120 mm.

(a) (b) (c)

Figure 3.19: Surface current distributions for the proposed balanced antenna at 2.4 GHz for various ground plane lengths: a) 120 mm, (b) 80 mm, (c) 60 mm

3.6.3 Measuring the Input Impedance of the Improved Version of the Proposed Antenna

For the sake of convenience whilst investigating the antenna's radiation performance, the wideband planar balun applied in previous section was used as a part of the feeding network, to provide the necessary balanced feed from an unbalanced source. For the physical realisation, a copper sheet of thickness 0.15 mm was used to fabricate the balanced antenna. The ground plane was printed on one side of the dielectric substrate and the planar balun was placed on the other side, as illustrated in Figure 3.20. The same procedure of positioning the two balanced outputs from the balun in order to share the same ground plane, and constitute a fully integrated system, was followed as mentioned earlier.

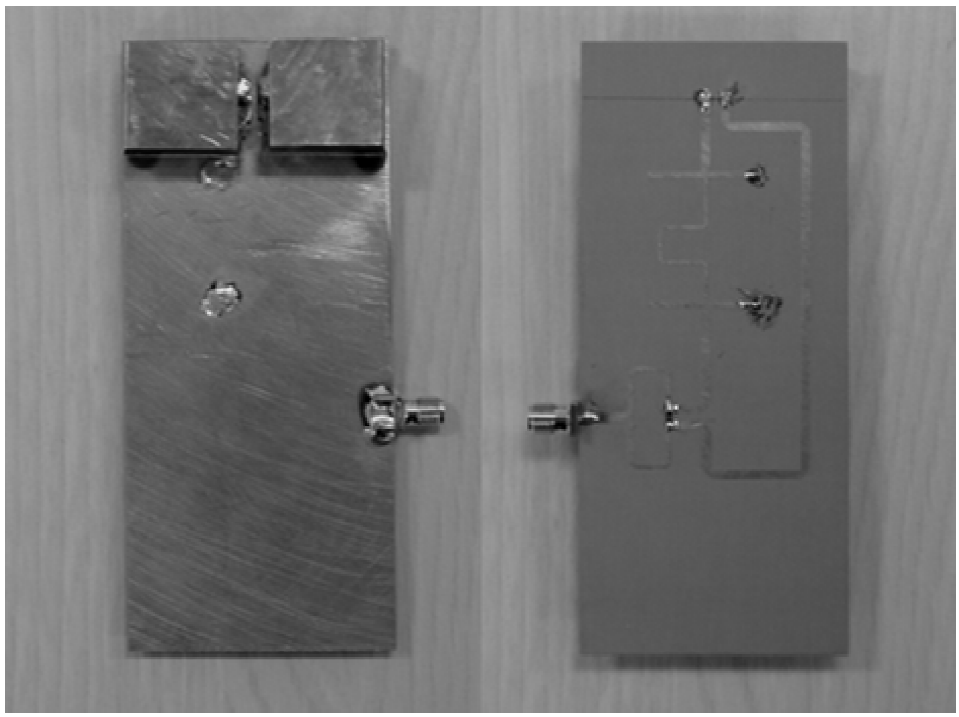

Figure 3.20: The fabricated prototype balanced antenna, together with its feeding network.

Figure 3.21 shows the measured return loss of the prototype antenna, using both the two-port direct measurement and the antenna with integrated planar wideband balun. Both are compared against the simulation model. There is a generally good agreement between the simulated and measured return loss, also there are some slight discrepancies between the fabricated antenna and its simulation model. This result verifies the actual impedance of the antenna, as well as the effectiveness of the antenna system with an integrated balun, and confirms the validity of using it for the evaluation of radiation performance of the system.

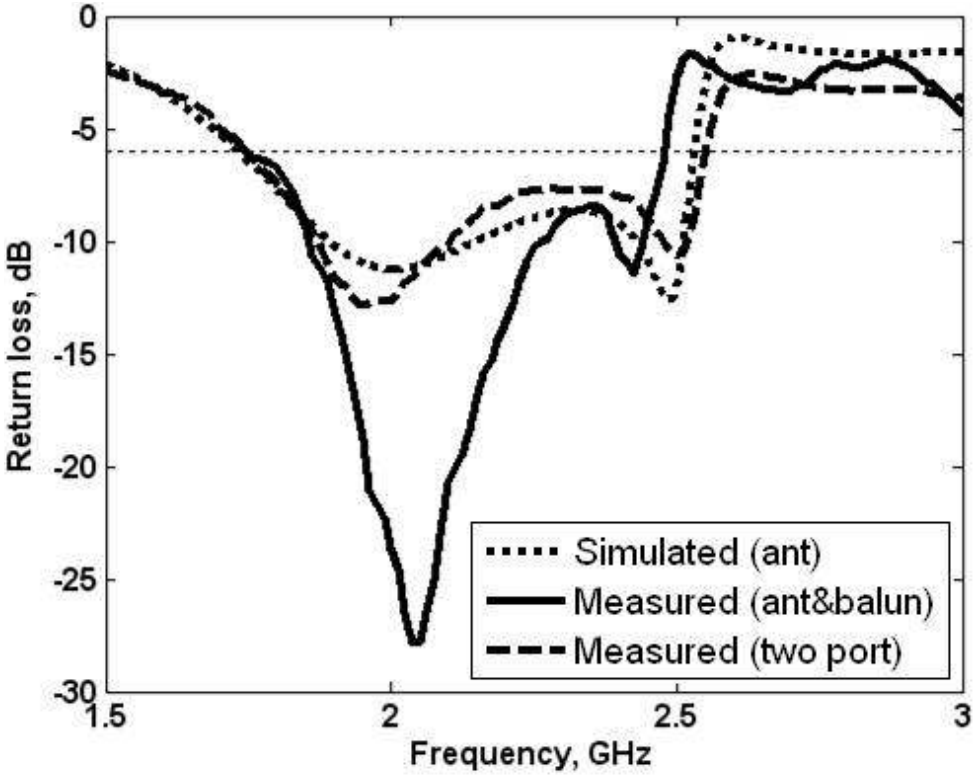

Figure 3.21: The simulated and measured return loss against operating frequency.

3.6.4 Radiation Pattern and Power Gain of the Improved Version of the Antenna

Measurements of the far field radiation patterns of the prototype were carried out in a far-field anechoic chamber using an elevation-over-azimuth-positioner, with the elevation axis coincident with the polar axis ($\theta = 0°$) of the AUT's co-ordinate system. The azimuth drive thus generates cuts at constant ϕ. The fixed antenna (reference antenna) was a broadband EMCO horn (type 3115) positioned at 4 m. The elevation positioner was rotated from $\theta = -180°$ to 180° with increments of 5° for the selected measurement. Two pattern cuts (i.e. $\phi = 0°$ and $\phi = 90°$) were taken at four selected operating frequencies covering the required bandwidth. The radiation patterns for the AUT at 1795, 1920, 2045 and 2445 MHz were measured and the corresponding results were verified and plotted against the predictions in Figure 3.22. The patterns of the AUT are quite similar to each other for the first three cases. Moreover, the x-z plane presents a nearly omni-directional radiation pattern in the three lower frequency bands, whereas at 2445 MHz it tends to radiate at the +z direction in both planes. In this case, the ground plane acts as a good reflector in this band.

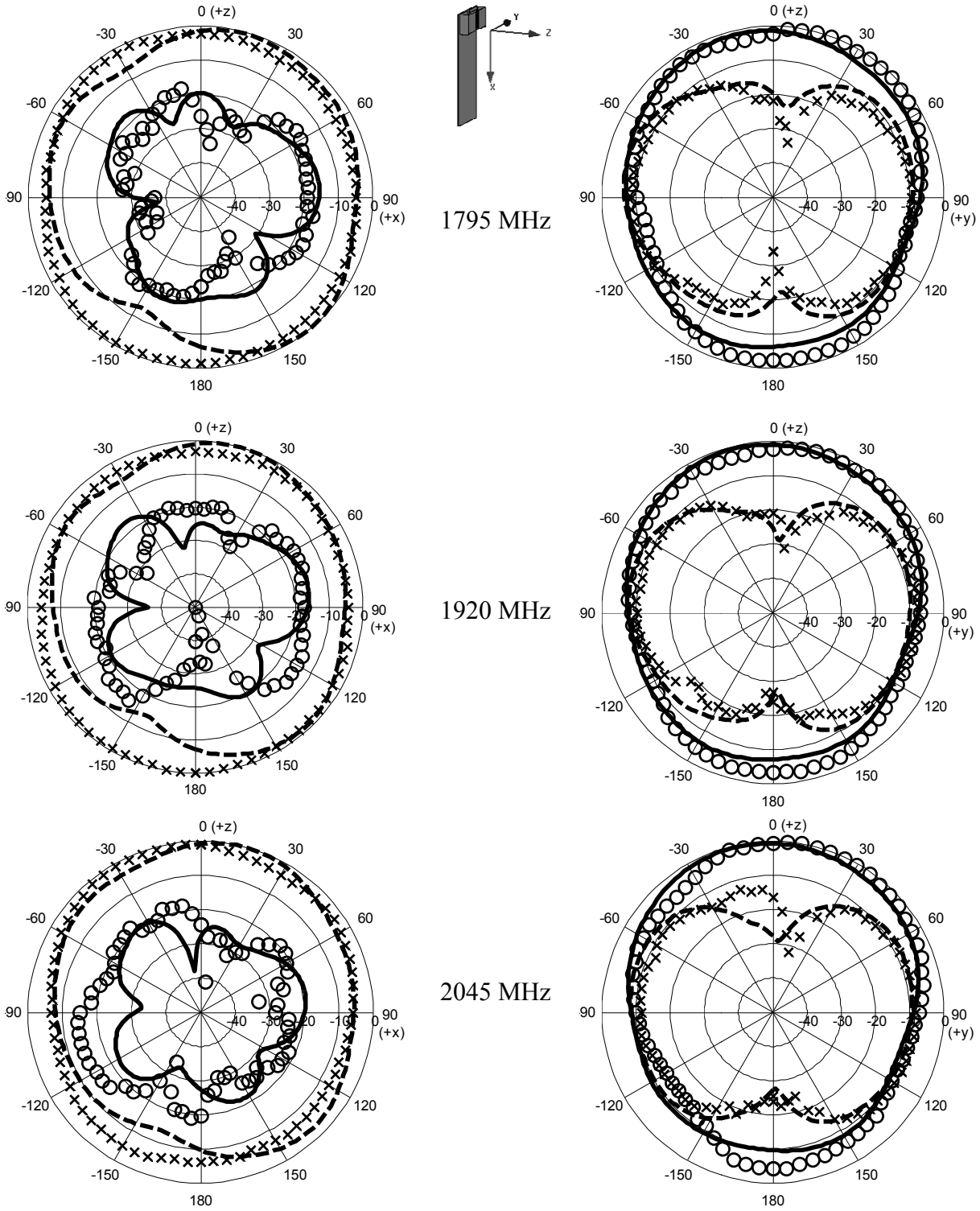

Figure 3.21: Radiation patterns of the antenna at 1795, 1920, 2045 and 2445 MHz in (a) the x-z plane and (b) the y-z plane. 'ooo' measured E_θ '——' simulated E_θ 'xxx' measured E_ϕ '----' simulated E_ϕ

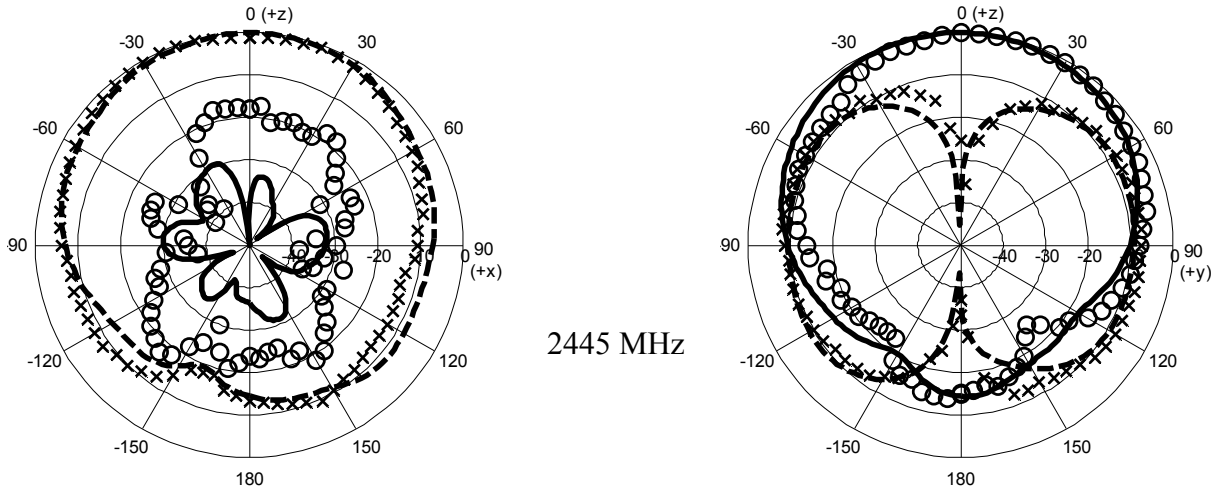

(a) (b)

Figure 3.22: Radiation patterns of the antenna at 1795, 1920, 2045 and 2445 MHz in (a) the x-z plane and (b) the y-z plane. 'ooo' measured E_θ '——' simulated E_θ 'xxx' measured E_ϕ '----' simulated E_ϕ

Figure 3.23 illustrates the calculated and measured antenna gain in the broadside direction for the frequencies across the GSM 1800, GSM 1900, UMTS and 2.45-GHz bands. It should be noted that the simulated gain curve assumes an ideal feed network, whereas the measured results include the insertion loss of the feed network, hence the local discrepancies. The measured antenna gain varied between 3.8 dBi and 5 dBi over the entire bandwidth. This variation is believed to be caused through the introduction the balun, and the connections between the antenna and the balun. On average, it can be said that the measurements are comparable with the prediction.

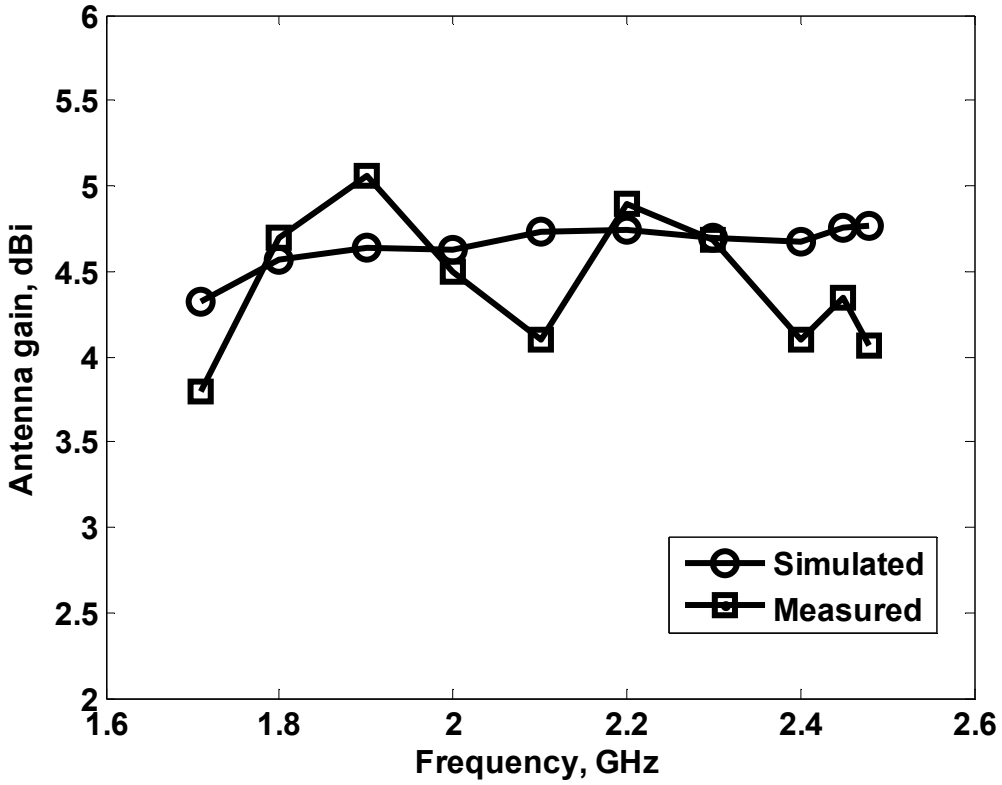

Figure 3.23: Comparison of simulated and measured antenna gain of the proposed antenna.

3.7 Conclusions

The main subject of this chapter has been a new wideband folded dipole antenna design, operating over the GSM 1800/1900 and UMTS service bands. The dipole is fed by a planar wideband balun network. The design was successfully expanded to include the 2.45 GHz WLAN band. The antenna impedance was determined using the two methods described in the previous Chapter, and the balanced operation of the antenna was verified. Comparison of the return loss and far field radiation pattern showed good agreement between the prototype assembly and the simulation models. These results indicate that the ground plane had a minimal effect on the operating characteristics with the user, in particular these characteristics seem to be independent of the length of the

ground plane. Therefore, it is reasonable to conclude that the user-handset interaction has been minimised, and that the antenna may be seen as a possible candidate for use in mobile handsets.

3.8 References

[1] Z. Li and Y. Rahmat-Sammii, "Optimization of PIFA-IFA combination in handset antenna designs," *IEEE Trans. On Antennas and Propagation,*, vol. 53, pp. 1770-1778, May 2005.

[2] Y.-S. Wang, M.-C. Lee, and S.-J. Chung, "Two PIFA-related miniaturized dual-band antennas," *IEEE Trans. on Antennas and Propagation*, vol. 55, pp. 805-811, March 2007.

[3] J. Janapsatya, K. P. Esselle, and T. S. Bird, "A dual-band and wideband planar inverted-F antenna for WLAN applications," *Microwave and Optical Technology Letters*, vol. 50, pp. 138-141, January 2008.

[4] S.-Y. Lin, "Multiband Folded Planar Monopole Antenna for Mobile Handset," *IEEE Trans. Antennas and Propagation*, vol. 52, pp. 1790-1794, July 2004.

[5] M.-C. Huynh and W. Stutzman, "Ground plane effects on planar inverted-F antenna (PIFA) performance," *IEE Proc.-Microw. Antennas Propag.,*, vol. 150, pp. 209-213, August 2003.

[6] H. Morishita, H. Furuuchi, and K. Fujimoto, "Performance of balance-fed antenna system for handsets in the vicinity off a human head or hand," *IEE Proceeding Microwave Antennas Propagation*, vol. 149, pp. 85-91, 2002.

[7] R. A. Abd-Alhameed, P. S. Excell, R. A. K. Khalil, and J. Mustafa, "SAR and radiation performance of balanced and unbalanced mobile antennas using a hybrid computational electromagnetics formulation," *IEE Proceedings-Science, Measurement and Technology special issue on Computational Electromagnetics*, vol. 151, pp. 440-444, 2004.

[8] C. N. Chiu and H. R. Chen, "A New Compact Balance-Fed T-Monopole Antenna for UMTS Mobile Applications," *Microwave and Optical Technology Letters* vol. 49, pp. 1904-1907, 2007.

[9] H. Morishita, H. Furuuchi, and K. Fujimoto, "Balance-fed L-type loop antenna system for handset," *IEEE Vehicular Technology Conference*, vol. 3, pp. 1346-1350, 1999.

[10] H. Morishita, Y. Kim, H. Furuuchi, K. Sugita, Z. Tanaka, and K. Fujimoto, "Small balance-fed helical dipole antenna system for handset," *IEEE Vehicular Technology Conference Proceedings VTC* vol. 2, pp. 1377 - 1380 2000.

[11] Y. X. Guo, Y. F. Ruan, Z. Y. Zhang, L. C. Ong, and X. Q. Shi, "New Balanced UWB Planar Antenna," *Microwave And Optical Technology Letters* vol. 49, pp. 114-118, 2007.

[12] D. Sasaki and e. al, "A Planar Folded Dipole Antenna for Mobile Handset," *IEEE International Workshop on Antenna Technology* pp. 133-136, March 2005.

[13] C.-N. Chiu and W.-C. Hsu, "A Balanced T-Shaped Antenna for 3G Imt2000 Mobile Handsets for WLAN," *Microwave and Optical Technology Letters* vol. 48, pp. 131-133, January 2006.

[14] U. Navsariwaln and J. Svigetj, "A reduced sized balanced antenna for 2.4 GHz WLAN," *IEEE Antennas and Propagation Society International Symposium*, vol. 2, pp. 6 - 9 2003

[15] Hisashi Morishita, Syogo Hayashida, Jun Ito, and K. Fujimoto, "Analysis of Built-in Antennas for Handset Using Human (Head, Hand, and Finger) Model," *Electronics and Communications in Japan*, vol. 86, pp. 35–45, 2003.

[16] B. S. Collins, S. P. Kingsley, J. M. Ide, S. A. Saario, R. W. Schlub, and S. G. O'Keefe, "A Multi-Band Hybrid Balanced Antenna," *IEEE International Workshop, Antenna Technology Small Antennas and Novel Metamaterials*, pp. 100-103, 2006

[17] H. Morishita, H. Furuuchi, Z. T. H. Ide, and K. Fujimoto, "A balance-fed loop antenna system for handset," *IEICE Trans. Fundamentals*, vol. E82-A, pp. 1138-1143, 1999.

[18] J. J. Arenas, J. Anguera, and C. Puente, "Balanced and single-ended handset antennas: free space and human loading comparison," *Microwave And Optical Technology Letters*, vol. 51, pp. 2248-2254, September 2009.

[19] K. Ogawa, H. Iwai, and Y. Koyanagi, "Balance-fed planar built-in antenna," *IEEE, Electronics Letters*, vol. 37, pp. 476 - 478, 2001.

[20] "High Frequency Structure Simulator, Version 11, Ansoft Corporation, USA.."

[21] M. J. Ammann and Z. N. Chen, "Wideband Monopole Antennas for Multi-Band Wireless Systems," *IEEE Antennas and Propagation Magazine*, vol. 45, pp. 146-150, 2003.

[22] D. Valderas, J. Legarda, I. Gutierrez, and J. I. Sancho, "Design of UWB folded-plate monopole antennas based on TLM," *IEEE Transactions on Antennas and Propagation*, vol. 54, pp. 1676-1687, June 2006.

[23] M. J. Ammann, "Control of the impedance bandwidth of wideband planar monopole antennas using a bevelling technique," *Microwave and Optical Technology Letters* vol. 30, pp. 229–232, August 2001.

[24] T. Tanaka, S. Hayashida, H. Morishita, Y. Koyanag, and K. Fujimoto, "Built-in Folded Dipole Antenna for Handset," vol. 1, pp. 451-454, Jun, 2003.

[25] S. Hayashida, T. Tanaka, H. Morishita, Y. Koyanagi, and K. Fujimoto, "Built-in half size of folded dipole antenna for handsets," *IEEE Antennas and Propagation Society International Symposium*, vol. 3 pp. 2759- 2762, 2004.

[26] H. Morishita, Y. Kim, Y. Koyanagi, and K. Fujimoto, "A folded loop antenna system for handsets," *IEEE Antennas and Propagation Society International Symposium*, vol. 3, pp. 440-443, 2001.

[27] Y. Kim, H. Morishita, Y. Koyanagi, and K. Fujimoto, "A folded loop antenna system for handsets developed and based on the advanced design concept," *IEICE Trans. Commun.*, vol. E84-B, pp. 2468-2475, September 2001.

[28] Y. Tikhov, Y. J. Kim, and Y. H. Min, "Compact low cost antenna for passive RFID transponder," *IEEE Antennas and Propagation Society International Symposium*, pp. 1015-1018, 2006.

[29] S. Tanaka, S. Hayashida, H. Morishita, and Y. Atsumi, "Wideband and Compact Folded Loop Antenna," *IEEE Electronics Letters*, vol. 41, pp. 945 - 946 2005.

[30] Z. Y. Zhang, Y. X. Guo, L. C. Ong, and M. Y. W. Chia, "A New Wide-band Planar Balun on a Single-Layer PCB," *IEEE Microwave and wireless components letters*, vol. 15, pp. 416-418, June 2005.

[31] "Agilent Technologies, Advanced Design System, ADS2005A.."

[32] K. Tilley, X.-D. Wu, and K. Chang, "Coplanar waveguide fed coplanar strip dipole antenna," *Electronics Letters*, vol. 30, pp. 176 - 177, Feb 1994.

[33] J. Toftgard, S. N. Hornsleth, and J. B. Andersen, "Effects on portable antennas of the presence of a person," IEEE Transactions on Antennas and Propagation, vol. 41, pp. 739 - 746, 1993.

[34] H. Morishita, H. Furuuchi, and K. Fujimoto, "Performance of balance-fed antenna system for handsets in the vicinity off a human head or hand," IEE Proceeding Microwave Antennas Propagation, vol. 149, pp. 85-91, 2002.

[35] S.-W. Su, K.-L. Wong, and C.-L. Tang, "Ultra-wideband Square Planar Monopole Antenna for IEEE 802.16a Operation in the 2-11-GHz Band," Microwave and Optical Technology Letters, vol. 42, pp. 463-466, 20 September 2004.

CHAPTER FOUR

SAR Measurement for Compact Wideband Balanced Antenna for Mobile Handsets

4.1 Introduction

Progress toward worldwide wireless communication continues at a remarkable pace, and the antenna element of the technology is crucial to its success. Trends in system evolution indicate the gap between cellular and WLAN technologies is narrowing, and developments in Software Defined Radio (SDR) point strongly to the need for new antenna designs to permit user terminals to access several different radio resources at different frequencies according to the service requirements. Also, as radio connected services become increasingly commonplace, the possible implications of user exposure to emissions from hand-held terminals are causing increasing concern. Therefore, in addition to the traditional design objectives of small size and low cost it is now essential to address the need for (a) wide, or multi-band operation, (b) compliance with international safety guidelines on Specific Absorption Rate (SAR) [1, 2] and (c) weak coupling of the antenna with the handset case in order to achieve a good impedance match that is stable in the presence of a human body.

As mentioned previously, balanced antennas may be used to reduce the coupling of the mobile antenna to the handset. This contrasts with unbalanced antennas, which drive current into the handset chassis. These induced currents can interact unfavourably with the complex characteristics of the body [3-5]. The maximum SAR values have been shown to be substantially reduced when placed next to the human head, compared with conventional unbalanced antennas, if these antennas are well-designed [6,7]. For example in [8], it was demonstrated the corresponding computed peak SAR values for the balanced antenna were 0.17674 (W/kg) and 0.64243 (W/kg) for balanced and unbalanced respectively. In addition the computations indicate that approximately 20% to 25% (balanced) and between 26% and 41% (unbalanced) of the total delivered power was absorbed by the head.

In this chapter, the design of a compact balanced folded dipole antenna, with a novel dual-arm structure, is introduced. A multi-band design is considered from the start, with the following service bands: DCS, PCS, UMTS and WLAN (2.4 GHz). The broadband balun circuit used in the previous chapter is adopted in the realization of this design. The simulation model was build using a commercial EM solver based on the finite integration technique [9]. The mutual effect of the proposed antenna system in the presence of a human hand phantom is also addressed, and the SAR performance is evaluated by experiment. Finally, the calculated and measured results for the constructed prototype are presented and discussed.

4.2 Antenna Design Theory and Structure

The basic design concept is optimised and developed using the design procedure established in the previous chapter as the starting point. The technique for optimising

the impedance bandwidth by symmetrically trimming a triangle at the monopole edge close to the feed point, to give a tapered feed, was used. In addition, a slot is introduced into each of the arms of the planar dipole. This mitigates the effect of the ground plane, and helps to maintain a good antenna performance.

The computer modelling was used for this design. Greater refinement is required in the mechanical realisation for a more efficient, and compact, layout for the antenna assembly. This is needed to meet the expanded multi-band requirements in the electrical specification. The modelling was used to gain a better understanding of the compromise between the antenna volume and the mutual interaction with the ground plane. In contrast with the design in Ch. 3, where the slot on each arm of the folded dipole antenna is removed, this design uses a relatively thin metal strip. The technique for introducing multiple resonances to the folded dipole structure was refined further for this design. The discussion concludes with the impedance bandwidth required to enable multiple-band operation.

Firstly, a single arm balanced folded dipole antenna was developed for operation around 2 GHz. Tapering was introduced at the edge near the feed point. To achieve a more compact design, the top end of the folded arm was extended and bent downwards (see parameter ‘h1’ in Figure 4.1) to satisfy the required length for each arm to generate and locate the target resonances. Subsequently, an additional thin-strip arm was introduced and inserted in each arm of the planar dipole to generate the additional resonance around 2.4 GHz as shown in Figure 4.1. Using this technique, the singly resonant antenna was modified and developed as a wideband dual-resonant variant for multi-band operation.

The lateral length of the tapered feed, and its location on the antenna, together with the length and location of the additional arm, and other parameters of the proposed antenna, was adjusted and a further optimisation process was carried out to ensure that the design entirely covered the required frequency bands (1.710 - 2.485 GHz) at VSWR ≤ 3.

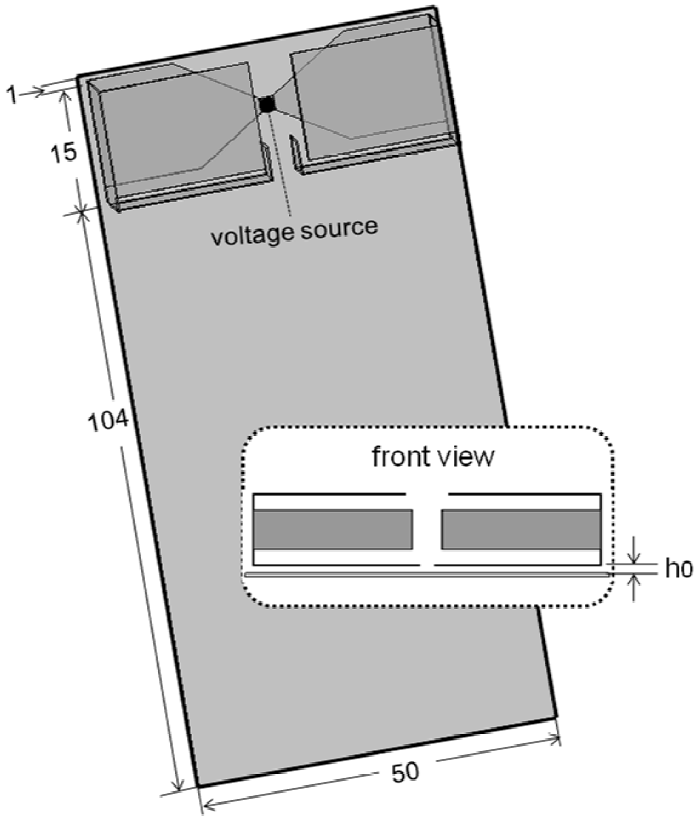

(a)

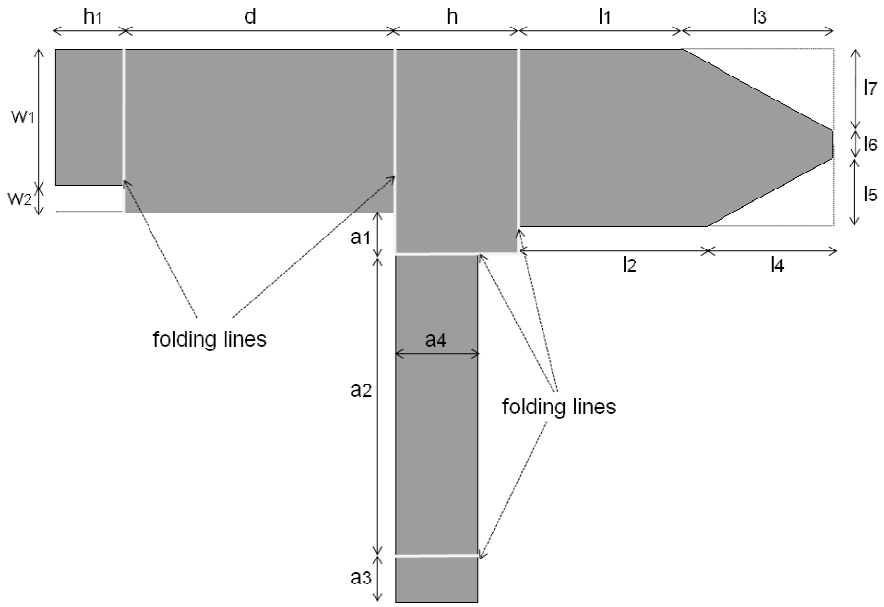

(b)

Figure 4.1: Antenna configuration studied. (a) Balanced antenna with conducting plate; (b) important parameters of the proposed antenna.

Figure 4.2: Photograph of prototype of the proposed balanced antenna design.

4.3 Measuring Input Impedance of Balanced Antenna

The volume constraint for this radiator assembly was 48 (l) × 15 (w) × 9 (h) mm^3, which includes a 2 mm gap source for the feed. The simulation model was developed according to these constraints, resulting in 'first cut' dimensions shown in Table 4.1 for the prototype. This is achieved through systematically evaluating the consequences of optimising a number of antenna parameters and carefully monitoring the impact of such

changes, these include (d, w_1, h, h_1, a_3, a_4). The impact of making changes to the antenna is monitored and verified through using the software modelling tool to ensure accuracy and verification of the results.

A prototype balanced dipole and ground plane assembly was cut from copper sheets of thickness 0.35 mm and 0.5 mm, respectively (Figure 4.2).

Table 4.1: The parameters of the antenna

Parameter	Value / mm
d	20
w_1	10
w_2	2
h	9
h_1	5
h_0	1
l_1	12
l_2	14
l_3	11
l_4	9
l_5	5
l_6	2
l_7	6
a_1	3
a_2	22
a_3	3.5
a_4	6

Figure 4.3 presents the measured return loss of the prototype antenna against the computed one. There is a reasonable level of agreement between the calculated and measured return losses. It should be noted that the two impedance measurement methods presented in chapter two were used here. The first was observed at the input ports of the balanced antenna using the S-Parameter method in which the antenna is considered as a two-port device. The second impedance was considered at the input port of the balun.

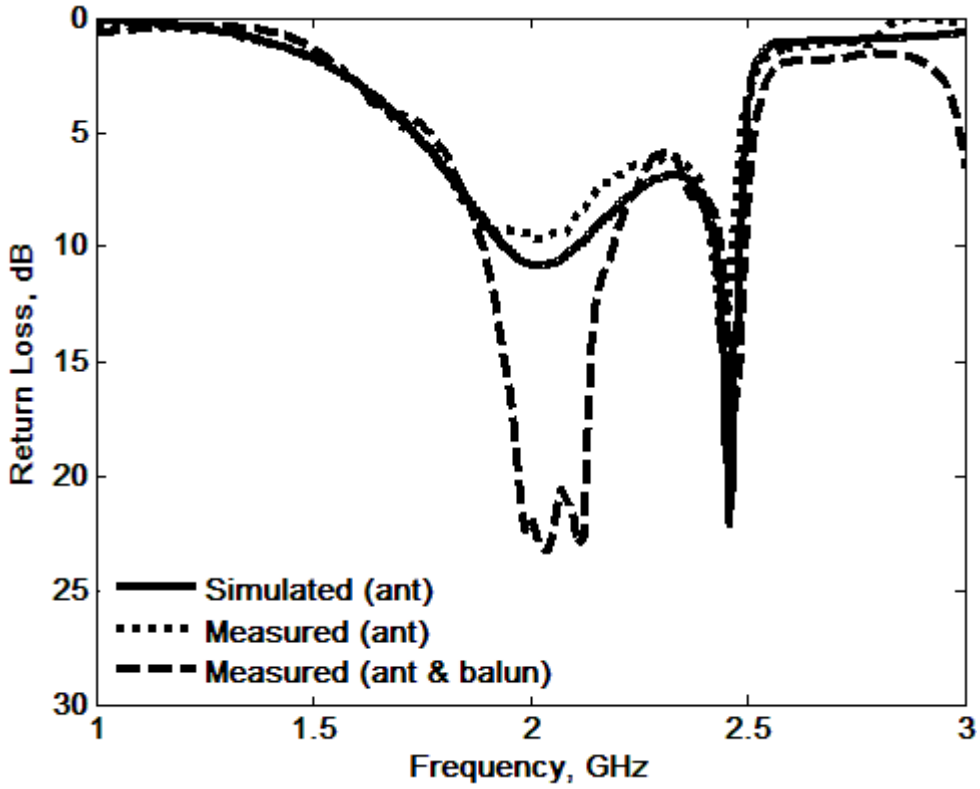

Figure 4.3: The simulated and measured return loss versus the operating frequency.

4.4 Analysis Stability Performance for the Antenna and Hand Model

The mutual effect between the antenna and the human hand model was investigated in order to evaluate its impact on the proposed design. The hand was modelled as a lossy dielectric with an equivalent conductivity of 1.45 S m-1 and a permittivity of 54, for a reference frequency of 2 GHz. In addition, the dimensions and position of the hand model are illustrated in Figure 4.4 and listed as follows: g_1 = 8.5, h_h = 80, h_1 = 39.5, h_w = 30 and m_1 = 24 (all dimensions in mm). The gap between the hand model and the metallic ground plate is 4 mm.

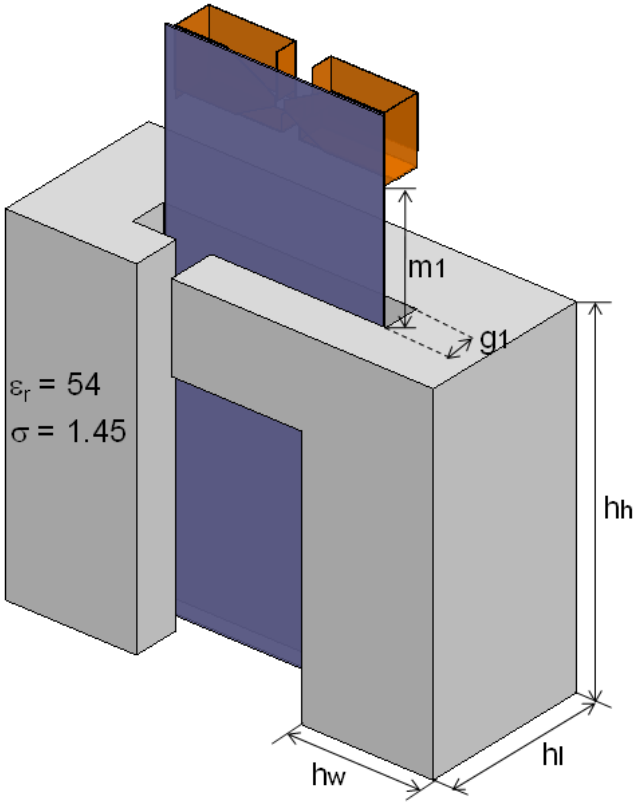

Figure 4.4: Hand phantom model with the proposed design.

The antenna performance in presence of human hand model was characterised in terms of the antenna return loss and radiation patterns.

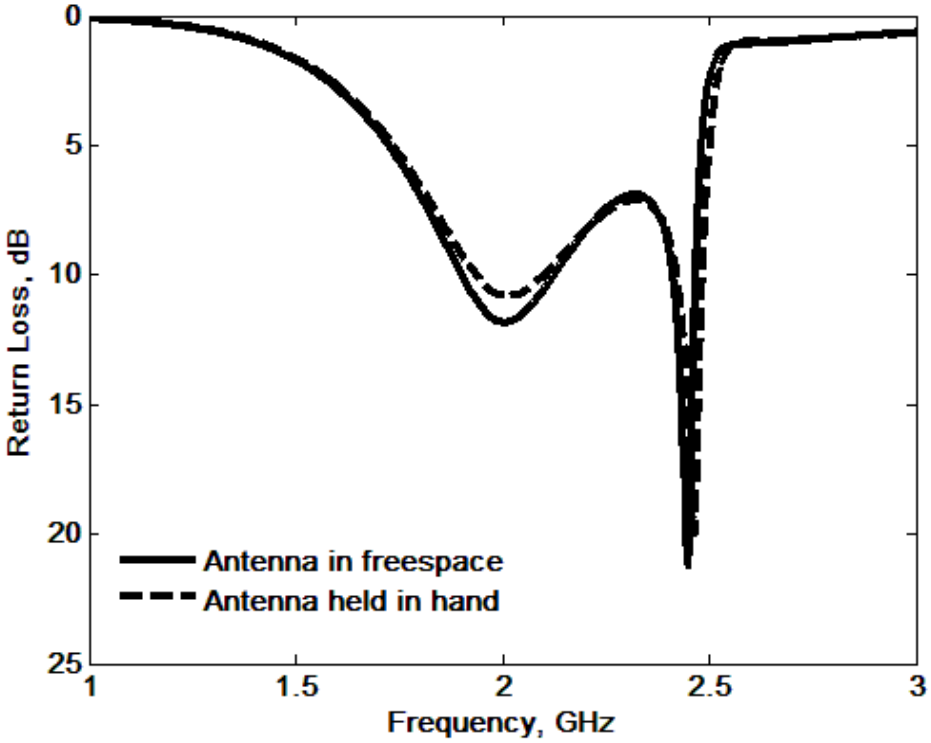

Figure 4.5: Comparison of antenna return loss in free space and in presence of hand model.

Figure 4.5 shows the antenna return loss with and without hand model, with the hand model m_1 was chosen to be 50 mm in the analysis. As can be seen, the resulting two plots have almost identical variations. The results indicate the proposed design features have low sensitivity for impedance de-tuning when the phone is held, and a reduced dependence of the antenna on the ground plane. The effects on various positions of the hand (i.e. m_1) were also studied. The distance between the antenna and the hand (i.e. parameter 'm_1') was varied from 30 mm to 60 mm in increments of 10 mm. The corresponding return loss results are presented in Figure 4.6.

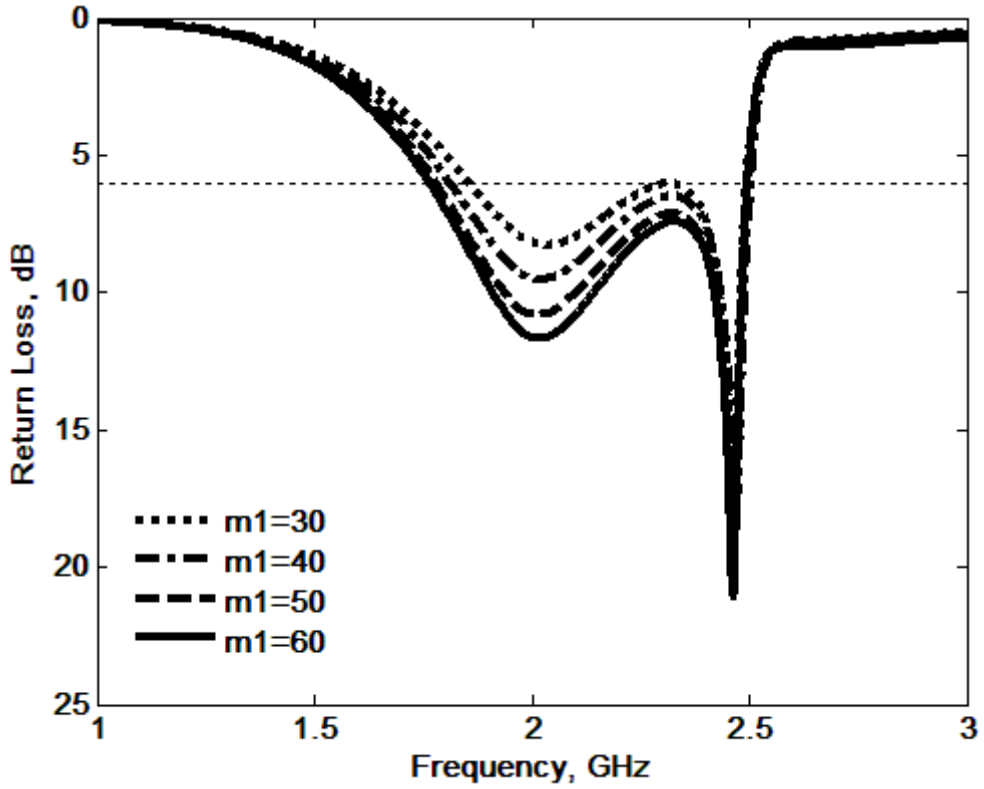

Figure 4.6: The parametric study on parameters *m1* against operating frequency.

As can be seen there is little variation of the calculated return loss observed for the varied cases. These results agree well with [10, 11] in which they show negligible induced surface currents on the handsets expect underneath the antenna. Similarly, the radiation patterns were examined for the case m_1 = 30 mm. The calculated patterns of the proposed antenna, with and without the hand model, at frequencies of 2 GHz and 2.45 GHz were presented in Figure 4.7 and Figure 4.8. The results found to vary by no more than 2 dB at the maximum when the hand model is included, which suggests that this antenna induced very little current into the ground plane.

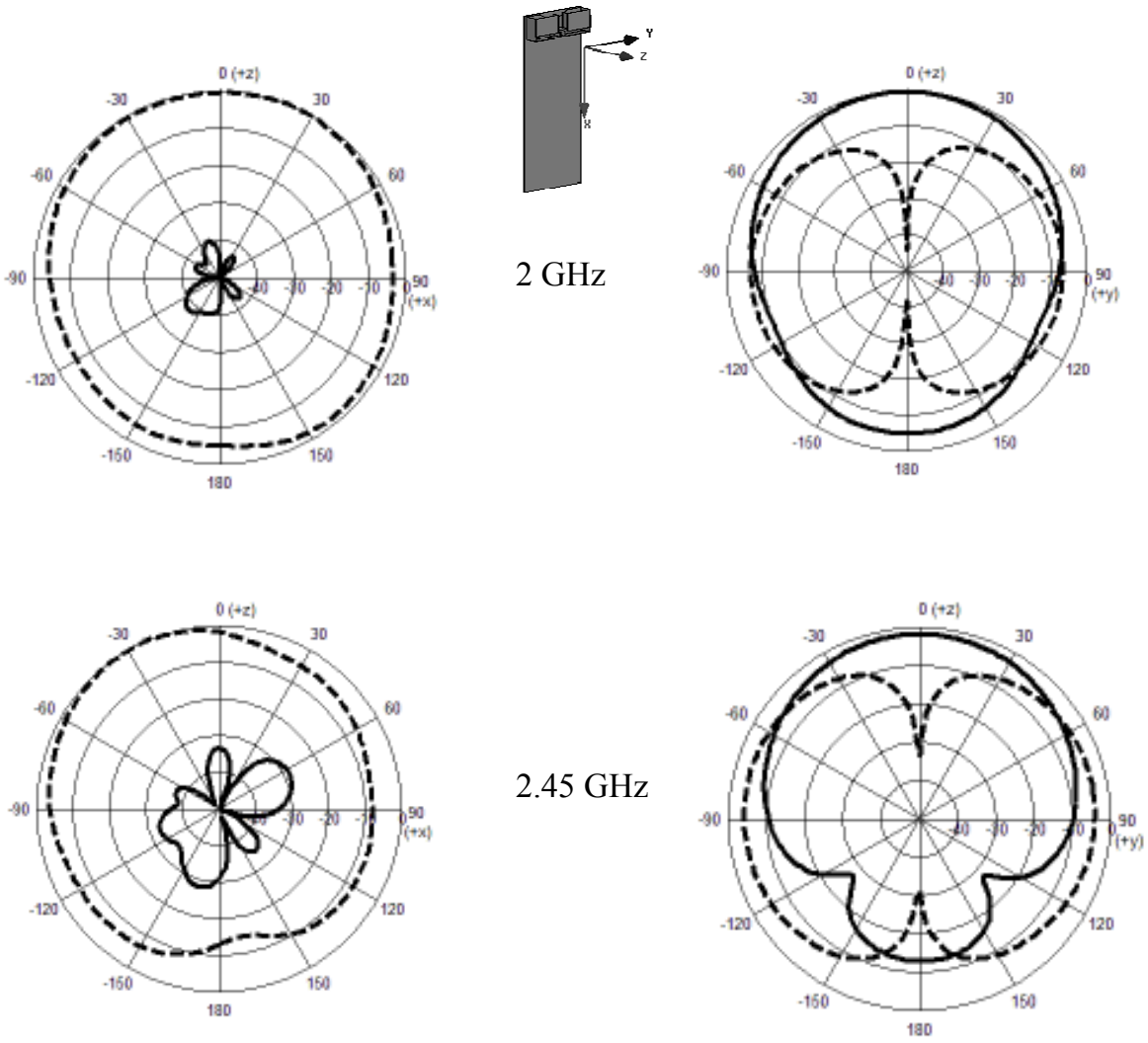

Figure 4.7: Comparison of radiation patterns in free space at 2 GHz and 2.45 GHz. '——' calculated E_θ, '----' calculated E_ϕ.

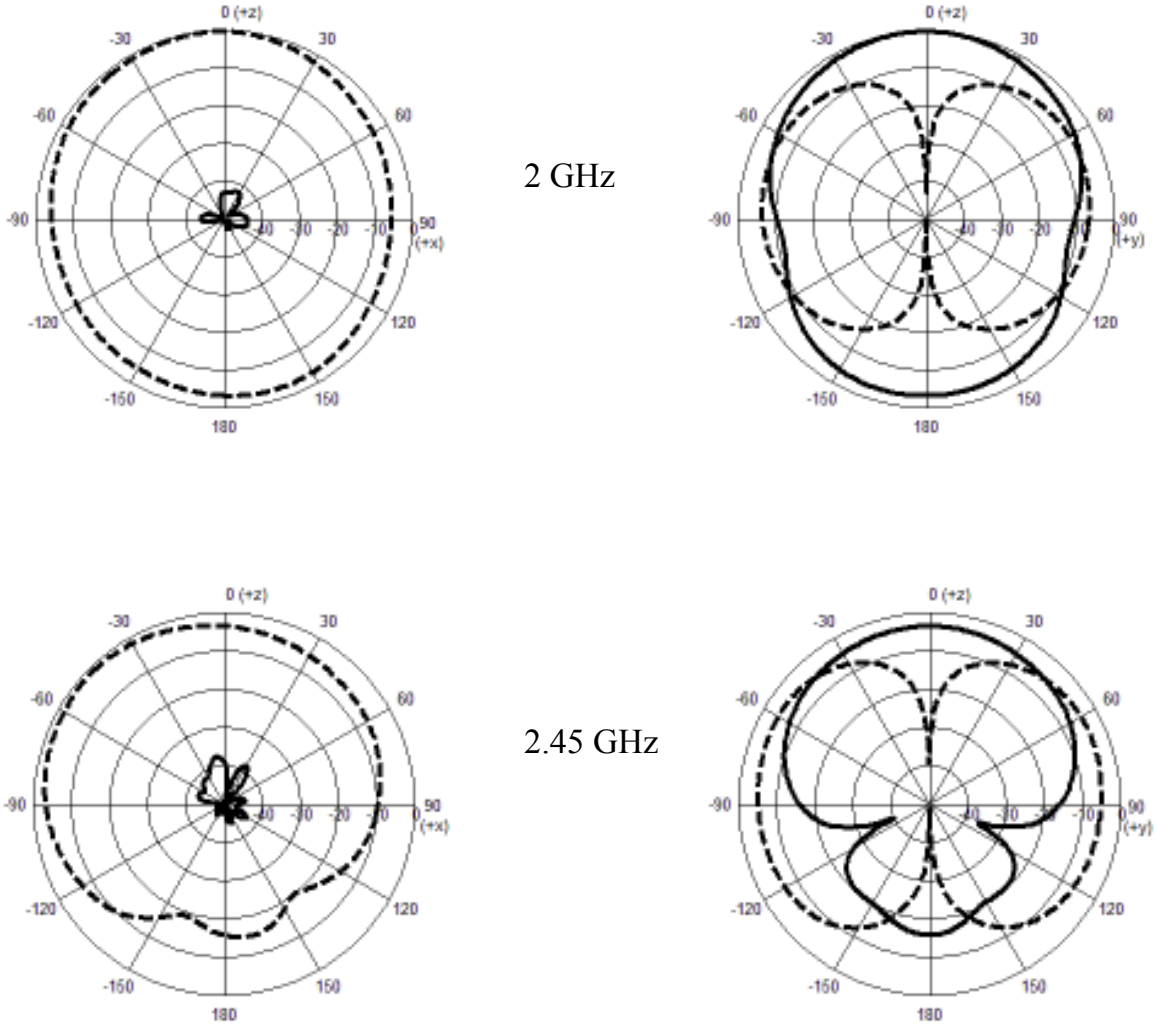

Figure 4.8: Comparison of radiation patterns in presence of hand model at 2 GHz and 2.45 GHz. '——' calculated E_θ, '----' calculated E_ϕ.

4.5 Near Field Measurement

The experimental SAR measurement for the antenna was carried out in an anechoic chamber using the equipment illustrated in Figure 4.9, which includes a cubic phantom model and computer controlled 3-D stepper motor to position the probe. The head model was considered as a single homogenous layer, which is good enough compared to a multi-layered spherical head [12].

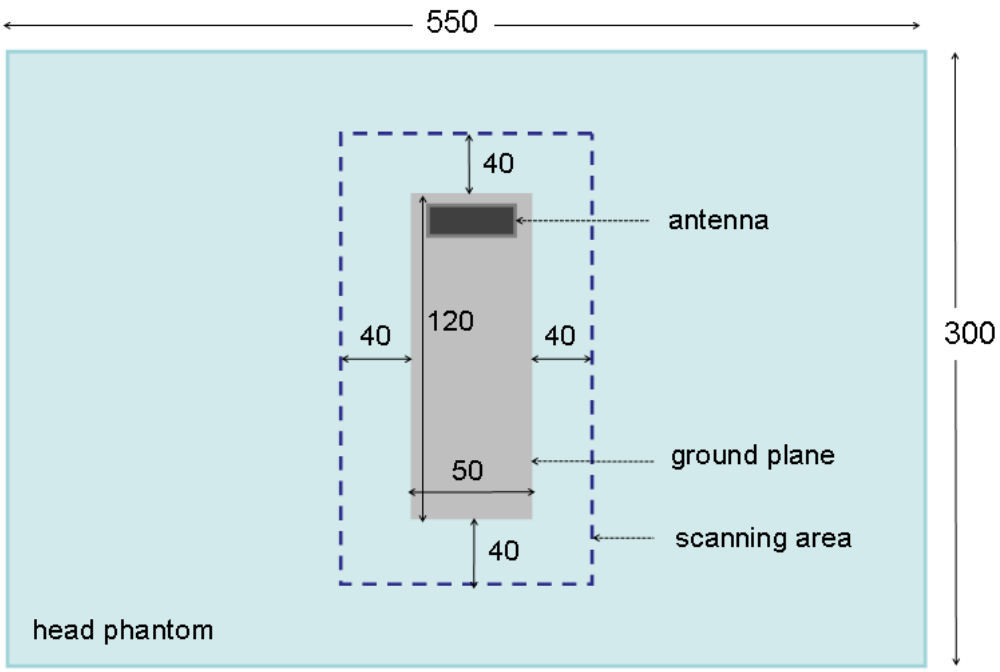

(a)

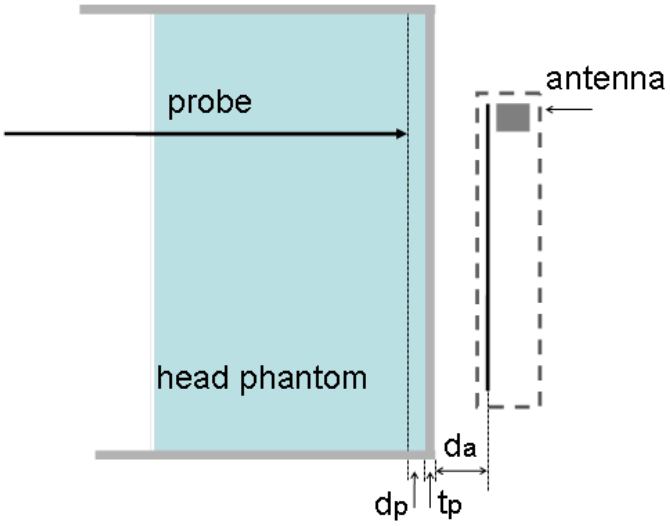

(b)

Figure 4.9: Diagram of near field measurement set-up for the proposed antenna (a) bottom view; (b) side view.

A simple phantom was constructed from plastic of thickness 5 mm (t_p), and dimensions 550 mm (L) × 300 mm (W). The phantom was filled with 5 litres of lossy tissue analogue, representing the brain matter. This material was modelled as a lossy dielectric

with conductivity 1.3 Sm-1 and $\varepsilon_r = 41.8$, for a reference frequency of 1.8 GHz. The fluid composition was 54.90% de-ionised water, 44.92% (2-Butoxyethoxy) ethanol or diethylene glycol monobutyl ether and 0.18% NaCl salt, as set out in IEEE-1520-200x for the frequency band 1800 MHz – 1900 MHz [13, 14]. The top surface is left open, allowing a non perturbing electric field probe to be inserted and held in position for the measurement; repeatability is ensured by use of a stepper motor, the measurement tolerance being ± 5 mm. A commercial Schmid Associates (SPEAG) electric field probe and near field measurement system was used for the measurement [15]. The normalized measured, and simulated, SAR values are shown in Figure 4.10. The probe and antenna distances shown in Figure 4.9 were 2 mm (d_p) and 3 mm (d_a) respectively.

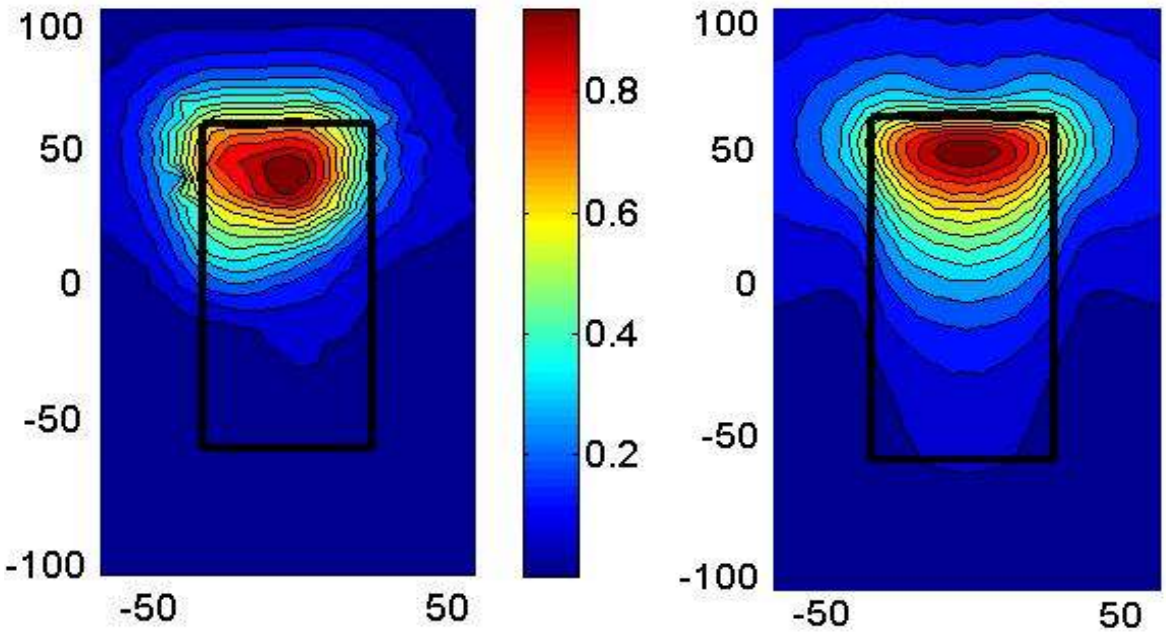

(a) (b)

Figure 4.10: The normalized SAR distribution at 1.8 GHz; (a) measured SAR, (b) computed SAR.

A reasonable agreement in SAR distribution between the measured and computed results can be noted from Figure 4.10. The maximum unaveraged measured and

computed SAR values for one watt of input power are 3.2 W kg-1 and 3.02 W kg-1 respectively. These results are much lower than those reported in [14] for a GSM 1800 terrestrial handset, for which the peak SAR in the head was between 10 and 21 W kg-1 for a head-handset separation of 7.5 mm.

4.6 Antenna Radiation Pattern

The radiation pattern measurements of the prototype were carried out in a far-field anechoic chamber. Two pattern cuts were taken for four selected operating frequencies covering the designated bandwidth. The radiation patterns in the zx plane and zy plane were measured for 1.795, 1.920, 2.045 and 2.445 GHz, respectively. These results are presented in Figure 4.11. These patterns seem to be quite similar to one another. The pattern similarities for the first three selected frequencies (i.e., 1.795, 1.920 and 2.045) were quite reasonable. In addition, the zx plane presents a nearly omni-directional radiation pattern in all three intended frequency bands; whereas, the proposed antenna at 2.445 GHz tends to radiate at the -x direction in the zx plane cut and at the +z direction in the zy plane cut, in which the ground plane for this band acts as a good reflector.

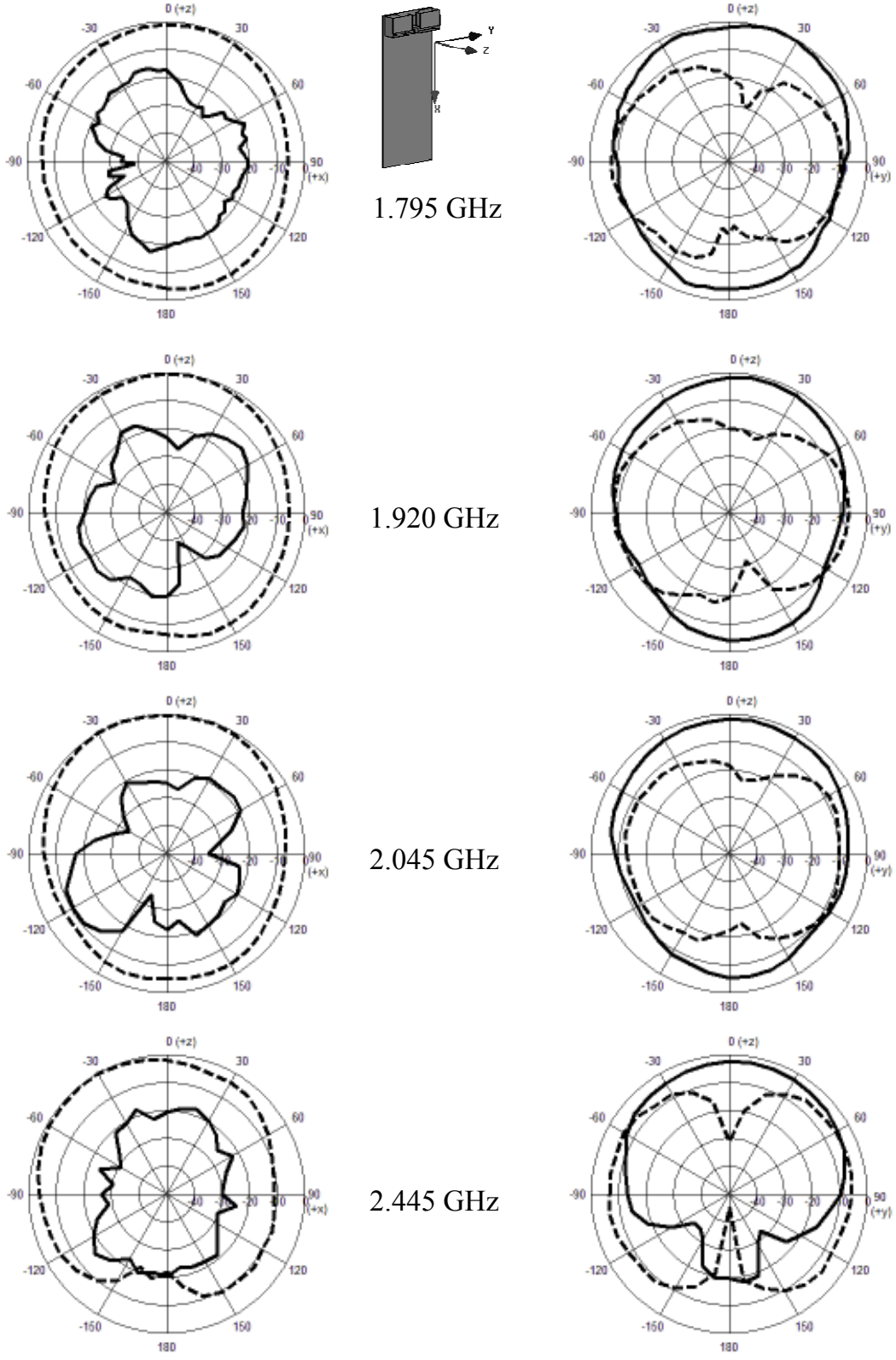

Figure 4.11: Measured radiation patterns for the proposed antenna at 1.795 GHz, 1.920 GHz, 2.045 GHz and 2.445 GHz at : (left) xz plane; (right) yz plane, where '——' measured E_θ and '- - -' measured E_ϕ.

4.7 The Power Gain and Efficiency of the Antenna

Table 4.2 shows the measured broadside antenna power gain for the frequencies across the DCS, PCS, UMTS and 2.4-GHz WLAN bands. It should be noted that the insertion loss of the feeding network was subsequently compensated for each measured power gain over all the bands. As observed, the measured antenna gain varied between 2.7 dBi and 5.4 dBi over the entire bandwidth considered. In addition, the gain value of this antenna is quit comparable with the gain values of the antenna in previous chapter.

Table 4.2: Measured antenna gain of the proposed design.

Frequency (GHz)	Antenna gain (dBi)
1.75	2.7
1.80	3.2
1.85	3.6
1.90	4.3
1.95	4.2
2.00	4.2
2.04	4.3
2.10	4.2
2.15	5.4
2.40	3.2
2.44	3.6
2.48	4.1

The radiation efficiency is an important measure of antenna performance, but is often over looked as it is difficult to measure with precision. A convenient indoor radiometric method reported in [16] was used to obtain an efficiency value for this prototype; the measured results are given in Table 4.3. The antenna has very high efficiency over the

target frequency bands. These efficiency results may be seen as encouraging, and provide further support to the balanced antenna approach.

Table 4.3: Measured antenna efficiency of the proposed design.

Frequency (GHz)	1.75	1.80	1.845	1.90	1.95	2.01
Antenna Efficiency (%)	91.2	90.7	94.5	93.1	97.2	95.2

4.8 Conclusions

A new compact wideband balanced folded dipole antenna design, operating over the DCS, PCS, UMTS and 2.4-GHz WLAN bands, has been presented. The antenna design was characterized in terms of the return loss, radiation pattern, power gain and radiation efficiency. Comparison of return loss measurements showed good agreement with the computational predictions. The analysis of the design in the presence of a human hand model confirmed that the antenna induces little current into the ground plane. In addition, the antenna performance was stable since the interaction between the antenna and the hand is minimized. The specific absorption rate (SAR) performance of the antenna is also studied experimentally by measuring near field exposure. The measured results have shown low induced current in the ground plane and thus confirm minimisation of performance variations and SAR. The antenna efficiency has been measured using a radiometric technique. The results provided further supporting evidence for the balanced technique. However, the current design has some practical limitations since it does not cover the GSM 900 frequency band, which remains in

demand or in the 5 GHz band for WLAN, which is often required in new mobile handsets. Looking to the future, further development of balanced antennas will be required for multi-band implementation.

4.9 References

[1] FCC, "Evaluating compliance with FCC guidelines for human exposure to radio frequency electromagnetic fields," Federal communication Commission, Washington, DC, OET Bulletin 65, Aug. 1997.

[2] "ICNIRP Guidelines, Guidelines for limiting exposure to time-varying electric, magnetic, and electromagnetic fields (up to 300 GHz)', Health Phys.," vol. 74, pp. 494-522, 1998.

[3] K. Ogawa, H. Iwai, and Y. Koyanagi, "Balance-fed planar built-in antenna," *IEEE, Electronics Letters*, vol. 37, pp. 476 - 478, 2001.

[4] S. Kingsley, "Advances in handset antenna design, ," *RF Design*, May 2005.

[5] B. S. Collins, S. P. Kingsley, J. M. Ide, S. A. Saario, R. W. Schlub, and S. G. O'Keefe, "A Multi-Band Hybrid Balanced Antenna," *IEEE International Workshop, Antenna Technology Small Antennas and Novel Metamaterials*, pp. 100-103, 2006

[6] R. A. Abd-Alhameed, P. S. Excell, R. A. K. Khalil, and J. Mustafa, "SAR and radiation performance of balanced and unbalanced mobile antennas using a hybrid computational electromagnetics formulation," *IEE Proceedings-Science, Measurement and Technology special issue on Computational Electromagnetics*, vol. 151, pp. 440-444, 2004.

[7] H. Morishita, H. Furuuchi, and K. Fujimoto, "Performance of balance-fed antenna system for handsets in the vicinity off a human head or hand," *IEE Proceeding Microwave Antennas Propagation*, vol. 149, pp. 85-91, 2002.

[8] R. Alias, "Hybrid Finite Element and Finite Difference-Time Domain Technique for Personal Mobile Handset Antenna Design," in Electronics and Telecommunication Engineering, vol. PhD. Bradford: University of Bradford, 2004.

[9] "Computer Simulation Technology Corporation, CST Microwave Studio, Version 5.0, Germany."

[10] Y. Kim, H. Morishita, Y. Koyanagi, and K. Fujimoto, "A folded loop antenna system for handsets developed and based on the advanced design concept," *IEICE Trans. Commun.*, vol. E84-B, pp. 2468-2475, September 2001.

[11] S. Hayashida, H. Morishita, and K. Fujimoto, "Self-balanced wideband folded loop antenna," *IEE Proceeding Microwave Antennas Propagation*, vol. 153, pp. 7-12, 2006.

[12] O. Kivekäs, J. Ollikainen, T. Lehtiniemi, and P. Vainikainen, "Bandwidth, SAR, and Efficiency of Internal Mobile Phone Antennas," *IEEE transactions on electromagnetic compatibility* vol. 46, pp. 71-86, 2004.

[13] J Mustafa, R. A. Abd-Alhameed, P. S. Excell, and N. J. McEwan, "SAR Reduction using phased antenna array mobile handset," *Applied Computational Electromagnetics Journal, Special Issue on Phased and Adaptive Array Antennas*, vol. 21, pp. 196-205, November 2006.

[14] J. Mustafa, "Mobile communication handset antennas with reduced user coupling: design of array and balanced antennas for 1.8 GHz personal communication handset to reduce specific absorption rate," vol. PhD thesis: Submitted to Bradford University, July 2005.

[15] "Schmid & Partner Engineering AG, Switzerland, http://www.speag.com/speag/index.php."

[16] N.J. McEwan, R. A. Abd-Alhameed, and M. N. Z. Abidin, "A modified radiometric method for measuring antenna radiation efficiency," *IEEE Transaction on antennas and propagation*, vol. 51, pp. 2099-2105, 2003.

CHAPTER FIVE

Dual-band and Multi-band Balanced Mobile Handset Antennas

5.1 Introduction

Many mobile handsets have design constraints on size and weight; this is driven by customer expectations, and the pervasive impact of location-aware services. From an antenna design perspective, these constraints may be summarised thus:

- to reduce the antenna size with unchanged, or improved, performance characteristics
- to continue to seek reductions in the degradation of antenna performance when in proximity with the operator's body [1].

It has been established that balanced antennas offer a genuine choice for the designer in mitigating the effects of the user on the antenna performance [2], since balanced currents only flow on the antenna element, thus dramatically reducing the effect of current flow on the ground plane. Hence, balanced antennas are generally efficient and, more importantly, maintain their performance when held or positioned adjacent to the human body [3].

Recently, several novel designs of such antenna types have been successfully developed and demonstrated [3-6], most of them being designed and implemented for operations in

the current 2G and 3G mobile service bands. However, not much work has been carried out for the potential frequency bands beyond the current frequency ranges, as expected future integration of mobile applications. Therefore, there is motivation to develop this balanced antenna technique for future mobile device applications.

Wireless local area network (WLAN) technology is a rapidly expanding area in the modern wireless communication. The trend of integrating WLAN communication system into the mobile electronic products leads to a great demand in developing dual-band or multi-band antennas with compact size [7, 8]. In this chapter, the design of a built-in multi-band balanced-dipole antenna is presented, and optimized for WLAN and WiMAX applications over the corresponding frequency bands. The study covers the full WLAN requirement, and the lower WiMAX service bands, via 2.4 GHz and 5.2 GHz WLAN bands and 2.5 and 3.5 WiMAX bands.

Some success in reducing the size of the antenna has been achieved by introducing a long slot into each folded arm of the dipole radiator. The performance of the proposed antennas have been analysed and optimised for the targeted frequency bands. For validation purposes, antennas prototypes were fabricated and tested. The prototypes performance are characterised in terms of the antenna reflection coefficient, radiation pattern, power gain and surface current distribution. The predicted and measured results show acceptable agreement, and the results also confirm good impedance bandwidth characteristics with excellent dual-band operation. In addition, a new design with wideband impedance bandwidth for the future mobile communication systems is introduced at the end of this chapter.

5.2 First Design (Multi-band Balanced Antenna for WLAN/WiMAX Operation in Handheld Devices)

The design concept established in the previous chapter is applied to a new multi-band antenna. The requirements specification is based on the full WLAN and lower WiMAX service bands for handset applications, additionally the design may also cover the 2.4 GHz remote control band (RF4CE – remote control using radio frequency for consumer applications). A working model was constructed using CST Microwave Studio [9], and performance guidelines for input return loss, power gain and radiation pattern were established.

5.2.1 Antenna Structure

The antenna design is fundamentally based on the realisation of a folded dipole structure. This is due to its symmetrical layout, and the fact that the structure easily lends itself to low profile packaging. The geometrical antenna model is shown in Figure 5.1, the radiator structure is mounted 1 mm above a rectangular conducting plate (40 mm × 100 mm) which may be regarded as the base or chassis of the device, and which acts as an effective ground plane. The positioning of the antenna is set with a spacing of 1 mm to all surrounding edges of the ground plane, making the total antenna length 38 mm (including 1 mm gap between the two arms for feeding purposes). The simulation model is effectively tuned in terms of three structure parameters: the height (h) of the folded dipole, the antenna width (w), and the length (d).

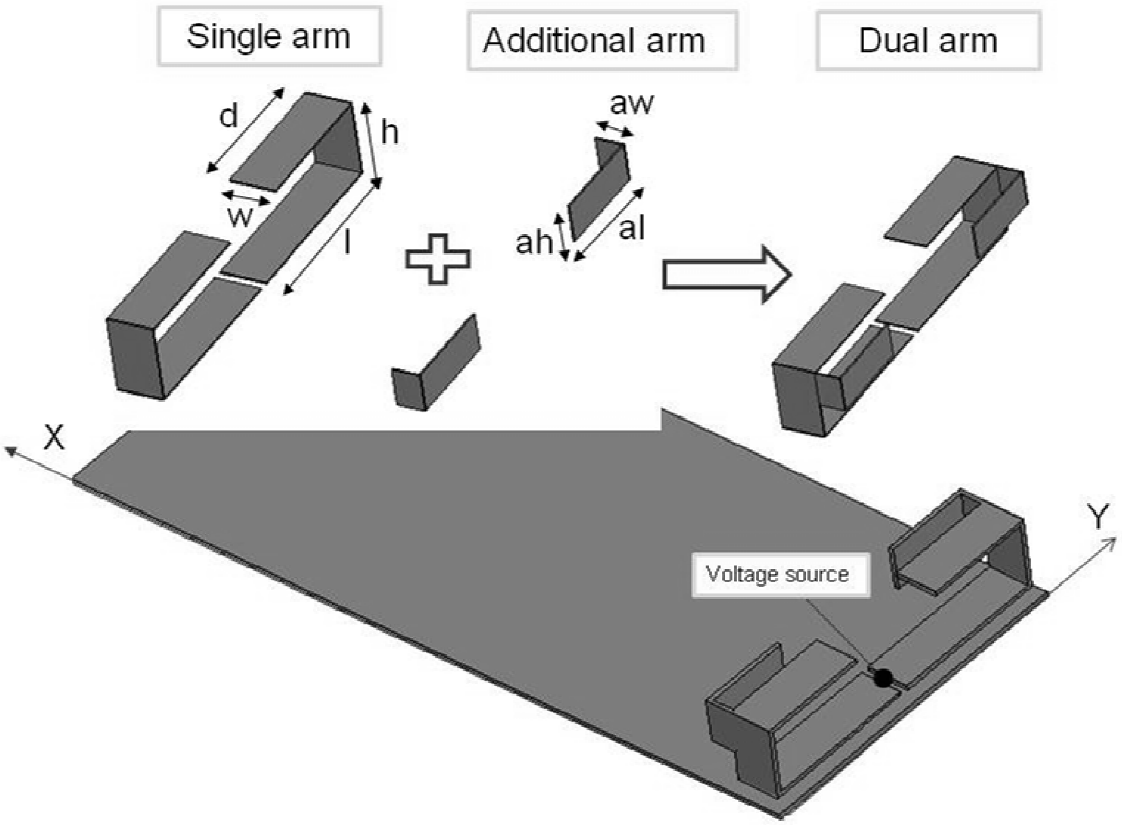

Figure 5.1: Balanced mobile antenna configuration studied.

5.2.2 Parametric Study of the Antenna

In order to fully understand the influence of these parameters on the impedance bandwidth, a parametric study was carried out by varying each parameter, while holding the remaining parameters at the assumed optimum values. The effect of varying h on the input return loss was studied, where the parameters *d* and *w* were set to be 15 mm and 5 mm, respectively. It was found that the variation of the folded antenna height influences the shifting of resonant frequency dramatically, as shown in Figure 5.2. Figure 5.3 illustrates the effect of varying the length of the folded arms, where *h* and *w* are 8 mm and 5 mm, respectively. The antenna resonant frequency is observed to rise as the parameter d decreases, which is as expected, since this is equivalent to decreasing the

total length of a simple dipole antenna. On the other hand, the width of the arms (w) principally affects the broadband impedance matching as it is varied (where h = 8 mm and d = 14.5 mm), this is shown in Figure 5.4.

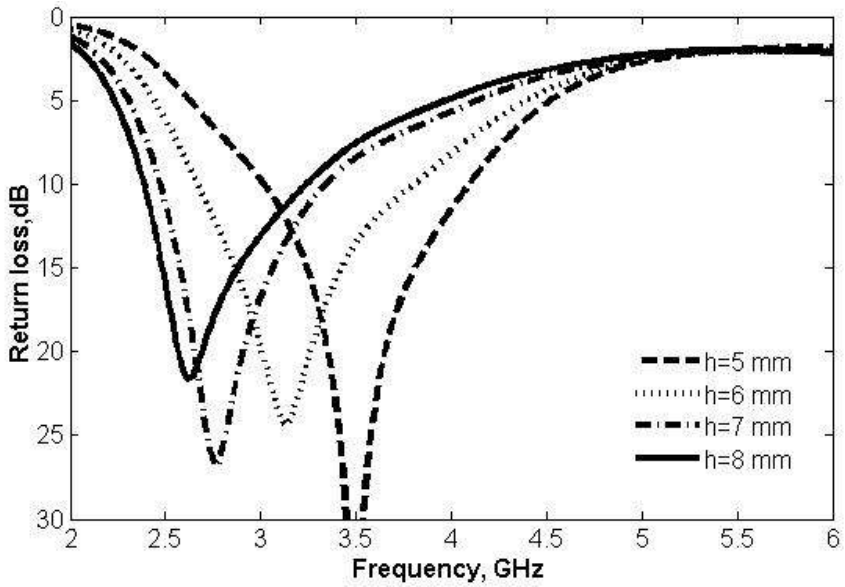

Figure 5.2: Effect of variation of the parameter h on the input return loss.

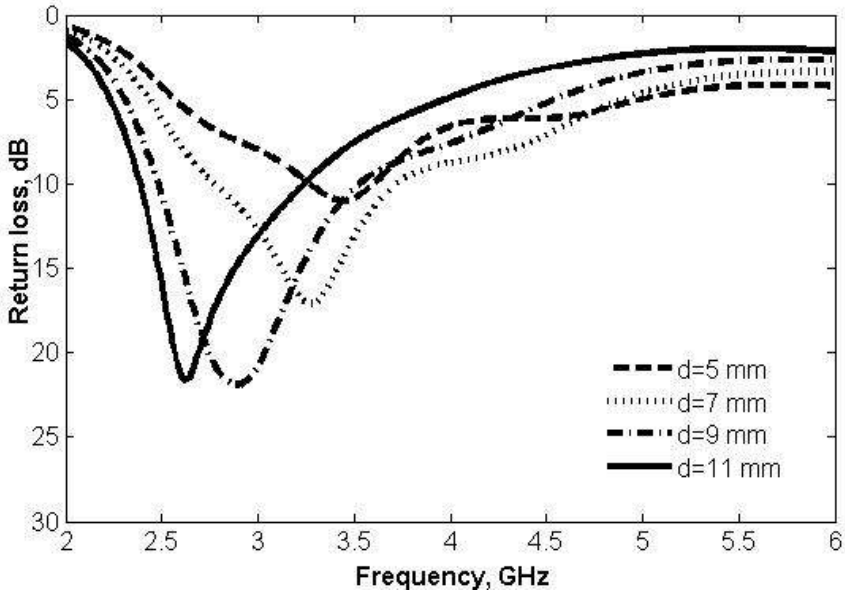

Figure 5.3: Effect of variation of the parameter d on the input return loss.

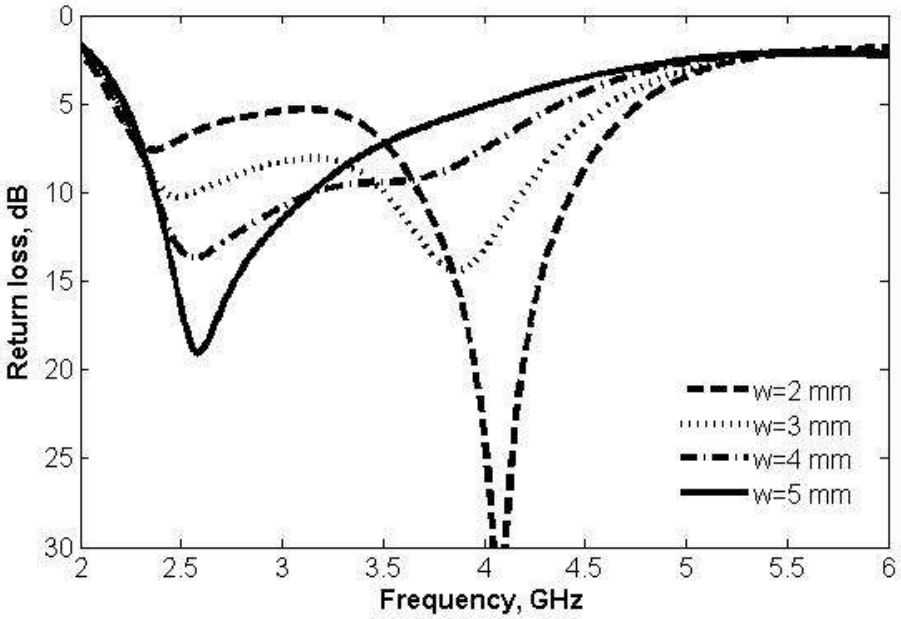

Figure 5.4: Effect of variation of the parameter *w* on the input return loss

A first working design may be created as a result of this parameter study, with the folded dipole covering all of the bands of interest, except for the 5.2 GHz WLAN. In order to realise a design variant which includes this band, a technique was applied by inserting an additional thin-strip at the side of each main arm of the folded structure, see Figure 5.1. This produces the additional resonant frequency for the 5.2 GHz band. The optimal length and width of this added arm was found, subject to the input return loss required of the antenna in the 5.2 GHz band. It should be noted that this added arm has little effect on the return loss of the main radiator. Therefore, the desired multiple frequency operation of this balanced handset antenna, together with low profile, is achieved with the dual-arm structure.

The optimised configuration of this dual-arm structure was studied in terms of return loss, radiation patterns and power gain. The principal dimensions of this configuration are tabulated in Table 5.1. The new compact design has overall dimensions of 38 (L) × 8 (W) × 8 (H) mm. The total physical length of the main radiator at 2.5 GHz is 35.5

mm, which is longer than a quarter wavelength at this frequency in free space. This is mainly because the bending and the proximity (1 mm) to the ground plane of the radiator affect the resonance length.

Table 5.1: Summary of the principal dimensions of the antenna.

Parameters	Value (mm)
l	18.5
d	9
w	5
h	8
a_l	9.5
a_w	3
a_h	5

5.2.3 Prototyping of Antenna and Test Results

For practical optimisation, the simulation model was studied in terms of return loss, radiation patterns and power gain, and then realized as a first cut design as follows. Copper sheet with thickness 0.15 mm was used for fabricating the antenna, and 0.5 mm for the associated ground plane. The prototype is presented in Figure 5.5. As can be seen from the photograph, some of the non-conductive material was used to support the radiator's arms in order to constrain them at the same level, and to suspend the antenna uniformly from the ground plane with distance of 1 mm.

Figure 5.5: Photograph of prototype of the proposed balanced antenna design

5.2.3.1 Return Loss of the Antenna

The return loss measurement for this prototype uses a balun circuit as the feed network. In addition, the impedance at the input port of the antenna was examined using the S-Parameter method described in [10] (see Chapter 2). In this case, balanced antennas are considered as two-port devices, and the S-Parameters can be obtained by using a calibrated network analyser. A simple formula is then used to derive the differential input impedance of the balanced antenna. Figure 5.6 gives the two versions of measured return loss, both compared against the simulation model. The results are in fairly close agreement.

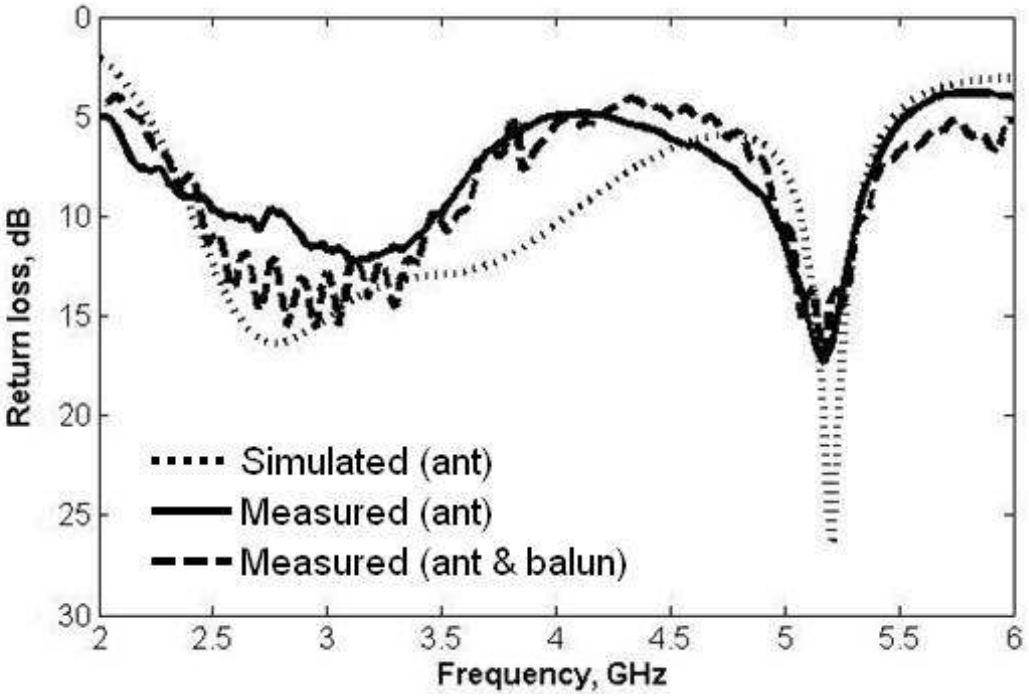

Figure 5.6: Comparison of simulated and measured return loss

5.2.3.2 The Radiation Pattern of the Antenna

Measurement of the radiation patterns of the prototype were carried out in a far-field anechoic chamber, using an elevation-over-azimuth positioner, with the elevation axis coincident with the polar axis ($\theta = 0°$) of the antenna's co-ordinate system. The azimuth drive thus generates cuts at constant ϕ. The fixed antenna was a broadband horn (EMCO type 3115) fixed at a distance of 4 m. The elevation positioner was rotated over $180° \leq \theta \leq 180°$, with an increment of 5° for principal plane measurements. Three principal-plane pattern cuts were taken for the four designated WLAN/WiMAX operating frequencies. The radiation patterns in the y-z, x-z and x-y planes for the design at 2.45 GHz, 2.6 GHz, 3.5 GHz and 5.2 GHz were measured and compared with the simulation, as shown in Figure 5.7. The measured patterns at frequencies above the lower band (e.g. in the 2.6 and 3.5 GHz bands) are similar to the patterns at 2.45 GHz presented in

Figure 5.7. This is because the antenna's behaviour at the lower operating frequencies is controlled by the basic single-arm folded dipole, whereas at 5.2 GHz the antenna tends to radiate with a partial bias towards the +z direction, since the ground plane acts as a reflector in this band.

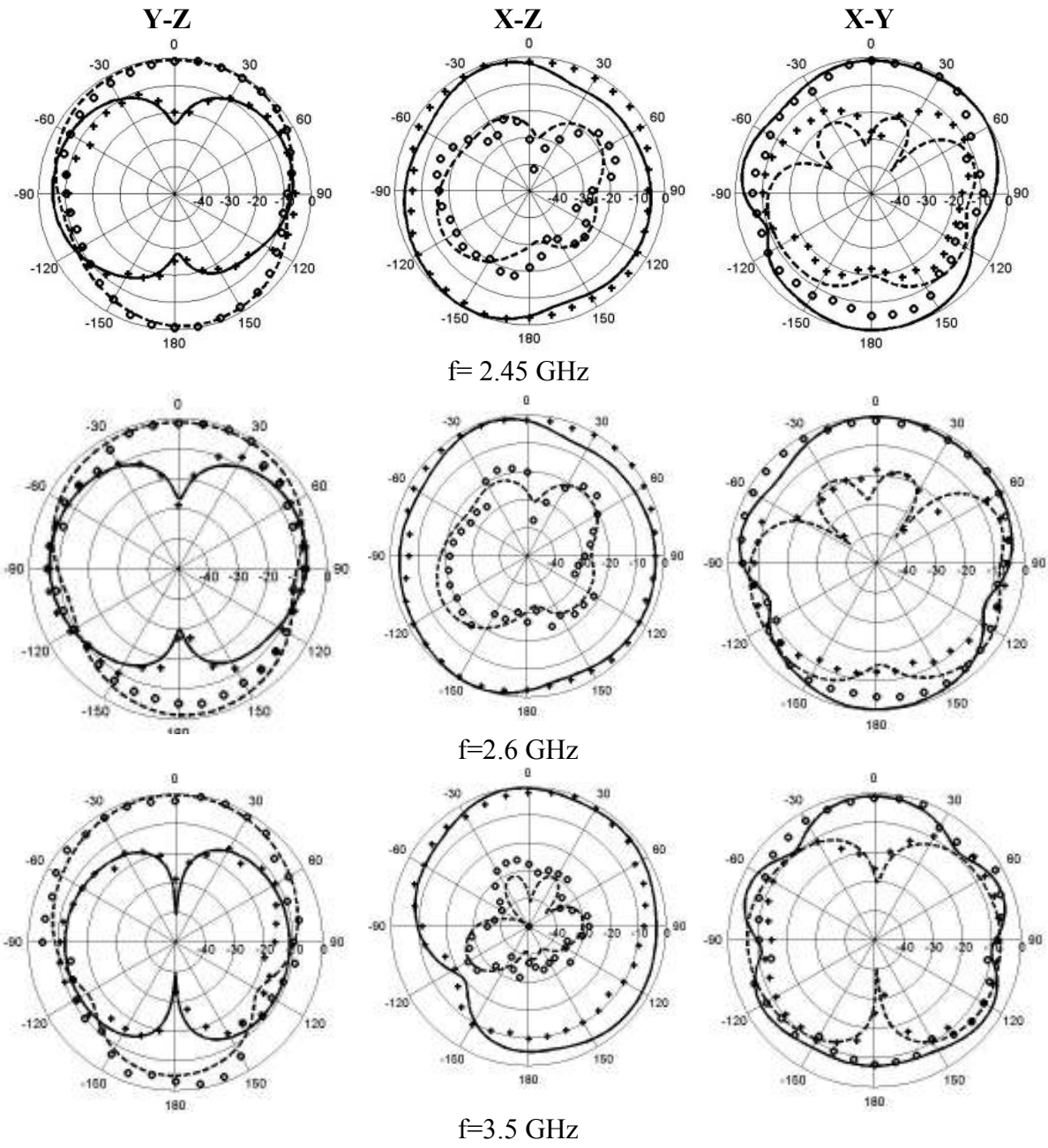

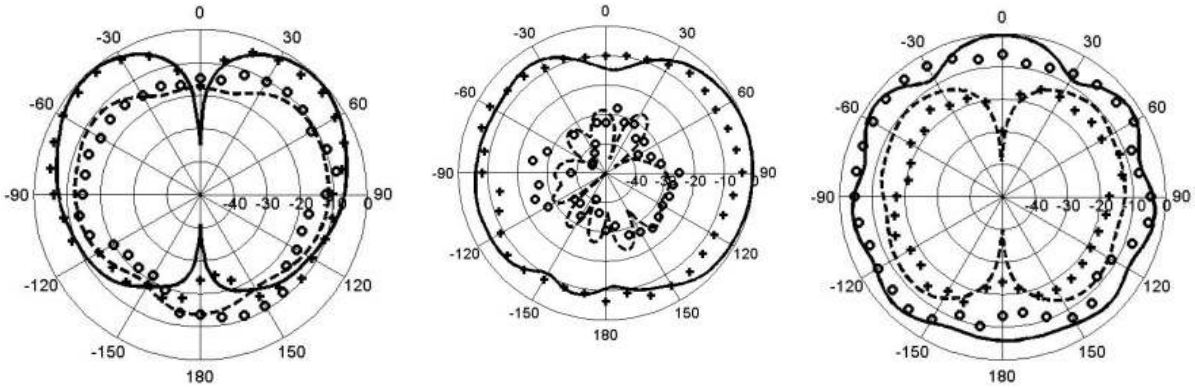

Figure 5.7: Radiation patterns of the proposed antenna at 2.45, 2.6, 3.5 and 5.2 GHz for y-z, x-z and x-y planes, where 'ooo' measured E_θ ,' ----' simulated E_θ ,'xxx' measured E_ϕ '——' simulated E_ϕ

5.2.3.3 Power Gain and Current Distribution of the Antenna

The measured broadside antenna power gain for frequencies across the 2.4 and 5.2 GHz WLAN bands and 2.5 and 3.5 GHz WiMAX bands were also investigated. The measured antenna gains across the frequency bands of interest are shown in Figure 5.8. The insertion loss of the feed network was adjusted to compensate the measured power gain, to give uniform values over each band, where necessary. The basic antenna gain varied over the range of from 2.12 dBi to 5.26 dBi over the frequency bands of interest.

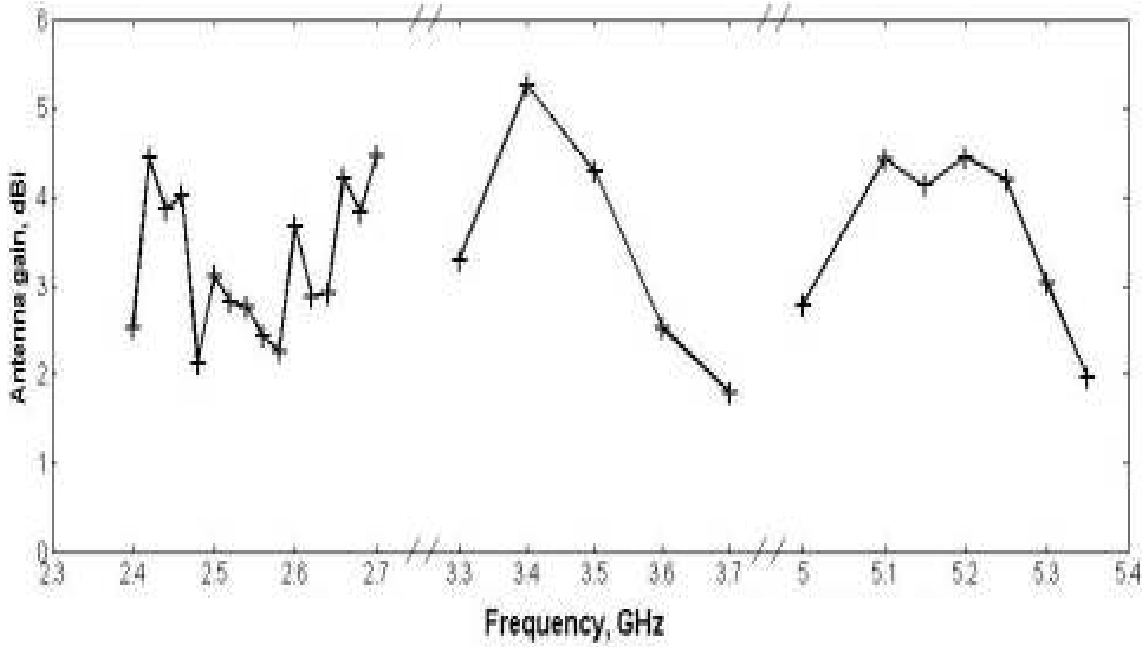

Figure 5.8: Measured power gain of the proposed antenna

Furthermore, the current distribution on the mobile handset ground plane was analysed using the EM simulator. This confirms that most of the current induced on the ground plane was at a maximum in the area beneath the antenna, and that a relatively weak current distribution appeared on the rest of the ground plane. This prototyping study clearly illustrates the advantages of the balanced design concept, and the next logical step is to pursue the interaction of the user with the antenna (or handset), with particular reference to radiation characteristics and SAR performance.

5.3 Second Design (Low Profile Dual-Band Balanced Handset Antenna for WLAN Application)

By extending the work from previous section, a dual-band balanced antenna for mobile handset applications covering the 2.4 GHz (2.4-2.484 GHz) and 5 GHz (5.15-5.35 GHz

& 5.725–5.825 GHz) bands, is proposed. Up to 50% height reductions were achieved as compared with the previous designs. This was achieved by introducing a long slot into each folded arm of the dipole radiator, and the new low-profile design is therefore realised.

5.3.1 Antenna Structure

In the first instance, the aim was to design a dual-band balanced antenna using two clearly separated resonant modes. This design was approached using a two-tier process. Firstly, each monopole arm of a planar strip dipole was folded. In order to achieve a low-profile folded (i.e. minimised height) balanced antenna, whilst maintaining sufficient impedance bandwidth to support the targeted WLAN bands, a long slot was introduced into each folded arm of the dipole radiator, as in Figure 5.9. In this way, the equivalent wavelength of the surface current at 2.4 GHz was increased, compared to the case without the long slot. Thus, the folded antenna height (h) can be reduced by 50%, and revised the low-profile design realised. Secondly, a technique for introducing another resonant frequency was applied to the antenna after the first stage. A metal strip with appropriate length and width was inserted into each arm of the planar dipole with folded structure (see Figure 1.9c). This additional arm was exploited to generate the second resonant frequency for the 5 GHz frequency band [11]. The proper length and width of this added arm was found with the aid of the structure parameters in the simulation model, subject to the input impedance matching required for the 5 GHz band. It was noticed that this addition had only a slight effect on the resonant frequency for the 2.4 GHz band. Therefore, a dual-frequency operation with low profile was achieved with the dual-arm structure, as shown in Figure 5.9.a.

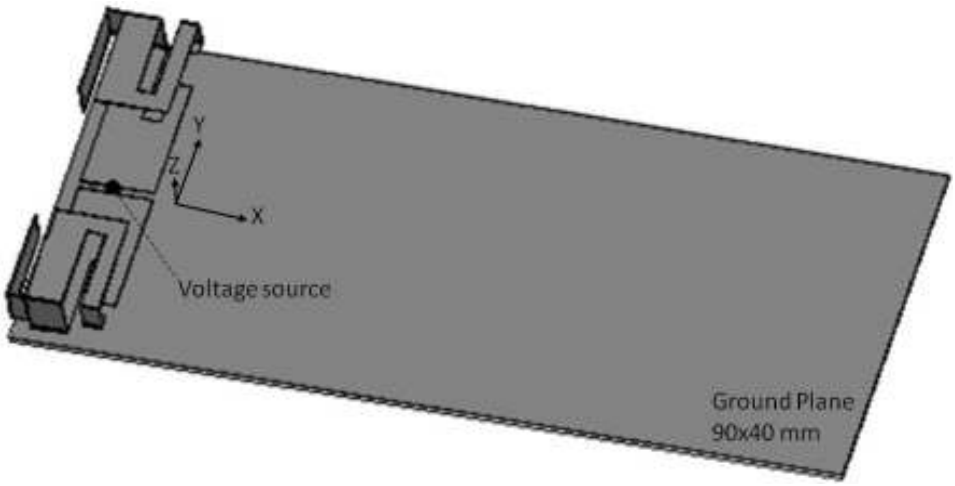

(a)

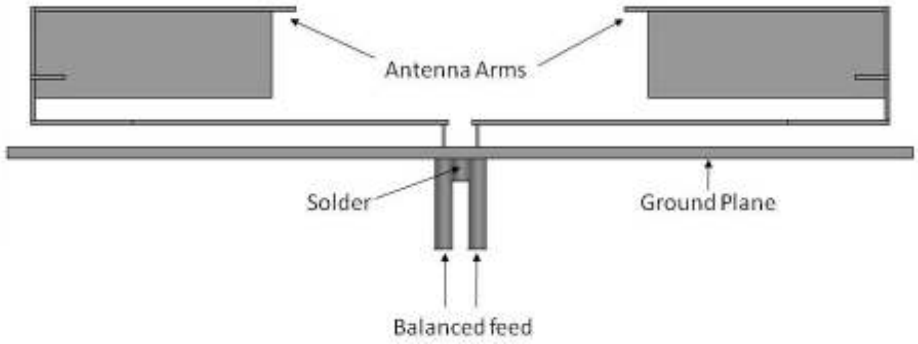

(b)

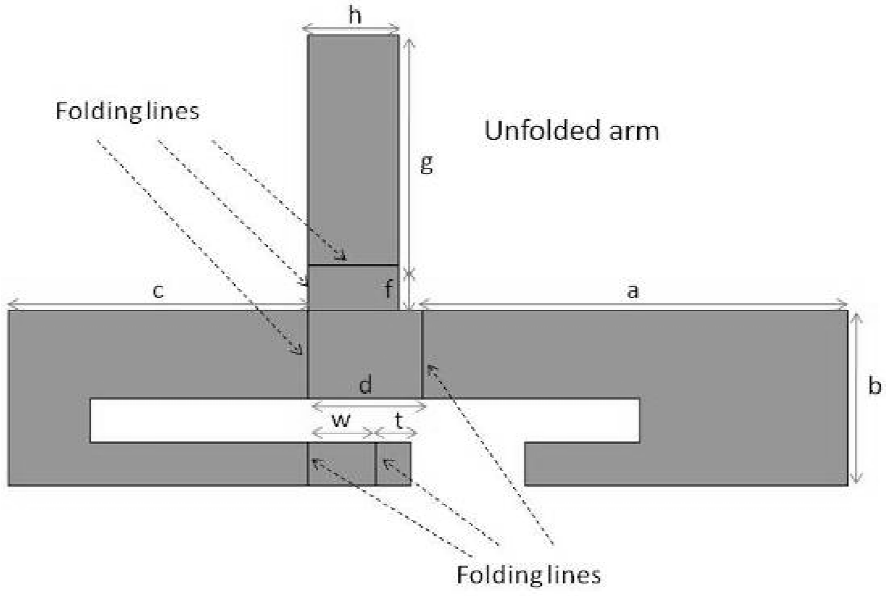

(c)

Figure 5.9: Geometry model of the proposed balanced mobile antenna, (a) 3D balanced mobile antenna configuration, (b) Side view of the balanced antenna with connected feed, (c) Unfolded arm of the balanced mobile antenna configuration studied

5.3.2 Parametric Study of the Antenna

The dimensions of this antenna geometry must remain within realistic handset sizes constraints. A parametric model was built up to establish the relationship between the principal structure parameters, and the realisable impedance bandwidth. The model is used to guide the optimisation of the impedance bandwidth, to include the WLAN band. The antenna height parameters (*h* and *w*) have a dominant effect on the impedance bandwidth. The optimal value of h was found to be 4 mm, based on a sweep over the range $2 \le h / mm \le 5$, this is shown in Figure 5.10. The corresponding value for w was 3 mm, based on the range $1 \le w / mm \le 4$, see Figure 5.11. As discussed in the previous section, the purpose of the additional strip was to produce the upper resonance of the antenna. The controlling parameters are the dimensions f and g, as these values are increased; the upper resonant frequency decreases (see Figure 5.12). This does have a slight effect on the lower band.

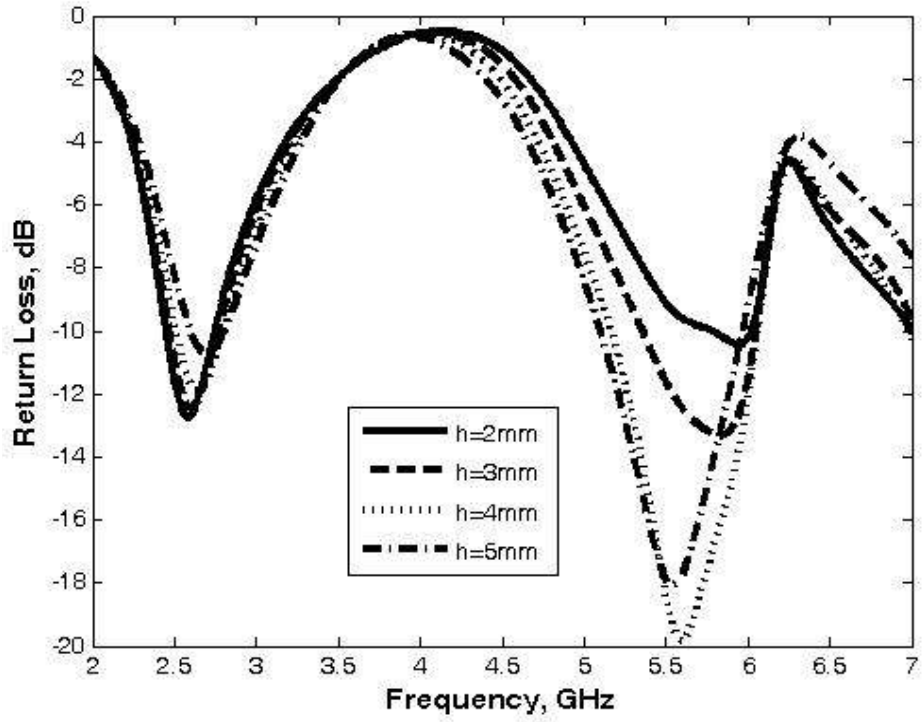

Figure 5.10: Effect of variation of the parameter *h* on the input return loss

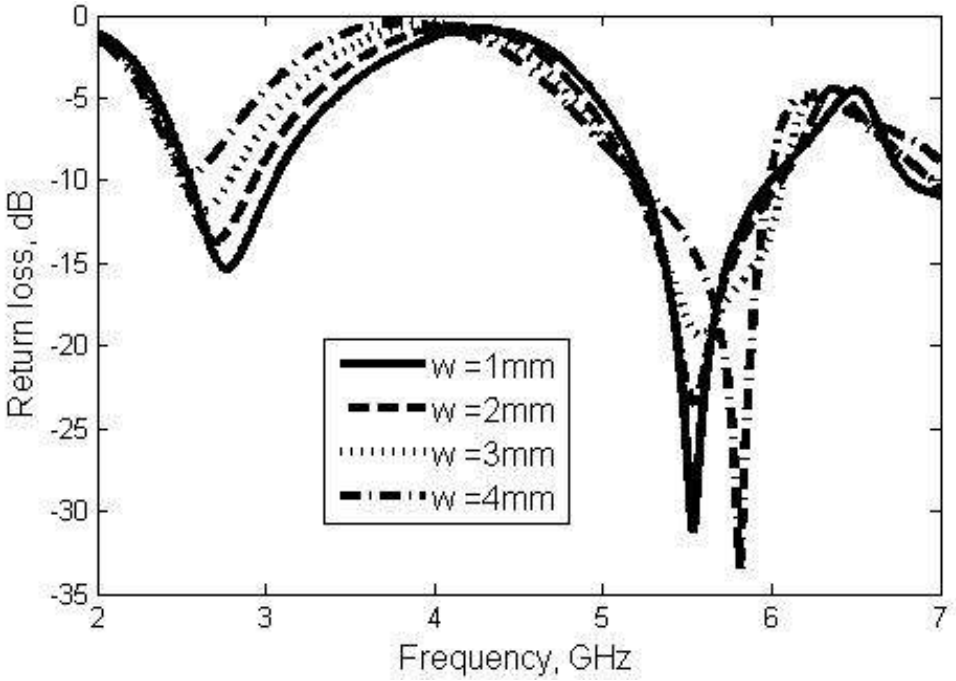

Figure 5.11: Effect of variation of the parameter *w* on the input return loss.

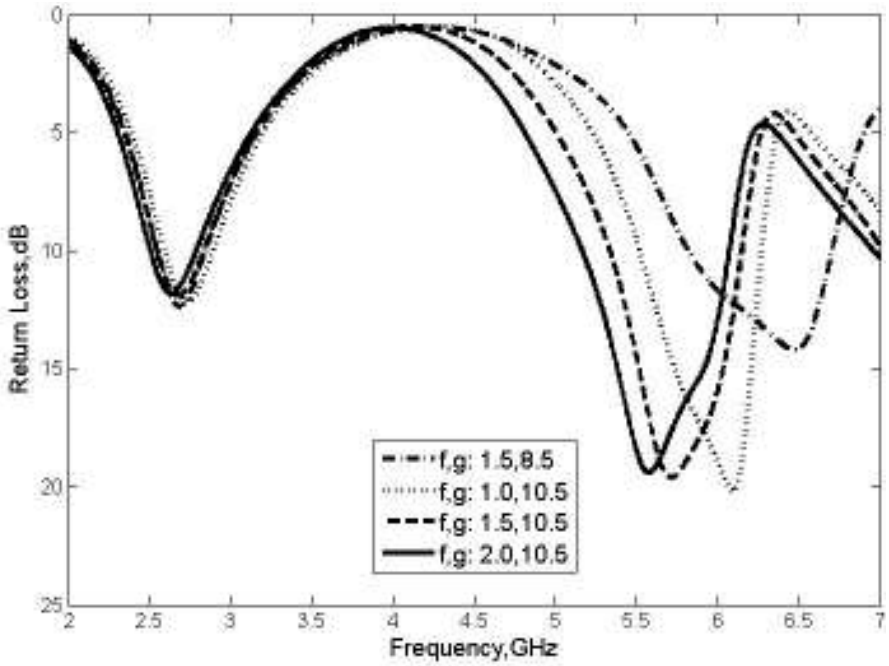

Figure 5.12: Parametric study of parameters *f* and *g* (in mm) against operating frequency.

The actual design values for this model analysis are summarised in Table 5.2. The antenna is placed 1 mm above the ground plane (90 mm × 40 mm), and the equivalent volume is 38 × 10 × 4 mm^3. The length and positioning of each arm were fine tuned,

together with second order effects from the remaining parameters to achieve a return loss better than 10 dB over the WLAN band.

Table 5.2: Summary of important parameters defining the proposed antenna.

Parameters	Value (mm)
a	18.5
b	8
c	11.5
d	5
w	3
h	4
t	1.5
f	2
g	10.5

5.3.3 Simulation and Measurement Return Loss

A prototype antenna was constructed using copper sheet of thickness 0.15 mm (Figure 5.13). A commercial balun (ET Industries, [12]) operating over 2 GHz to 12 GHz was used as the feed network (see Figure 5.14).

Figure 5.13: Fabricated prototype of the proposed balanced antenna design.

Figure 5.14: Photograph of prototype of the balun.

Figure 5.15 compares the return loss of the simulation model (ant) against the prototype (ant) and the full assembly (ant & balun), the results are in general agreement, and sufficient to verify the impedance response of the design.

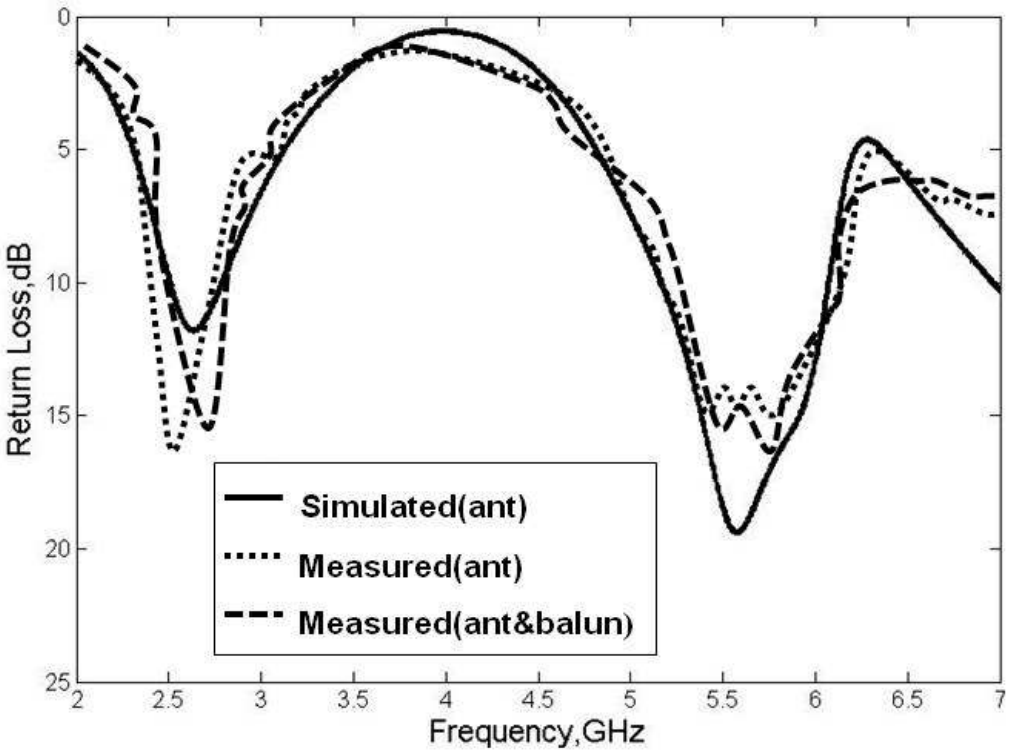

Figure 5.15: Comparison of simulated and measured return loss.

5.3.4 Measurement of Radiation Pattern and Power Gain

Measurements of the balanced prototype radiation patterns were carried out in a far-field anechoic chamber. Three principal-plane pattern cuts (i.e. zx, zy and xy planes) were taken for three WLAN operating frequencies covering the designated bandwidth. The radiation patterns were measured at selected frequencies of 2.4 GHz, 2.45 GHz, 5.2 GHz and 5.8 GHz, respectively; the measured patterns were normalised and presented in Figure 5.16. The results indicate a reasonable agreement between simulated and measured radiation patterns.

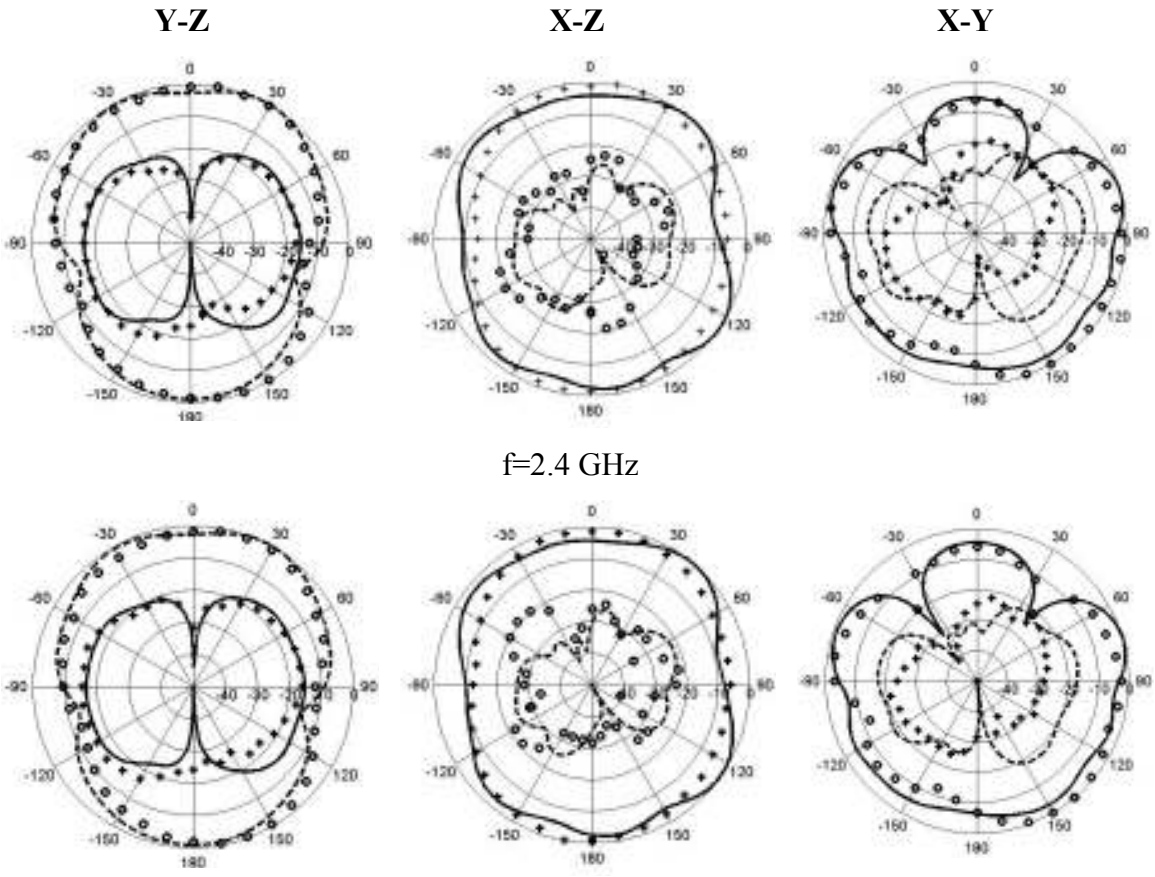

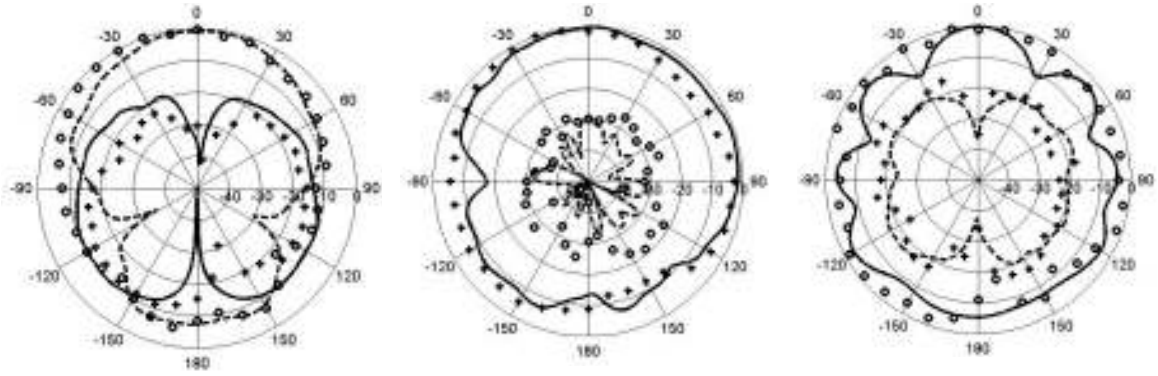

f=5.2 GHz

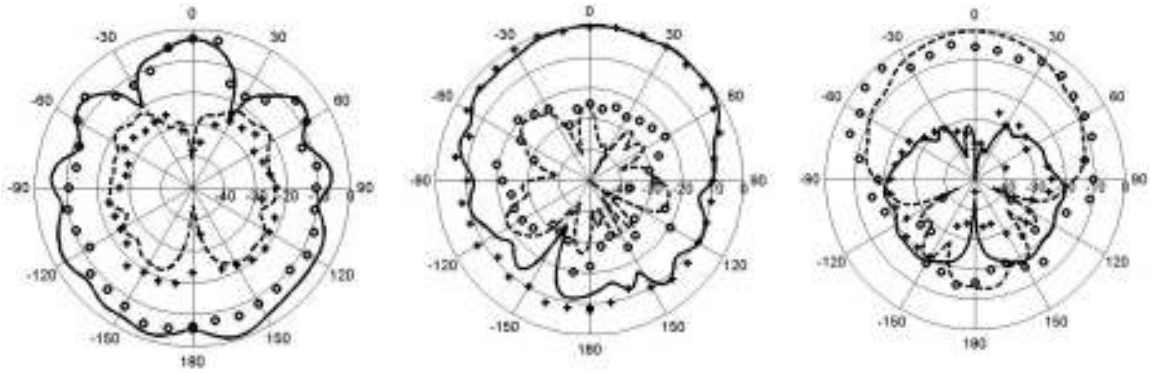

f=5.8 GHz

Figure 5.16: Radiation patterns of the proposed antenna at 2.4, 2.45, 5.2 and 5.8 GHz for yz, xz and xy planes. 'ooo' measured E_θ ,' ----' simulated E_θ ,'xxx' measured E_ϕ '——' simulated E_ϕ

The antenna gain of the final assembly was also measured in the broadside direction for frequencies centred on 2.4 GHz and 5 GHz see Figure 5.17, it should be noted that the insertion loss of the feed network was added to the measured power gain at each specified frequency in the plot. The measured antenna gain varied approximately between 2.3 dBi and 4.3 dBi over the 2.5 GHz band and between 3.5 dBi and 5.3 dBi over 5.2 GHz band. The variations in the measured antenna gains were mainly caused by the balun, and from the wire connections between the antenna and the balun. The peak antenna gain variations for the 2.4 GHz and 5 GHz bands are less than 1.0 dBi, as compared with the simulation model.

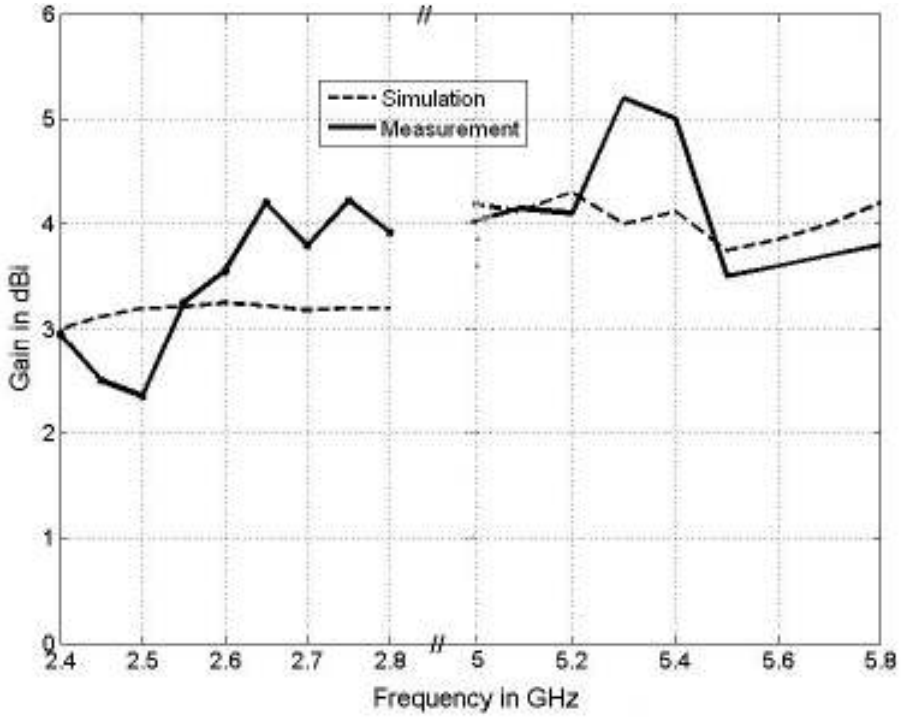

Figure 5.17: Simulated and measured power gain of the proposed antenna

5.3.5 The Current Distribution

The current distribution on the ground plane was studied in the simulation model, using the three specified frequencies, 2.45 GHz, 5.2 GHz, and 5.8 GHz. The results are shown in Figure 5.18, where most of the induced current on the ground can be seen to be concentrated in the region beneath the radiator. The distribution elsewhere is minimal. This is in close agreement with the established results of Kim et al [13] and Hayashida et al [14], in which only negligible induced surface currents were shown to exist on the underside handset chassis structures. Once again it may be safely inferred that this balanced design will be insensitive to the loading effect of the user's hand.

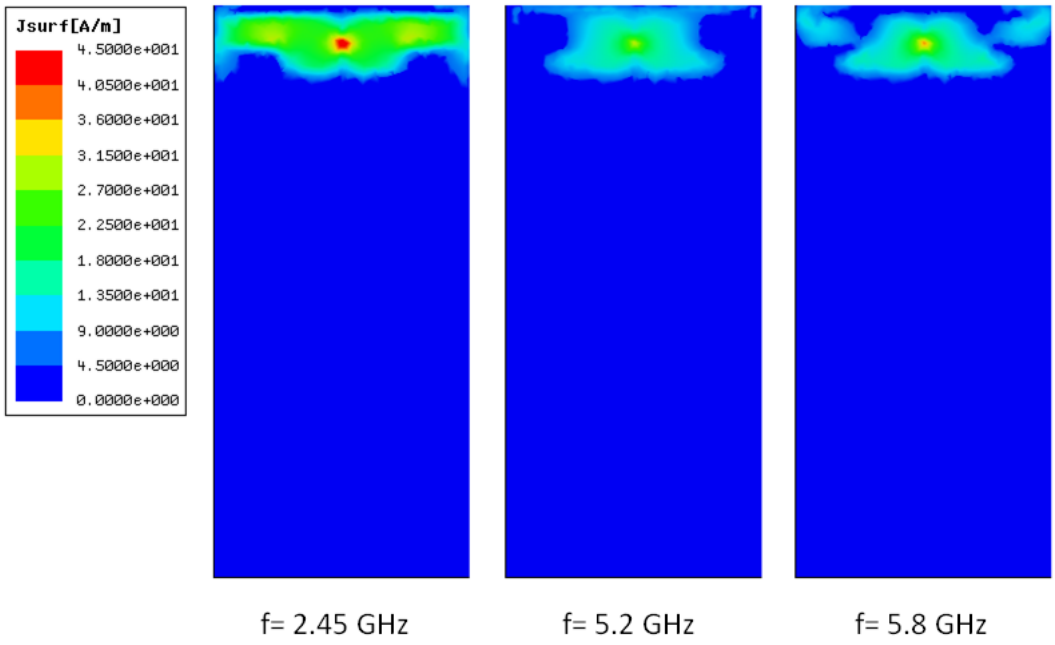

Figure 5.18: Surface current distributions for the proposed balanced antenna at 2.4 GHz, 5.2 GHz and 5.8 GHz, respectively.

5.4 Antenna for Future Mobile Application

To date, most of the balanced antenna designs have been implemented for operations in the contemporary 2.5G and 3G service bands. Therefore, there is a substantial motivation to look beyond these immediate requirements for the folded balanced-dipole antenna designs presented in this chapter. The usual mechanical constraints are anticipated, i.e. small size, low profile, and internalised construction. On this basis a more speculative folded structure may be proposed.

5.4.1 The Antenna Design Concept, and Basic Mechanical Structure

The initial building block of this design concept, ‘antenna 1’, is shown on Figure 5.19. The eventual goal will be a wideband folded dipole. The antenna 1 structure was

systematically modified to enhance its wideband performance; the dipole was mounted over a rectangular conducting plate with dimensions 120 mm × 40 mm.

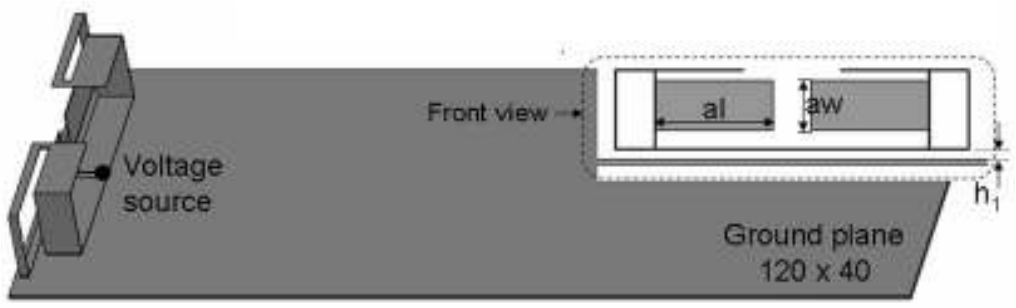

Figure 5.19: Geometry of wideband balanced antenna for future mobile communication system

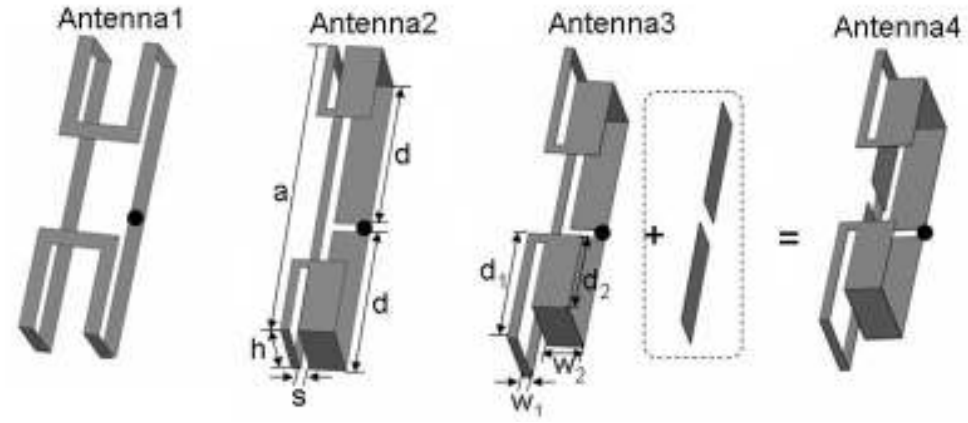

Figure 5.20: Antenna elements configuration

The initial basis for Antenna 1 is the single band folded design reported by Zhou et al [15], which had a design frequency of 1.8 GHz. The detailing was provided via a genetic algorithm, using a goal function derived from the impedance bandwidth requirement. A second building block, 'Antenna 2', was designed for a higher resonant frequency (2.68 GHz) [16], the structure is shown in Figure 5.20. This variant produces an intrinsically wider bandwidth, which may be tuned in terms of the strip width parameter w_2, this may be easily seen from the reference model calculation in Figure

5.20. Further analysis clarifies the tuning process in terms of *a* 'fine tuning' parameter *d*, which is varied whilst keeping the main parameter (*a*) constant. For example, consider 'Antenna 3', shown in Figure 5.20. In this variant, the principal dimensions are summarised in Table 5.3. The corresponding return loss is given in Figure 5.21. The design concept from the last section may be employed at this stage, and a further resonant frequency may be incorporated. An additional thin metal strip was inserted into each arm of the planar dipole; this structure ('Antenna 4') is given in Figure 5.20, with return loss given in Figure 5.21. The result of these actions is a single dual-resonant wideband variant of the folded planar dipole antenna, which is capable of operating over a comparatively large bandwidth. The influence of the geometry on return loss, radiation pattern and power gain was investigated in a detailed simulation model constructed using CST [9]. The parameter table was seeded with the values quoted above, and the frequency tuning was carried out using {*al* and *d*}, which control the total length of the folded loop. The main effect is summarised in Figure 5.21. The trend in the structure parameters is understood in terms of their impact on the impedance bandwidth; it can be seen with reference to Figure 5.22 and Figure 5.23 that the optimal values of *d* and *al* are 13.5 mm and 12.5 mm, respectively. These results should also be understood in terms of the constraint on available volume for the final assembly. The final dimensions for this design are 36 (*l*) mm × 6 (*w*) mm × 8 (*h*) mm, which are fully consistent with Hayashida et al [16]. A small amount of further optimisation was required as a result of the added volume on the arms, with respect to the bandwidth requirement, i.e. $2.6 \leq f\,(GHz) \leq 5.8$ and VSWR ≤ 2.

Table 5.3: Summary of important parameters of the antenna.

Parameters	Value (mm)
a	35.8
d	13.5
h	8
s	1
w_1	1
w_2	4
d_1	13
d_2	9
a_l	12.5
a_w	5
h_1	1

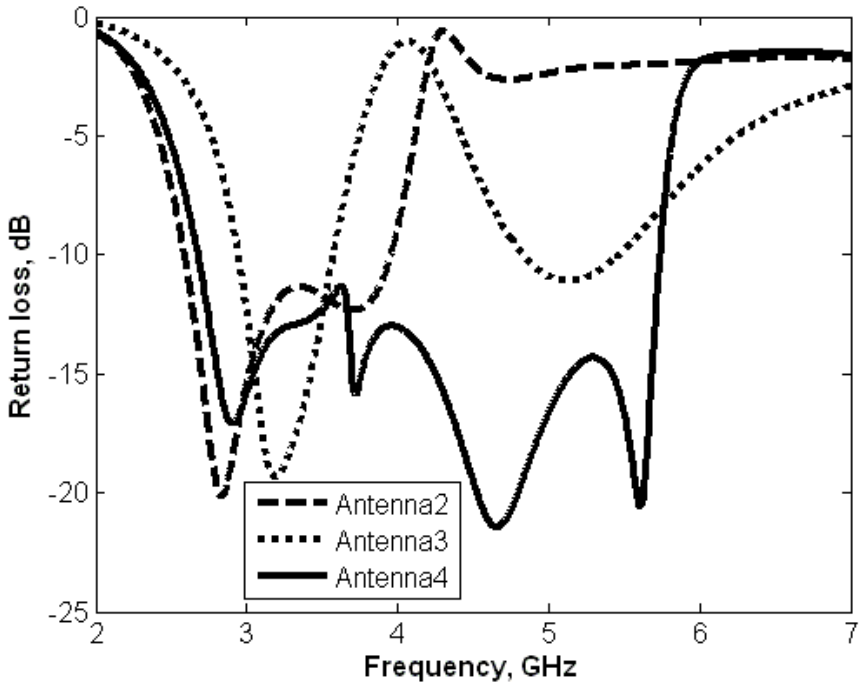

Figure 5.21: Calculated return loss of the antennas presented in Figure 5.22

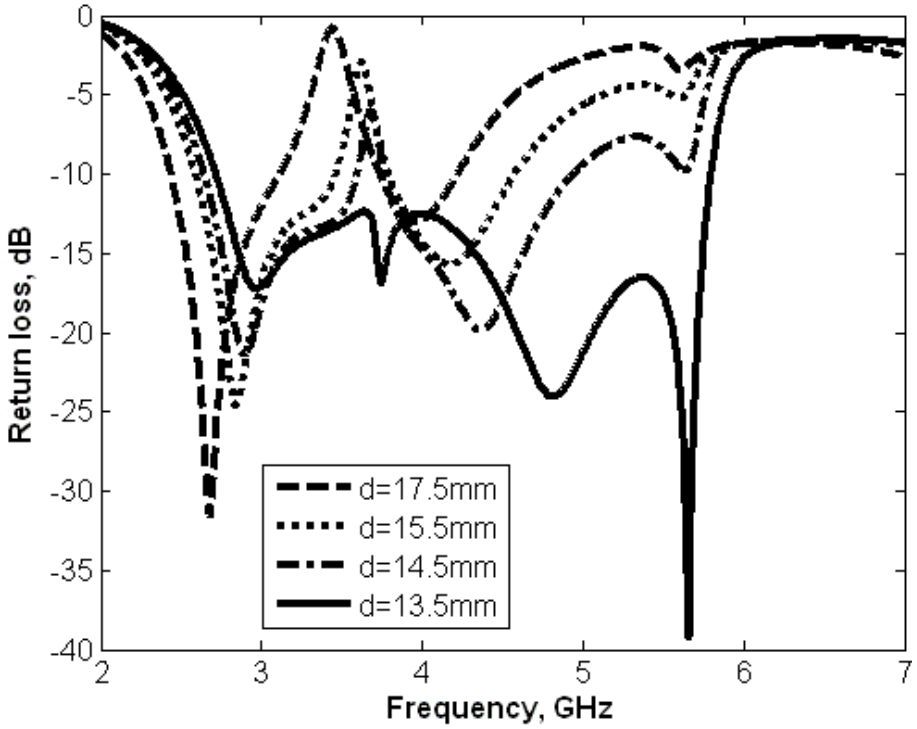

Figure 5.22: Variation of the parameter *d* on the effect of return loss.

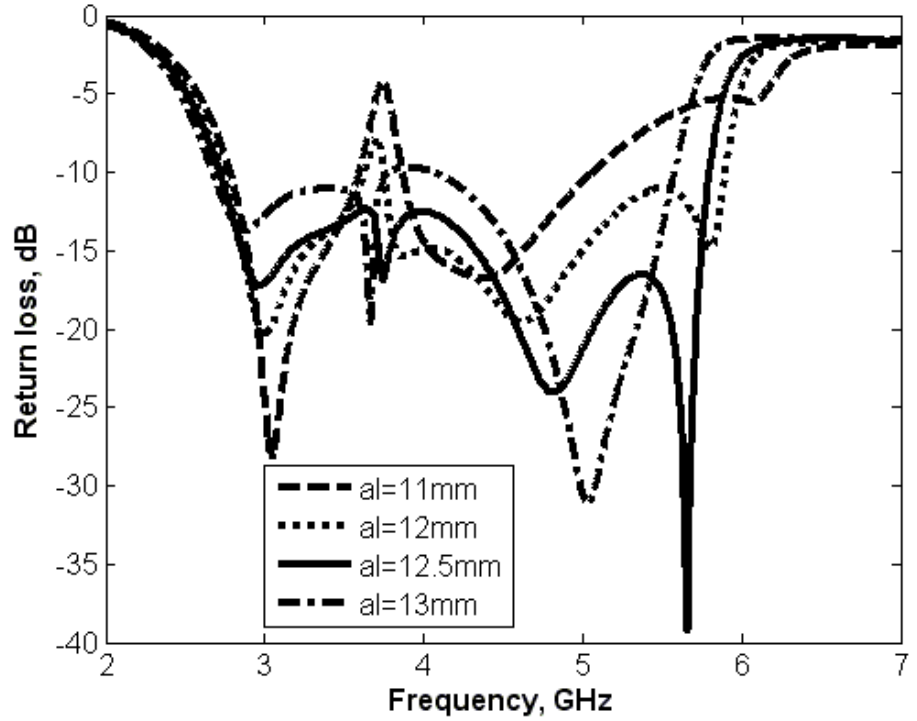

Figure 5.23: Variation of the parameter a_1 on the effect of return loss.

5.4.2 Simulation and Measurement Results

A prototype antenna and ground plane assembly was constructed from copper sheet with thickness 0.35 mm and 0.5 mm, respectively, see Figure 5.24. The ET industries balun circuit was used again to provide the balanced feed.

Figure 5.24: Photograph of the prototype antenna.

The return loss for the simulation model and prototype are shown in Figure 5.25. The model was cross validated using a different calculation method, i.e. CST vs. IE3D [17]. Taking into account that some of the practical detail of the prototype is not present in the simulation, the results are in acceptably close agreement.

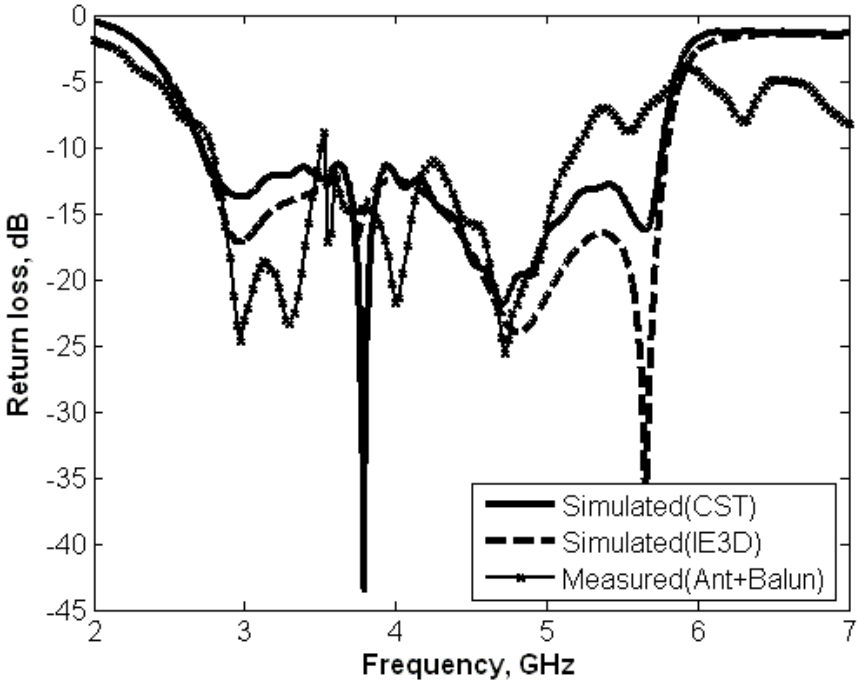

Figure 5.25: Comparison of simulated and measured return loss.

The simulated, normalised, radiation patterns are shown in Figure 5.26. Five specific frequencies of the radiation patterns in the xz plane and yz plane of the prototype antenna were selected in this study. These are 2.9 GHz, 3.5 GHz, 4.6 GHz, 5.2 GHz and 5.8 GHz. It can also be seen from Figure 5.26, that similar radiation patterns were observed at yz plane, except for the one at 2.9 GHz. This prototype tends to radiate in the +z direction, and the peak (simulated) gain was found to vary between 4.5 dBi to 6.6 dBi over the full band.

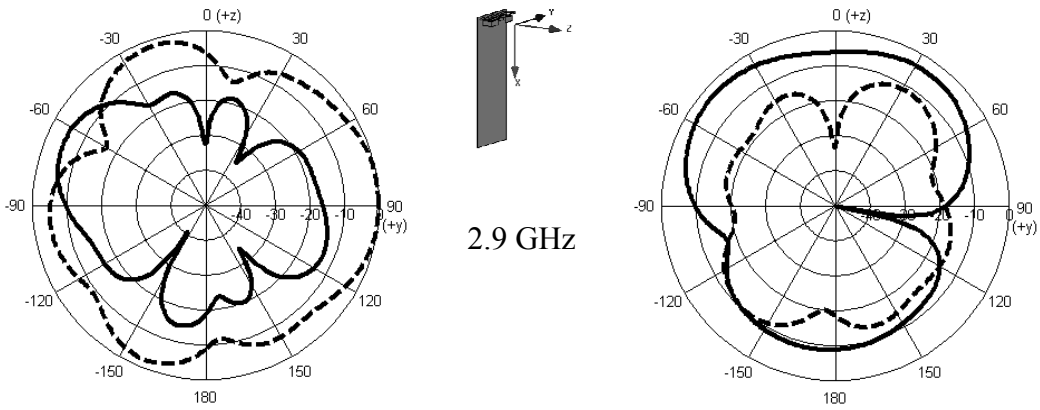

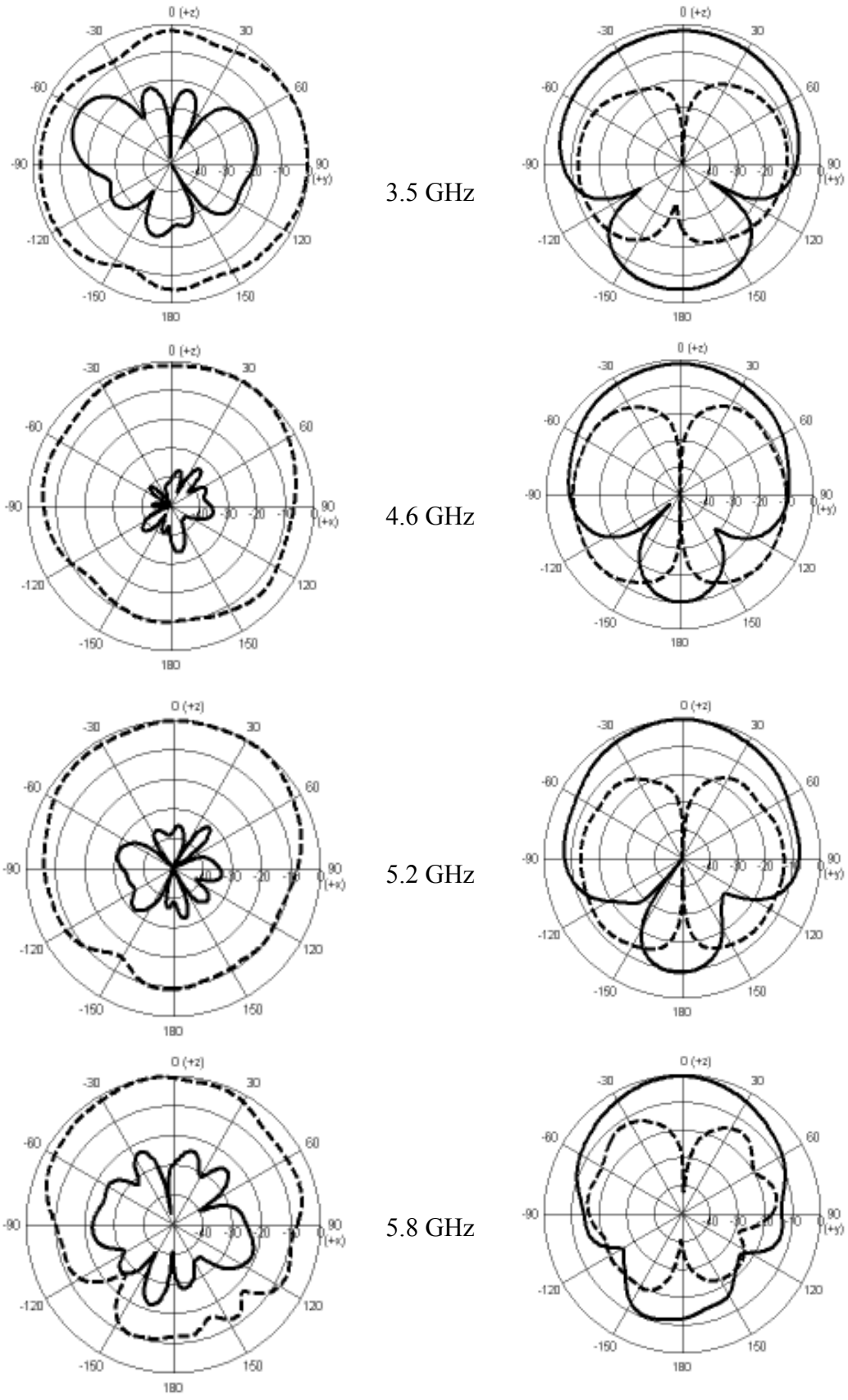

Figure 5.26: Radiation patterns of the proposed antenna for 2.9 GHz, 3.5 GHz, 4.6 GHz, 5.2 GHz and 5.8 GHz at: (left) xz plane; (right) yz plane; ('——' calculated E_θ, and '- - -' calculated E_ϕ).

5.5 Conclusions

Three new folded planar dipole antennas, with some novel design features, have been presented for dual-band and multi-band mobile handset applications. The first antenna was designed to operate over both low (2.4 GHz) and high (5.2 GHz) WLAN bands, and the low (2.5 GHz) and mid (5.2 GHz) WiMAX bands. This was achieved by cutting a long slot into each folded arm of the planar dipole, and the resulting height of the new structure may be reduced by up to 50%, this size reduction was realised in the second variant. The design concept was motivated in part by the desire to look beyond 3G, and anticipate the possible evolution of mobile handset requirements. Therefore, new design operating over wide frequency band (i.e. 2.6-5.8 GHz) has been proposed and studied. These antenna designs concept have been studied through detailed simulation models, with some level of cross validation where necessary. The simulation models have been experimentally verified through physical prototypes. These antennas are seen to be viable in performance terms, via antenna return loss, radiation pattern and power gain. In addition, the stability and low SAR inherent in the balanced design is proven for these designs. The simulated and measured results over the various frequency bands show good agreement, making these designs attractive candidates for handheld device applications.

5.6 References

[1] H. Morishita, H. Furuuchi, and K. Fujimoto, "Performance of balance-fed antenna system for handsets in the vicinity off a human head or hand," *IEE Proceeding Microwave Antennas Propagation*, vol. 149, pp. 85-91, 2002.

[2] R. A. Abd-Alhameed, P. S. Excell, R. A. K. Khalil, and J. Mustafa, "SAR and radiation performance of balanced and unbalanced mobile antennas using a hybrid computational electromagnetics formulation," *IEE Proceedings-Science, Measurement and Technology special issue on Computational Electromagnetics*, vol. 151, pp. 440-444, 2004.

[3] D. Zhou, R. A. Abd-Alhameed, C. H. See, A. G. Alhaddad, and P. S. Excell, "Compact wideband balanced antenna for mobile handsets," *IET Microwaves, Antennas and Propagation*, vol. 4, pp. 600-608, 2010.

[4] H. Morishita, H. Furuuchi, Z. T. H. Ide, and K. Fujimoto, "A balance-fed loop antenna system for handset," *IEICE Trans. Fundamentals*, vol. E82-A, pp. 1138-1143, 1999.

[5] Hisashi Morishita, Syogo Hayashida, Jun Ito, and K. Fujimoto, "Analysis of Built-in Antennas for Handset Using Human (Head, Hand, and Finger) Model," *Electronics and Communications in Japan*, vol. 86, pp. 35–45, 2003.

[6] B. S. Collins, S. P. Kingsley, J. M. Ide, S. A. Saario, R. W. Schlub, and S. G. O'Keefe, "A Multi-Band Hybrid Balanced Antenna," *IEEE International Workshop, Antenna Technology Small Antennas and Novel Metamaterials*, pp. 100-103, 2006

[7] J. Janapsatya, K. P. Esselle, and T. S. Bird, "A dual-band and wideband planar inverted-F antenna for WLAN applications," *Microwave and Optical Technology Letters*, vol. 50, pp. 138-141, January 2008.

[8] C. H. See, R. A. Abd-Alhameed, D. Zhou, and P. S. Excell, "Dual-frequency planar inverted F-L-antenna (PIFLA) for WLAN and short range communication systems," *IEEE Transactions on Antennas and Propagation*, vol. 56, pp. 3318-3320, October 2008.

[9] "Computer Simulation Technology Corporation, CST Microwave Studio, Version 5.0, Germany.."

[10] R. Meys and F. Janssens, "Measuring the impedance of balanced antennas by an S-Parameter method," *IEEE antennas and propagation magazine*, vol. 40, pp. 62-65, 1998.

[11] A. G. Alhaddad, R. A. Abd-Alhameed, D. Zhou, I. T. E. Elfergani, C. H. See, P. S. Excell, and M. S. Bin-Melha, "Low Profile Balanced Handset Antenna with Dual-Arm Structure for WLAN Application," *In Proceedings of Mosharaka International Conference on Communications, Propagation, and Electronics, Amman, Jordon*, pp. 1-4, 5-7 March 2010.

[12] "ET Industries, USA, http://www.etworld."

[13] Y. Kim, H. Morishita, Y. Koyanagi, and K.Fujimoto, "A folded Loop Antenna System for Handset Developed and Based on the Advanced Design Concept," *IEICE Transaction Communication*, vol. E84-B, pp. 2468-2475, September 2001.

[14] S. Hayashida, H. Morishita, and K. Fujimoto, "Self-balanced wideband folded loop antenna," *IEE Proceeding Microwave Antennas Propagation*, vol. 153, pp. 7-12, 2006.

[15] D. Zhou, R. A. Abd-Alhameed, and P. S. Excell, "Bandwidth enhancement of balanced folded loop antenna design for mobile handsets using genetic algorithms," *National URSI symposium, University of Portsmouth, Portsmouth, UK*, 2007.

[16] S. Hayashida, H. Morishita, Y. KIM, Y. Koyanagi, and K. Fujimoto, "Wideband folded loop antenna for handsets," *IEEE AP-S Proc.*, vol. 3, pp. 2-5, Jun. 2002.

[17] "IE3D User's Manual, Zeland Software Inc., Release 5, 2000."

CHAPTER SIX

Interaction between Electromagnetic Field and Human Body for Dual Band Balanced Antenna Using Hybrid Computational Method

6.1 Introduction

The finite difference time domain (FDTD) method is used extensively in wireless communications both as a design tool, and for the general numerical simulation of complex systems. FDTD was introduced into the electrical engineering community in the late 1960s by Kane Yee [1, 2], its widespread applicability is in part due to its comparative simplicity, especially for very large scale computations, and its natural representation of complex inhomogeneous materials within the calculation domain [3-7]. The equations linking the electric and magnetic field variables are offset in time over a dual grid complex, the equations being updated using the leap-frog method. A major practical advance on Yee's basic scheme was Taflove's total-scattered field formulation which allowed the algorithm to be implemented using plane wave excitation from arbitrary directions.

The computational grid is discretised into a number of cells which are scaled as a fraction of the wavelength. The associated time step must be kept small during the simulation to satisfy the Courant-Freiderichs stability criterion [2, 8]. An absorbing boundary condition (ABC) must be applied to the outer boundary of the FDTD space to obtain the necessary spatial resolution to represent electromagnetic wave interactions in unbounded regions i.e. to simulate the extension of the finite lattice to infinity. The ABC should be able to absorb the outwardly travelling waves with an extremely low reflection. The perfectly matched layer introduced by Berenger [9] allows boundary reflections better than -80 dB to be realised. FDTD is currently the most widely used method for numerical dosimetry, particularly for the field analysis required to estimate mobile handset radiation effect on the human body [10-14]. In [10], an efficient numerical technique based on the FDTD technique was used to investigate radiation pattern distortion for three types of body-worn antennas. It was reported; the antenna with the ground plane has the least effect from the presence of the human body but suffers from a narrow bandwidth. The variation of path loss with the transmitter–receiver distance also was investigated for propagation along the human body torso, and it demonstrated that an antenna close to the omnidirectional source has the least spread in a linear-fit path-loss curve.

This chapter focuses on the practical modelling of the human body interaction with the dual balanced antenna structure detailed in the previous chapter [15], using a modified FDTD approach. The antenna operates over bands centred at 2.4 GHz and 5.2 GHz, respectively. The near and far field performance of this antenna is studied for several locations in close proximity to the human body, and the radiated and absorbed power distributions are computed at these locations, and for different polarizations. This allows the radiation efficiency of this antenna to be inferred from the ratio of the absorbed

power to the radiated power, under the operating conditions described. The cumulative distribution function (CDF) of the radiation efficiency and the location based power ratios are used to summarise the data.

6.2 A hybrid Method

The antenna – body interaction model is developed using a hybrid FDTD code. The first stage in the modelling requires the definition of a Huygens' surface around the antenna as illustrated in Figure 6.1 and Figure 6.2 for linear horizontal (HOR) and vertical (VER) polarisation **s**tate**s**, respectively. Equivalent electric and magnetic sources on this Huygens' surface are generated at each time step from the electric and magnetic fields created by the antenna in free space using NEC [16]. This field data is the used as an input source for an in-house FDTD code.

The human body is represented by a very detailed tissue classified anatomical model known as 'Visible Man' [17]. This model comprises forty-nine tissue types, and has a resolution of 1 mm. However, the FDTD cell size of the present simulation model for both frequency bands was 3 mm; forty-two tissue types were included. This cell size was chosen to speed up the computational time required by the hybrid method, and work within the available computer memory. The positions of the antenna on the human model are shown in Figure 6.3.

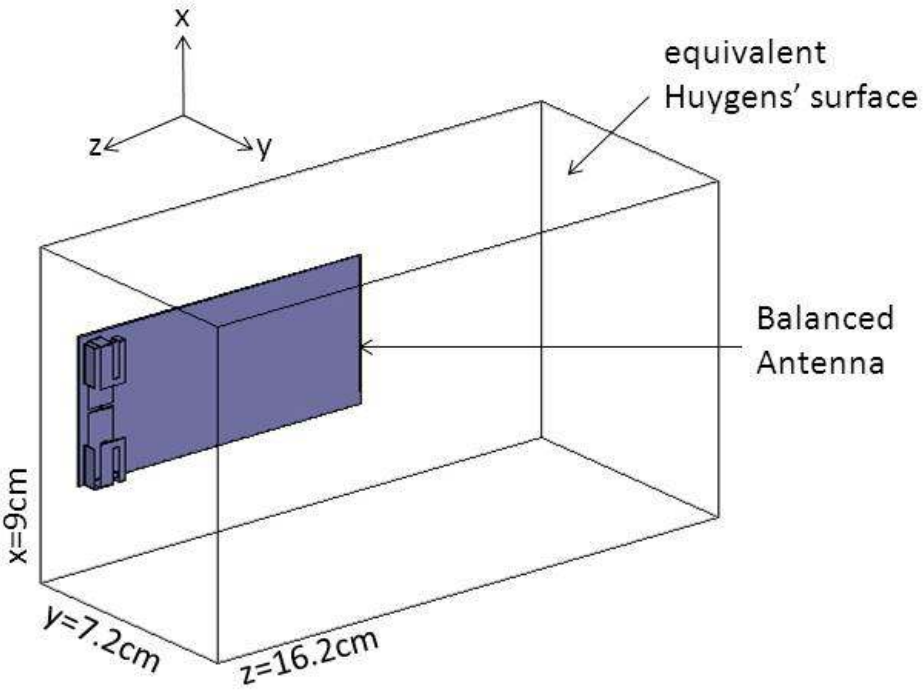

Figure 6.1: The balanced antenna with the equivalent Huygens box for linear horizontal polarisation.

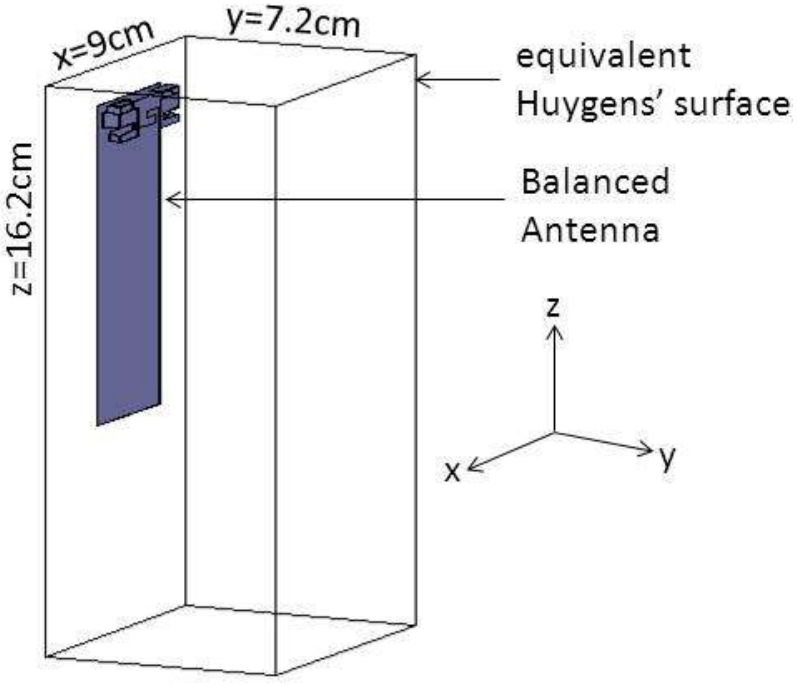

Figure 6.2: The balanced antenna with the equivalent Huygens box for linear vertical polarisation.

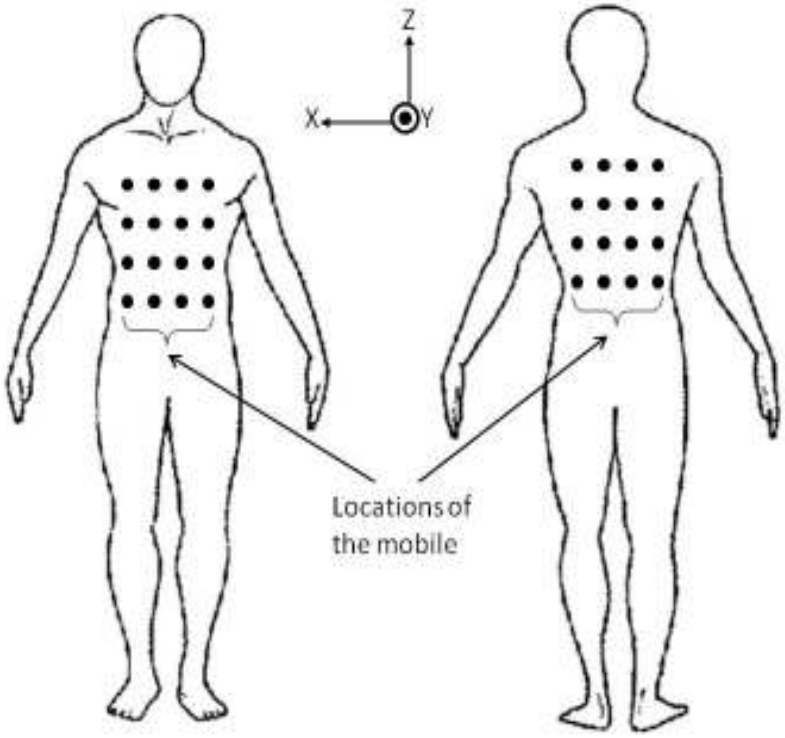

Figure 6.3: Human body model and the balanced antenna locations

The electrical properties of different type of human tissues at 2.45 GHz and 5.20 GHz are shown Table 6.1 and Table 6.2 respectively. Figure 6.4 shows the FDTD domain, displayed in the xz plane (i.e. the front view), with different tissue at different cross-sections for values of y (i.e., y = 30, y = 38 and y = 42). Figure 6.5 illustrates the FDTD domain model, displayed in the yz plane (i.e. the side view from left of the human to the right) with different tissue at different cross-sections for values x (i.e., x = 34, x = 50 and x = 67). Figure 6.6 shows the human body model at xy plane (top view) with different tissue at different cross-section of different values z (i.e., z = 15, z = 60, z = 100, z = 140, z = 165 and z = 205).

The human body was placed on a perfectly conducting ground plane, and the antenna was replaced by an equivalent Huygens' surface. The physical size of the Huygens' surface was 9 cm × 7.2 cm × 16.2 cm and this is equivalent to 30 × 24 × 54 FDTD cells

for horizontal and vertical polarisation as illustrated in Figure 6.1 and Figure 6.2 respectively. The Huygens' surface was carefully placed at the surface of the human model, where the distance between the antenna, and human tissues was only two cells. The FDTD method is applied over the entire computational domain. The equivalence principle is carried out in 3D by applying the hybrid electromagnetic method described in [18, 19] with cell size dx = dy = dz = 3.0 mm, and time step dt = 5 ps. The FDTD problem space was 180 × 118 × 633 cells, at which it is terminated by a PML with a thickness of 6 cells. The number of running cycles was set to 40 for both WLAN frequencies. It should be noted that in all cases shown in Figure 6.3 the antenna handset was between the antenna and the human tissues.

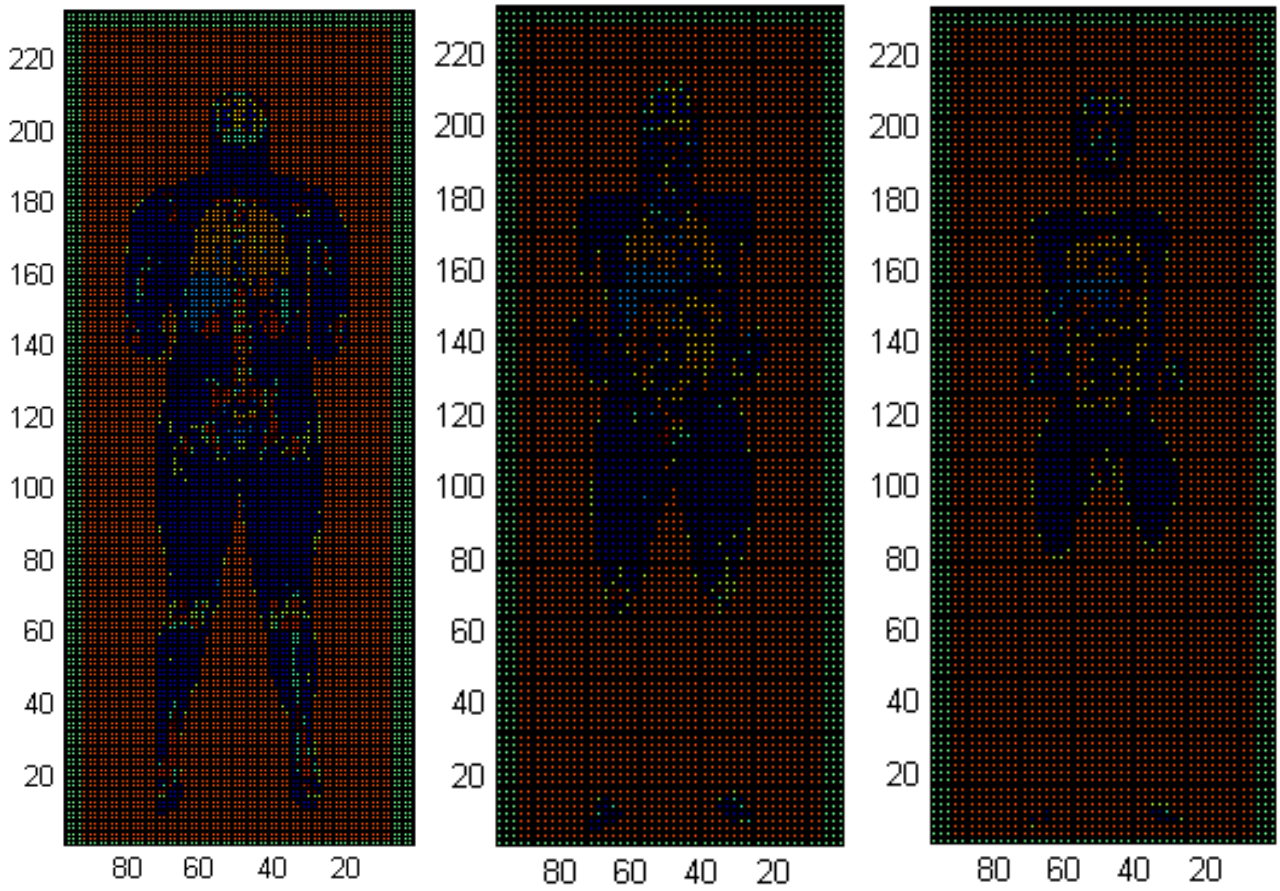

Figure 6.4: The human body model in *xz* plane of the computational domain. Cross-section at: (a) y = 30, (b) y = 38, (c) y = 42.

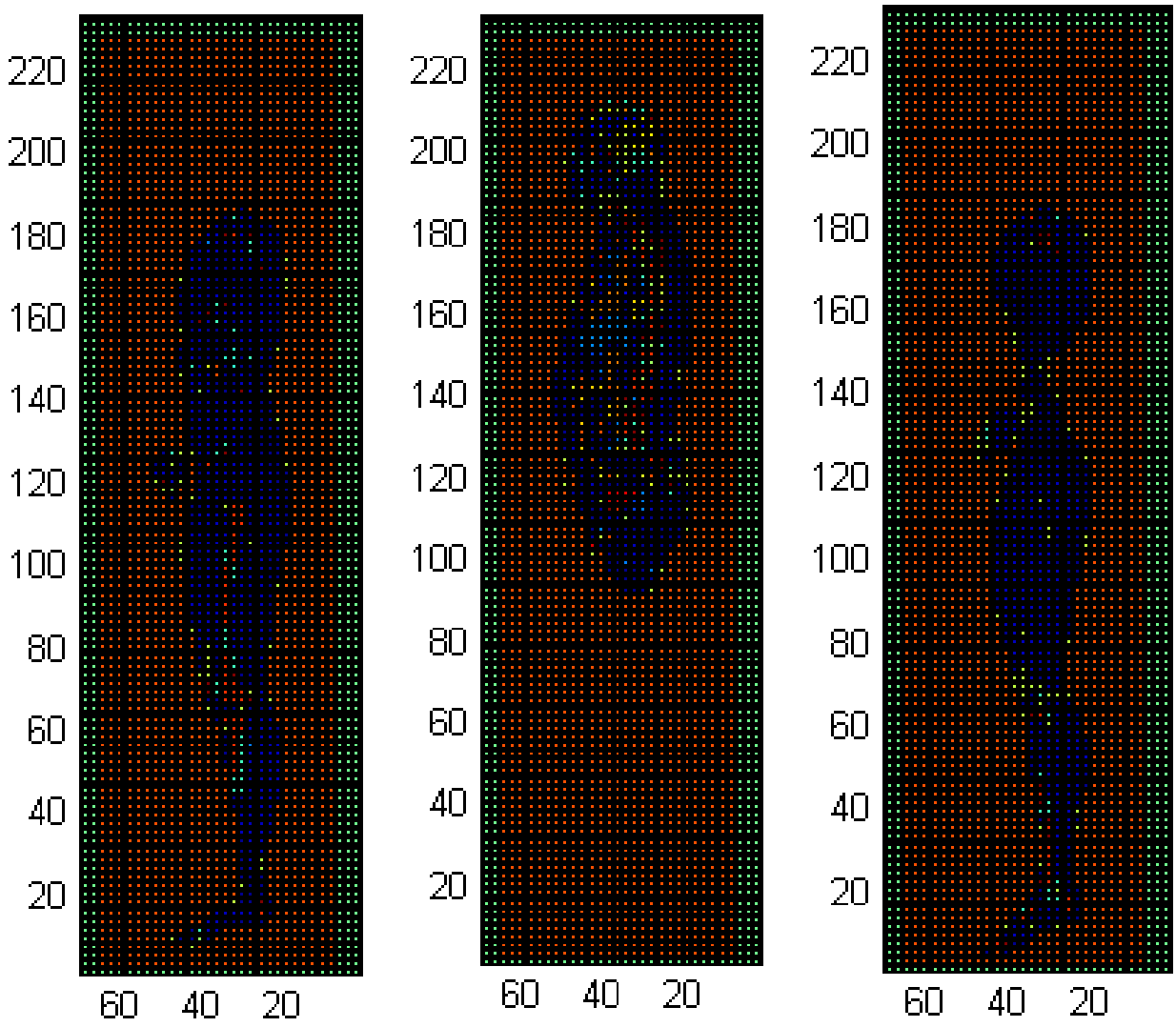

Figure 6.5: The human body model in *yz* plane of the computational domain. Cross-section at: (a) $x = 34$, (b) $x = 50$, (c) $x = 67$

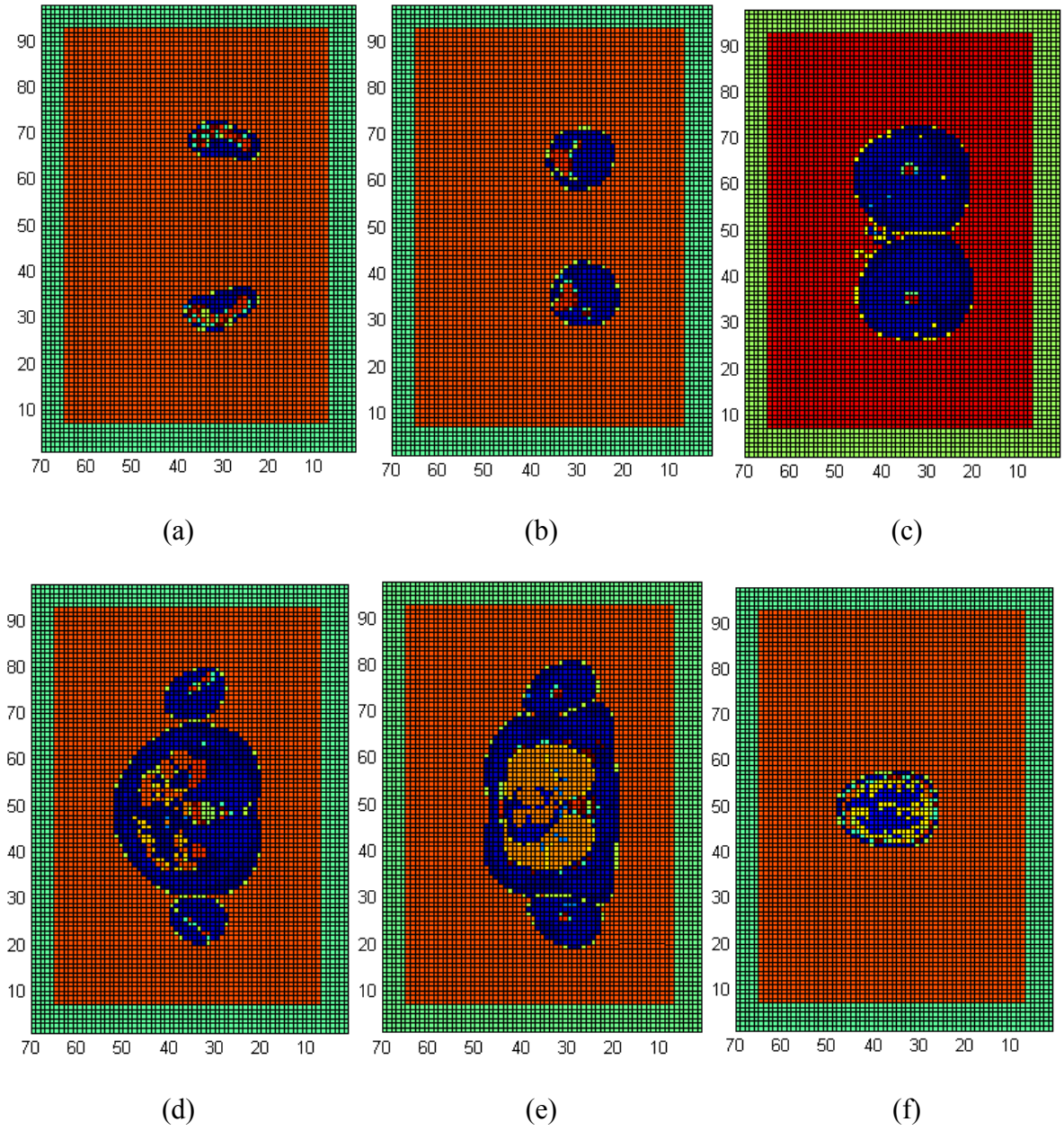

Figure 6.6: The human body model in *xy* plane of the computational domain. Cross-section at: (a) $z = 15$, (b) $z = 60$, (c) $z = 100$. (d) $z = 140$, (e) $z = 165$, (f) $z = 205$

Table 6.1: Human tissues properties at 2450 MHz

Tissue	ε_r	σ (S / m)	ρ (kg / m^3)
AIR.(internal)	1	0	1300
BILE	68.361	2.8007	1010
BODY.FLUID	68.208	2.4781	1010
EYE.(cornea)	51.615	2.2954	1076
FAT	5.2801	0.10452	916
LYMPH	57.201	1.9679	1040
MUSCOUS.MEMBRANE	42.853	1.5919	1040
NAILS.(toe.&.finger)	11.381	0.39431	1030
NERVE.(spine)	30.145	1.0886	1038
MUSCLE	52.729	1.7388	1047
HEART	54.814	2.2561	1030
WHITE.MATTER	36.167	1.215	1038
STOMACH	62.158	2.2105	1050
GLANDS	57.201	1.9679	1050
BLOOD.VESSEL	42.531	1.4353	1040
LIVER	43.035	1.6864	1030
GALL.BLADDER	57.634	2.059	1030
SPLEEN	52.449	2.238	1054
CEREBELLUM	44.804	2.1014	1038
BONE.(cortical)	11.381	0.39431	1990
CARTILAGE	38.77	1.7559	1097
LIGAMENTS	43.121	1.6847	1220
SKIN/DERMIS	38.007	1.464	1125
INTESTINE.(large)	53.879	2.0383	1043
TOOTH	11.381	0.39431	2160
GRAY.MATTER	48.911	1.8077	1038
EYE.(lens)	44.625	1.504	1053
LUNG.(outer)	48.381	1.6825	1050
INTESTINE.(small)	54.425	3.1731	1043
EYE.(sclera/wall)	52.628	2.0332	1026
LUNG.(inner)	20.477	0.80416	260
PANCREAS	57.201	1.9679	1045
BLOOD	58.264	2.5448	1058
CEREBRAL.SPINAL.FLUI	66.243	3.4578	1007
EYE.(retina)	52.628	2.0332	1026
EYE.(aqueous.humor).	68.208	2.4781	1009
KIDNEYS	52.742	2.4295	1050
BONE.MARROW	5.2969	0.095037	1040
BLADDER	18.001	0.68532	1030
TESTICLES	57.551	2.1676	1044
BONE.(cancellous)	18.548	0.80517	1920

Table 6.2: Human tissues properties at 5200 MHz

Tissue	ε_r	σ (S / m)	ρ (kg / m^3)
AIR.(internal)	1	0	1300
BILE	64.5985	6.22219	1010
BODY.FLUID	65.5629	5.71315	1010
EYE.(cornea)	47.4335	4.95126	1076
FAT	5.0104	0.254695	916
LYMPH	53.0226	4.91859	1040
MUSCOUS.MEMBRANE	39.3647	3.76124	1040
NAILS.(toe.&.finger)	9.94599	1.0101	1030
NERVE.(spine)	27.7218	2.55136	1038
MUSCLE	49.2781	4.26699	1047
HEART	49.9416	5.10584	1030
WHITE.MATTER	33.2379	3.01319	1038
STOMACH	57.5392	5.43749	1050
GLANDS	53.0226	4.91859	1050
BLOOD.VESSEL	39.0306	3.73086	1040
LIVER	38.9769	4.02641	1030
GALL.BLADDER	54.4994	4.9104	1030
SPLEEN	47.8811	4.94994	1054
CEREBELLUM	40.7832	4.38914	1038
BONE.(cortical)	9.94599	1.0101	1990
CARTILAGE	33.2496	4.28557	1097
LIGAMENTS	37.9105	4.53603	1220
SKIN/DERMIS	35.61	3.21864	1125
INTESTINE.(large)	49.4063	4.82415	1043
TOOTH	9.94599	1.0101	2160
GRAY.MATTER	44.8612	4.31515	1038
EYE.(lens)	41.4273	3.757	1053
LUNG.(outer)	44.5829	4.15506	1050
INTESTINE.(small)	49.6503	5.99481	1043
EYE.(sclera/wall)	48.7005	4.73333	1026
LUNG.(inner)	18.8515	1.80831	260
PANCREAS	53.0226	4.91859	1045
BLOOD	53.6	5.66509	1058
CEREBRAL.SPINAL.FLUI	61.5861	6.89839	1007
EYE.(retina)	48.7005	4.73333	1026
EYE.(aqueous.humor).	65.5629	5.71315	1009
KIDNEYS	47.7298	5.1747	1050
BONE.MARROW	5.01891	0.246337	1040
BLADDER	16.5669	1.61034	1030
TESTICLES	53.2	5.14175	1044
BONE.(cancellous)	15.8811	1.89535	1920

6.3 Validation of FDTD Technique

The FDTD technique was validated by calculating the electric field at a line located 4 cm from the balanced antenna, as shown in Figure 6.7, a flow chart summarising the calculation process is given in Figure 6.8. The process is launched from the hyb.90 code which generates the free space fields inside the Huygens' surface box, these fields act as the input to the gen.90 code which calculates the back-scattered fields inside the Huygens' surface. From here, the new surface currents were inferred. Later, Js in the source code was run to compute the new E and H values as the new input source to the gen.90 code. This process will continue until the maximum number of iteration was achieved.

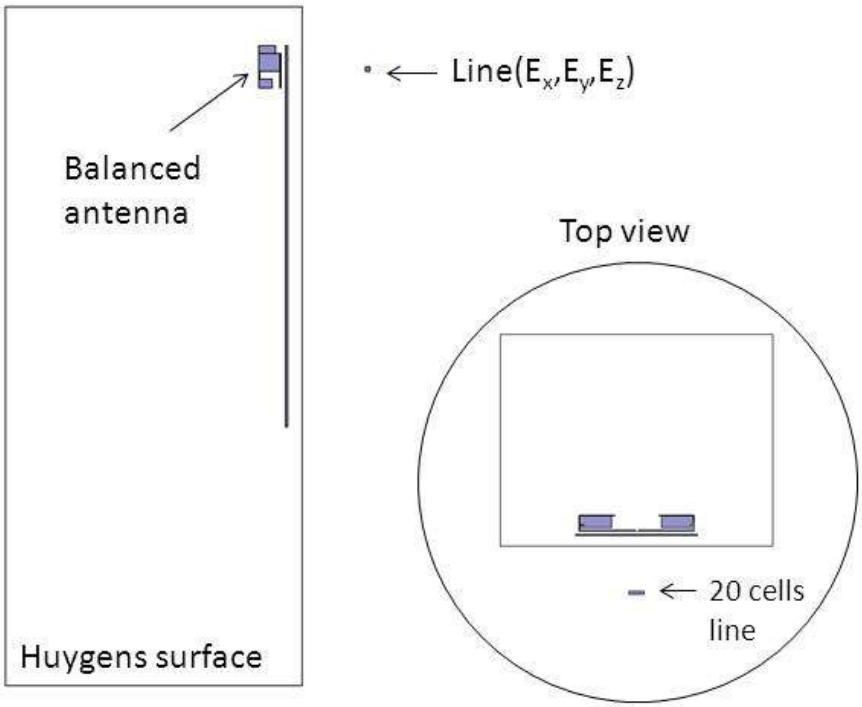

Figure 6.7: The position of electric field at a line 4 cm from the balanced antenna

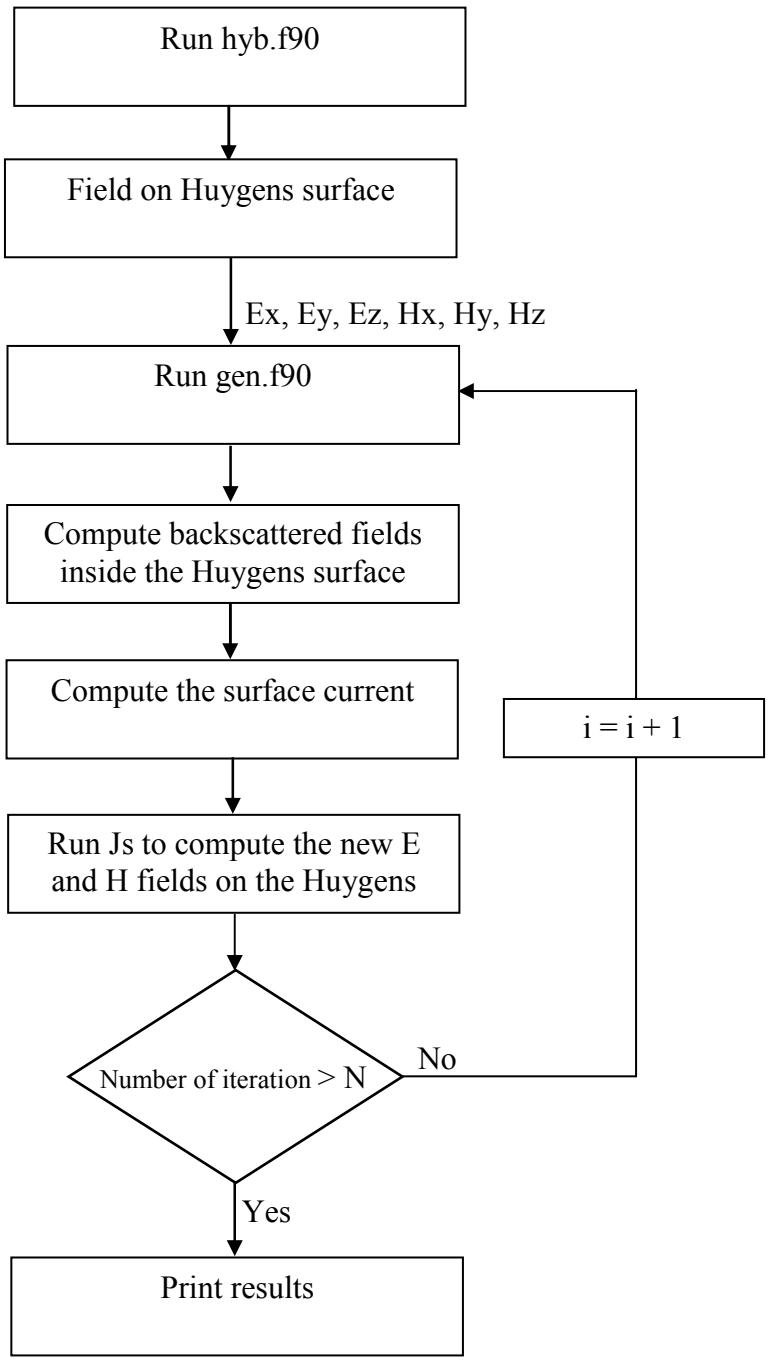

Figure 6.8: Flow chart to simulate the fields located 4 cm from the balanced antenna.

Two cases were considered; near field and far field. In line with our expectations, Figure 6.9 showed that the magnitude of the electric field has similar output for the FDTD and MoM methods, for both Ex and Ez. In regards to the far field, Figure 6.10 illustrates the far field components of the cases under investigation for yz and xy planes. From the pattern in the variations it is clear that the fields are quite similar to each other. It can be safely concluded that proof of concept has been made.

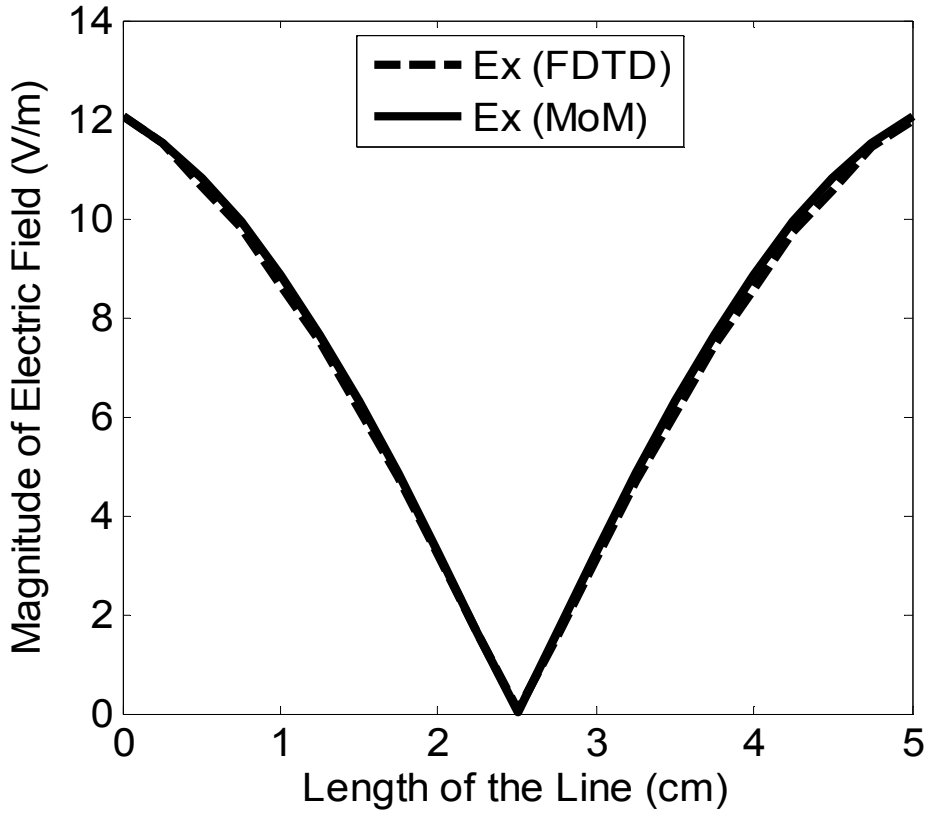

(a)

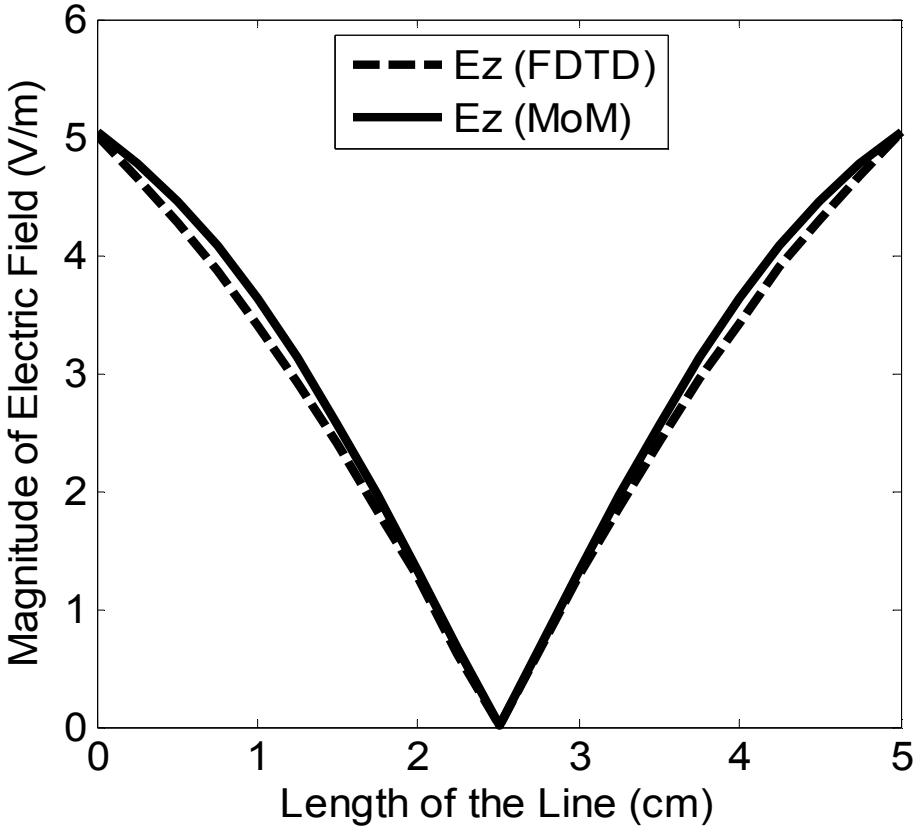

(b)

Figure 6.9: The electric field obtained from FDTD and MoM: (a) Ex; (b) Ez

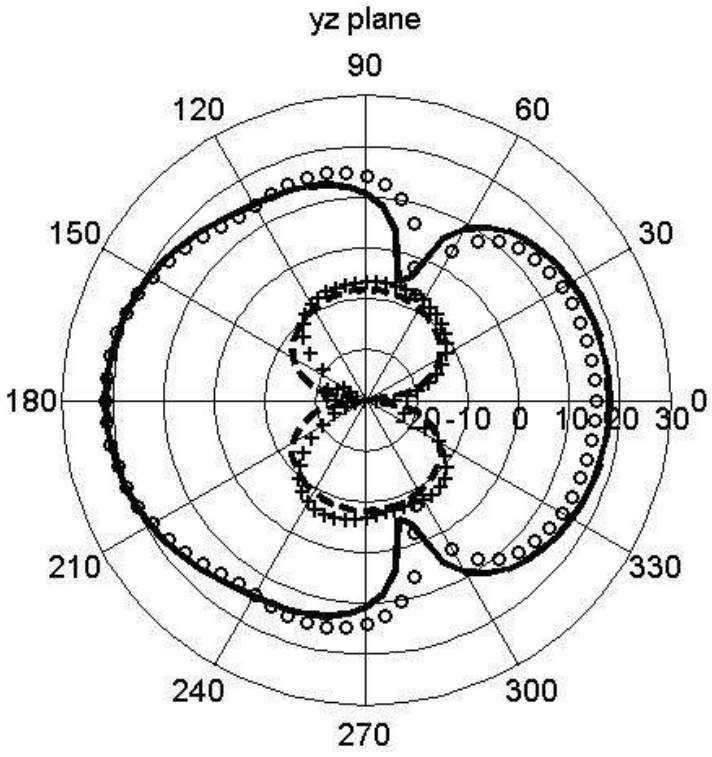

(a)

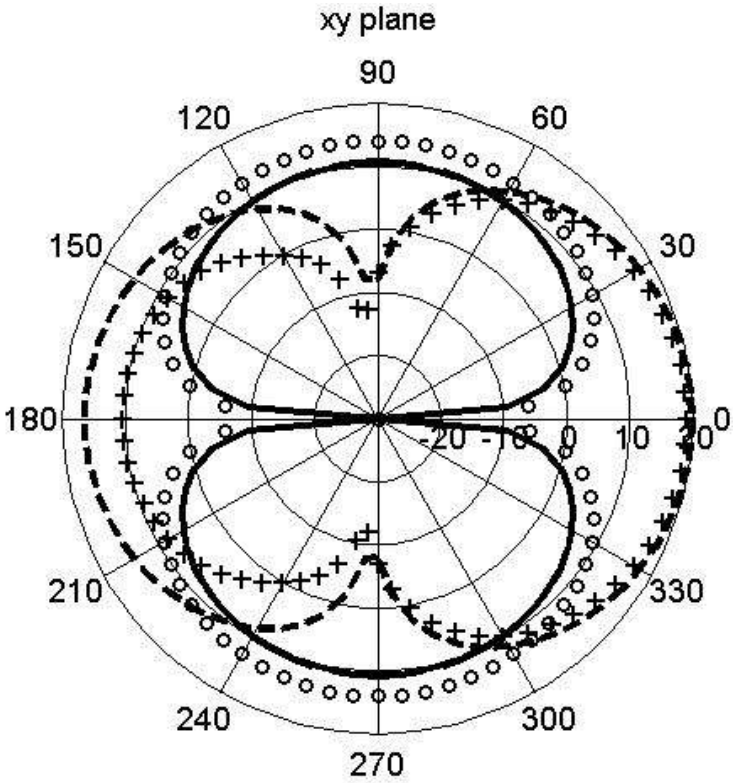

(b)

Figure 6.10: The far field obtained from FDTD and MoM: (a) yz; (b) xy

6.4 Near Field and Far Field

In order to investigate the performance of the antenna in proximity to the human body, the near and far field radiation of the antenna for different locations has been considered, as illustrated in Figure 6.3. A total of 32 locations were investigated: 16 locations on the back, and 16 on the front. Due to the electric field distribution of these points being quite similar to one another, only one position for each case was demonstrated. The total near field distribution at 2.45 GHz for two central vertical slices is shown in Figure 6.11 for the vertically polarised antenna position. These fields are normalised to 1 watt input power and the scale shown is in dB. It is clear that the distributions within the human tissues, and in their immediate neighbourhood, were not comparable to the fields pointing away from the antenna and the human body. This figure also shows the variations of the standing wave due to the conducting ground.

Further simulations were performed on the radiation performance using the same antenna locations, but with different polarisations and they are shown in Figure 6.12. Similarly, the near field distributions at 5.2 GHz are presented in Figure 6.13 and Figure 6.14 for horizontal and vertical polarization respectively. It can be also observed when the antenna is very close to the human tissue, the surrounded fields are much stronger, as indicated by the red colour distribution in the figures.

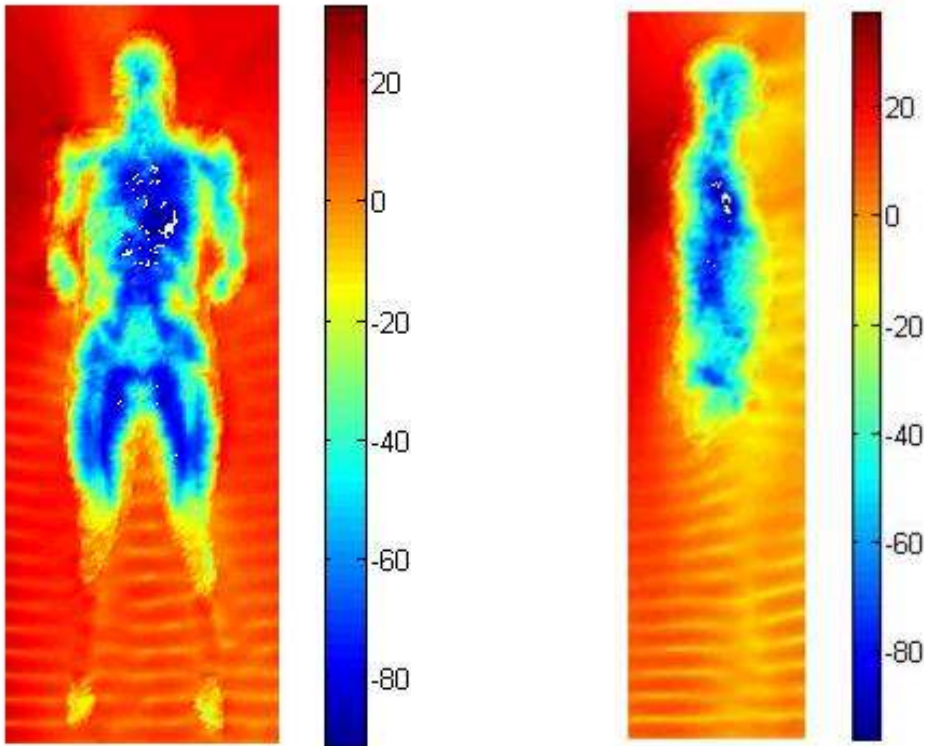

(a)

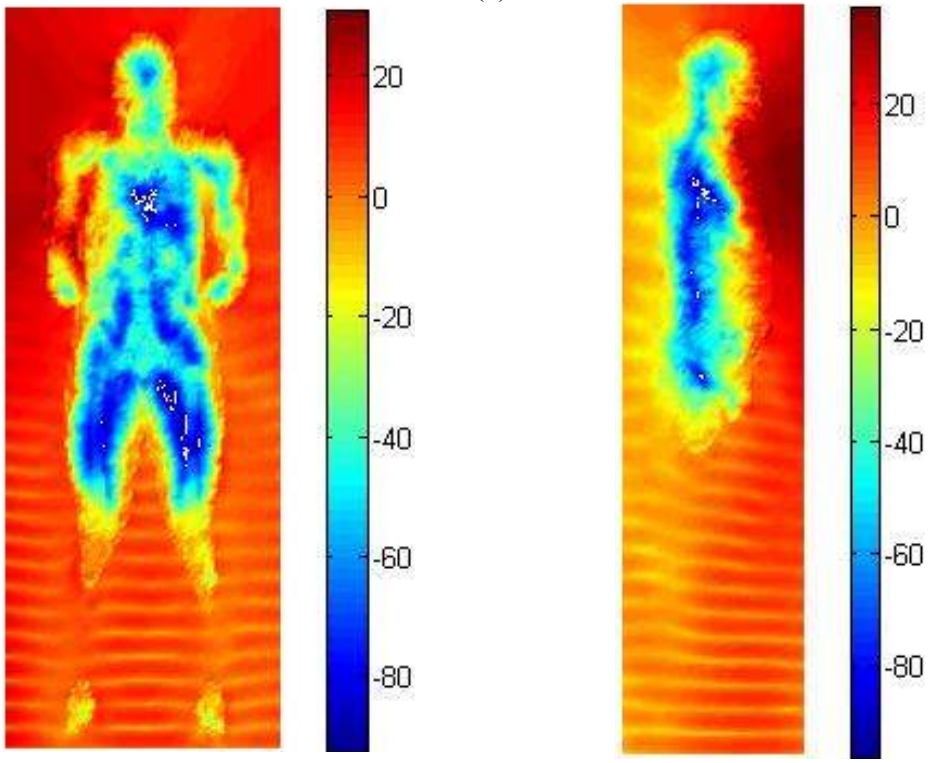

(b)

Figure 6.11: Total electric field (dB) distributions at 2.45 GHz when the mobile located in vertical position, (a) Back Location, (b) Front Location

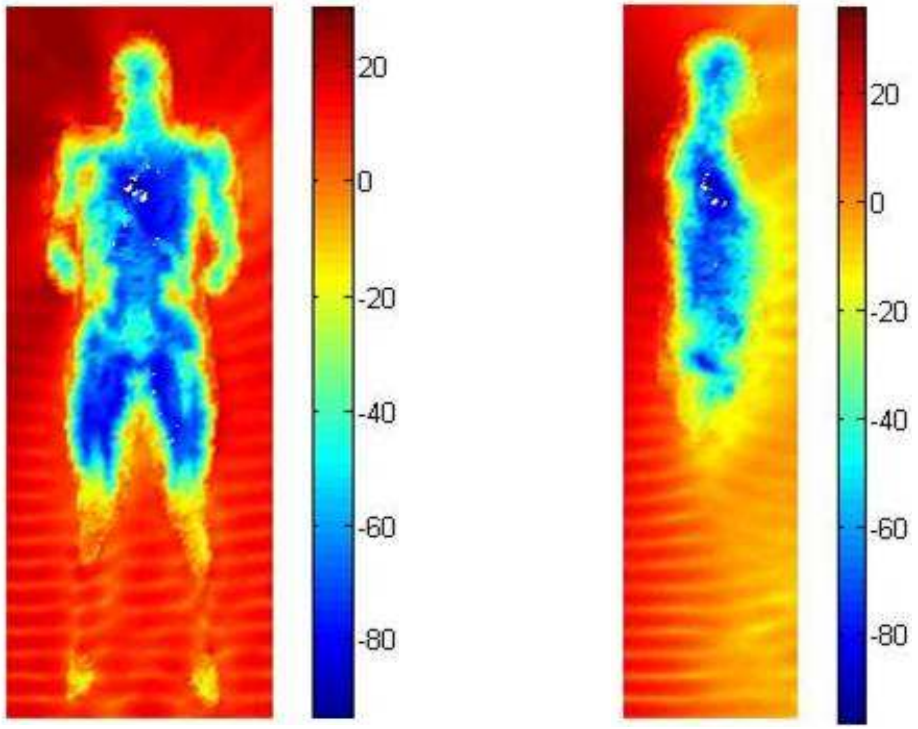

(a)

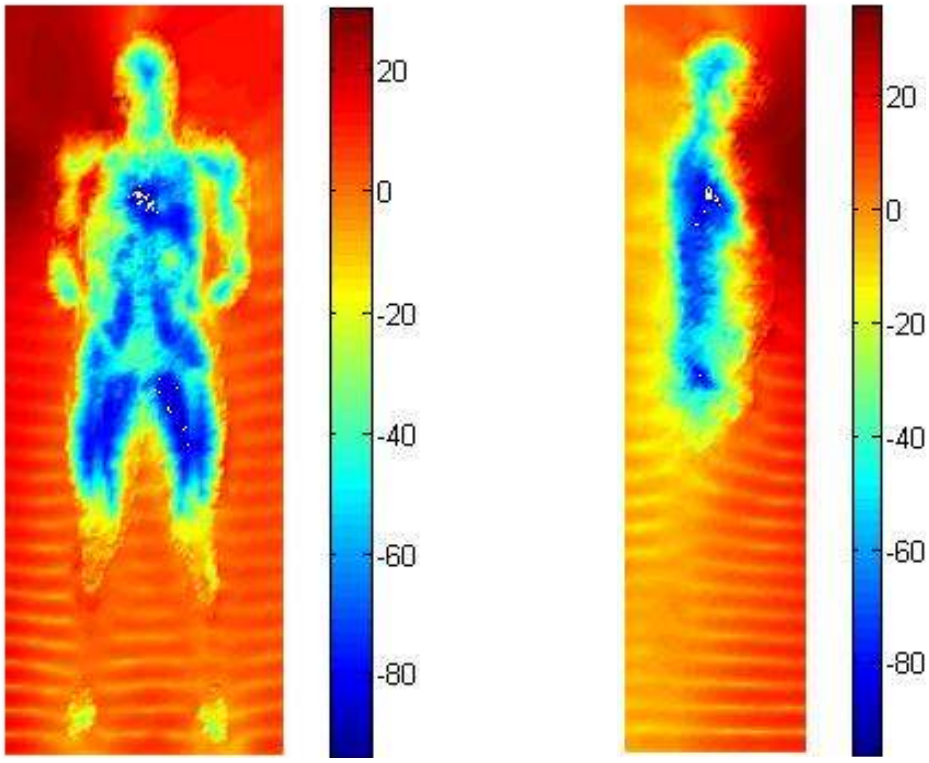

(b)

Figure 6.12: Total electric field (dB) distributions at 2.45 GHz when the mobile located in horizontal position, (a) Back Location,(b) Front Location

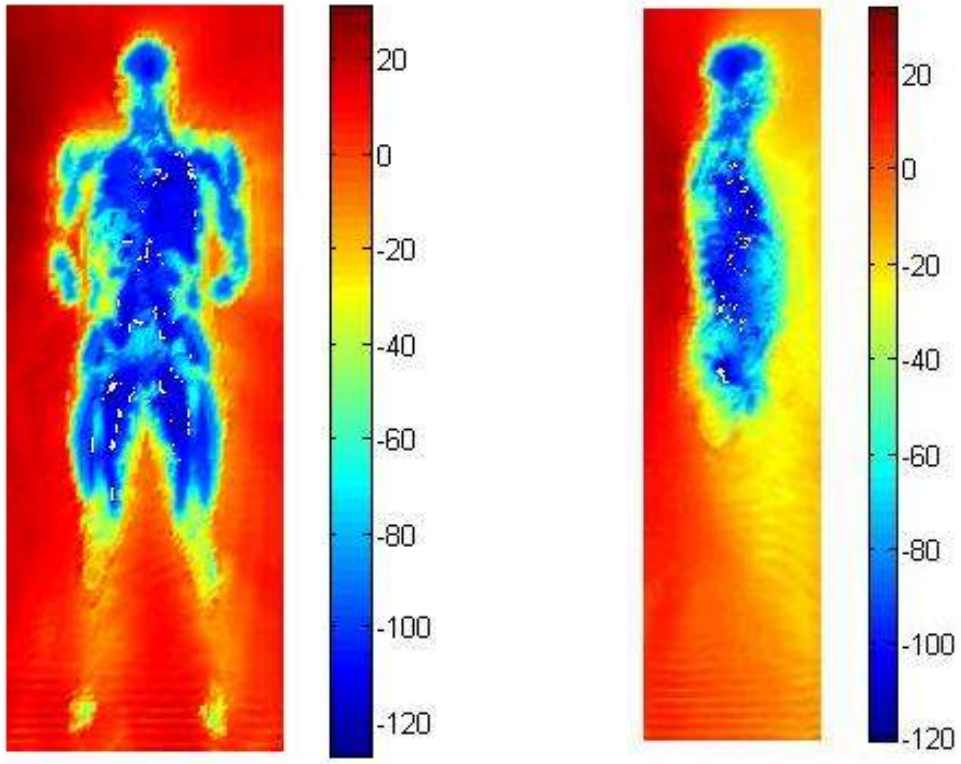

(a)

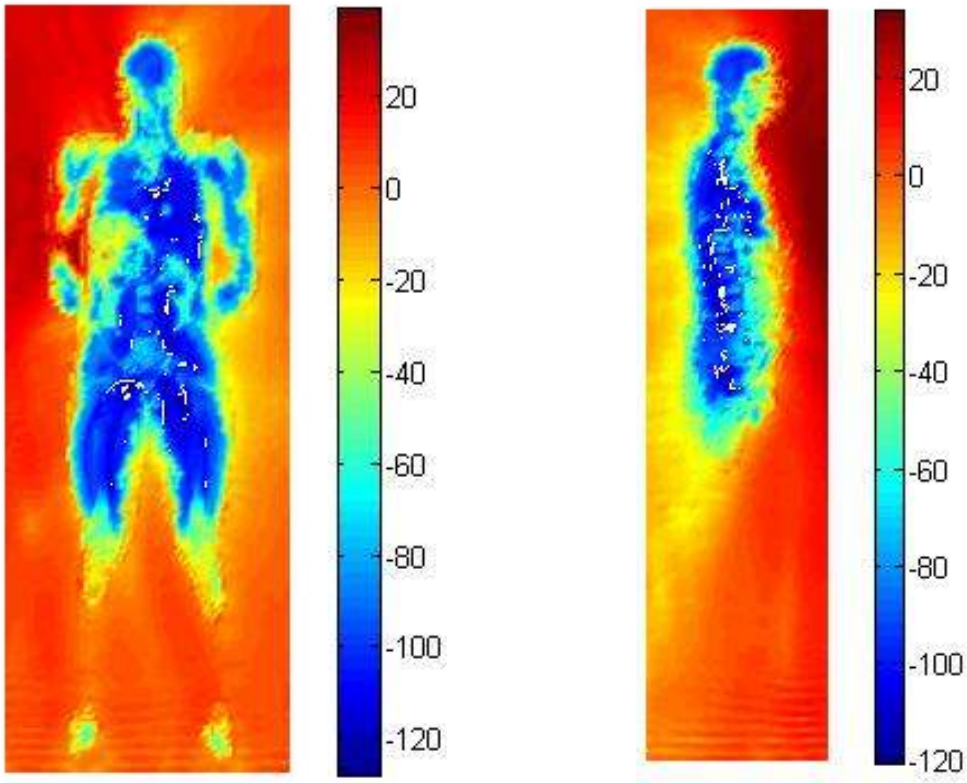

(b)

Figure 6.13: Total electric field (dB) distributions at 5.2 GHz when the mobile located in vertical position, (a) Back Location, (b) Front Location

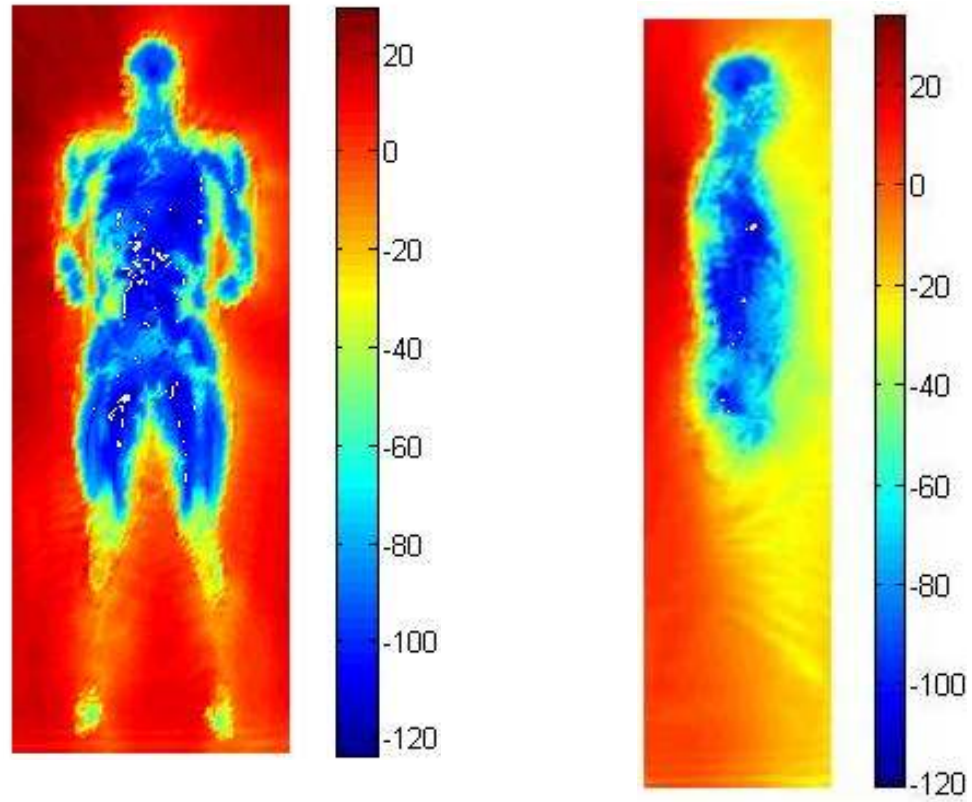

(a)

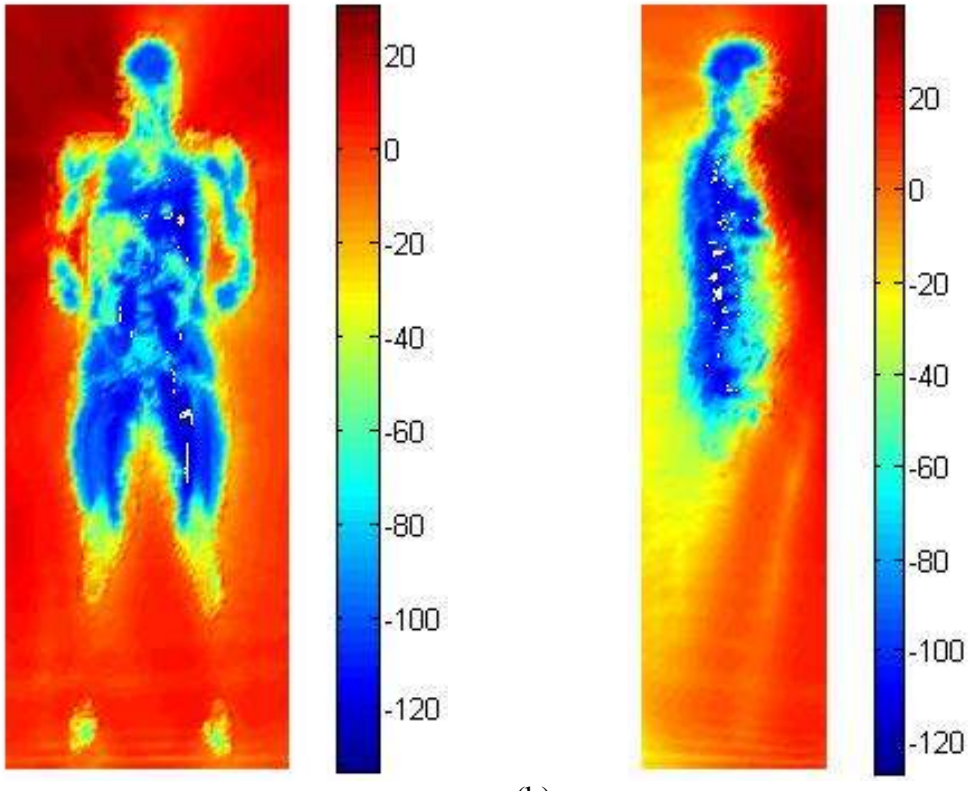

(b)

Figure 6.14: Total electric field (dB) distributions at 5.2 GHz when the mobile located in horizontal position, (a) Back Location,(b) Front Location

The results of the investigation were conclusive, and made clear that regardless any change in the polarisation, the electric field distribution was almost the same when the mobile positions were changed. Again, as one may expect with the electric field distribution of these points being quite similar to each other, only one position for each case was demonstrated.

The far field components at 2.45 GHz for the cases under investigation are shown in Figure 6.15 and Figure 6.16. Figure 6.17 and Figure 6.18 are presented the far field distribution for 5.2 GHz. The fields presented are normalised to one 1 watt input power for all y-z, x-z and x-y planes. The pattern variations in each case show that the fields were stronger in the direction pointing to the normal axis of the handset antenna, and away from the human body. It is clear from the results that the reduced field magnitudes caused by the shadowing effect of the human body fall approximately between 20 dB and 25 dB. In addition, due to strong coupling of the human tissue with induced surface currents of the antenna structure, the cross polar filed components were increased as indicated in the figures.

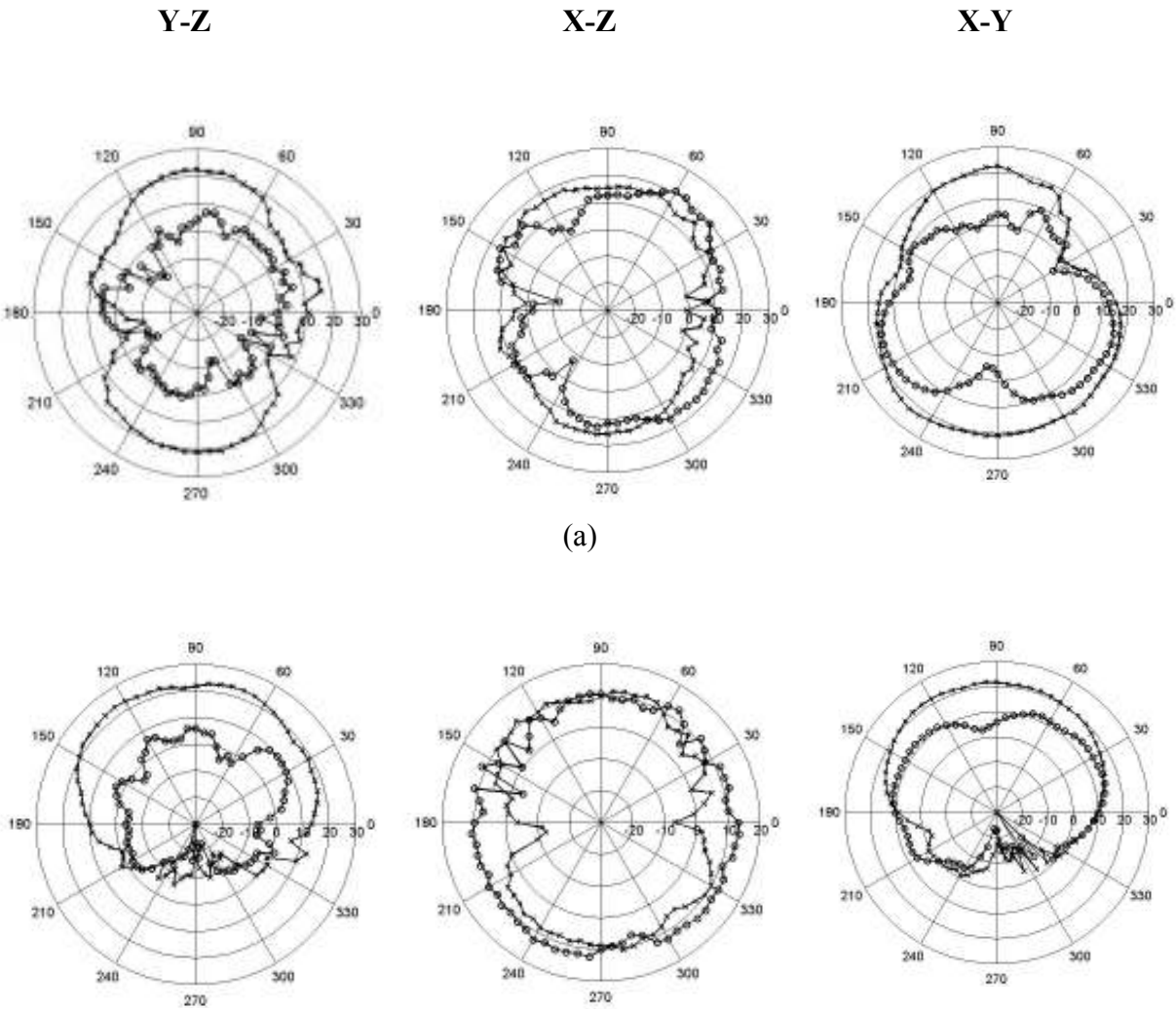

Figure 6.15: The far field patterns at 2.45 GHz yz, xz and xy planes; for vertical polarisation (a) Back Location,(b) Front Location; where 'o-o-o' computed E_θ and 'x-x-x' computed E_ϕ.

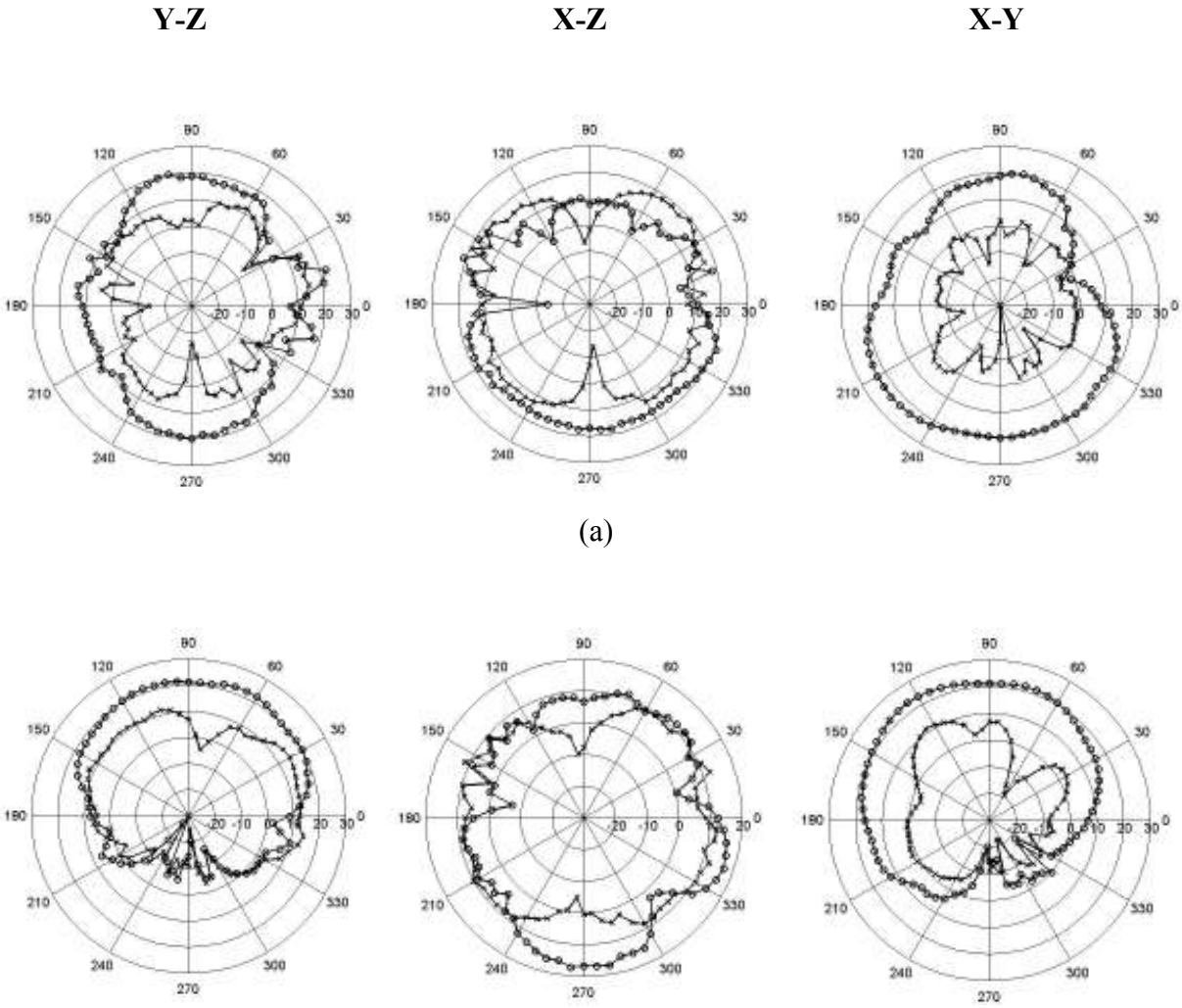

Figure 6.16: The far field patterns at 2.45 GHz yz, xz and xy planes; for horizontal polarisation (a) Back Location, (b) Front Location; where 'o-o-o' computed E_θ and 'x-x-x' computed E_ϕ.

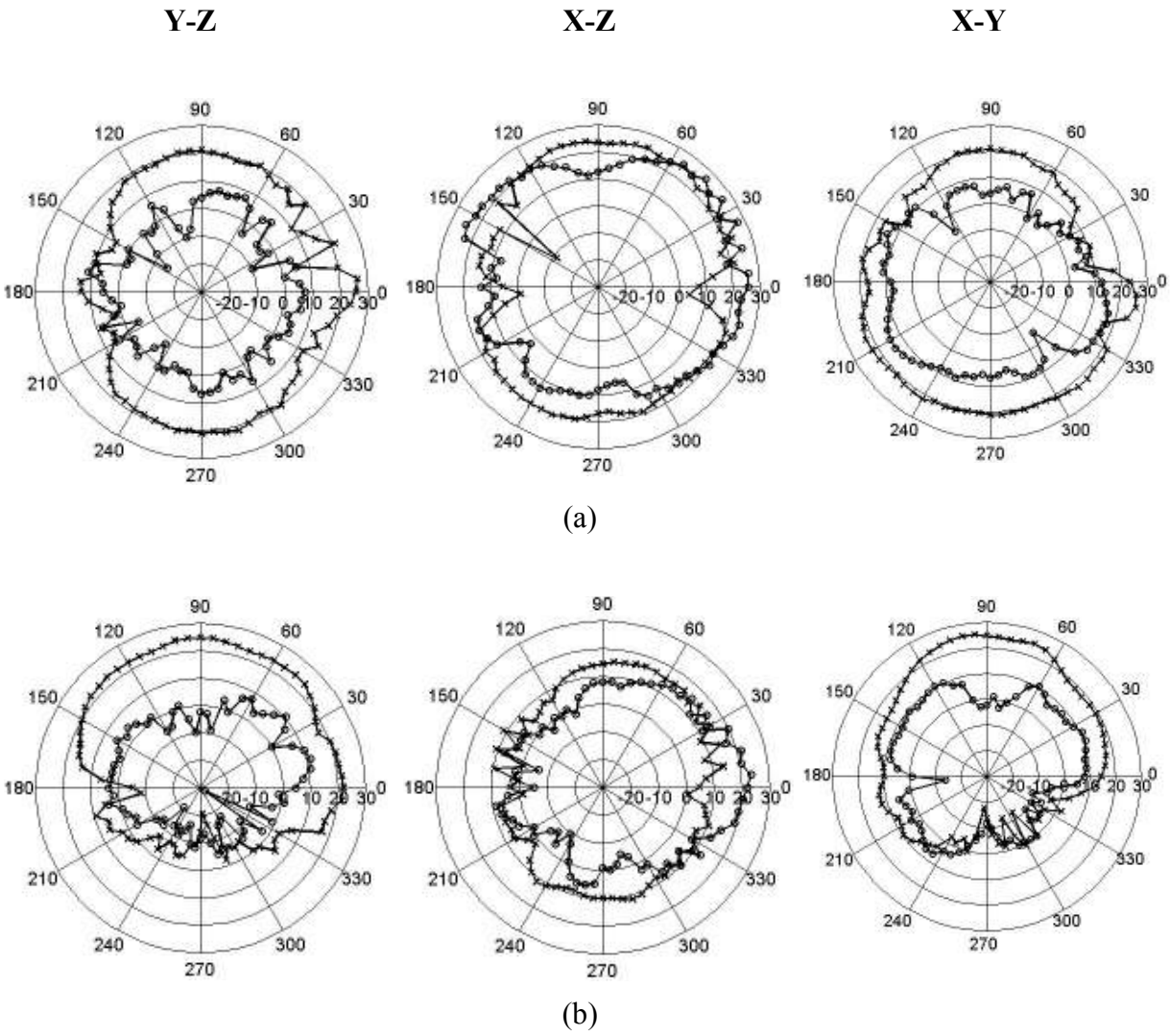

Figure 6.17: The far field patterns at 5.2 GHz yz, xz and xy planes; for vertical polarisation, (a) Back Location, (b) Front Location; where 'o-o-o' computed E_θ and 'x-x-x' computed E_ϕ.

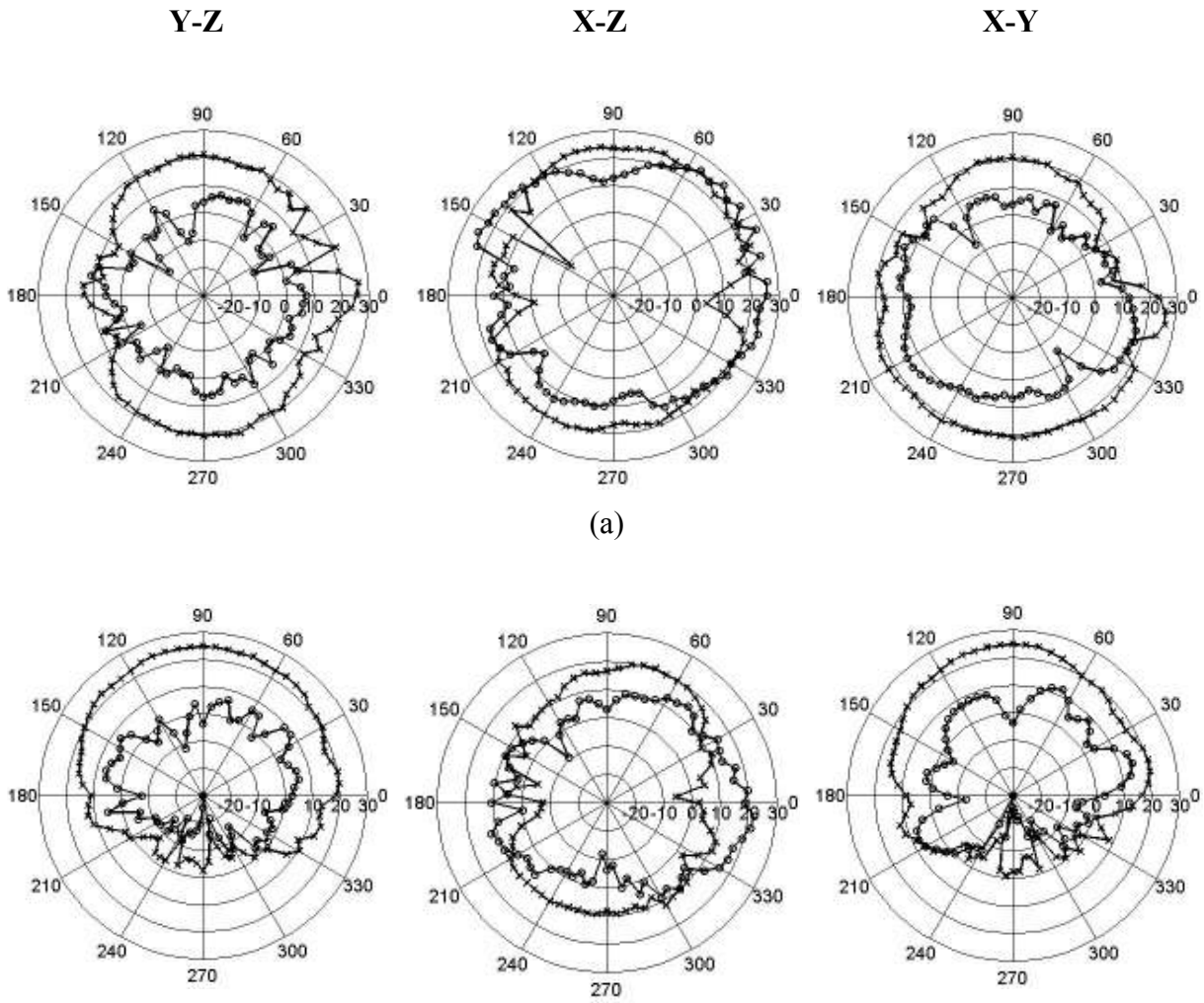

Figure 6.18: The far field patterns at 5.2 GHz yz, xz and xy planes; for horizontal polarisation, (a) Back Location, (b) Front Location; where 'o-o-o' computed E_θ and 'x-x-x' computed E_ϕ.

6.5 Cumulative Distribution Function of the Radiation Efficiency

The absorbed power and radiated power are recorded from the simulation results. The radiation efficiency for the balanced antenna can be calculated using the following formula:

$$\text{efficiency } (\eta) = \frac{\mathrm{P_{radiated}}}{\mathrm{P_{radiated}} + \mathrm{P_{absorbed}}}$$

The cumulative distribution function (CDF) is evaluated for each location in order to estimate the probability of the power absorbed and radiation efficiency on the human body. Figure 6.19 shows the radiation efficiency and the associated CDF evaluated when the mobile placed on these locations for horizontal and vertical polarisation. Figure 6.20 shows the absorbed power over radiated power ($P_{absorbed} / P_{radiated}$), and the associated CDF evaluated when the mobile placed on these locations for horizontal and vertical polarisation. Figure 6.21 and Figure 6.22 illustrate the related histogram of radiation efficiency and $P_{absorbed} / P_{radiated}$ for horizontal polarised antenna. It is a display of statistical data that shows the power ratio distribution function for various locations. It is more or less shown indication of the areas where radiation efficiency and $P_{absorbed} / P_{radiated}$ can be identified somehow from the graph. However, for the limited data collected, it is difficult to have a strong confidence on these distributions. In addition, it should be noted that the probability density function has been drawn subject to 16 points over the width 0 to 1 as illustrated in the figures. The histogram of radiation efficiency and $P_{absorbed} / P_{radiated}$ for vertical polarised antenna is illustrated in Figure 6.23 and Figure 6.24 respectively.

The CDF of radiation efficiency and absorbed power over radiated power is difficult to predict from the results collected due to the limited sample size generated through the simulation. Recognising the constraints surrounding memory and simulation time, a total of 32 different locations (in line with the rest of the simulation) have been considered, with a view to extrapolating the necessary data. The data from these locations was combined to obtain probability of the radiation efficiency and absorbed power over radiated power, and can be obtained from Figure 6.19 and Figure 6.20.

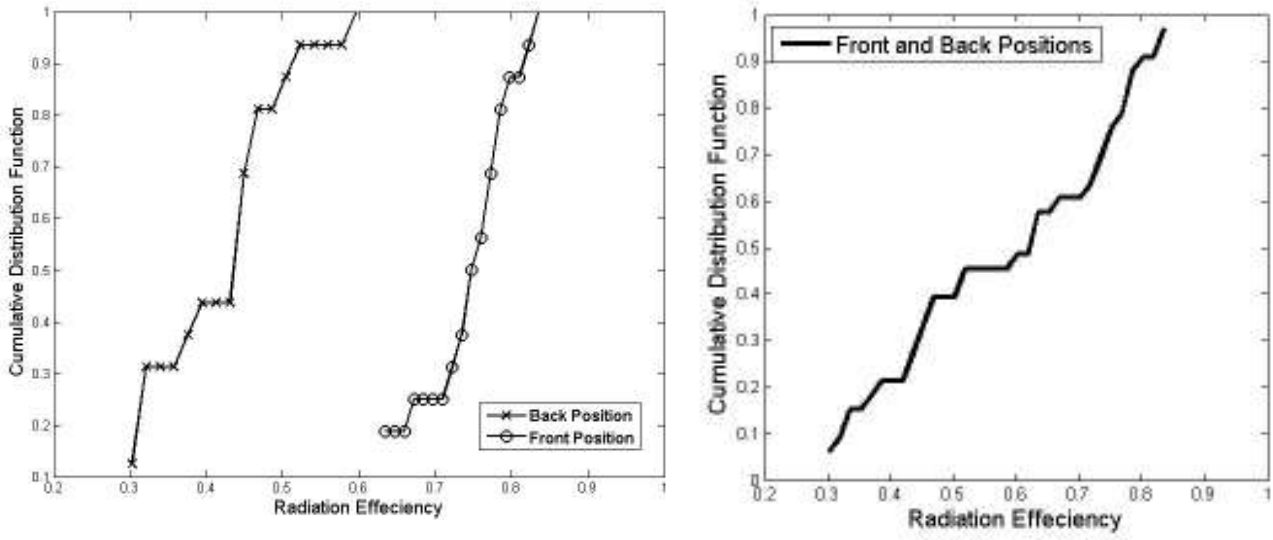

(a)

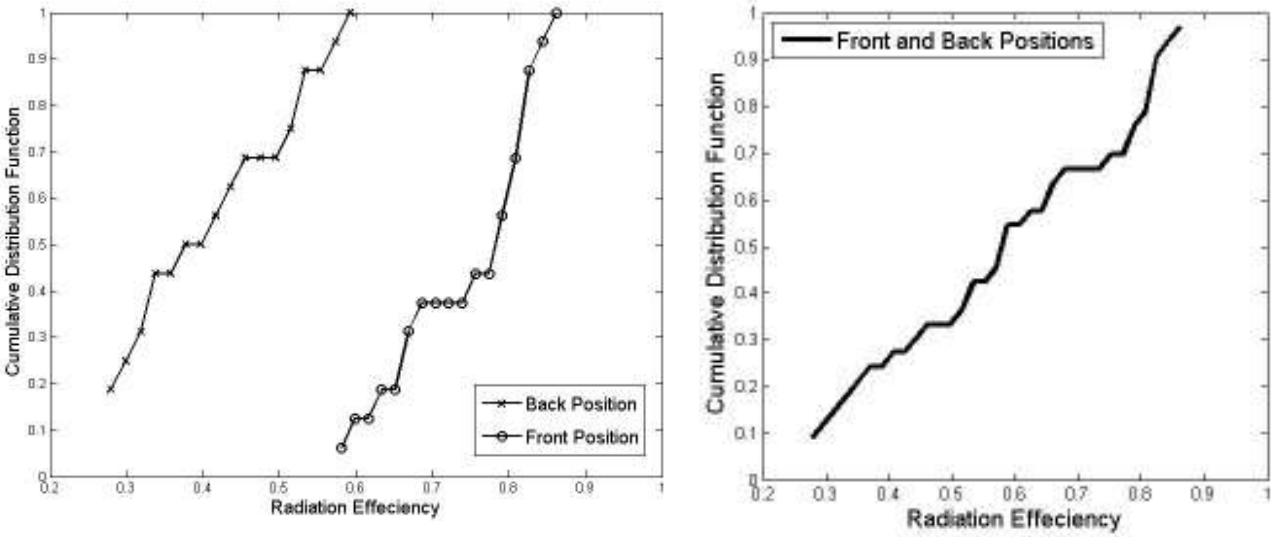

(b)

Figure 6.19: the cumulative distribution function of the radiation efficiency when (a) Vertical polarisation , (b) Horizontal polarisation

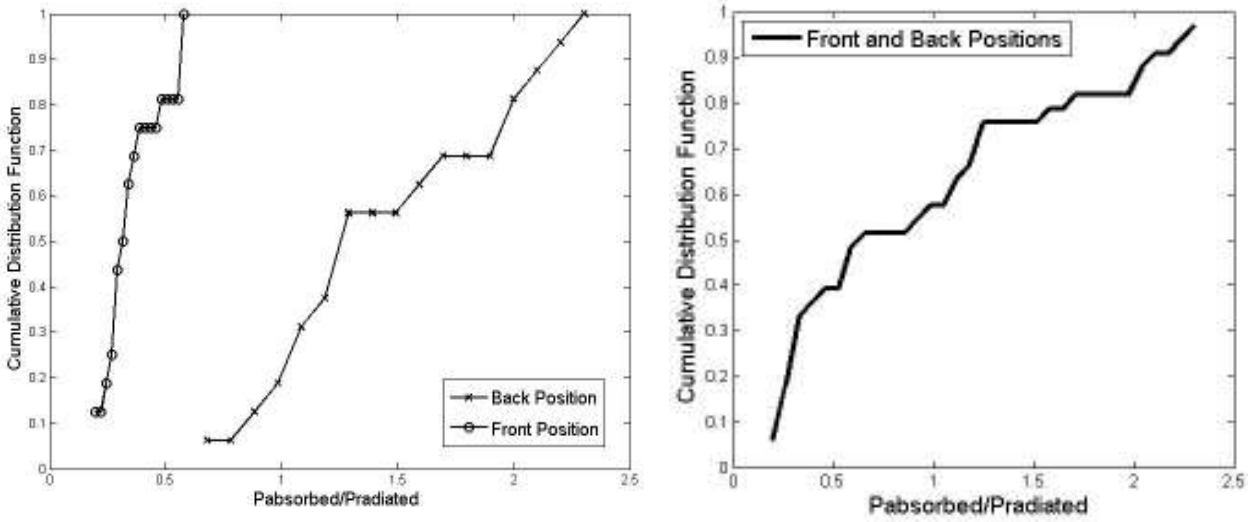

(a)

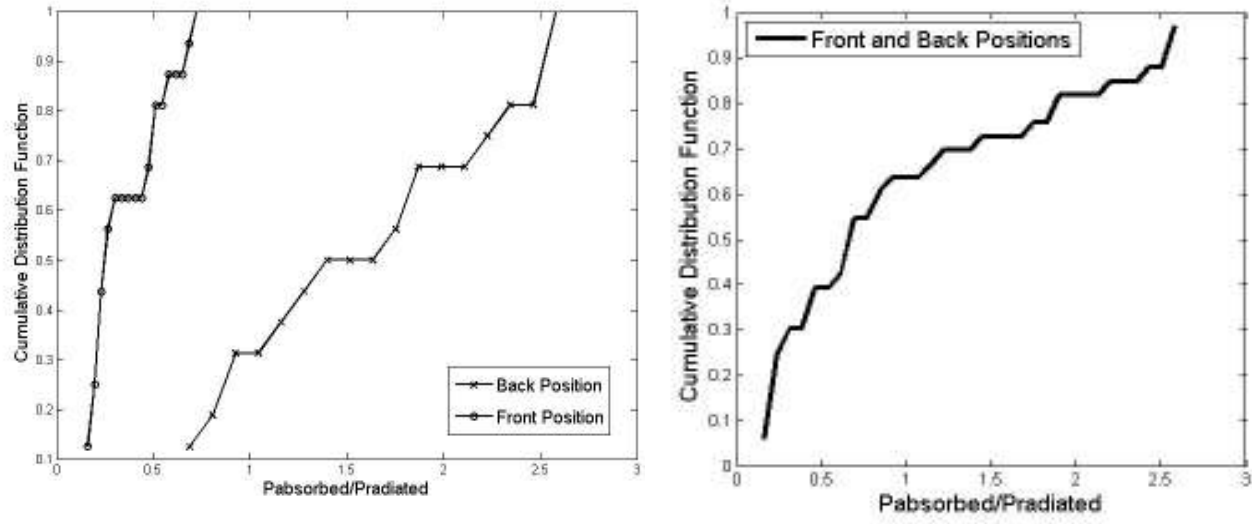

(b)

Figure 6.20: the cumulative distribution function of the $P_{absorbed}/P_{radiated}$ when (a) Vertical polarisation, (b) Horizontal polarisation

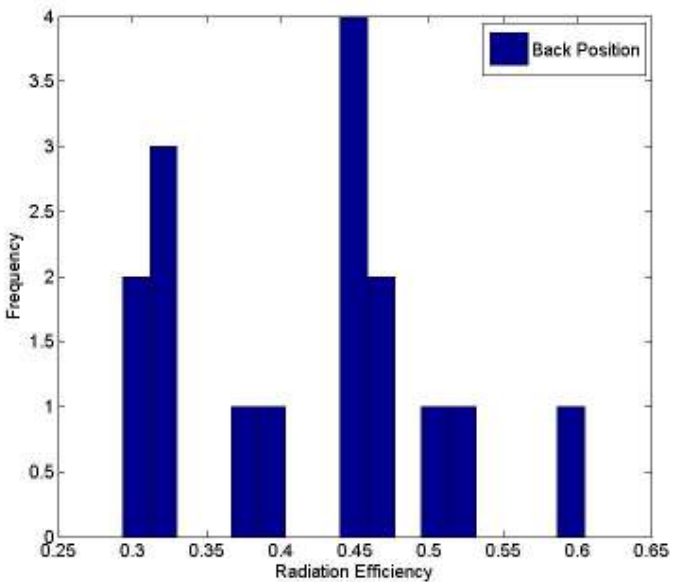

(a)

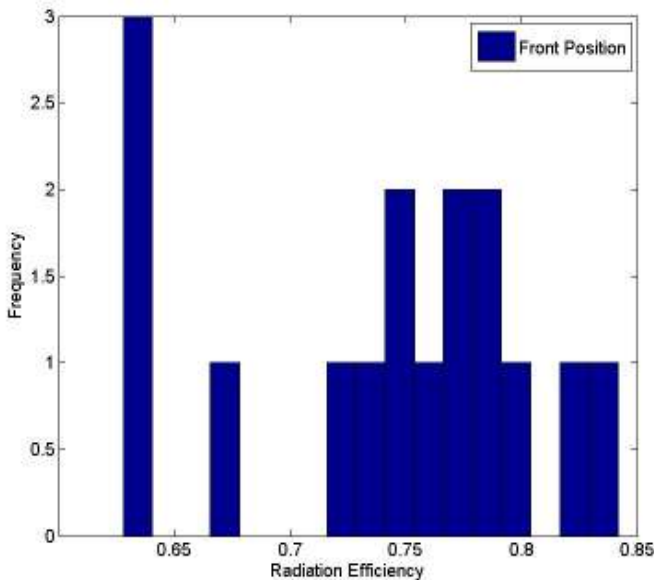

(b)

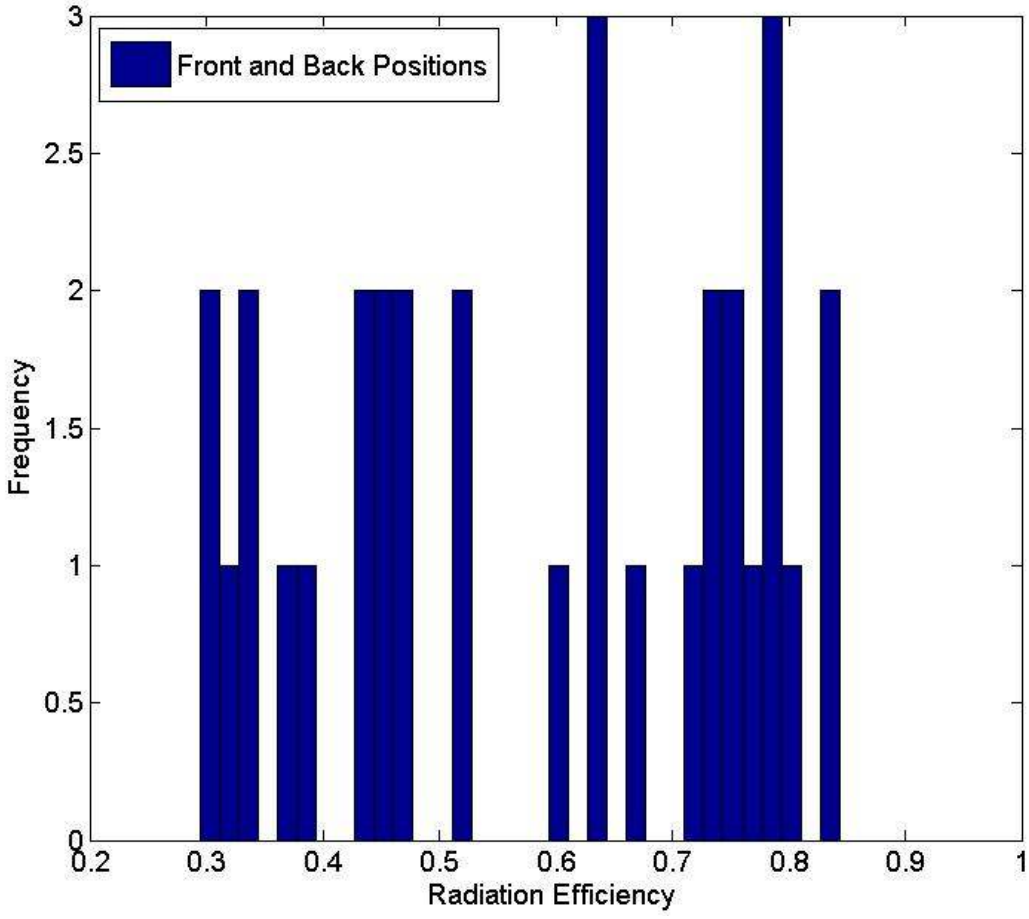

(c)

Figure 6.21: Histogram of radiation efficiency: (a) back position, (b) front position, (c) total, for horizontal polarised antenna

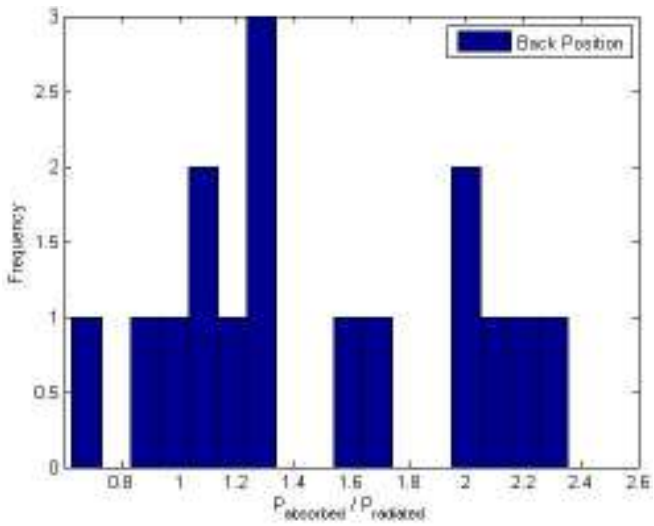

(a)

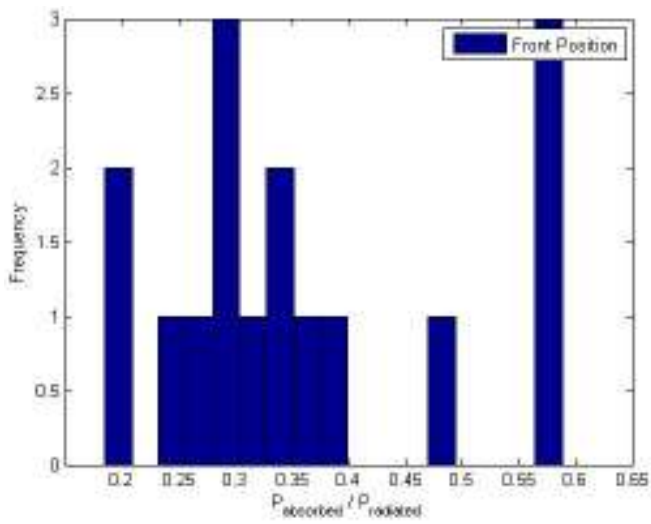

(b)

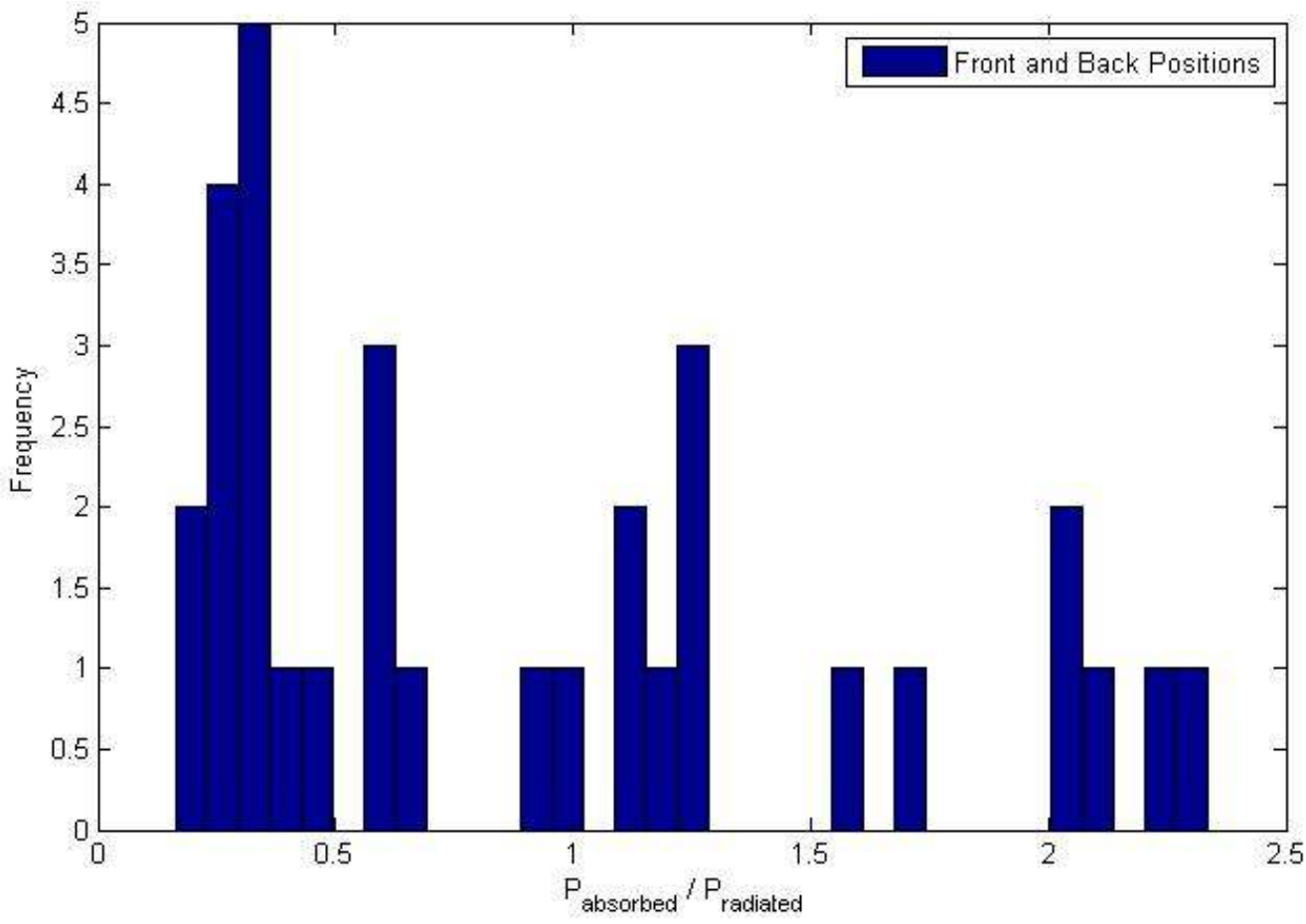

(c)

Figure 6.22: Histogram of $P_{absorbed} / P_{radiated}$,: (a) back position, (b) front position, (c) total, for horizontal polarised antenna

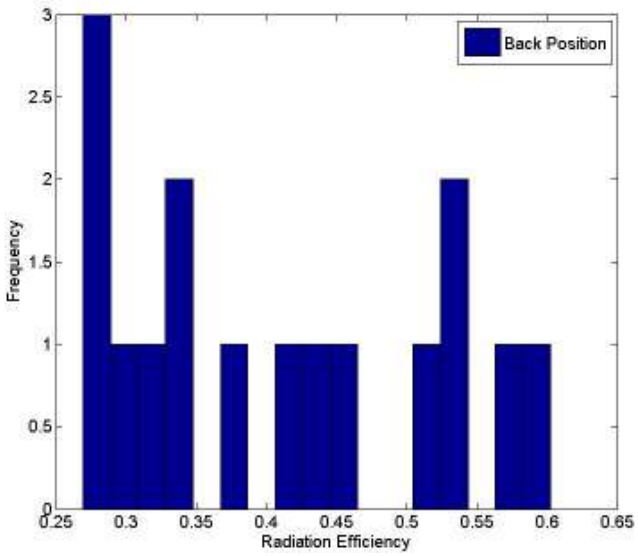

(a)

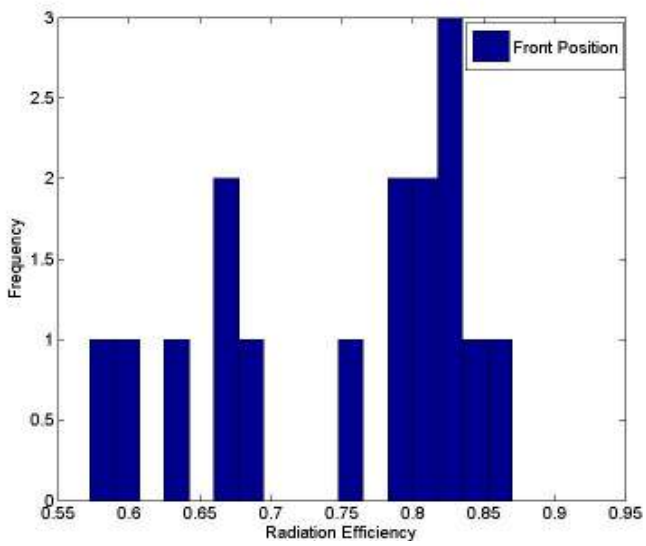

(b)

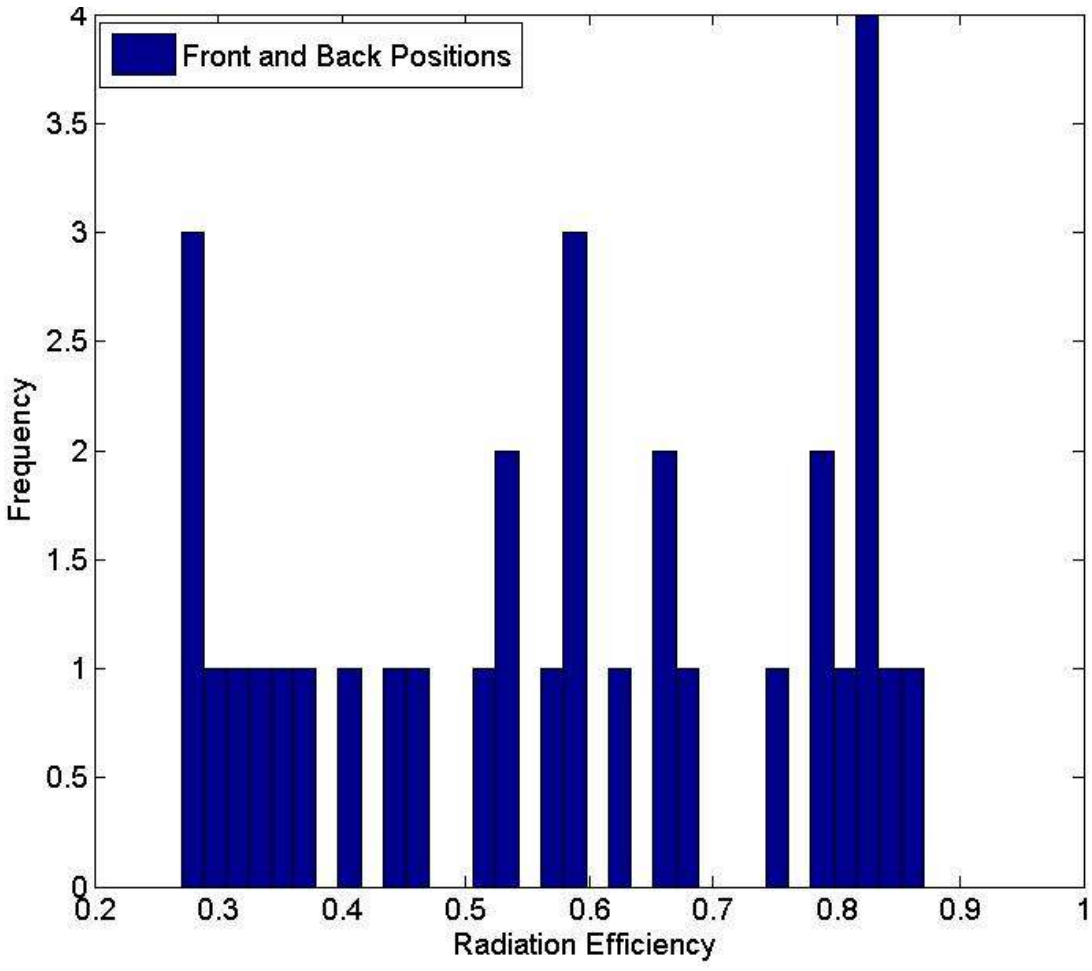

(c)

Figure 6.23: Histogram of radiation efficiency: (a) back position, (b) front position, (c) total, for vertical polarised antenna

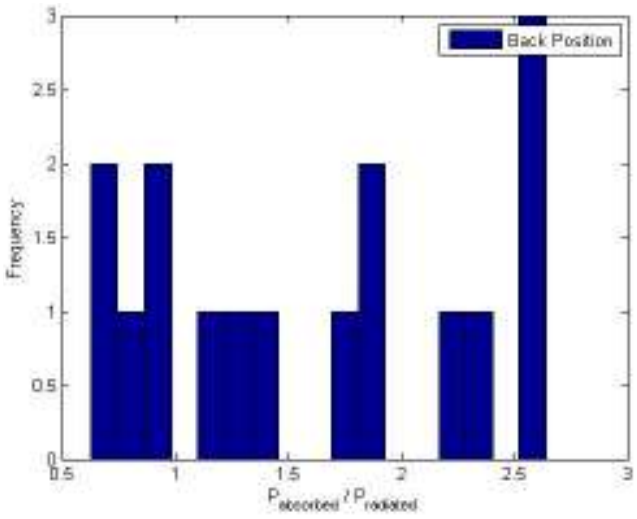

(a)

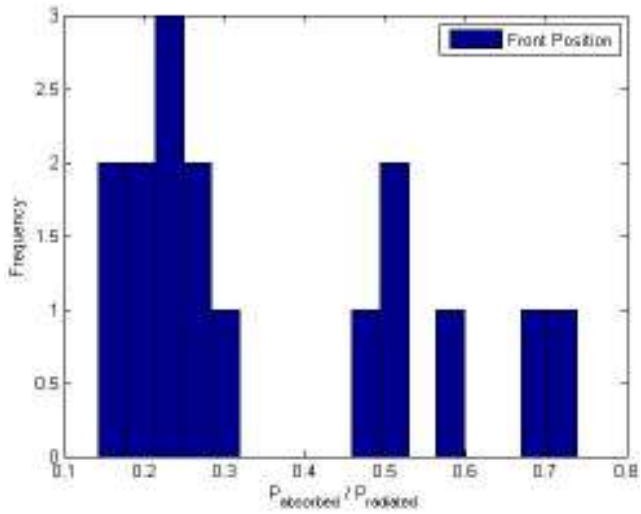

(b)

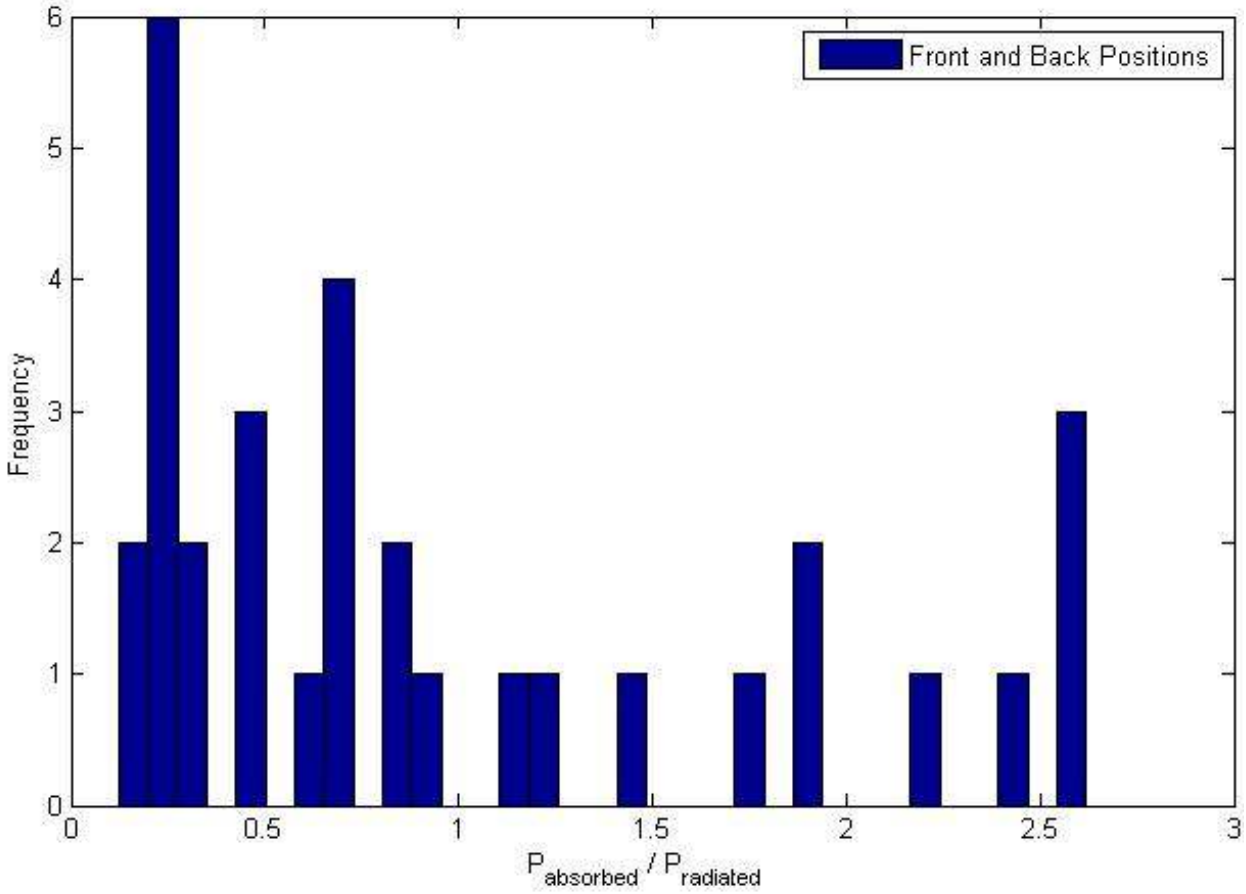

(c)

Figure 6.24: Histogram of $P_{absorbed}$ / $P_{radiated}$: (a) back position, (b) front position, (c) total, for vertical polarised antenna

The radiation efficiency values increase as the handset moves from the back to the front of the human body. Hence, these figures clearly indicate that the CDF achieves better radiation efficiency (typically 40% better) and consistent impedance matching for both horizontal and vertical polarisations when the mobile been placed on the front of the human model compared to the case of the back position. This may be accounted for by a loss of tissue characteristics in the front region, and the greater degree of absorbed power, as may be seen in the figure.

Further comparison of the figures shows that the qualitative details of the CDF results, for the horizontal and vertical polarisations, at each location are very similar, which is in line with expectations. Furthermore, using the data from Figure 6.19, it can be seen that the standard deviation of the radiation efficiency is less for the mobile in the front facing, as distinct from back facing positions. Taking the previous simulation results into account, we may safely conclude that altering the position of the antenna over the front region will not result in a large dispersion in the radiation efficiency.

6.6 Conclusions

Effective simulation techniques for antenna performance when in close proximity to the human body are needed for a variety of potential applications. This chapter has considered the practical application of a hybrid FDTD / MoM simulation technique in characterising the impact of the human body on the performance of a dual band balanced antenna. The antenna design from the previous chapter was used, and a total of thirty-two body locations were selected, front and back, each point being evaluated for horizontal and vertical polarisation states. The MoM calculation, based on NEC, was used to obtain the free space electric and magnetic fields generated by the antenna, from which the equivalent magnetic and electric source conditions were derived on a Huygens' surface for each time step of the FDTD code. The FDTD analysis applies to the whole structure at the point of interest, particularly within the human body in the neighbourhood of the excitation source. Full near and far field data was extracted, this was used to develop a better understanding of the impact of regions of tissue facing, and offset from, the antenna. The results were presented statistically, using the cumulative distribution function of the radiation efficiency and absorbed power to radiated power ratio over the various locations. The results support the conclusion that there was a clear improvement in the front compared to the back.

6.7 References

[1] K. S. Yee, "Numerical solution of initial boundary value problems involving Maxwell's equations in isotropic media," *IEEE Transactions on Antennas and Propagation*, vol. AP-14, pp. 302-307, 1966.

[2] A. Taflove and S. C. Hagness, *Computational electrodynamics: The finite-difference time-domain method*, vol. 3rd ed. Boston: MA: Artech House, 2005.

[3] A. Taflove and M. E. Brodwin, "Numerical solution of steady-state electromagnetic scattering problems using the time-dependent Maxwell's equations," *IEEE Transactions on Microwave Theory and Techniques*, vol. 23, pp. 623-630, 1975.

[4] A. Taflove and M. E. Brodwin, "Computation of the electromagnetic fields and induced temperatures within a model of the microwave-irradiated human eye," *IEEE Transactions on Microwave Theory and Techniques*, vol. 23, pp. 888-896, 1975.

[5] R. Holland, "THREDE: A free-field EMP coupling and scattering code," *IEEE Transactions on Nuclear Science*, vol. NS-24, pp. 2416-2421, 1977.

[6] K. S. Kunz and K. M. Lee, "A three-dimensional finite-difference solution of the external response of an aircraft to a complex transient EM environment: Part I-The method and its implementation," *IEEE Transactions on Electromagnetic Compatibility*, vol. EMC-20, pp. 328-333, 1978.

[7] A. Taflove, "Application of the finite-difference time-domain method to sinusoidal steady-state electromagnetic-penetration problems," *IEEE Transactions on Electromagnetic Compatibility*, vol. EMC-22, pp. 191-202, 1980.

[8] K. S. Kunz and R. J. Luebbers, The finite difference time domain method for electromagnetics, vol. Boca Raton: FL: CRC Press, 1993.

[9] J. P. Berenger, "A perfectly matched layer for the absorption of electromagnetic waves," *Journal of Computational Physics*, vol. 114, pp. 185-200, 1994.

[10] A. Sani, Y. Zhao, Y. Hao, A. Alomainy, and C. Parini, "An Efficient FDTD Algorithm Based on the Equivalence Principle for Analysing Onbody Antenna Performance," *IEEE Transactions on Antennas and Propagation,* , vol. 57, pp. 1006 - 1014, April, 2009.

[11] M. F. Wong and J. Wiart, "Modelling of electromagnetic wave interactions with the human body," *Comptes Rendus Physique*, vol. 6, pp. 585-594, 2005.

[12] J. Wang, O. Fujiwara, S. Watanabe, and Y. Yamanaka, "Computation with a parallel FDTD system of human-body effect on electromagnetic absorption for portable telephones," *IEEE Transactions on Microwave Theory and Techniques*, vol. 52, pp. 53-58, 2004.

[13] O. P. Gandh and J. Chen, "Numerical dosimetry at power-line frequencies using anatomically based model," *Bioelectromagnetics*, vol. 13, pp. 43-60, 1992.

[14] K. Fujii, M. Takahashi, K. Ito, and N. Inagaki, "Study on the electric field distributions around whole body model with a wearable device using the human body as a transmission channel," *First European Conference on Antennas and Propagation EuCAP* pp. 1 - 4, 6-10 Nov. 2006

[15] A. G. Alhaddad, R. A. Abd-Alhameed, D. Zhou, I. T. E. Elfergani, C. H. See, P. S. Excell, and M. S. Bin-Melha, "Low Profile Balanced Handset Antenna with Dual-Arm Structure for WLAN Application," *In Proceedings of Mosharaka International Conference on Communications, Propagation, and Electronics, Amman, Jordon*, pp. 1-4, 5-7 March 2010.

[16] G. J. Burke and A. J. Poggio, "Numerical electromagnetics code (NEC): method of moments," *US Naval Ocean Systems Centre, Rep, No. TD116*, 1981.

[17] P. A. Mason, W. D. Hurt, T. J. Walters, J. A. D'Andrea, K. L. R. P. R. Gajsek, K. I. S. D. A. Nelson, and J. M. Ziriax, "Effects of frequency, permittivity, and voxel size on predicted specific absorption rate values in biological tissue during electromagnetic-field exposure," *IEEE Transactions on Microwave Theory and Techniques*, vol. 48, pp. 2050 - 2058, Nov 11, 2000.

[18] R. A. Abd-Alhameed, P. S. Excell, and J. Vaul, "Currents Induced on wired I.T. Networks by Randomly distributed phones –A Computational study," *IEEE Trans on Electromagnetics and Compatibility*, vol. 48, pp. 282-286, May 2006.

[19] M. A.-A. Mangoud, "Hybrid Computational Electromagnetics Methods for Personal Communications Applications," in *Department of Electronic and Electrical Engineering*, vol. PhD Thesis: University of Bradford, 2001.

CHAPTER SEVEN

Ultra Wide Band Balanced Antenna

7.1 Introduction

Ultra-wideband (UWB) technology allows new services to co-exist alongside current radio systems with minimal or no interference. In 2002 the FCC approved the use of the unlicensed UWB spectrum, in the 3.1–10.6 GHz range, for commercial purposes [1]. The proposed technologies are based on the use of extremely narrow RF pulses for communication between TX and RX nodes. The system operates at low RF power levels, and operates over a relatively short range. Such systems are relatively immune to multipath fading. In summary, any UWB antenna design should be capable of operating over the bandwidth allocated by the FCC, whilst at the same time, providing a satisfactory radiation performance over the entire frequency range. This requires a suitable time domain characteristic.

Some of the more common issues in handset antenna design have a follow through with the extension to UWB. The general volume constraint remains ever present, along with other practical integration issues. Planar metal-plate antennas may be designed with ultra wide-band (UWB) characteristics [2-15] taking advantage of their simple geometry and wide bandwidth [16]. They are suitable for several UWB communication systems which require full, or substantial coverage of the available bandwidth [3]. As the name

suggests these antennas use a planar metal plate as the radiator and this radiating patch is placed over a finite ground plane.

Thus far the more commonly reported configurations include simple monopoles over a ground plane [17-19], modified monopoles [20-27], dipoles [28], T-structures [29-31], U-structures [31-33], meandered striplines [34] and planar inverted L (PILA) [11, 35-37], and planar inverted F (PIFA) structures [26, 38-41]. Most of these designs operate in an unbalanced configuration. Hence, there is an obvious motivation to apply the balanced technique to develop antennas for UWB applications with particular reference to mobile terminals.

It is obvious choice to select a wide band monopole antenna [42] and then extend the design concept to balanced configuration by placing another element with less coupling using parametric study. In this work, the orientation, locations of the monopoles including the necessary feeding network are optimized to meet as possible as small compact balanced antenna structure.

7.2 Design Structure of Ultra-Wide Band UWB Balanced Antenna

The geometry of the proposed antenna is shown in Figure 7.1. Two metal ground planes are used for this particular antenna design; the vertical ground plane is constructed from copper sheeting with dimensions of 0.5 mm × 75 mm × 60 mm (see Figure 7.1.a). The horizontal ground plane is constructed from a different copper sheet with thickness 0.035 mm, the gap h is 10 mm and it lies below the substrate (see Figure 7.1.b and c). The substrate is FR4 and with relative permittivity of 4.4, and thickness is 0.8 mm. It should also be noted that printed feed lines of thickness 0.035 mm, length of 18 mm and

width of 1.5 mm (see Figure 7.1.c), are used on the horizontal ground plane to feed the radiating patches. The antenna is fed at the centre. The radiating patches are made up of copper ($c = d = 20$ mm) with thickness of 0.5 mm and have square slot shapes of 8 mm as shown in Figure 7.1.a.

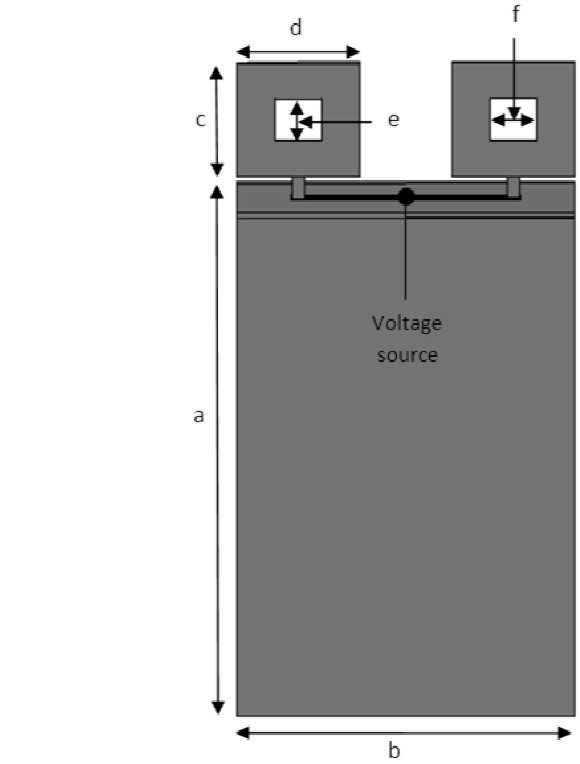

a) Top view

b) Side view

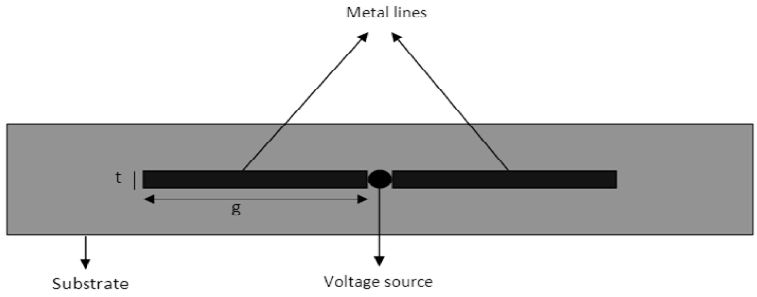

c) Substrate and metal lines

Figure 7.1: Antenna configuration, a) Top view, b) Side view, c) Substrate and metal lines

7.3 UWB Prototype Antenna, and Results

A development prototype for the balanced UWB antenna design is shown in Figure 7.2. The internal input impedance for this antenna is 100Ω; a balun circuit acts as a transformer, the detailed design and layout are given below.

Figure 7.2: The prototype of proposed antenna

7.3.1 Balun Design

Two baluns were designed for this prototype development using ADS. It is obvious by using the ADS; the execution time can be lee compare to other software (i.e. HFSS). This can be attributed to the fact that the mutual coupling between the elements on the structure is not incorporated in the design circuit configuration. In addition, an optimized circuits with better performance can be achieved using such tools but with less accuracy. One of the baluns is used for the lower frequency band, operating over the interval 1.9 GHz to 3.6 GHz, whilst the other is for the upper frequency band which extends from 3.0 GHz to 6.5 GHz. Figure 7.3 shows the lower band balun and its measurement results.

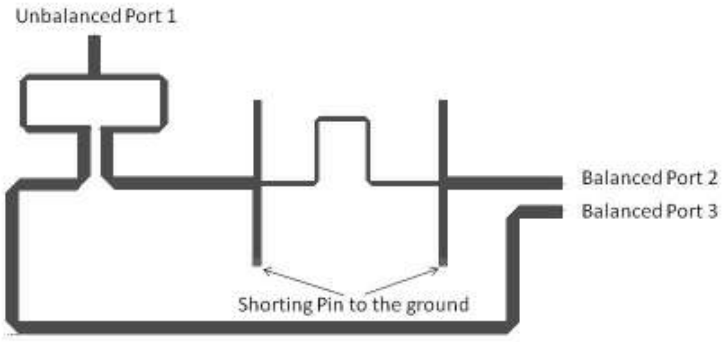

Figure 7.3: Balun for lower frequency band

It can be seen from the Figure 7.4 that the simulated input return loss of the unbalanced port (i.e., port at unbalanced port 1 in Figure 7.3) was less than 10 dB over the required bandwidth. Similarly, the other ports (ports that represent the balanced feed) were showing same return loss variations. It should be noted that the characteristics impedances of ports 2 and 3 are considered to be 100 Ω.

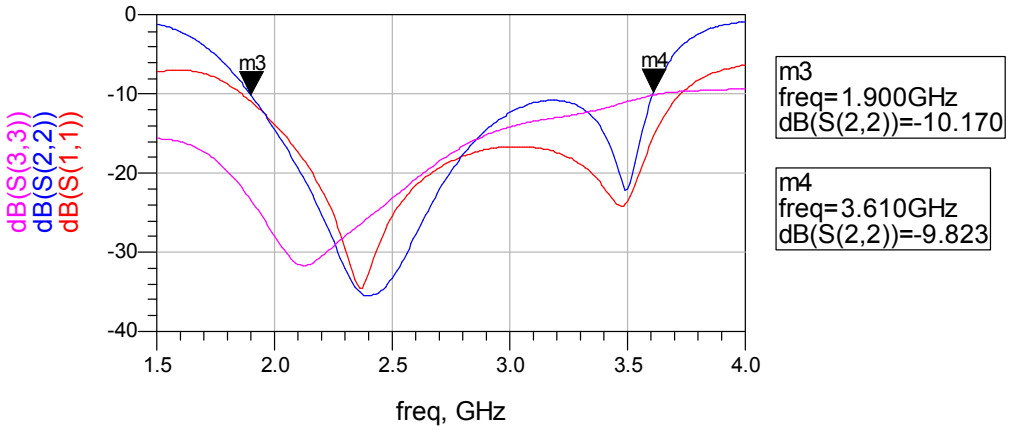

Figure 7.4: Calculated return loss for the lower band balun

The phase and amplitude responses are calculated in order to validate the balun performance for the specified frequency band. In Figure 7.5 the phase difference was approximately 180° between given markers m_1, m_5, and m_6. In addition, the amplitude difference of the two output ports of the balun is shown in Figure 7.6. The maximum

amplitude difference observed between these ports was approximately ± 0.6 dB, which is quite reasonable for this design.

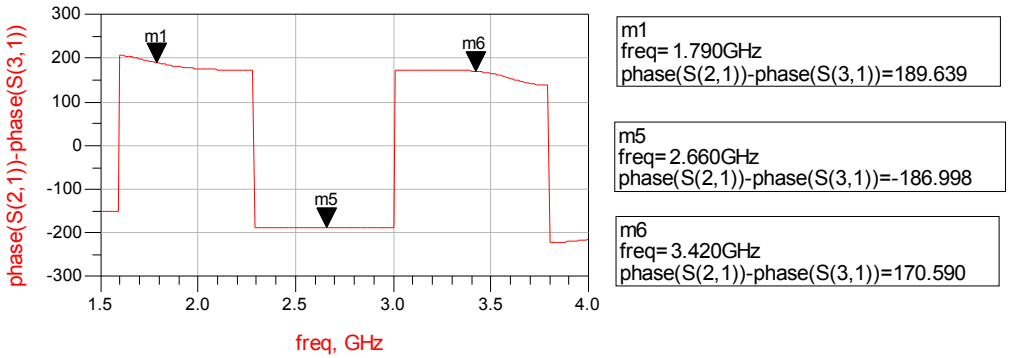

Figure 7.5: Phase difference between the two output ports of the balun at lower frequency band.

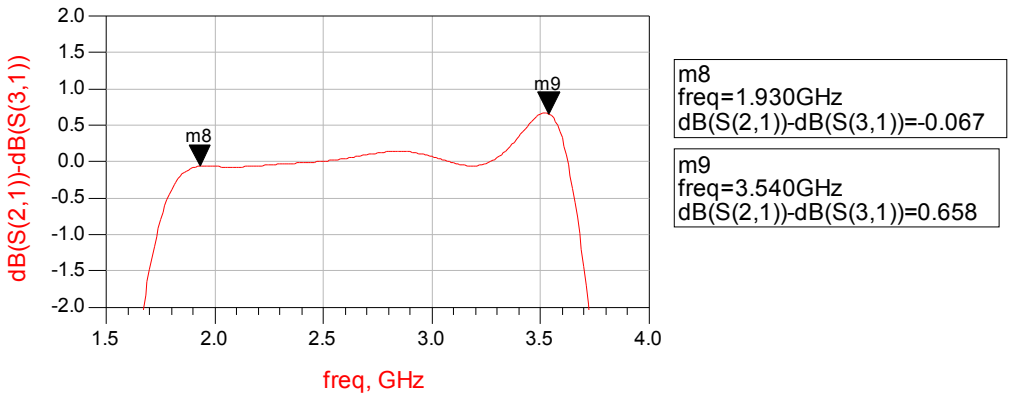

Figure 7.6: Amplitude difference between the two output ports of the balun at lower frequency band.

The second balun covers the upper band 3.0 GHz to 6.5 GHz, and is shown in Figure 7.7. Similar port notations are used, and the characteristic impedance was kept same as for the lower band.

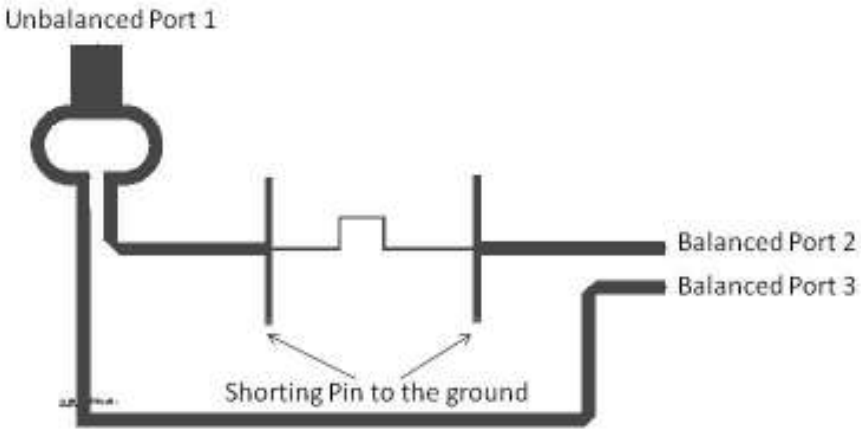

Figure 7.7: The upper band Balun

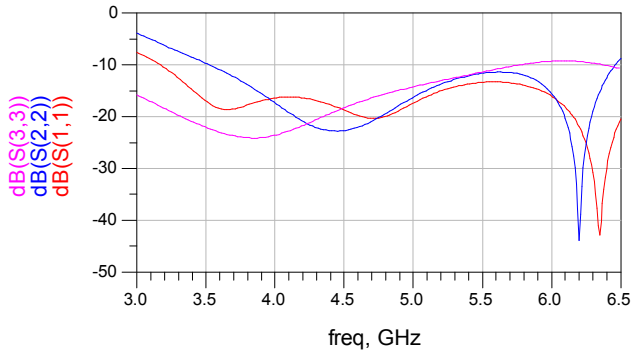

Figure 7.8: Simulated return loss of the upper band balun

Figure 7.8 shows the return loss of the given upper frequency balun for the three ports p_1, p_2, p_3 respectively. Similar results were observed for all input return losses over the considered bandwidth. Similarly, the phase and magnitude differences between the two output ports are shown in Figure 7.9 and Figure 7.10. The maximum variations in the phase and magnitude responses of the output ports were ± 3º and - 0.9 dB respectively.

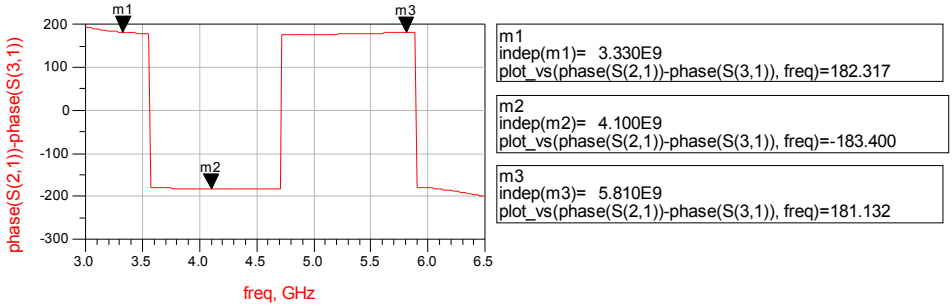

Figure 7.9: Phase difference of the upper band balun

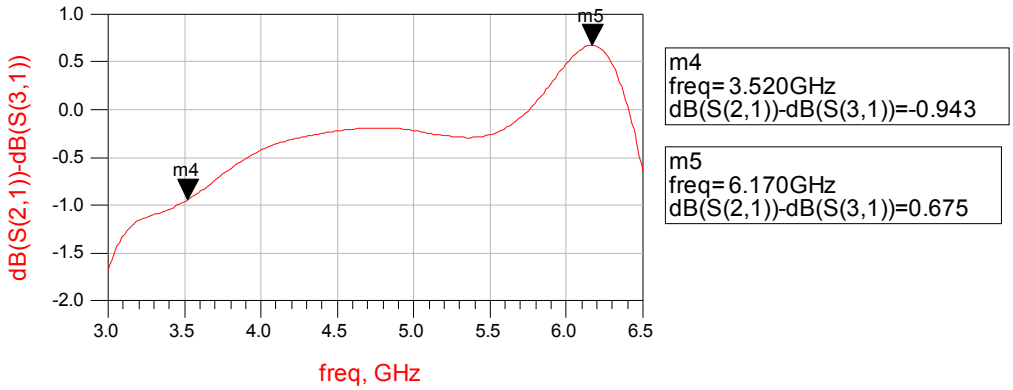

Figure 7.10**:** Amplitude difference between the two output ports of the balun at upper frequency band.

7.4 The Return Loss and Radiation Pattern of the Proposed Antenna

The effects of the ground plane size on the input return loss were systematically investigated. The length of the ground plane was reduced from the far side of the antenna, and varied from 75 mm to 60 mm in increments of 5 mm. The length of the horizontal ground plane was varied from 10 mm to 4 mm in increments of 2 mm. The corresponding results are presented in Figure 7.11 and Figure 7.12, respectively. As can be seen, slight variations in the calculated return loss were observed for the four cases. This implies that the realised antenna has very little sensitivity with respect to ground plane size.

The relative impedance bandwidth and the centre frequency can be stated respectively, as follows:

$$\text{B.W} = \frac{F_h - F_l}{F_c} \tag{7.1}$$

$$F_c = \frac{F_h + F_l}{2} \tag{7.2}$$

Where F_h, F_l, and F_c are the upper, lower and centre frequency components respectively. The computed frequency band achieved at an input return-loss of -8 dB was between 1.7 to 6.3 GHz (i.e., relative bandwidth is 115 %). The centre frequency is approximately 4 GHz.

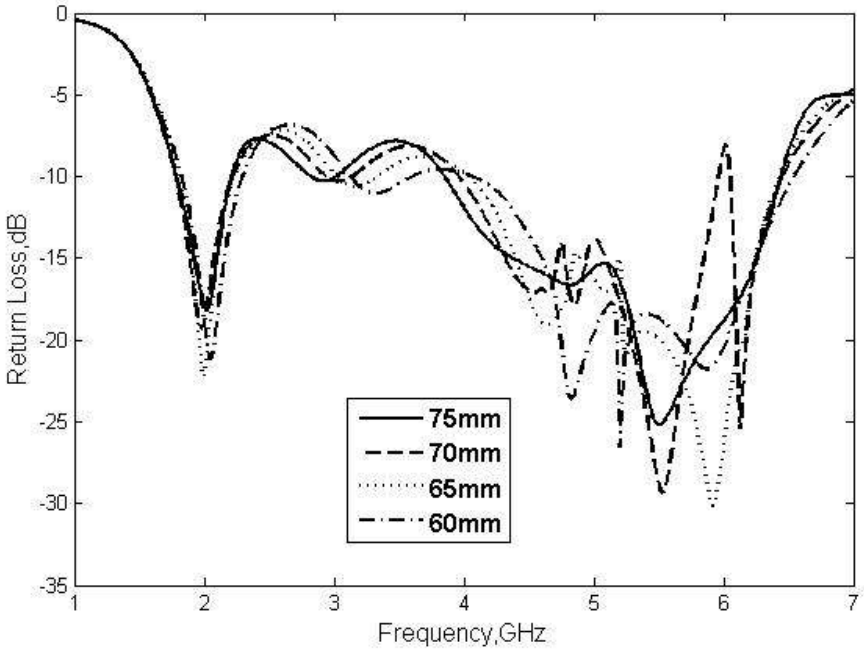

Figure 7.11: Antenna return loss characteristics against the length of the ground plane; lengths: 60 mm, 65 mm, 70 mm and 75 mm

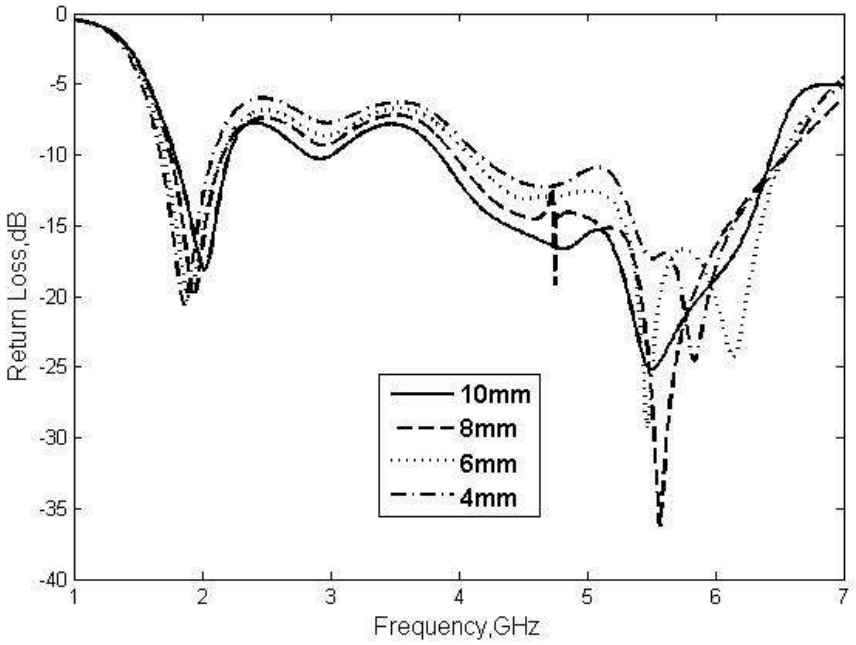

Figure 7.12: Antenna return loss characteristics versus the width of the ground plane; widths: 4 mm, 6 mm, 8 mm and 10 mm

By inspecting Figure 7.13, and taking into account any errors caused by the manufacturing process, it can be seen the antenna covers an ultra-wide band-width with promising performance. In addition, the agreement with simulations is very satisfactory as presented in Figure 7.11. Furthermore it can be seen that the effect of the operator's hand and head on the antenna performance is very small, which implies that the antenna has a reasonable balanced structure.

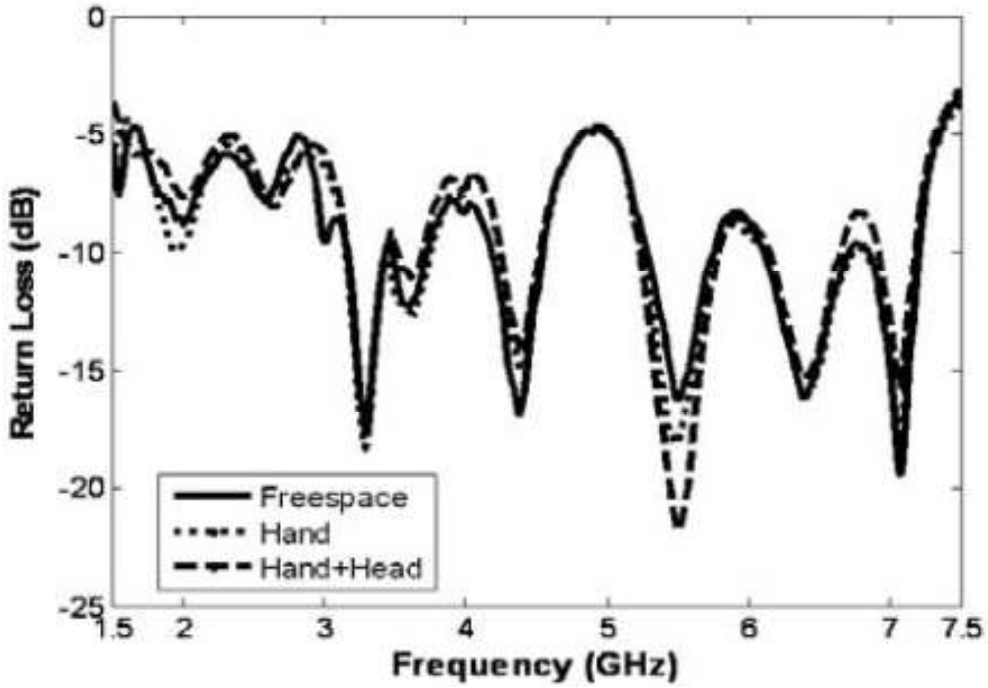

Figure 7.13: Measured input return loss of the proposed antenna

The radiation patterns of the prototype antennas were measured inside a far-field anechoic chamber, by placing the antenna under test (AUT) at one end of the chamber, while placing a standard gain horn antenna at the other end of the room. Two pattern cuts were taken for four selected operating frequencies that cover the designated whole bandwidth in this study. The radiation patterns in the zx plane and zy plane for the antenna were measured at 2000, 4900 and 5900 MHz, and presented in Figure 7.14. The patterns of the prototypes are seen to be quite similar to each other for all three cases. Moreover, as expected the figures presented a nearly omni-directional radiation pattern in all intended three frequency components.

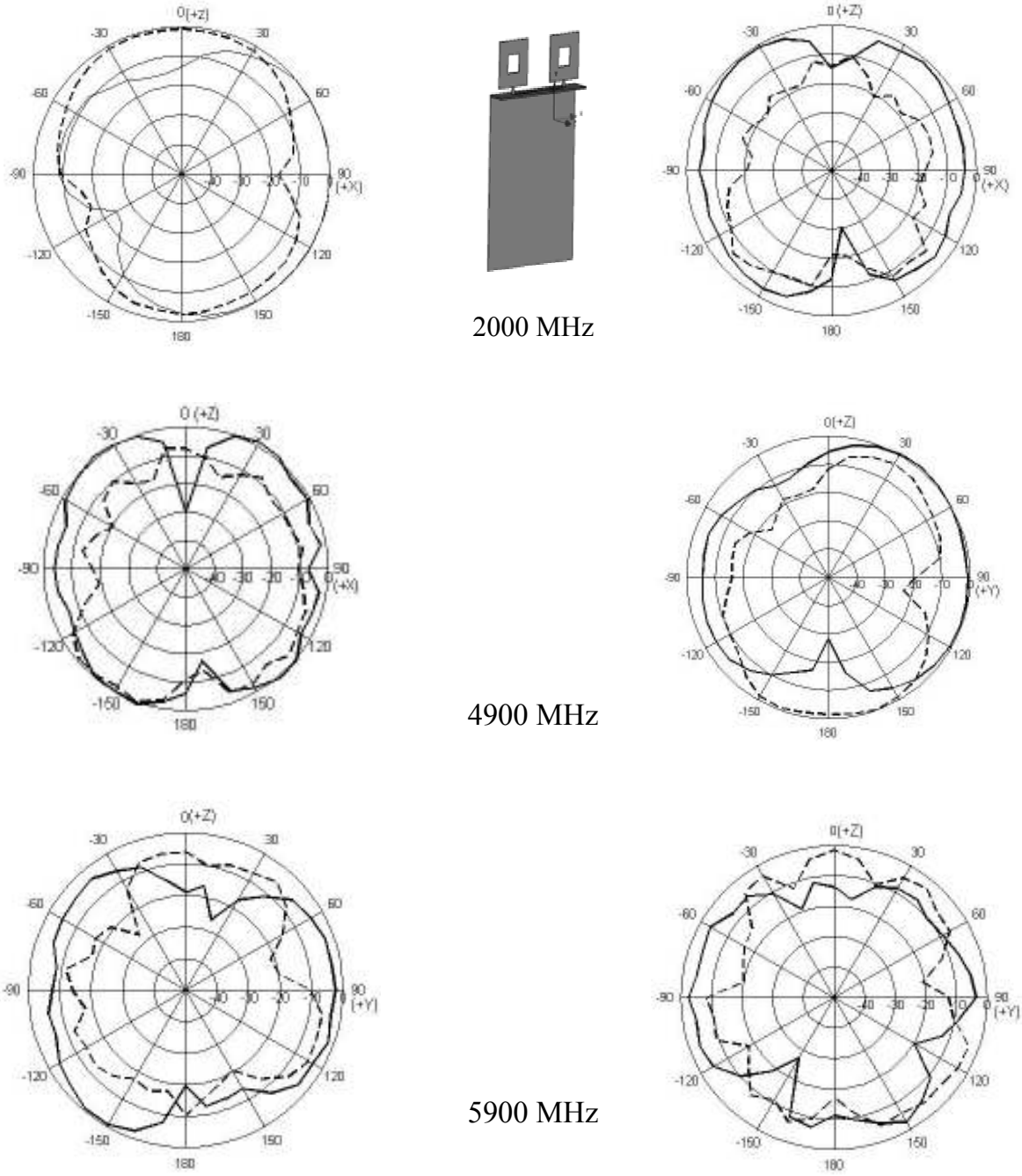

Figure 7.14: Radiation patterns of the proposed antenna for 2450 MHz, 4900 MHz and 5900 MHz at: (left) xz plane; (right) yz plane, where '——' measured E_θ and '- - -' measured E_ϕ.

7.5 Modified UWB Balanced Antenna

In this section a variant of the previous antenna design is considered in which the antenna size was reduced, along with the printed feed network. The first design iteration was obtained by decreasing the antenna arms to 18.5 mm × 18.5 mm, whilst keeping the same dimensions for the slots (i.e., 8 mm × 8 mm). In order to maintain the existing compact profile, these arms were printed on FR4 using a 0.035 mm copper process.

A tapered microstrip layout with a 0.5 mm reduced line width was introduced on three lines in order to obtain an extended bandwidth response, as discussed in [25], see Figure 7.15. In addition, it was also found that by introducing this type of line transition between the original 50 Ω feeding lines and the antennas arms (i.e. the input impedance of the antenna is 50 Ω.), the conversion from the normal 50 Ω to 100 Ω impedance as the previous design is no longer required.

The resulting design was prototyped on the usual FR4 material; the dimensions were set to be representative of the final handset: 60 mm (h) × 94 mm (b) × 10 mm (h). The thickness of the copper for the handset (i.e., ground plane in vertical position) including the ground part in the horizontal position, from which the feed network tracks are implemented, and the antenna arms is 0.035 mm (see Figure 7.16).

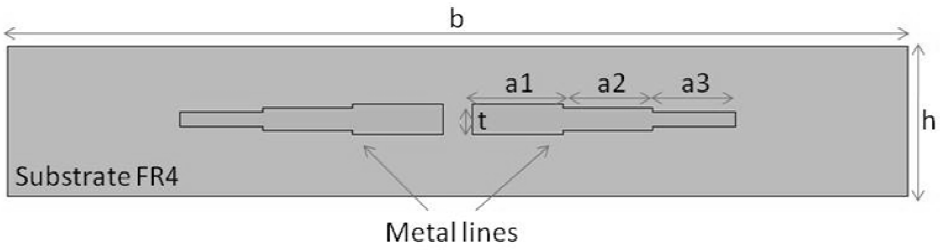

Figure 7.15: Top view of the feeding network; a_1 = 5.5 mm, a_2 = 6 mm, a_3 = 6 mm, t = 2 mm, h = 10 mm, b = 60 mm.

Figure 7.16: Prototype of the modified antenna

7.5.1 Simulation and Results

Figure 7.17 shows the simulated and measured return loss of the current UWB antenna design. Allowing consideration of the difficulties and errors caused in custom manufacture of the antenna, the results gave much confidence in the simulation carried out. This can be seen from the generally good agreement results of the measured return loss and the values from simulation over a wide frequency range from 2 GHz to 8 GHz. Although there are some slight discrepancies between the fabricated antenna and its simulation model, ultra wideband characteristics with less than -8 dB return loss can also be confirmed.

Figure 7.18 shows the measured return losses of the antenna in free space, with operator's hand and in held in the talk position adjacent to the head. By inspection, it

may be observed that when the antenna is held in the hand, or in talk position, the antenna input return losses were not significantly affected. This is as expected for the operation of a balanced antenna, in which the induced currents in the handset are minimal; this is clearly shown in Figure 7.19.

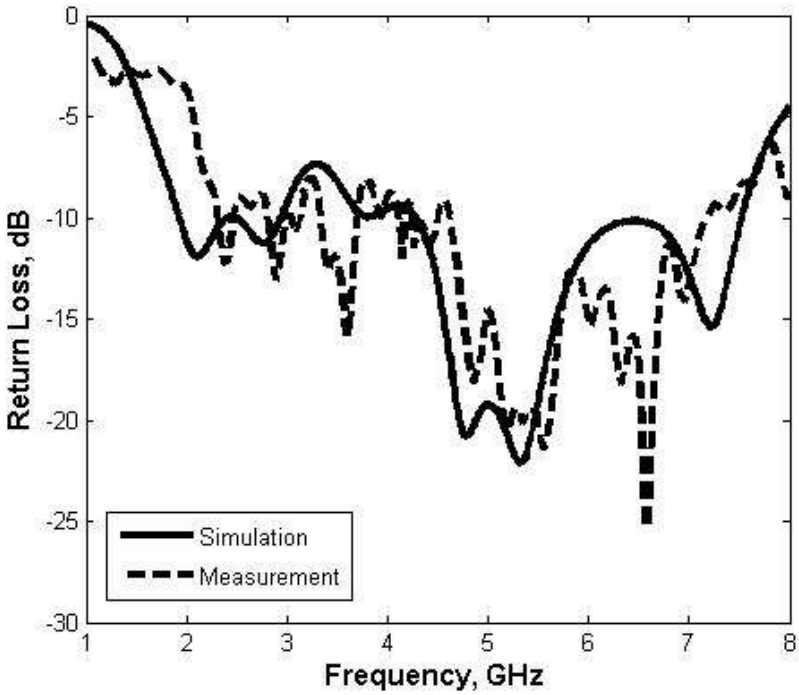

Figure 7.17: simulated and measured return loss

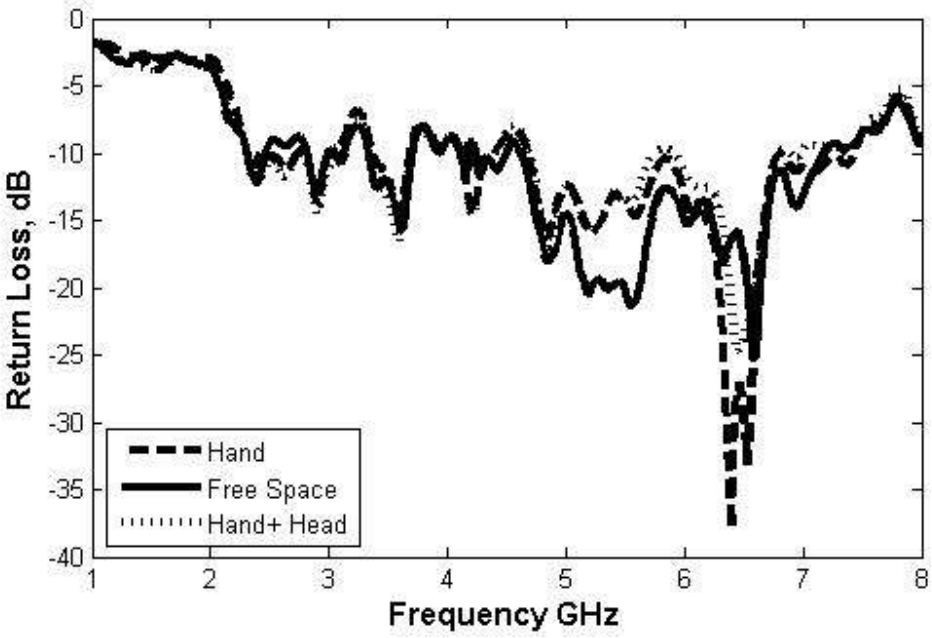

Figure 7.18: Measured Return loss of the proposed antenna

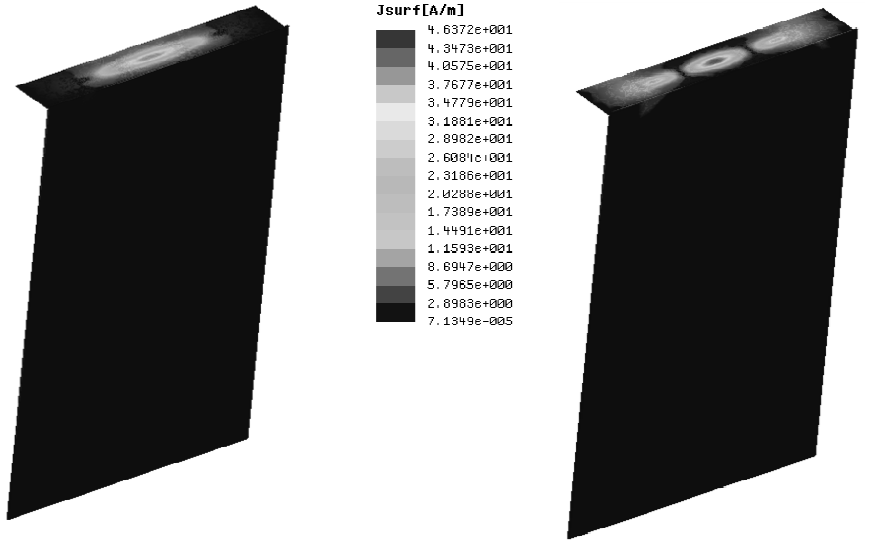

3.0 GHz 4.5 GHz

5.5 GHz 6.5 GHz

Figure 7.19: Surface current distribution of the UWB antenna in its vertical and horizontal ground plane at 3.0 GHz, 4.5 GHz, 5.5 GHz and 6.5 GHz

It should be noted that the measured relative bandwidth at input return loss (≤ -8 dB) is 106 %, as extended over the frequency band from 2.3 GHz and 7.5 GHz. This bandwidth is slightly less than in the previous design but it falls comfortably within the FCC guidelines. The antenna size was reduced, along with the new feed network.

Figure 7.20 and Figure 7.21 summarise the simulated radiation patterns of the modified prototype. Two pattern cuts (i.e. xz plane and yz plane) were considered for evaluation purposes, and taken across the whole frequency bandwidth. The spot frequencies considered were 2.45 GHz, 4.0 GHz, 5.0 GHz and 7.0 GHz. The antenna performance is essentially omni-directional over much of the frequency range, except at the higher end, where the balun performance appears to degrade. The simulated antenna gain values were quite encouraging and fall into the range from 1.9 to 4.5 dBi.

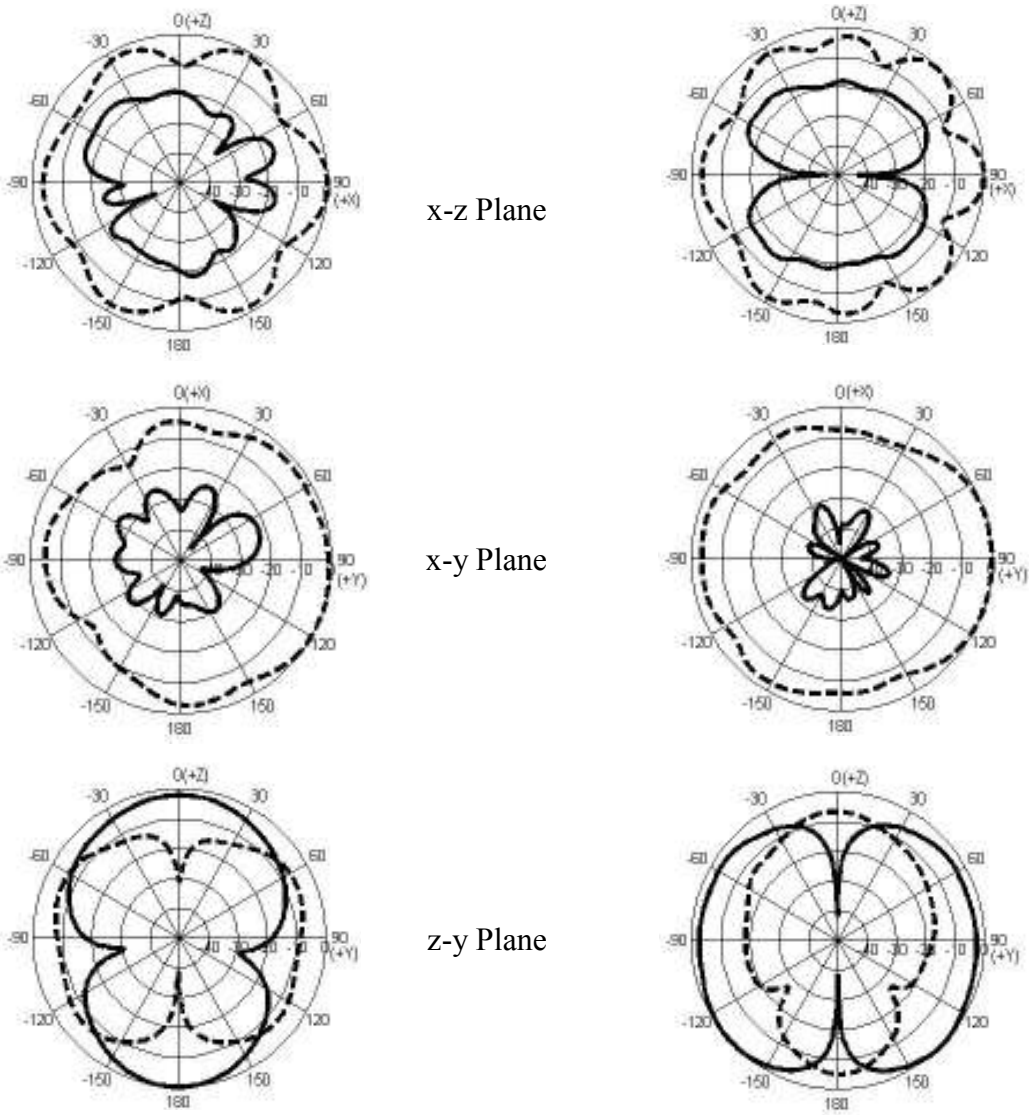

Figure 7.20: Radiation patterns of the proposed antenna for 2.45 GHz, 4.0 GHz at: xz plane; yz plane and xy plane, where '——' calculated E_θ and '- - -' calculated E_ϕ.

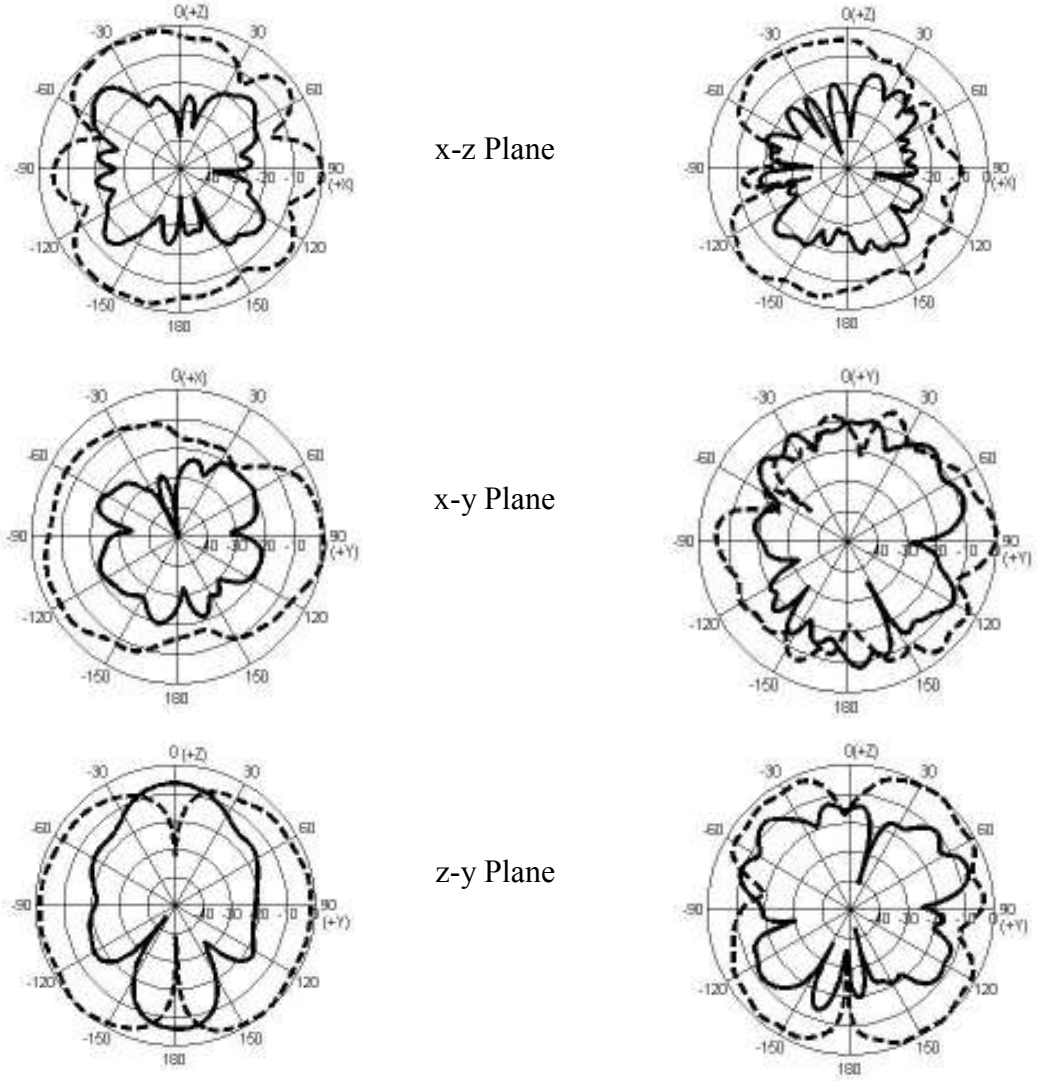

Figure 7.21: Radiation patterns of the proposed antenna for 5.0 GHz and 7.0 GHz at: xz plane; yz plane and xy plane, where '——' calculated E_θ and '- - -' calculated E_ϕ.

7.6 Conclusion

In this chapter, two different planar UWB antenna geometries have been presented. These proposed designs have simple configurations and should be easy to implement at low cost. Prototypes have been constructed and studied, the simulated and measured input returns losses of both antennas showed a reasonable agreement. In addition, a nearly omni-directional characteristic of radiation pattern is obtained over the entire frequency range. The relative antenna bandwidth achieved was between 106% and 115% for the considered designs. The modified UWB antenna can be recommended as an attractive candidate for mobile handset applications. In addition, the analysis of the proposed antenna design in the presence of human hand and head was tested, and it can be confirmed that the antenna exhibited low induced currents on the handset since the input return losses were unchanged for all operated configurations.

7.7 References

[1] "FCC, First Report and Order 02-48. February 2002."

[2] Kin-Lu Wong, T.-c. Tseng, and P.-L. Teng, "Low Profile ultra wideband Antenna For Mobile Phone Applications," *Microwave and Optical Technology Letters*, vol. 43, pp. 7-9, October 2004.

[3] K.-L. Wong, C.-H. Wu, and S.-W. Su, "Ultrawide-band square planar metal-plate monopole antenna with a trident-shaped feeding strip," *IEEE Transaction on antennas and propagation*, vol. 53, pp. 1262-1269, April 2005.

[4] M. J. Ammann, "Control of the impedance bandwidth of wideband planar monopole antennas using a beveling technique," *Microwave and Optical Technology Letters* vol. 30, pp. 229–232, August 2001.

[5] S.-H. Choi, H.-C. Lee, and K.-S. Kwak, "Clover-Shaped Antenna for Ultra-Wideband Communications," *Microwave and Optical Technology Letters* vol. 48, pp. 2111-2113, October 2006.

[6] J. Jung, Y. Yu, and J. Choi, "A Small Wideband Planar Monopole Antenna for Mobile Wireless Devices," *Microwave and Optical Technology Letters* vol. 48, April 2006.

[7] D. Valderas, J. Mele´ndez, and I. Sancho, "Some Design Criteria For UWB Planar Monopole Antennas: Application to A Slotted Rectangular Monopole," *Microwave and Optical Technology Letters* vol. 46, pp. 6-11, July 2005.

[8] N. Fortino, G. Kossiavas, J. Y. Dauvignac, and a. R. Staraj, "Novel Antennas for Ultrawideband Communications," *Microwave and Optical Technology Letters*, vol. 41, pp. 166-169, May 5 2004.

[9] W.-C. Liu and P.-C. Kao, "CPW-Fed Triangular Monopole Antenna For Ultra-Wideband Operation," *Microwave and Optical Technology Letters*, vol. 47, December 2005.

[10] J. Liang, "Antenna Study and Design for Ultra Wideband Communication Applications," in *Department of Electronic Engineering Queen Mary,* , vol. degree of Doctor of Philosophy: University of London, July 2006.

[11] A. A. Eldek, "A Small Ultra-Wideband Planar Tap Monopole Antenna With Slit, Tapered Transition, and Notched Ground Plane," *Microwave and Optical Technology Letters*, vol. 48, pp. 1650-1654, August 2006.

[12] F.-R. Hsiao and K.-L. Wong, "An Internal Ultra-Wideband Metal-Plate Monopole Antenna For UMTS/WLAN Dual-Mode Mobile Phone," *Microwave and Optical Technology Letters*, vol. 45, pp. 265-268, May 5 2005.

[13] M. Ding, R. Jin, J. Geng, and Q. Wu, "Design of A CPW-Fed UWB Fractal Antenna," *Microwave and Optical Technology Letters*, vol. 49, pp. 173-176, January 2007.

[14] S.-Y. Lin and K.-C. Huang, "Printed Pentagon Monopole Antenna With A Band-Notched Function," *Microwave and Optical Technology Letters*, vol. 48, pp. 2016-2018, October 2006.

[15] D.-B. Lin, T. Tang, and M.-Y. Tsou, "A Compact UWB Antenna With CPW-Fed," *Microwave and Optical Technology Letters*, vol. 49, pp. 564-567, March 2007.

[16] Z. N. Chen, "Broadband planar monopole antenna,," *IEE Proc Microwave Antennas Propagat*, vol. 147, pp. 526–528, December 2000.

[17] E. Antonino-Daviu, M. Cabedo-Fabre´s, M. Ferrando-Bataller, and A. Valero-Nogueira, "Wideband double-fed planar monopole antennas," *Electronics Letters* vol. 39, 13th November 2003.

[18] S.-W. Su, K.-L. Wong, Y.-T. Cheng, and W.-S. Chen, "Finite-Ground-Plane Effects on The Ultra-Wideband Planar Monopole Antenna," *Microwave and Optical Technology Letters* vol. 43, pp. 535-537, December 20 2004.

[19] S.-W. Su, K.-L. Wong, and C.-L. Tang, "Ultra-Wideband Square Planar Monopole Antenna for IEEE 802.16a Operation in The 2–11-Ghz Band," *Microwave And Optical Technology Letters* vol. 42, pp. 463-466, September 20 2004.

[20] E. Lee, P. S. Hall, and P. Gardner, "Compact Wideband Planar Monopole Antenna," *Electronics Letters* vol. 35, pp. 2157-2158, 9th December 1999.

[21] N. P. Agrawall, G. Kumar, and K. P. Ray, "Wide-Band Planar Monopole Antennas," *IEEE Transactions on Antennas and Propagation*, vol. 46, pp. 294-295, FEBRUARY 1998.

[22] Z. N. Chen, M. J. Ammann, M. Y. W. Chia, and T. S. P. See, "Annular planar monopole antennas," *IEE Proceeding Microwave Antennas Propagation*, vol. 149, Aug 2002.

[23] A. M. Abbosh and M. E. Bialkowski, "Design of Ultrawideband Planar Monopole Antennas of Circular and Elliptical Shape," *IEEE Transactions on Antennas and Propagation*, vol. 56, pp. 17-23, JANUARY 2008.

[24] M. Sun and Y. P. Zhang, "Miniaturization of Planar Monopole Antennas for Ultrawide-Band Applications " *Antenna Technology: Small and Smart Antennas Metamaterials and Applications, IWAT '07. International Workshop* pp. 197 - 200, 2007.

[25] M. N. Srifi, S. K. Podilchak, M. Essaaidi, and Y. M. M. Antar, "Planar circular disc monopole antennas using compact impedance matching networks for ultra-wideband (UWB) applications," *Microwave Conference, 2009. APMC 2009. Asia Pacific*, pp. 782 - 785, 2009.

[26] S.-H. Yeh, K.-L. Wong, T.-W. Chiou, and S.-T. Fang, "Dual-Band Planar Inverted F Antenna for GSM/DCS Mobile Phones," *IEEE Transactions on Antennas and Propagation*, vol. 51, pp. 1124-1126, 2003.

[27] Y. Gao, B.-L. Ooi, and A. P. Popov, "Band-Notched Ultra-Wideband Ring-Monopole Antenna," *Microwave and Optical Technology Letters* vol. 48, pp. 125-126, January 2006.

[28] C.-D. Zhao, "Analysis on the Properties of a Coupled Planar Dipole UWB Antenna," *IEEE Antennas and Wireless Propagation Letters*, vol. 3, pp. 317-320, 2004.

[29] S.-B. Chen, Y.-C. Jiao, W. Wang, and F.-S. Zhang, "Modified T-Shaped Planar Monopole Antennas for Multiband Operation," *IEEE Transactions on Microwave Theory and Techniques*, vol. 54, pp. 3267-3270, August 2006.

[30] J.-Y. Jan and L.-C. Tseng, "Planar monopole antennas for 2.4/5.2 GHz dual-band application," *IEEE Antennas and Propagation Society International Symposium*, vol. 4, pp. 158 - 161, 2003.

[31] W.-S. Lee, D.-Z. Kim, and J.-W. Yu, "Wideband Crossed Planar Monopole Antenna with the Band-Notched Characteristic," *Microwave and Optical Technology Letters*, vol. 48, pp. 543-545, March 2006.

[32] K.-L. Wong, L.-C. Chou, and F.-S. Chang, "Printed Short-Circuited Wideband Monopole Antenna with Band-Notched Operation," *Microwave and Optical Technology Letters*, vol. 46, pp. 58-61, July 5 2005.

[33] W.-S. Lee, K.-J. Kim, D.-Z. Kim, and J.-W. Yu, "Compact Frequency-Notched Wideband Planar Monopole Antenna With An L Shape Ground Plane," *Microwave and Optical Technology Letters*, vol. 46, August 2005.

[34] J. F. Wu, C. J. Panagamuwa, P. McEvoy, J. C. Vardaxoglou, and O. A. Saraereh, "Switching a dual band PIFA to operate in four bands,," *IEEE Antennas and Propagation Society International Symposium*, pp. 2675 - 2678 2006.

[35] J.-Y. Jan and L.-C. Tseng, "Small Planar Monopole Antenna With a Shorted Parasitic Inverted-L Wire for Wireless Communications in the 2.4-5.2-, and 5.8-GHz Bands," *IEEE Transactions on Antennas and Propagation*, vol. 52, July 2004.

[36] L. Lu and J. C. Coetzee, "A Wideband Planar Monopole Microstrip Antenna with Coupled Parasitic Lines," *Microwave and Optical Technology Letters*, vol. 48, pp. 1507-1509, 8, August 2006.

[37] S. Tarvas and A. Isohatala, "An internal dual-band mobile phone antenna," *IEEE Antennas Propagat. Soc. Int. Symp., Salt Lake City, UT*, pp. 266–269, 2000.

[38] Hoon Park, K. Chung, and J. Choi, "Design of a Planar Inverted-F Antenna With Very Wide Impedance Bandwidth," *IEEEMicrowave and Wireless Components Letters*, vol. 16, pp. 113-115, 2006.

[39] J.-S. Row, "Dual-Frequency Triangular Planar Inverted-F Antenna," *IEEE Transactions on Antennas and Propagation*, vol. 53, pp. 874-876, 2005.

[40] P. Nepa, G. Manara, A. A. Serra, and G. Nenna, "Multiband PIFA for WLAN Mobile Terminals," *IEEE Antennas and Wireless Propagation Letters*, vol. 4, pp. 349-350, 2005.

[41] C. H. See, R. A. Abd-Alhameed, D. Zhou, and P. S. Excell, "Dual-frequency planar inverted F-L-antenna (PIFLA) for WLAN and short range communication systems," *IEEE Transactions on Antennas and Propagation*, vol. 56, pp. 3318-3320, October 2008.

[42] M. J. Ammann and Z. N. Chen, "Wideband Monopole Antennas for Multi-Band Wireless Systems," IEEE Antennas and Propagation Magazine, vol. 45, pp. 146-150, 2003.

CHAPTER EIGHT

Folded Loop Balanced Coplanar Antenna for WLAN Applications

8.1 Introduction

It has been established throughout this work that balanced antenna systems offer a substantial advantage to mobile antenna designs, this is due to their stable performance when held in close proximity to the user's body [1]. The feed networks for balanced antennas such as dipoles usually include a balun circuit, which in practice may result in a narrowing of the achievable bandwidth of the antenna, compromising the intended performance [2]. The symmetry of the antenna's radiation pattern is determined by the efficiency of the balun, and thus sub-optimal pattern shaping might be obtained [3]. This has the potential to limit the use of balanced antennas in many handset applications.

A convenient alternative approach is through the use of coplanar structures. Coplanar transmission line antenna configurations are attractive for antenna designers due to their simplicity, and ease of integration with active and passive components in the same layer [4]. The term "coplanar" has been used for those transmission lines and antennas in which all the conductors are in the same plane, namely, on the top surface of the dielectric substrate [5]. The coplanar structure as a transmission line has become an

intensive topic of recent research due to its attractive characteristics, such as a possibility for a wider impedance matching bandwidth and easy fabrication process [6, 7]. Moreover, coplanar antenna structures show less peak gain variation and higher minimum peak gain [7-10].

In this chapter a new printed circuit antenna using coplanar waveguide structures, covering the 2.4 GHz and 5.2 GHz WLAN frequency bands is described, analysed and tested. The antenna is intended to eliminate the need for a balanced feed network. This is achieved through systematically evaluating the consequences of modifying a number of antenna parameters and carefully monitoring the impact of such changes. The impact of making changes to the antenna is monitored and verified through using two standard software modelling tools to ensure accuracy and verification of the results. The optimised antenna was fabricated and tested, and its characteristics were experimentally verified confirming the design concept a having good impedance bandwidth characteristics and excellent dual-band performance.

8.2 Theory of the Shielded Balanced Loop

The balanced shielded loop is made from coaxial cable with a narrow gap in the outer conductor (or shield). The basic loop antenna is modified for use with an unbalanced coaxial line by incorporating a simple balanced to unbalanced transformer (balun) within it [11]. The inner of the coaxial line (or equivalent coplanar transmission structure) is terminated on the outer conductor or the grounded sheath (this is also equivalent to the coplanar ground plane) of the opposite half loop at the gap. Energy will still be transferred to the load Z_L [12]. The balanced coaxial (or coplanar) structure incorporating a balun transformer is shown in Figure 8.1.

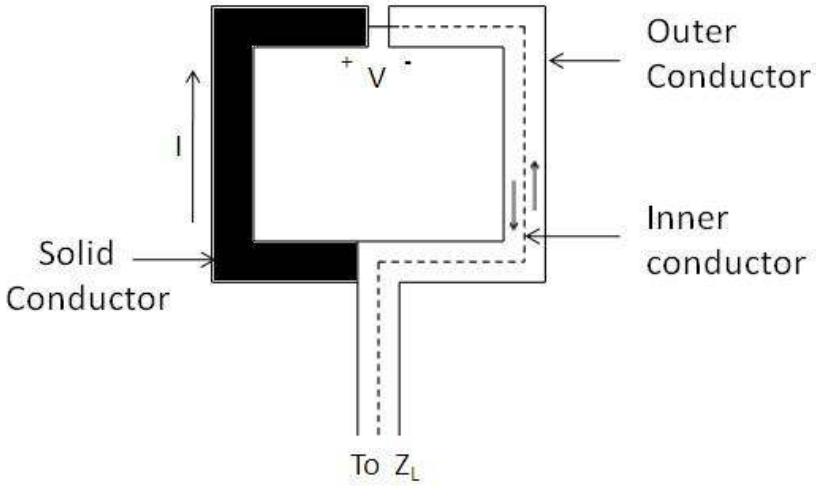

Figure 8.1: Balanced structure with incorporated balun

8.3 Microstrip Patch Antenna

Microstrip technology is one of the most common techniques used to design planar antennas, and they have an obvious attraction for mobile terminal designs. Microstrip characteristics have the potential to deliver significant reductions in size, and low costs in production [13]. Microstrip antennas possess four generic features namely, a thin flat metallic radiator, known as the patch, a dielectric substrate, a ground plane and a feed network that supplies the radiator with RF power as illustrated in Figure 8.2. The radiating patch could be of any arbitrary shape e.g. square, rectangular, circular, triangular, semi-circular, and annular rings [13]. All microstrip antennas can be divided into four basic categories: microstrip patch antennas, microstrip dipoles, printed slot antennas, and microstrip travelling wave antennas [14].

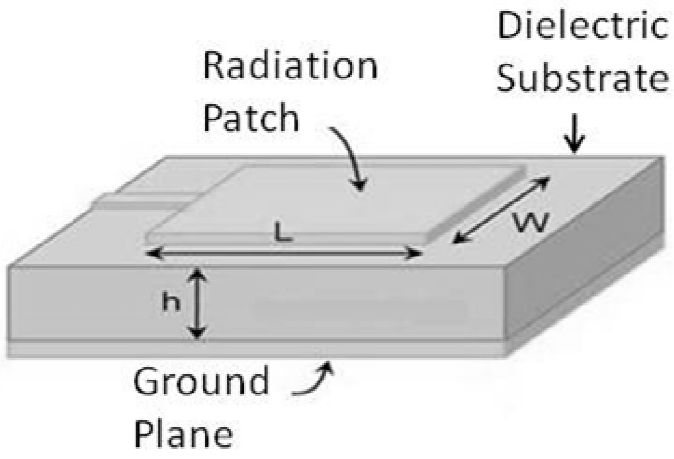

Figure 8.2: Microstrip patch antenna

Microstrip antennas can be easily integrated with other active, and passive components, onto the printed circuit board of the handset [15]. The main issue however is the size of the antenna. For operation in the low microwave frequency spectrum, a conventional patch is simply too large to be accommodated within a handset terminal. These antennas radiate due to the presence of the fringing field between the patch edges and the ground plane [15].

For a microstrip antenna to perform satisfactorily, three loss mechanisms need to be considered: conducting, dielectric, and surface waves. All are material dependent, so substrate materials need to be carefully selected for good overall efficiency. If the thickness and the dielectric constant of the substrate are kept at a minimal level, this will result in improving the efficiency, bandwidth, and the size of the antenna [14].

Microstrip antennas have radiating elements on one side of a dielectric substrate, and thus early microstrip antennas were fed either by a microstrip line or a coaxial probe through the ground plane. Since then a number of new feeding techniques have been developed. Major among these are coaxial feed, microstrip (coplanar) feed, proximity-

coupled microstrip feed, aperture-coupled microstrip feed, and coplanar waveguide feed [14].

8.4 Coplanar Waveguide (CPW) Antennas

When microstrip technology is applied to planar antennas, fabrication on both sides of the substrate is required. This means that microstrip antennas must have ground planes on the opposite side of the substrate material to support the feeding microstrip line. They will need a ground plane on the opposite side of the substrate for electromagnetic waves to travel along the feed line. However, by applying a coplanar waveguide (CPW) feed network, only one side of the substrate needs to be processed. Both radiating elements and ground planes are on the same side of the substrate. Therefore, most of the electromagnetic wave travels in the slots on the surface of the substrate, and less energy is lost in the substrate. If realisable, this a possibility for a wider impedance matching bandwidth [4]. A coplanar waveguide approach was proposed by Wen [5], it consists of a centre strip with two ground planes located parallel to it and in the plane of the strip as shown in Figure 8.3.

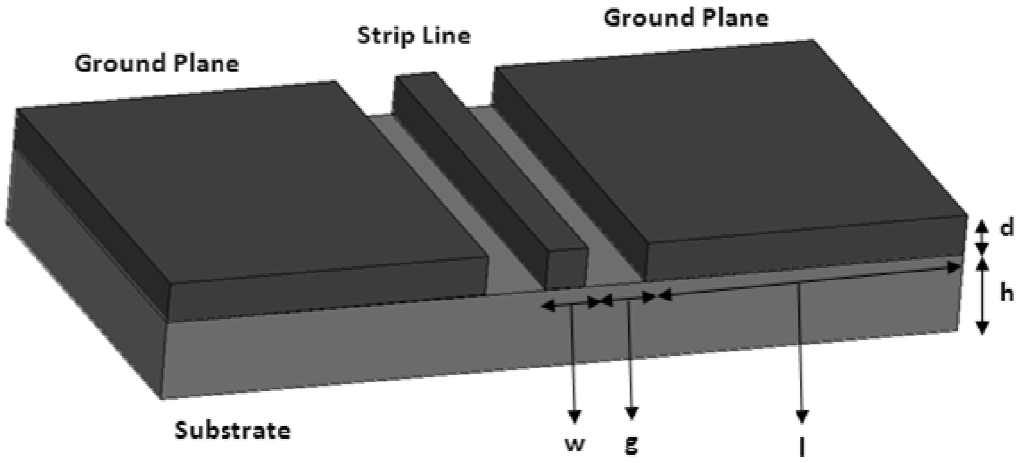

Figure 8.3: Coplanar waveguide structure

8.4.1 Advantages and Applications of CPW

Coplanar waveguide processes may be classified as conventional CPW, conductor CPW and micro machined CPW. The main advantages and applications of CPW are reviewed in [16-18]. Some of the more significant points are summarised as follows:

i. The dispersion properties, and hence losses, realisable impedances, and λ_g of CPW are comparable with microstrip, and may on occasions be superior.
ii. The coupling between the neighbouring lines is reduced due to the presence of the grounded lines between the signal lines.
iii. The characteristic impedance (Z_c) and phase velocity (v_p) of CPW are less dependent on the substrate and more on the dimensions of the plane of the conducting surface.
iv. Realisation of series and shunt elements are straight forward, and may be achieved without the need to drill holes through the substrate.

CPW processes are used across a wide range of applications, with particular reference to MMIC sub-systems, including attenuators, diplexers, antenna feeds and antennas. Some common discontinuities require detailed characterisation, e.g. CPW to slot line and CPW to waveguide [16, 17]. Detailed design strategies are not always available, and some of the applications alluded to here are still a specialised in nature, in general one of the major disadvantages in practice may be the lack of familiarity of CPW w.r.t. microstrip.

8.5 Antenna Structure

The coplanar antenna comprises three rectangular conducting strips; a centre strip and two similar lateral strips that can be regarded as the ground plane. Figure 8.4a shows the geometry of the proposed antenna in coplanar waveguide (CPW) technology for wideband application. The antennas were designed and optimised to work at 2.4 GHz and 5.2 GHz for WLAN. Here CPW is used as an antenna by extending the transmission lines along with the ground planes. The shape of the transmission line is like a letter 'P', with an open circuit at the top, this can be seen as the right part of the antenna in the Figure 8.4a. In order to have a balanced structure, the configuration is replicated, then inverted and connected to the original figure through the inner with the smallest possible gap. The antenna has a centre conductor of width n = 0.7 mm and the outer strips are both of the same width (5.45 mm). The gap m (0.2 mm) separates the centre strip and the two lateral conductors. The other parameters in this design are summarised in Table 8.1.

In order to obtain a compact size, the antenna is folded from both ends with the smallest height that can be achieved (3 mm), so that the antenna has a structure like a folded dipole. The layout of this antenna is presented in Figure 8.4b.

Table 8.1: The parameters of the coplanar antenna

Parameter	Value / mm
a	16.5
b	11
c	25
d	16.5
h	3
g	1
r	1
s	5.45
f	12
t	1
n	0.7
m	0.2
e	2.75

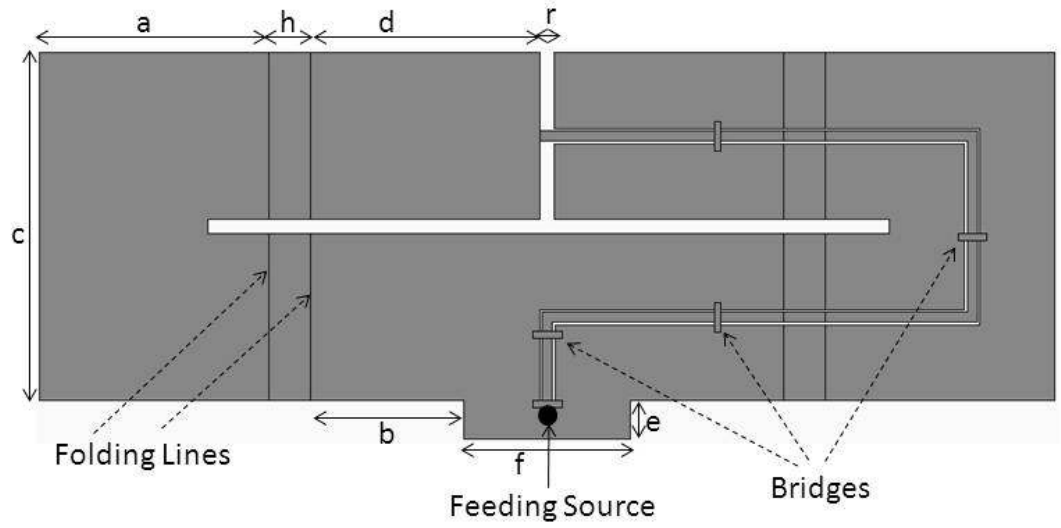

(a)

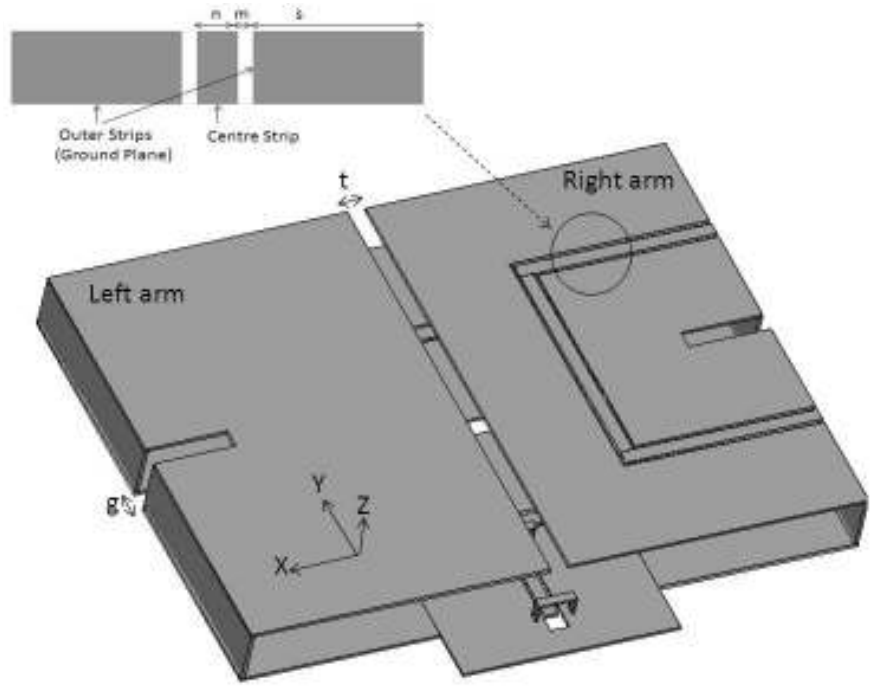

(b)

Figure 8.4: The proposed antenna configuration, (a) dimensions of the unfolded coplanar antenna, (b) The final folded antenna

8.6 Effect of Variation of Parameters on Return Loss

The most sensitive structure parameters of this antenna form a rather large parameter space, and a systematic modelling approach is essential. The simulation was carried out using the CST design suite [19]. The variables under consideration are:

i. The antenna height
ii. The antenna length
iii. The loop gap of the structure
iv. The space between the folded ends of the structure
v. The gap between the arms of the structure
vi. The ground plane size

8.6.1 Variation of the antenna height *h*

The effect of varying the antenna height on return loss is summarised in Figure 8.5. The height was varied over an interval from 2 mm to 6 mm, in 1 mm steps. The resonant frequency has an inverse relationship with *h*, as *h* is increased, then the resonant frequency shifts down in frequency. Therefore, changes to this parameter can be used to control the size of the antenna.

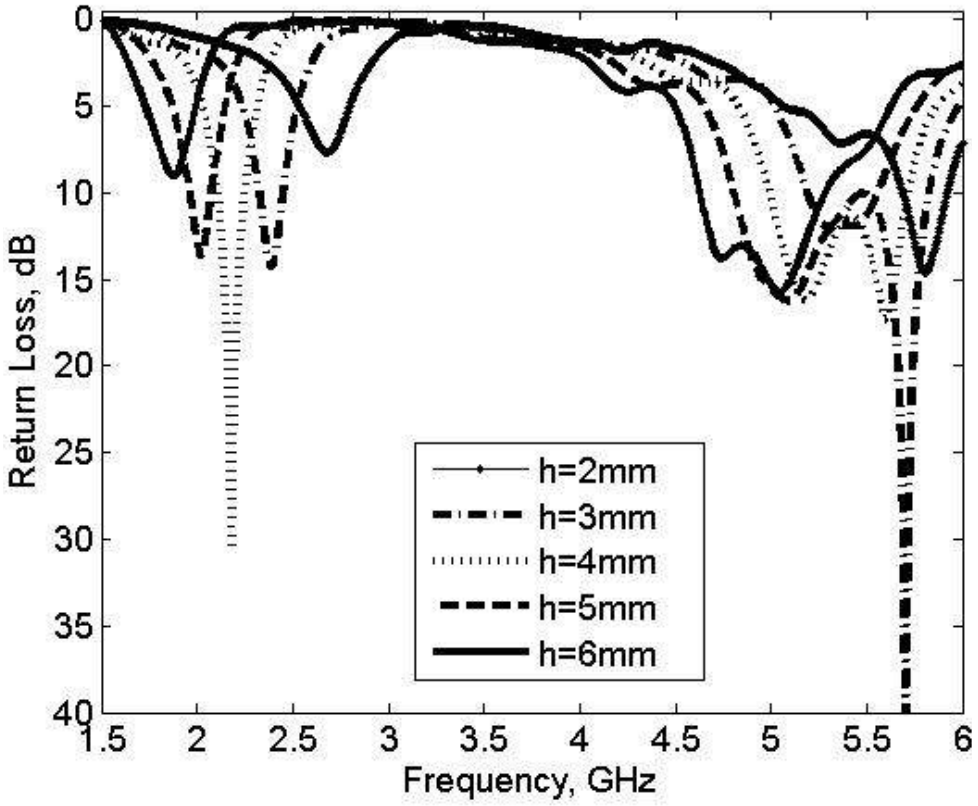

Figure 8.5: Effect of variation of the parameter *h* on the input return loss

8.6.2 Variation of the length of the antenna *b*

The direct effect of antenna length on impedance matching is summarised in Figure 8.6, the length (*b*) was varied from 9 mm to 13 mm, with the other structure parameters being held constant. These results indicate an inverse relationship between resonant

frequency and length, as the b is increased, then the resonant frequency moves down in frequency. This implies that b has a significant impact on the return loss.

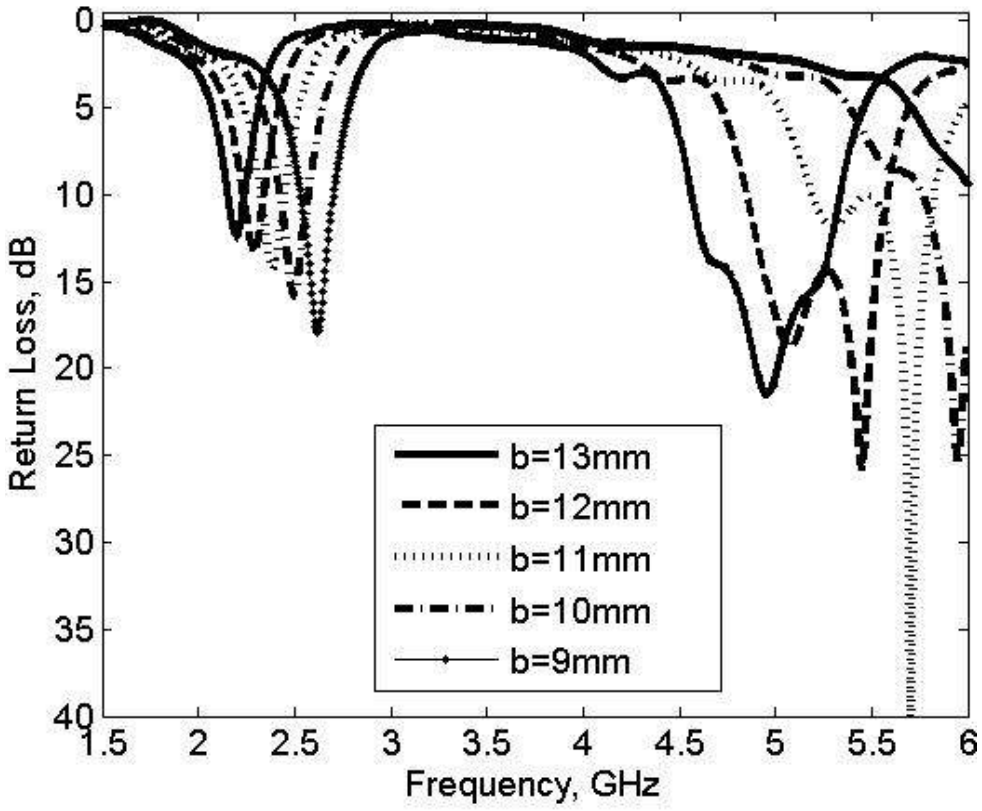

Figure 8.6: Effect of variation of the parameter *b* on the input return loss

8.6.3 Variation of the loop gap *g*

Figure 8.7 shows the return loss of the proposed antenna with variation of the loop gap *g*. The resonant frequency is found to be relatively insensitive to the variations of this parameter. However, there are small variations in the value of the return loss over 5.2 GHz. Therefore, it can be said that the impact of the loop gap *g* on impedance matching is limited.

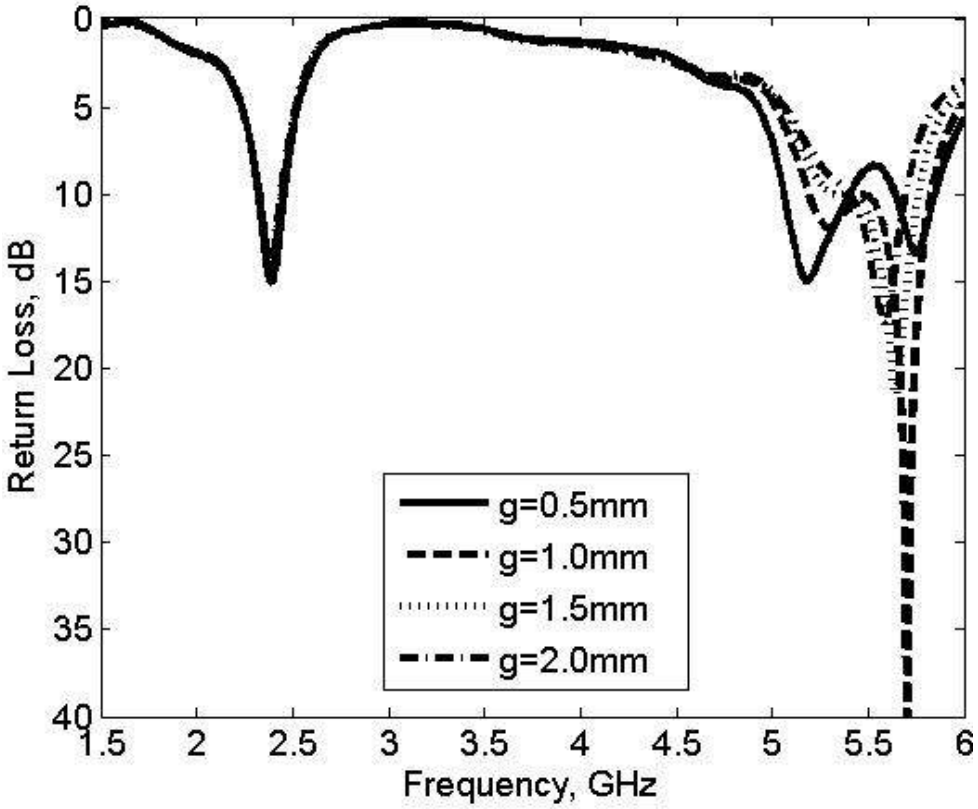

Figure 8.7: Effect of variation of the parameter *g* on the input return loss

8.6.4 Variation of the gap between the folded ends of the antenna *t*

Analysis of the return loss of the antenna with respect to the spacing between its folded ends (*t*) is shown in Figure 8.8 (the other antenna parameters are held constant). The resonant frequency is very sensitive to the variation of this parameter. The resonant frequency can be substantially decreased for small variations in *t* (~0.5 mm). Therefore, the gap *t* has a great effect on impedance matching, and good impedance matching can be obtained by selecting the spacing between the folded ends carefully.

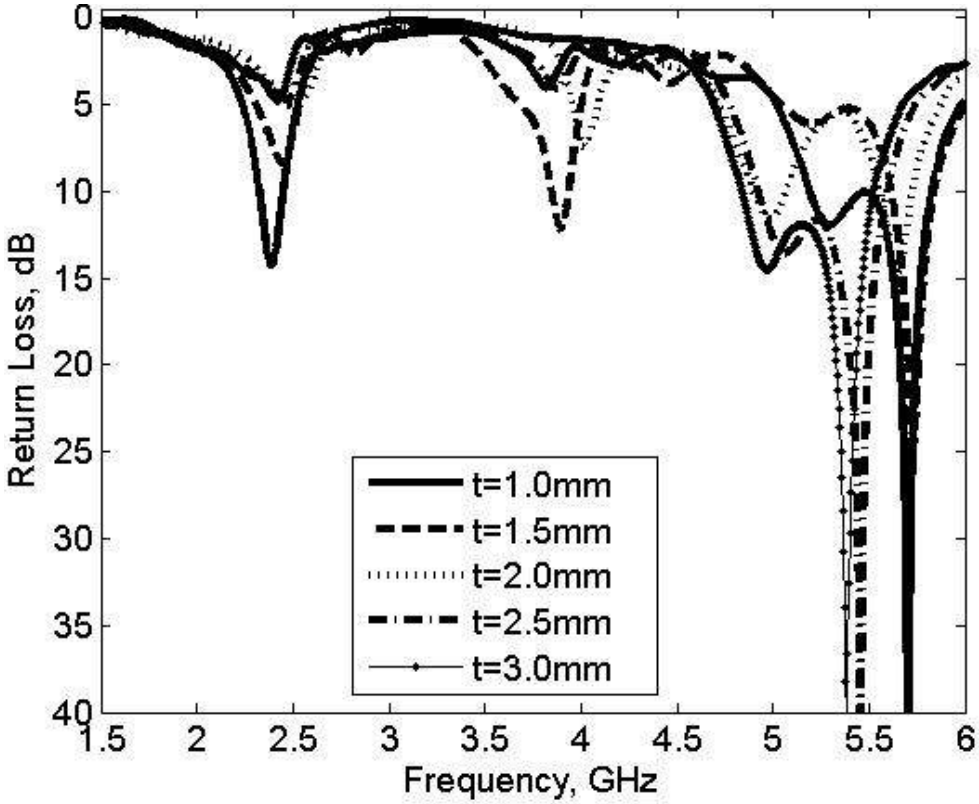

Figure 8.8: Effect of variation of the parameter *t* on the input return loss

8.6.5 Variation of the gap between the electrical ends of the antenna arms *r*

The gap between the ends of the armatures (*r*) is an important design parameter for defining the resonant frequency of this antenna. Figure 8.9 summaries the simulated return loss for different values of *r*. There is a considerable change in the resonant frequency when r is varied by a small amount (0.2 mm). Thus the smaller values of the gap (*r* = 0.6 mm and *r* = 0.8) will tend to degrade impedance matching characteristics, in particular at the higher frequency band. However, in the case of the lower band, the resonant frequency remains unchanged, the smallest gap that can be achieved with acceptable return loss is when *r* = 1 mm.

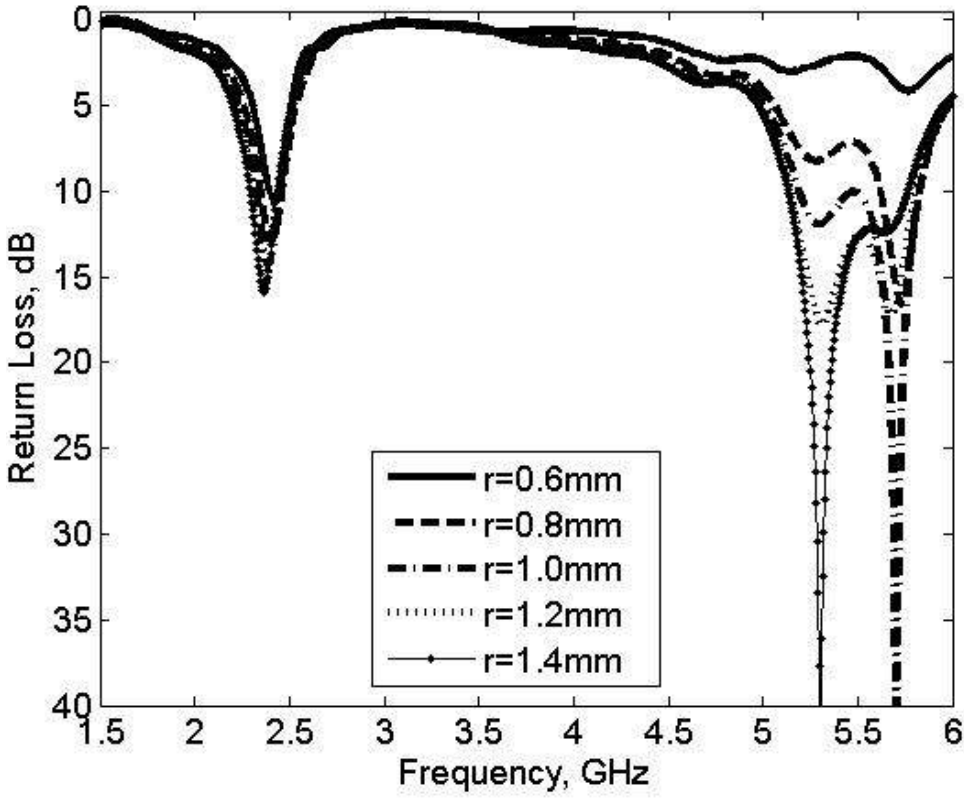

Figure 8.9: Effect of variation of the parameter *r* on the input return loss

8.6.6 The effect of the ground plane size

An investigation of the effect of handset size (equivalent ground plane) on the antenna performance was also carried out. The width of the handset was kept similar to the width of the antenna whereas the length (equivalent to parameter GND) was varied from 20 mm to 80 mm (see Figure 8.10). It is quite clear from Figure 8.11 that there is only an insignificant variation on the return loss when this parameter increased from 20 mm to 80 mm. Therefore, the resonant frequency is found to be relatively insensitive to variations in the ground plane dimensions.

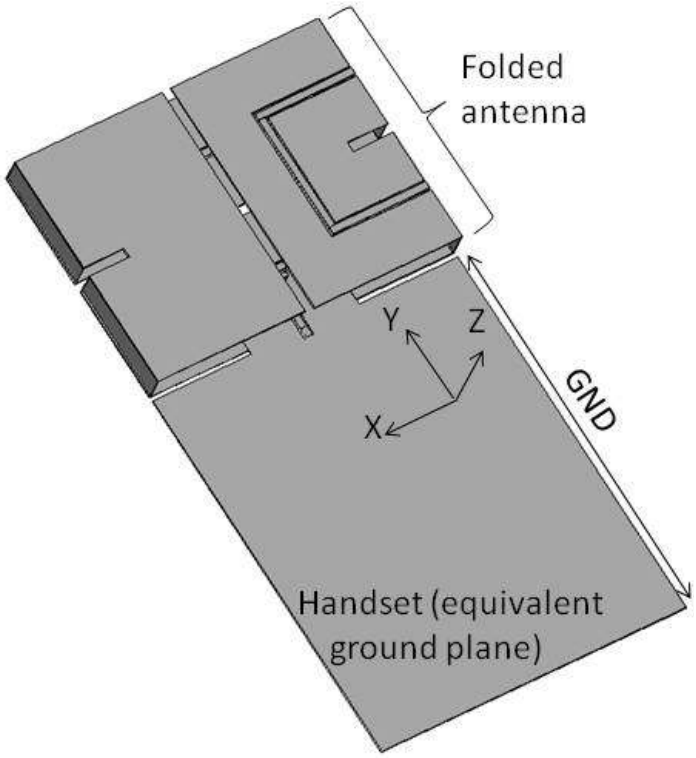

Figure 8.10: The coplanar antenna with equivalent ground plane

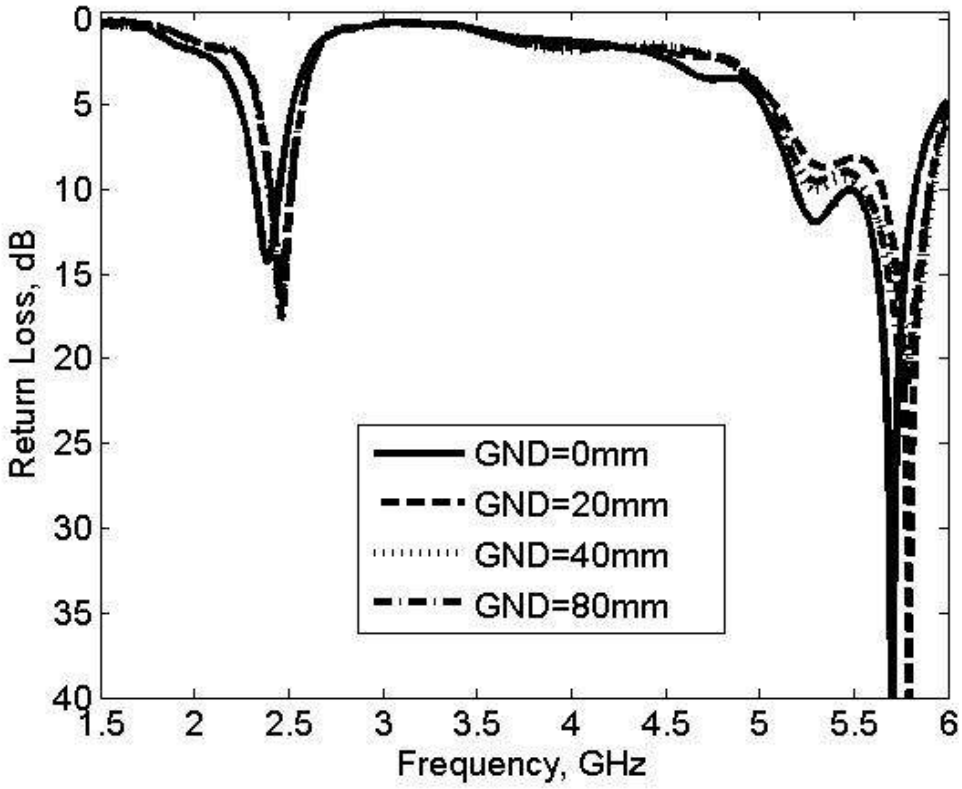

Figure 8.11: Effect of variation of the ground plane size on the input return loss

8.7 Prototyping of Antenna and Test Results

A prototype design using these simulation guidelines was constructed on a flexible foam substrate of thickness 2.5 mm and permittivity 1.1. This allows the antenna to be folded in such a way that the resulting armatures are held at a constant height above the common surface. This prototype is shown in Figure 8.12. A complex process of detaching the foam from the antenna was performed to ensure the most appropriate development in line with the simulation results. Moreover, the proposed antenna structure is completely composed of a CPW line that exhibits one dominant CPW mode. This mode has an electric field with opposite polarities between the two slots; therefore air bridges are placed along the CPW to keep the ground planes at the same potential. This has the effect of eliminating the slot line mode on the CPW line as shown in Figure 8.12a, and then the antenna response is checked to achieve balanced features. In addition, some dielectric material was added carefully between the antenna's top and bottom to support the arms in order to maintain them at the same height, and maintain the same surface structure.

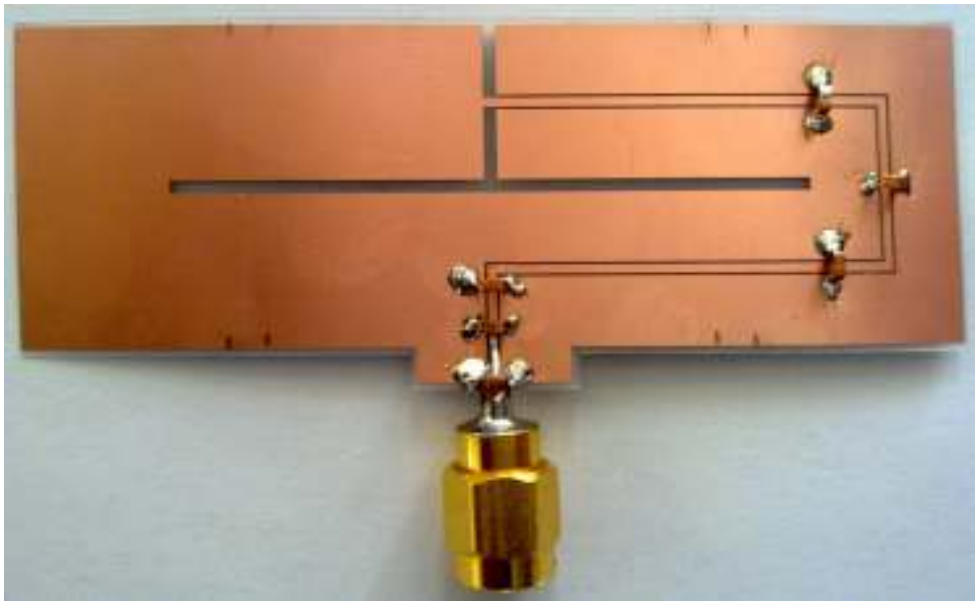

(a)

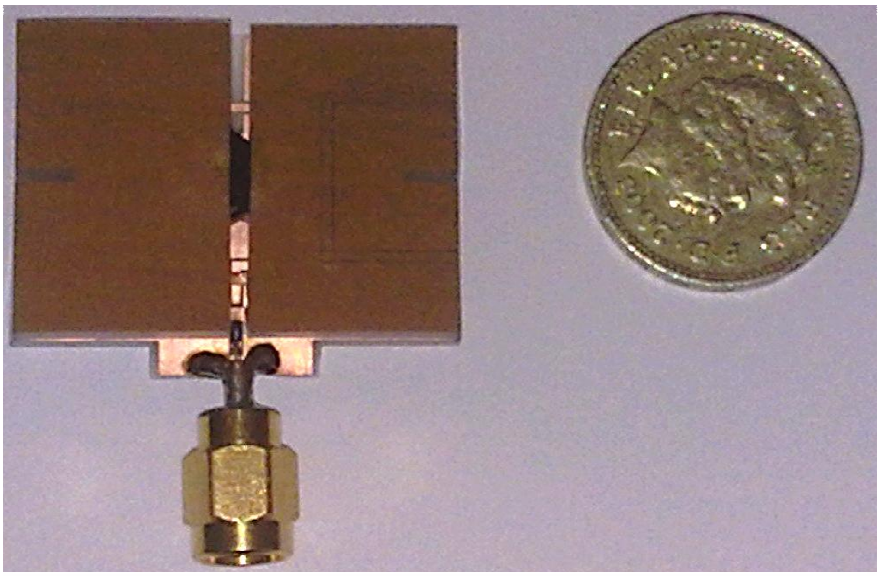

(b)

Figure 8.12: Photograph of prototype of the proposed folded balanced coplanar antenna design, (a) initial 2-dimensional structure, (b) folded in 3 dimensions

Figure 8.13 illustrates the current distribution in the antenna, with and without the air bridges. When the air bridges are implemented between the outer strips (ground plane), the induced current is much stronger, and this is clearly indicated in the figures.

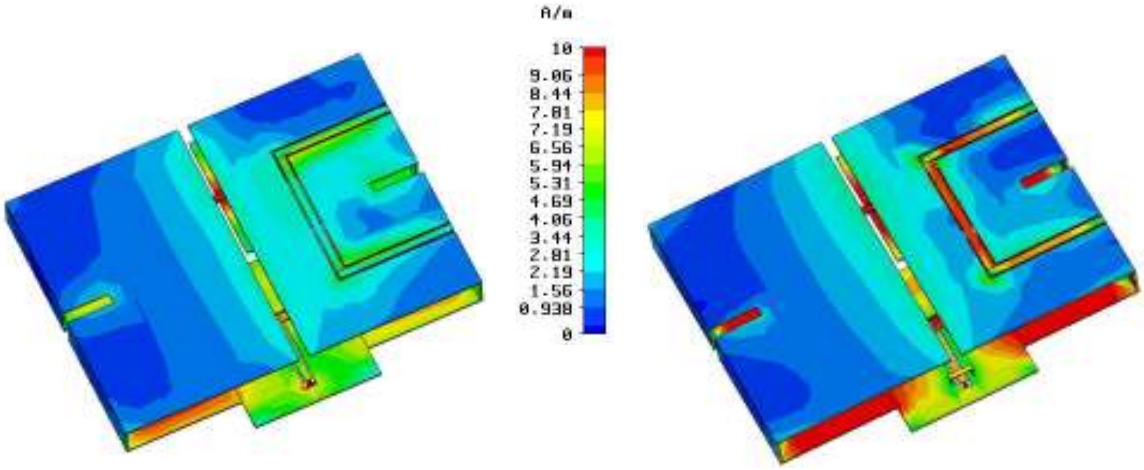

(a) (b)

Figure 8.13: The current distribution in the proposed folded balanced coplanar antenna, (a) without bridges, (b) with bridges

Simulation of prototype antenna shown in Figure 8.14 was carried out using CST; a further simulation was performed using HFSS [20] to verify the findings from the primary simulation model. Figure 8.14 also shows the measured return loss of the prototype antenna. Allowing for any minor errors in the build quality of the antenna, the results gave much confidence in the simulation model. This can be seen from the relatively well-correlated results of the measured return loss, and the values from both simulations, as shown in the figure.

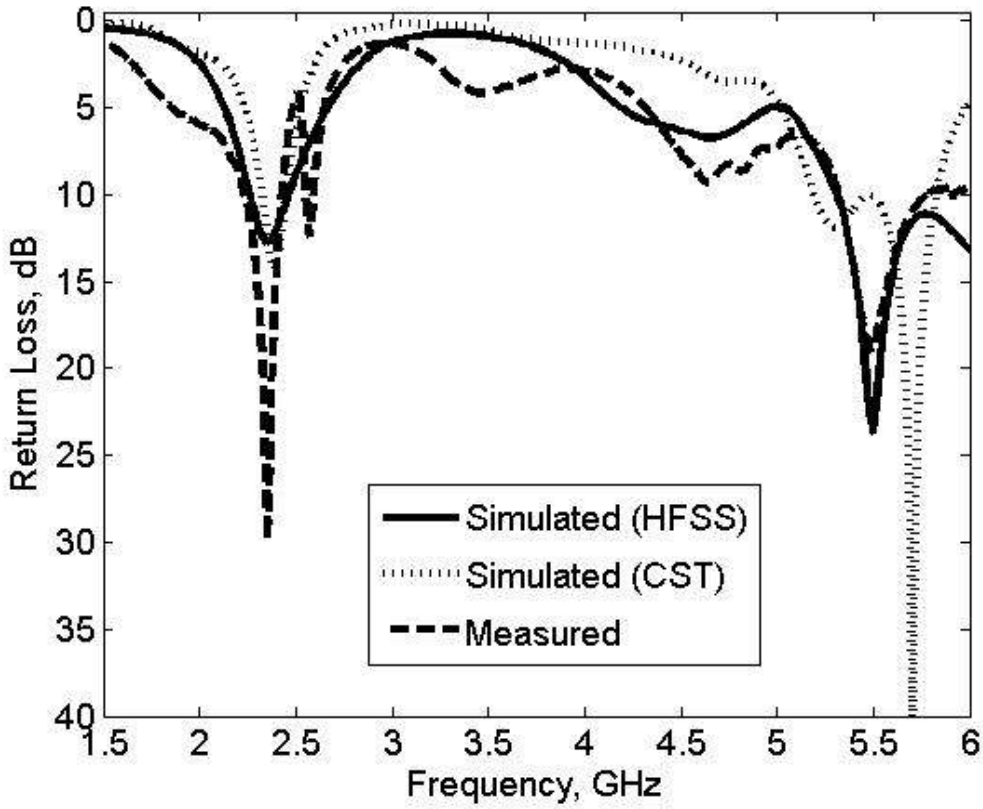

Figure 8.14: The simulated and measured return loss of the proposed antenna

8.8 The Radiation Pattern and Power Gain of the Antenna

Measurements of the radiation patterns of the prototype were carried out in a far-field anechoic chamber. Three principal-plane pattern cuts (i.e. zx, zy and xy planes) were taken for three frequencies that cover the whole designated WLAN operational bandwidth. The radiation patterns were measured at selected frequencies of 2.4 GHz, 2.45 GHz and 5.2 GHz, respectively; the measured patterns were normalized and presented in Figure 8.15. The results indicate a satisfactory agreement between simulated and measured radiation pattern. In addition as can be observed from the figure, these radiation patterns are approximately omni-directional.

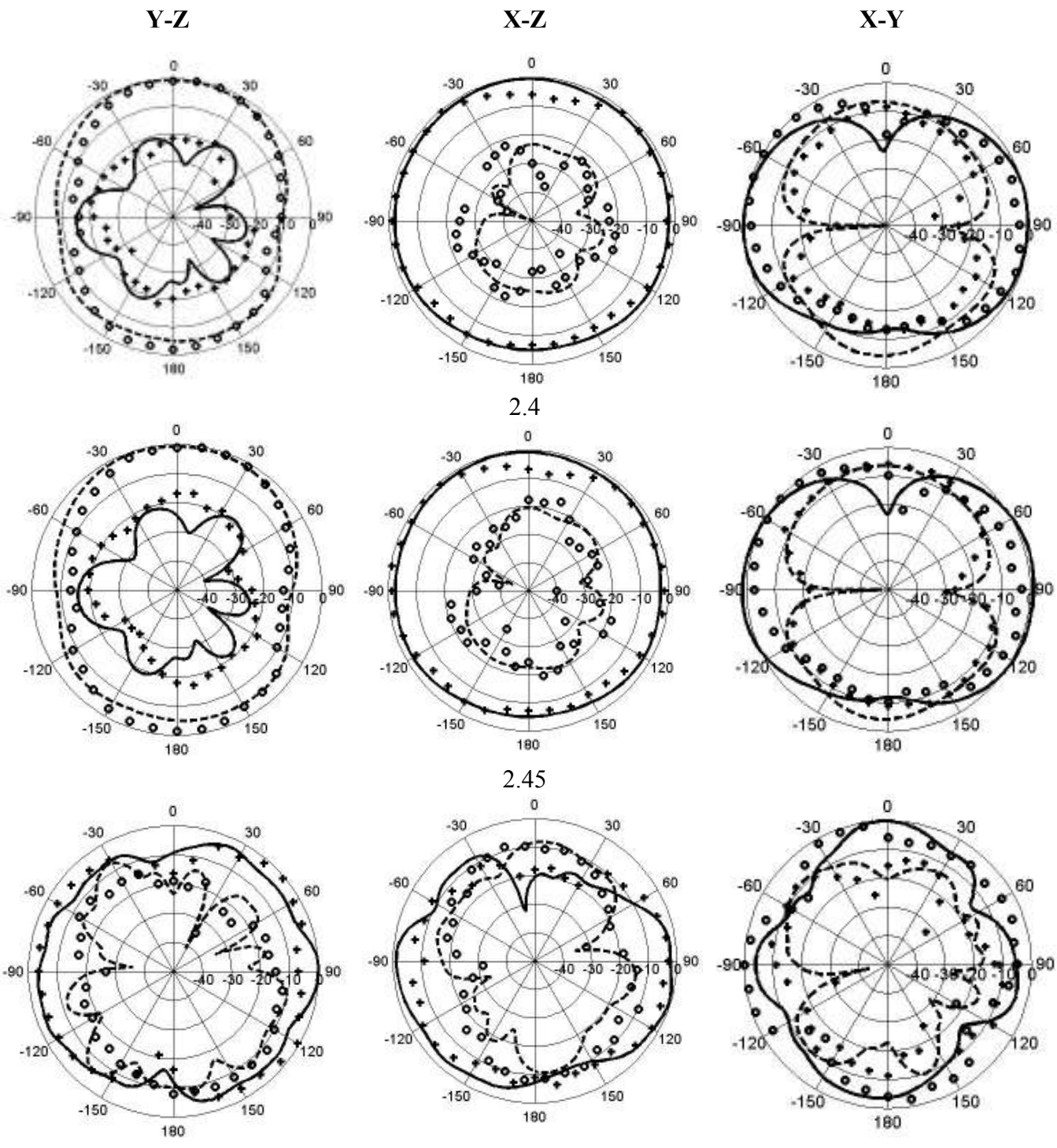

Figure 8.15: Radiation patterns of the proposed antenna at 2.4, 2.45 and 5.2 GHz for yz, xz and xy planes. 'ooo' measured, E_θ ,' ----' simulated, E_θ ,'xxx' measured, E_ϕ '——' simulated E_ϕ

Figure 8.16 illustrates the measured antenna gain in the broadside direction for frequencies across the 2.4 GHz and 5 GHz bands. As can be seen in the figure, the measured antenna gain varied between 1.5 dBi and 1.9 dBi in the 2.4 GHz band, and 1.4 dBi and 2.4 dBi in the 5.2 GHz band. For the bandwidths of the three specific operating bands, the peak antenna gain variations for the 2.4 GHz and 5 GHz bands are less than 1.0 dBi.

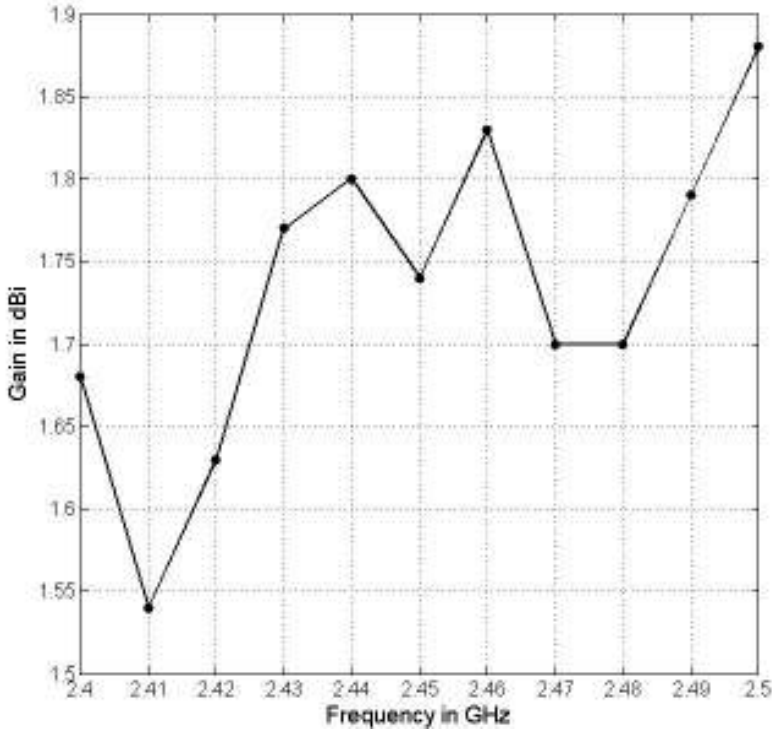

(a)

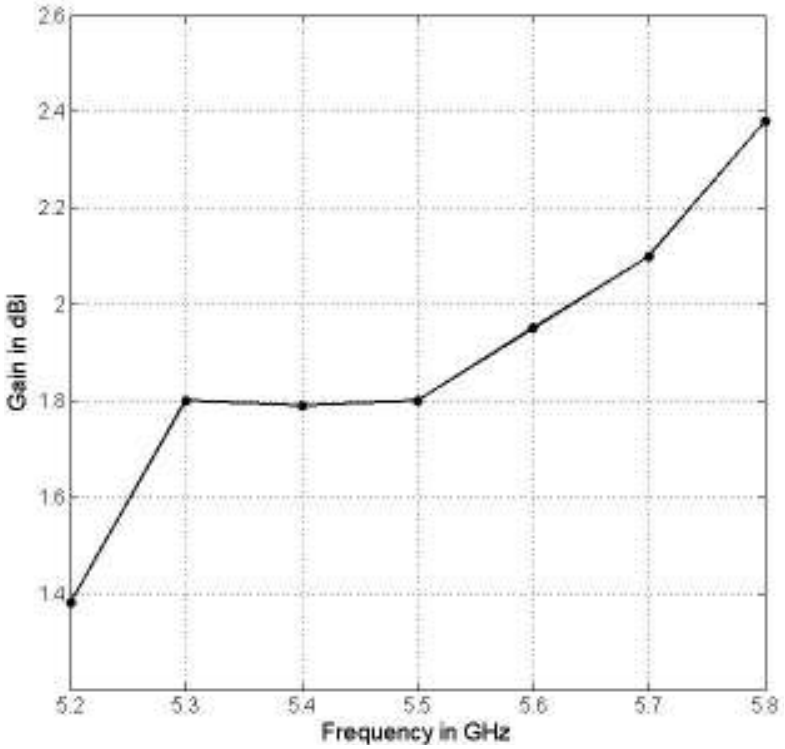

(b)

Figure 8.16: Measured antenna power gain at; (a) 2.4 GHz band,
(b) 5.2 GHz band.

Additionally, a Wheeler cap method for measuring radiation efficiency [21, 22] was applied to this prototype. Figure 8.17 illustrates the simulated and measured radiation efficiency of the antenna over the frequency ranges 2400 MHz to 2460 MHz and 5200 MHz to 5800 MHz. In the lower frequency band (see Figure 8.17a), the variations of measured radiation efficiency are 0.92 to 0.87 which correspond to average of 90% over the bands of interest. At the upper frequency band (see Figure 8.17b), the average radiation efficiency of 87% is achieved (the corresponding values are 0.84 to 0.90). These figures are in close agreement with those calculated from the simulation model.

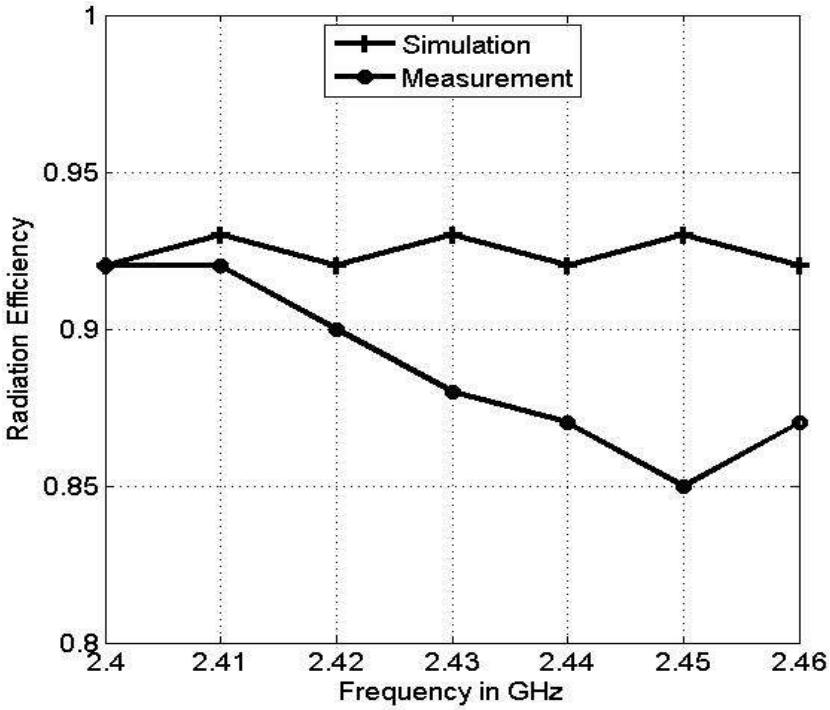

(a)

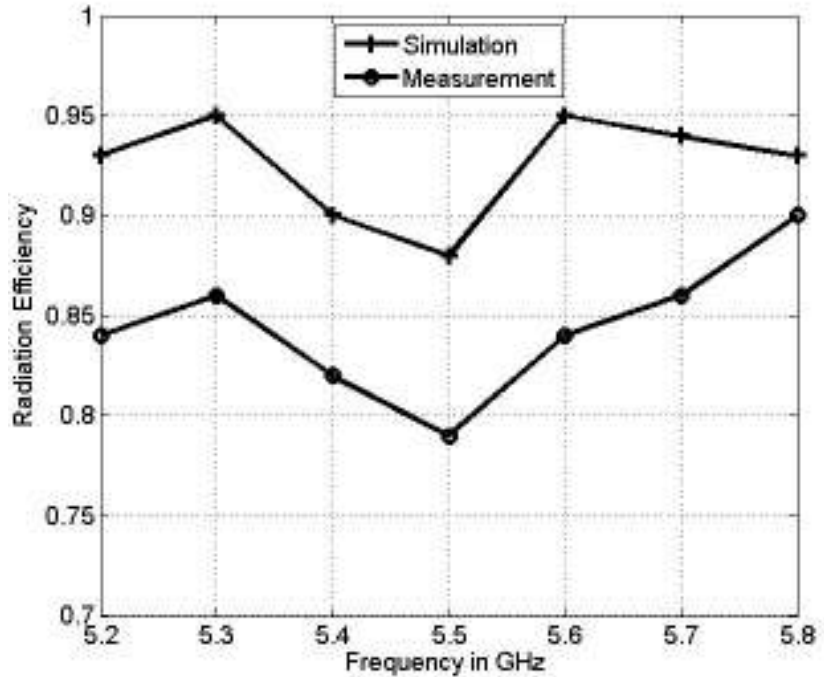

(b)

Figure 8.17: Measured and simulated radiation efficiency of the proposed folded balanced coplanar antenna at; (a) lower band, (b) upper band

8.9 Conclusions

A new class of dual band balanced antennas, with good impedance bandwidth characteristics, and excellent dual-band performance, has been studied in this chapter. The balanced feed network has been realised using a coplanar waveguide design. This design has enabled a selective optimisation of the antenna performance from a well-defined set of structural parameters. These include the height, length, ground plane size, the spacing between the folded arms, the gap between the arms, and the loop gap. The design was validated through detailed simulation of return loss, radiation pattern, power gain and radiation efficiency, which were then realised in a physical prototype.

8.10References

[1] H. Morishita, H. Furuuchi, and K. Fujimoto, "Performance of balance-fed antenna system for handsets in the vicinity off a human head or hand," *IEE Proceeding Microwave Antennas Propagation*, vol. 149, pp. 85-91, 2002.

[2] D. Zhou, R. A. Abd-Alhameed, C. H. See, A. G. Alhaddad, and P. S. Excell, "Compact wideband balanced antenna for mobile handsets," *IET Microwaves, Antennas and Propagation*, vol. 4, pp. 600-608, 2010.

[3] J. S. McLean, "Balancing Networks for Symmetric Antennas:part I: Classification and Fundamental Operation," *IEEE Transactions on Electromagnetic Compatibility*, vol. 44, pp. 503-514, 2002.

[4] G. Ghione and C. U. Naldi, "Coplanar Waveguides for MMIC Applications: Effect of Upper Shielding, Conductor Backing, Finite-Extent Ground Planes, and Line-to-Line Coupling," *IEEE Transactions on Microwave Theory and Techniques* vol. 35, pp. 260- 267, Mar 1987.

[5] C. P. Wen, "Coplanar waveguide: A surface strip Transmission line suitable for nonreciprocal gyromagnetic device applications," *IEEE Transactions on Microwave Theory and Techniques*, vol. MTT-17, pp. 1087-1090, Dec. 1969.

[6] R. L. Smith and J. T. Williams, "Coplanar Waveguide Feed for Microstrip Patch Antennas," *Electronics Letters*, vol. 28, December 1992

[7] S.-M. Deng, M.-D. Wu, and P. Hsu, "Analysis of coplanar waveguide-fed microstrip antennas," *IEEE Transactions Antennas and Propagation,* , vol. 43, pp. 734-737, Jul 1995.

[8] R. K. Raj, M. Joseph, C. K. Aanandan, K. Vasudevan, and P. Mohanan, "A new compact printed antenna with coplanar configuration," *Antennas and Propagation Society International Symposium, IEEE*, vol. 2A, pp. 442 - 445, 2005.

[9] K. Tilley, X.-D. W, and K. Chang;, "Dual frequency coplanar strip dipole antenna," *Antennas and Propagation Society International Symposium, IEEE*, vol. 2, pp. 928 - 931, 1994.

[10] Y. Jee and Y.-M. Seo, "Triple-band CPW-fed compact monopole antennas for GSM/PCS/DCS/WCDMA applications," *Electronics Letters*, vol. 45, pp. 446 - 448, 2009.

[11] M. N. Z. Abidin, "Measurement of current distribution on wire antennas", Master of Science Dissertation in Radio Frequency and Microwave Engineering"," University of Bradford, September 1993.

[12] L. L.L., "Special Aspects of Balanced Shielded Loops," *Proceedings of the IRE* vol. 34, pp. 641- 646, September. 1946.

[13] K.-L. Wong, *Compact and Broadband Microstrip Antennas*. New York: John Wiley&sons, Inc, 2002.

[14] R. Garg, P. Bhartia, I. Bahl, and A. Ittipihoon, *Microstrip antenna design handbook*: Artech House, Inc, 2001.

[15] G. Kumar and K.P.Ray, *Broadband Microstrip Antenna*: Artech house, Inc. Canton Str. US, 2003.

[16] R. N. Simons, *Coplanar Waveguide Circuits, Components, and Systems*: John Wiley & sons. Canada, April 2001.

[17] A. Z. Jakal, "New coplanar printed antennas : a family of broadband uniplanar printed antennas in endfire, broadside and omnidirectional forms, and suitable for integration with coplanar waveguide," PhD. Thesis, Department of Electronic and Electrical Engineering, University of Bradford, Bradford, UK, 1997.

[18] W. Menzel and W. Grabherr, "A Microstrip Patch Antenna With Coplanar Line Feed," *IEEE Microwave and Guided Wave Letters.*, vol. 1, pp. 340-342, NOVEMBER 1991.

[19] "Computer Simulation Technology Corporation, CST Microwave Studio, Version 5.0, Germany."

[20] "High Frequency Structure Simulator, Version 11, Ansoft Corporation, USA.."

[21] R. W. Johnston and J. G. McRory, "An improved Small Antenna Radiation-Efficiency Measurement," *IEEE Antenna and Propagation Society Magazine*, vol. 40, pp. 40-48, 1998.

[22] H. Choo, R. Rogers, and H. Ling, "On the Wheeler Cap Measurement of the Efficiency of Microstrip Antennas," *IEEE Trans. Antennas and Propagation*, vol. 53, pp. 2328-2332, 2005.

CHAPTER NINE

Conclusion and Future Work

9.1 Summary of Thesis

The fundamental objective of this thesis is the development of new balanced structures for antenna designs intended for use in mobile terminals and sensors held or positioned close to the human body. This is to avoid the drawbacks encountered with unbalanced antennas which suffer degraded radiation characteristics as a result of radiating current paths on the human body. The unity of this research can be appreciated through the following retrospective summaries of each of main the chapters.

Chapter 2 reviewed the characteristics of balanced and unbalanced antenna structures. Two measurement techniques to find the differential input impedance of balanced antennas were also presented in this chapter: (i) the monopole method, and (ii) the two-port network method. A symmetrical structure which is fed with balanced currents can achieve an electrically symmetrical operation, through which the balanced currents only flow on the radiating element, thus dramatically reducing the effect of the current flow on the ground plane or chassis. Therefore, if e.g. a mobile handset is held close to the body, no coupling takes place between the antenna and the human body, thus the performance of the antenna is not affected, and a reduced SAR may be achieved. This constitutes the rationale for further development of this field, and the subsequent designs presented in this thesis.

Chapter 3 presents a new wideband balanced folded-arm dipole antenna, operating over the GSM 1800, GSM 1900 and UMTS bands. A further improvement to the antenna has been achieved by covering the 2.45 GHz WLAN band. The input impedances of the proposed antennas were verified by the two measurement techniques described in chapter 2. The measured prototypes showed good agreement with the computational modelling. The performance of the prototype balanced antenna in terms the induced handset currents are derived, and in comparison with unbalanced designs, it was proved there exists an enhanced immunity to the effect of adjacent human body components. This results in an enhanced stability of the proposed antenna for realistic mobile operating conditions.

In chapter 4 a new compact wideband balanced folded dipole antenna, intended to operate over the DCS, PCS, UMTS and 2.4-GHz WLAN bands, was introduced and discussed. This antenna was simulated, prototyped, and tested. Some characteristics of the antenna were investigated in detail in order to validate the performance of the antenna. The measured and simulated differential input impedances were in good agreement. This chapter also introduced and analysed the antenna performance in the presence of a human hand. It was found that the antenna induces only a little current into the ground plane, and thus the desired performance stability of the antenna can be achieved. The antenna efficiency was tested using a radiometric technique, and the results show a favourable performance. The proof of the design concept is concluded by measurement of the gain and radiation pattern.

Chapter 5 presents two different antenna geometries covering the 2.4 GHz and 5.2 GHz WLAN bands, and the 2.5 GHz and 3.5 GHz WiMAX bands. The design concept of compact-planer folded-dipole balanced antennas was initially investigated using HFSS,

and then supported by intensive prototyping and measurement. A new technique was applied to the antenna, in which a long slot was introduced on the each folded arms of the dipole antenna. A significant size reduction was achieved after performing a detailed parametric study over several structural parameters. The antenna performances were characterised over their target bands in terms of return loss and radiation patterns, the return loss measurements were conducted as per discussion in chapter 2, and balun was introduced to verify the impedance of the antenna.

Chapter 6 describes a hybrid computational method which efficiently models the interaction between a small dual band balanced antenna, placed in proximity with the human body, and operating over the 2.4 GHz and 5.2 GHz WLAN frequencies. Results for several test cases of antenna placed in different locations on the body are presented and discussed. The near and far fields were incorporated into the study to provide a complete understanding of the impact on human tissue. Finally, the cumulative distribution function (CDF) of the radiation efficiency, and the ratio of the absorbed power to the radiated power of the identified locations were also provided. It was concluded that there was a clear improvement in the front compared to the back. The reason for this appeared to be due to a loss of characteristics in the tissue at the front, and a greater degree of absorbed power.

In chapter 7 a planar UWB antenna covering a wide range of frequencies has been presented. The antenna arms were considered as a wide planer monopole antennas, and then mounted on substrate for further improvement and easy implementation. These two wideband radiators were fed using tapered microstrip lines to meet the wide frequency response. The handset geometry was modified to meet these modifications, such as the feed network used in this particular design. Two baluns were utilised for this proposed

antenna, each covering single band. A parametric study was performed over several structural antenna parameters, to reduce the antenna's size, and to verify the optimum response. The prototype return loss and radiation pattern was in good agreement with expectations. In addition the computed effects of user hand and head on mobile performance were also investigated in this chapter.

A new idea of using a coplanar waveguide structure to implement the balanced feed network covering the 2.4 GHz and 5.2 GHz WLAN frequency bands has been presented in chapter 8. The antenna is intended to eliminate the need for a balanced feed network. This structure enabled modification to selected antenna parameters with a view to optimizing the antenna's performance. Results were obtained by varying the following antenna parameters: height; length; spacing between the folded ends; gap between arms; loop gap, and ground plane size. The antenna was fabricated and tested to evaluate and the design concept. The predicted and measured results for return loss, radiation pattern, power gain and radiation efficiency demonstrated considerable success in achieving this; with good impedance bandwidth characteristics, and an excellent dual-band performance.

9.2 Conclusion

Several new developments in balanced antenna structures have been described, and validated. The antenna designs have been motivated by applications in multi-band mobile terminals and handsets, wireless LANs and UWB radio. Different techniques have been applied to the antennas to meet the required design specification. These antennas have been fabricated, and tested, and compared with theoretical results.

Balanced antenna systems are of major interest to mobile phone antenna designers. This is due to their stable performance when held adjacent to the human body by their users, as compared with that of the unbalanced designs. It is believed that the mutual coupling of the balanced antenna is not totally affected by the induced currents in the mobile handsets. Consequently the resultant performance of these antennas would be preserved even when the handset is loaded or in contact with human hands. It should be noted that these antennas are fed by two sources carrying currents of equal magnitude and 180° out of phase. The result of this emergent symmetric geometry is that the induced currents appearing on the handset will be mostly cancelled (i.e., no current flows on the antenna ground plane). In fact, the effects of the antenna radiation next to the human head will also suggest reducing the possibility of electromagnetic energy absorption by the user's head.

9.3 Suggestions for Further Work

Throughout the course of this research it was observed that there were areas for further study that might be carried out.

- An important candidate for further development is the use of the coplanar technique. For mobile terminals there is considerable scope for further improvements to antenna performance, and extensions into more varied multi-band operation, including GSM 1800/1900 and UMTS. Further size reductions may also be achieved, without degrading overall antenna performance, and investigations into ‘best fit’ assembly configurations could be pursued using Genetic Algorithm (GA) optimisation [1].

- The results in chapters 3 and chapter 4 have proved the basic design concept for mobile antennas using balanced techniques. Although attractive in mobile phone design, there are still some substantial limitations in practice. This approach does not cover the lower frequency GSM 900 band, which is a continuing operational necessity, nor does it cover the 5 GHz WLAN band, which is an emerging requirement for mobile handsets and terminals. Therefore, further development of balanced antennas could be investigated to develop new techniques for multi-band design.
- There would also be considerable research value in establishing small balun designs which meet the required wideband response, and enable the module to fit a desirable volume size for mobile applications.
- The possible use of EBG material [2] on balanced antenna could add considerable value in studies to improve antenna performance. This is because the EBG structure has the capability to exhibit a distinct stop-band for surface waves [3, 4], whereby the gain and the efficiency of the antenna may be increased.
- One further possible study that might be considered relates to tuning balanced antennas [5]. These antennas could be operated on single and multi-band facilities on different frequencies which are not necessarily harmonically related [6].

9.4 References

[1] D. Zhou, R. A. Abd-Alhameed, and P. S. Excell, "Bandwidth enhancement of balanced folded loop antenna design for mobile handsets using genetic algorithms," *National URSI symposium, University of Portsmouth, Portsmouth, UK*, 2007.

[2] Z. Z. Abidin, R. A. Abd-Alhameed, N. McEwan, S. M. R. Jones, K. N. Ramli, and A. G. Alhaddad, "Design and analysis of UC-EBG on Mutual Coupling Reduction," *Loughborough Antennas & Propagation Conference*, pp. 693-696, November 2009.

[3] M. F. Abedin and M. Ali, "Effects of EBG Reflection Phase Profiles on the Input Impedance and Bandwidth of Ultrathin Directional Dipoles," *IEEE Transactions on Antennas and Propagation*, Vol. 53, pp. 3664-3672, November 2005.

[4] M. Z. Azad and M. Ali, "Novel Wideband Directional Dipole Antenna on a Mushroom Like EBG Structure, "*IEEE Transactions on Antennas and Propagation*, vol. 56, pp. 1242-1250, 2008.

[5] I. T. E. Elfergani, R. A. Abd-Alhameed, C. H. See, M. B. Child, and P. S. Excell, "A capacitively loaded antenna for use in mobile handsets," *Antennas and Propagation Conference (LAPC), 2010 Loughborough*, pp. 441 - 444, Nov. 2010.

[6] J. F. Wu, C. J. Panagamuwa, P. McEvoy, J. C. Vardaxoglou, and O. A. Saraereh, "Switching a dual band PIFA to operate in four bands,," *IEEE Antennas and Propagation Society International Symposium*, pp. 2675 - 2678 2006.

Author’s Publication Record

LIST OF PUBLICATIONS

JOURNAL ARTICLES

[1] **A. G. Alhaddad**, R. A. Abd-Alhameed, D. Zhou, C. H. See, I. T. E. Elfergani, and P. S. Excell, "Low Profile Dual-Band Balanced Handset Antenna with Dual-Arm Structure for WLAN Application," *IET Microwaves, Antennas and Propagation,* vol. 5, pp. 1045-1053, 2011.

[2] **A. G. Alhaddad**, R. A. Abd-Alhameed, D. Zhou, and P. S. Excell, "Folded Loop Balanced Coplanar Antenna for WLAN Applications," *IEEE Transactions on Antenna and Propagation,* June 2011 (in press.).

[3] D. Zhou, R. A. Abd-Alhameed, **A. G. Alhaddad**, C. H. See, P. S. Excell, and S. Gao, "Multi-band Weakly Ground-Coupled Balanced Antenna for Portable Devices," *IET Science, Measurmrnt & Technology*, July 2011 (in press.).

[4] D. Zhou, R. Abd-Alhameed, C. See, **A. G. Alhaddad**, and P. Excell, "Compact wideband balanced antenna for mobile handsets," *IET Microwaves, Antennas and Propagation*, vol. 4, pp. 600-608, 2010.

[5] **A. G. Alhaddad**, R. Abd-Alhameed, C. S. D Zhou, E. Elkhazmi, and P. Excell, "Compact dual-band balanced handset antenna for WLAN application," *The Electromagnetics Academy, PIERS Online*, vol. 6, pp. 11-15, 2010.

CONFERENCES AND WORKSHOPS

[1] I.T.E.Elfergani**,** R.A.Abd-Alhameed, **A. G. Alhaddad**, C.H.See, and E.H.Cabongomueba, "A Novel Dual Band Frequency Tunable Balanced Handset Antenna for WLAN Application", 18th IEEE International Conference on Electronics, Circuits and Systems (ICECS 2010), Beirut, Lebanon, pp. 516-519, December 11-14, 2011.

[2] I. T. E. Elfergani, A. S. Hussaini, R. A. Abd-Alhameed, C. H. See, M. M. Abusitta, H. I. Hraga, **A. G. Alhaddad**, and J. Rodriguez, "Frequency Tuned Planar Inverted F Antenna with L Shaped Slit Design for Wide Frequency Range," *Progress In Electromagnetics Research Symposium Proceedings, Marrakesh, Morocco*, pp. 443-447, March 2011.

[3] **A. G.Alhaddad**, R. A. Abd-Alhameed, D. Zhou, and P. S. Excell, "Folded Loop Balanced Coplanar Antenna for WLAN Applications " *Proceedings of 4rd International Conference on Internet Technologies and Applications*, Wrexham, North Wales, UK, pp.566-573, 8-11 September 2011.

[4] I.T.E.Elfergani, R. A. Abd-Alhameed, C. H. See, H. I. Hraga, T.sadeghpour, **A. G. Alhaddad**, and P. S. Excell, "Dual-Band and Wide Band Tuning Antennas for Mobile snd Wireless Communications" *Proceedings of 4rd International Conference on Internet Technologies and Applications*, Wrexham, North Wales, UK, pp.524-530, 8-11 September 2011.

[5] **A. G. Alhaddad**, K. N. Ramli, R. A. Abd-Alhameed, and D. Zhou, "Interaction between electromagnetic field and human body for dual band balanced antenna using hybrid computational method," *Antennas and Propagation Conference (LAPC), Loughborough*, pp. 449 - 452 November, 2010.

[6] **A. G. Alhaddad**, R. A. Abd-Alhameed, D. Zhou, I. T. E. Elfergani, C. H. See, P. S. Excell, and M. S. Bin-Melha, "Low Profile Balanced Handset Antenna with Dual-Arm Structure for WLAN Application," *Proceedings of Mosharaka International Conference on Communications, Propagation, and Electronics (ISBN: 978 - 9957- 486 - 10 - 5),Amman, Jordon*, pp. 1-4, 5-7 March 2010.

[7] Z. Z. Abidin, R. A. Abd-Alhameed, N. McEwan, S. M. R. Jones, K. N. Ramli, and **A. G. Alhaddad**, "Design and analysis of Uc-EBG on Matual Coupling Reductiobn," *Loughborough Antennas & Propagation Conference*, pp. 693-696, November 2009.

[8] **A. Alhaddad**, R. Abd-Alhameed, D. Zhou, C. See, M. Usman, Z. Z. Abidin, and P. Excell, "Novel balanced handset antenna design for 2.4 and 5.2 GHz bands application," *Loughborough antenna and propagation conference*, pp. 681-684, November 2009.

[9] D. Zhou, R. Abd-Alhameed, C. See, **A. Alhaddad**, and P. Excell, "New Dual-band Balanced Handset Antenna Design for 2.4 and 5.2 GHz Bands Application," *In proceeding of Mosharaka International Conference on Communications, Propagation and Electronics (ISBN: 978- 9957- 486- 06- 8), Amman, Jordon*, 6-8 February 2009.

[10] D. Zhou, R. Abd-Alhameed, C. See, **A. Alhaddad**, and P. Excell, "Wideband Reduced-Size Balanced Antenna Design for Mobile Handsets," *In proceeding of Mosharaka International Conference on Communications, Propagation and Electronics (ISBN: 978- 9957- 486- 06- 8), Amman, Jordon*, 6-8 February 2009.

[11] D. Zhou, R. Abd-Alhameed, C. See, **A. Alhaddad**, and P. Excell, "New mobile balanced mobile antenna with wide bandwidth performance," *In proceeding of the European Conference on Antennas and Propagation: EuCAP*, pp. 549-552, March 23-27, 2009, Berlin, Germany.

[12] D. Zhou, R. Abd-Alhameed, C. See, S. Chung, **A. Alhaddad**, and P. Excell, "Dual-frequency balanced mobile antenna for WLAN and short range communication systems," *In proceeding of Progress In Electromagnetics Research Symposium (ISBN: 978-1-934142-08-0)*, pp. 1277 – 1280, March 23-27, Beijing, China, 2009.

[13] **A. Alhaddad**, R. Abd-Alhameed, and D. Zhou, "Ultra-wideband balanced antenna for mobile handsets," *In proceedings of the ninth informatics workshop for research students (ISBN: 978-1-85143-251-6), University of Bradford, Bradford, UK*, pp. 36-37, 13 June 2008.

Selected Author's publications

IEEE Transactions on Antenna and Propagation, June 2011 (in press.)

Folded Loop Balanced Coplanar Antenna for WLAN Applications

A.G. Alhaddad[1], R.A. Abd-Alhameed[1], D. Zhou[2], C.H. See, P.S. Excell[3] and S.M.R. Jones[1]

Abstract— **A novel balanced rectangular loop antenna is proposed, having an ungrounded coplanar waveguide (CPW) configuration with folded structure at both ends. This antenna is designed for operation covering the 2.4 GHz and 5 GHz WLAN frequency bands. Bond-wire bridges are used along the CPW line to ensure the same potential across the CPW ground planes. The self-balancing structure of the CPW loop antenna offers the antenna's operation without the need of a separate balun for connecting to a RF source. A prototype of the optimized antenna with overall dimension of 51(l) x 16(w) x 3(h) is fabricated and tested. The calculated and measured results show good agreement, confirming good wideband characteristics with multiband operation. An example application of the proposed antenna is studied when used in handheld devices. The results show that this balanced antenna has performance largely independent of the variation of its associated ground plane. The use of an unbalanced CPW feeding technique confirmed the advantages of this new balanced antenna design.**

Index Terms— **Antenna, coplanar waveguide, balanced feed, WLAN**

I. Introduction

With continuing advancements in personal communications and the changing nature of consumer aspirations, the demand for compact antennas with wide impedance bandwidth and excellent radiation performance has grown radically. Over recent years, balanced antenna systems have become of interest as a means to satisfy some of these demands. For instance, they have been studied in applications for mobile handsets, for their superior performance compared with the unbalanced type (e.g. Planar Inverted-F Antenna) when held adjacent to the human body by the phone user [1-6]. Because balanced currents flow only on the antenna element in such antennas, this dramatically reduces the effect of induced current flow on the ground plane (i.e. phone chassis).

Generally, for balanced antennas (e.g. dipoles or other reported designs [1-5]), a balun (balanced to unbalanced transformer) is necessary to cover multiple operating frequency bands as a feeding network, and to provide a balanced feed from an unbalanced source. This can sometimes become a drawback when the balanced antennas are used in handheld devices, requiring a broadband balun to feed broadband or multi-band balanced antennas. In addition, the additional cost and performance degradation introduced by the balun are further drawbacks. A convenient alternative approach to overcome these drawbacks is to use integrated balun approach that is possible with a loop antenna, combined with realization in coplanar structure. Coplanar transmission line antenna configurations are an attractive option due to their simplicity and ease of integration with active and passive components on the same layer [7,8]. The coplanar waveguide (CPW) structure as a type of transmission line has become an intensive topic of recent research due to its attractive characteristics, such as the possibility of wider impedance matching bandwidth and easy fabrication process. Moreover, CPW antenna structures have demonstrated less peak gain variation and higher minimum peak gain across their operating bands, as reported in [9-11].

In this paper, a new dual-band balanced rectangular loop antenna in an ungrounded coplanar waveguide structure is introduced. A prototype of the antenna was designed and fabricated and its characteristics were experimentally verified through a hardware realization. In this study the antenna is assumed operating over the license-free 2.4 GHz bands and both 5 GHz bands (i.e. 2.4–2.483, 5.15-5.35 GHz & 5.725-5.825 GHz), as adopted for Wireless Local Area Network (WLAN) connectivity.

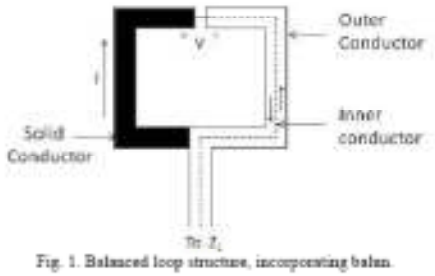

Fig. 1. Balanced loop structure, incorporating balun.

II. Principle of the Shielded Balanced Loop

A balanced shielded loop is made from coaxial cable with a narrow gap in the outer conductor (or shield) [12]. This basic balanced loop antenna can be driven directly with an

Manuscript received March 1, 2011. This work was supported by the UK Engineering and Physical Sciences Research Council (EPSRC) under grant EP/E022936/1.

[1]A.G. Alhaddad, R.A. Abd-Alhameed, C.H. See and S.M.R. Jones are with Mobile and Satellite Communications Research Centre, University of Bradford, Bradford, UK.

[2]D. Zhou is with Vertu Ltd, Church Crookham, Fleet, UK.

[3]P.S. Excell is with Glyndwr University, Wrexham, UK.

IEEE Transactions on Antenna and Propagation, June 2011 (in press.)

unbalanced coaxial feed by routing the coaxial feed around to the neutral point opposite the feedpoint, thus creating an integrated wideband balun [13]. The inner of the coaxial line (or equivalent coplanar transmission structure) is terminated onto the outer conductor, or sheath, (equivalent to the coplanar ground plane) of the opposite half loop at the gap. The e.m.f. induced in the outer conductor of the loop and appearing across the gap will still be transferred to the load Z_L. The balanced coaxial (or coplanar) structure, incorporating a balun transformer is shown in Fig. 1.

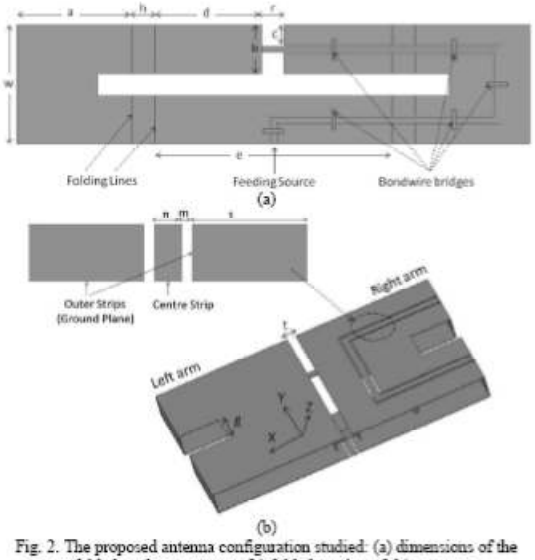

Fig. 2. The proposed antenna configuration studied: (a) dimensions of the unfolded coplanar antenna, (b) folded version of this antenna.

III. Antenna Structure

The coplanar antenna comprises three rectangular conducting strips; a centre strip and two similar lateral strips. Fig. 2a shows the geometry of the proposed antenna in coplanar waveguide technology in the unfolded version of the structure. Here the CPW is used as an antenna itself by extending the transmission lines along with the 'ground planes' (which actually radiate in this configuration). The shape of the transmission line is like a letter 'P', with an open circuit at the top (the right part of the antenna in Fig. 2a). In order to have a balanced structure, the configuration is replicated, then inverted and connected to the right part through the inner conductor, with a small gap (see parameter *r* in Fig. 2a). The antenna has a centre conductor of width n=0.7 mm and the outer strips are both of the same width c=2.7 mm. The gap m of 0.2mm separates the centre strip and the two lateral conductors. The other parameters in final design of this antenna are summarized in Table 1.

Bond-wires are also employed along the CPW lines to ensure the same potential across the CPW outer conductors. To obtain a compact design, the proposed antenna is folded again in a second plane by bending along the long lateral of the rectangular loop, while maintaining the smallest height that can be achieved (3mm), which must allow for the height of the bondwire bridges of 1mm. The layout of this antenna in folded version is presented in Fig. 2b.

TABLE I
The Parameters of the Coplanar Antenna

Parameter	Value (mm)	Parameter	Value (mm)
a	15	r	3
b	11	c	2.7
w	16	e	31
d	14	t	1
h	3	n	0.7
g	3	m	0.2

IV. Discussion and Analysis

The proposed antenna configuration was studied firstly by simulation and then in a hardware realization. In this section, the characteristics of the proposed design are analyzed in terms of antenna return loss, current distribution, radiation patterns, antenna gain and efficiency. In addition, the results of a study of an application of this antenna are presented. The measured results of the fabricated prototype are presented and compared with the simulation predictions.

A. Effect of Variation of Parameters on Return Loss

The importance of the parametric study is to help understand the behaviour of the antenna operation and sensitivity of antenna input impedance matching to the variation of the parameters. In this study, the balanced loop antenna is intended to achieve multi-band operation over the 2.4 GHz and 5 GHz bands. At the lower band, the loop antenna resonates when the structure has total electrical length of one wavelength at the resonant frequency, whereas it resonates in the harmonic mode at the upper band. According to the dimensions of the final design, the inner conductor of CPW structure has a total length of 71.7 mm (excluding the length of parameter *r*), which corresponds to 0.58λ (λ is wavelength in free space) at 2.45 GHz and 1.18λ at 5 GHz. It is noted that its total electrical length at the lower band is significantly less than a free-space wavelength, which is due to the modification of its electromagnetic behavior by folding the structure.

The most sensitive parameters of the antenna, including height, length, spacing between the folded ends, gap between arms and loop gap, were studied. The influence of these parameters on antenna impedance matching was explored using the Ansoft HFSS software [13].

Parameter c is an important design parameter to achieve a minimized design, since the overall length of the antenna (parameter e) in the folded structure is almost fixed in order to achieve the desired resonance at the lower band. Fig. 3 shows the variation of the parameter c while holding constant the rest of the parameters, as stated in Table I. As can be seen, in general the variations do not significantly influence the antenna resonance over both bands. The slight frequency shifting and the variation in input impedance matching can be easily tuned using other parameters. Thus, the smallest

IEEE Transactions on Antenna and Propagation, June 2011 (in press.)

possible value of parameter c, 2.7 mm, was chosen in the final design.

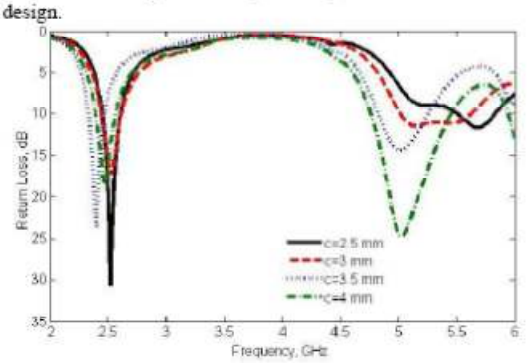

Fig. 3 Effect of variation of the parameter c on the input return loss.

Fig. 4 depicts the variation of simulated return loss for different values of the separation gap between the electrical ends of the arms of the antenna r, which corresponds to tuning the capacitance between the two ends of the loop antenna. As can be seen, the resonant frequency remains unchanged at the lower band; whereas there is considerable change in the input impedance matching when r is varied from 1 to 3 mm, especially over the upper band. This is because the impedance matching gradually changes from critical coupling to under-coupling as r decreases.

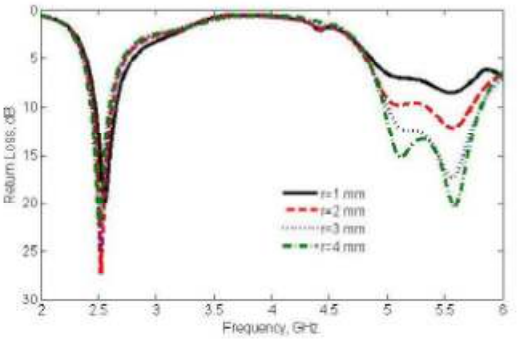

Fig. 4 Effect of variation of the parameter r on the input return loss.

B. *Effect of bondwire bridges on the antenna performance*

The CPW line exhibits one dominant CPW mode. The type of this mode has an electric field with opposite polarities between the two slots; therefore, bondwire bridges were placed along the CPW to keep the outer ('ground') planes at the same potential, thereby eliminating the parasitic slotline mode.

Fig. 5 clearly illustrates the current distribution in the antenna for two cases; with and without bondwire bridges at two different bands. When the bridges are implemented between the outer strips (ground planes), the induced current is stronger at 2.45 GHz than without bridges; whereas little difference in current distribution is observed at 5.2 GHz (similar behavior also observed at 5.8 GHz). In addition, the effects of bridges on the antenna return loss were examined and the corresponding results are shown in Fig. 6. These results show that the antenna matching and resonances deteriorate in the absence of the bridges, thus validating the necessity of using bondwire bridges in the proposed antenna.

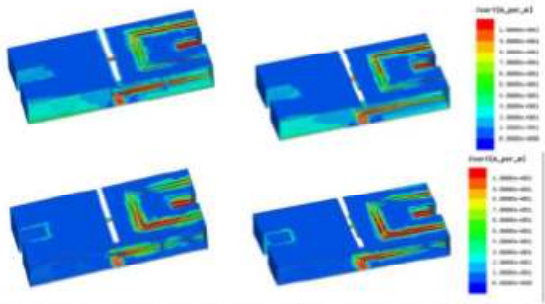

Fig. 5. The current distribution in the folded balanced coplanar antenna with bridges (left) and without bridges (right); at 2.45 GHz (upper) and 5.2 GHz (lower).

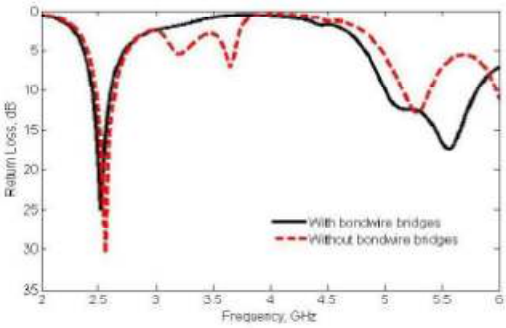

Fig.6. The antenna return loss with and without bondwire bridges.

(a) (b)

Fig. 7. Photograph of prototype of the folded balanced coplanar antenna design, (a) unfolded structure, (b) folded structure.

C. *Prototype realization of the antenna*

A prototype of the final antenna was fabricated on foam dielectric substrate with relative permittivity ε_r = 1.1 and thickness of 2.5 mm. This substrate is flexible PCB, which enables the antenna to fold into a 3-dimensional structure. The prototype of the proposed antenna is shown in Fig. 7. A spacer of dielectric slab (see Fig. 7b) was added carefully between the antenna's top and bottom to support the antenna's arms in order to maintain them at the same height and with the same surface structure. In order to be consistent with the simulation

IEEE Transactions on Antenna and Propagation, June 2011 (in press.)

model, the foam substrate of the flexible PCB was detached using an intricate process during the fabrication.

D. Characterization and analysis of the antenna

Results for the simulation of the antenna were cross-validated using Ansoft HFSS and CST MWS software [14] prior to the prototype fabrication. Fig. 8 illustrates both sets of simulated antenna return loss results, compared to those measured in the prototype. As can be seen, the prototype antenna has impedance bandwidth (10 dB) from 2.39 GHz to 2.575 GHz and from 5.1 GHz up to 6 GHz, respectively. Taking into consideration the difficulties and errors caused in custom manufacture of the antenna, the results give confidence in the simulations carried out. This can be seen from the relatively well-correlated results from both measurement and simulations.

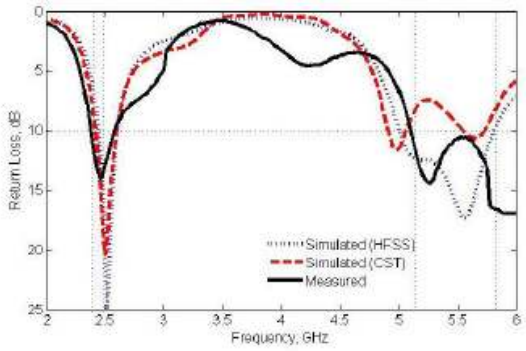

Fig.8. The simulated and measured return loss of the antenna

TABLE II
Measured Power Gain of the Antenna.

Lower band									
GHz	2.4	2.41	2.42	2.43	2.44	2.45	2.46	2.47	2.48
dBi	1.52	1.58	1.54	1.74	1.73	1.78	1.60	1.65	1.56
Upper band									
GHz	5.15	5.2	5.3	5.4	5.5	5.6	5.7	5.8	5.85
dBi	2.75	2.80	2.92	2.68	2.95	2.80	2.88	2.70	2.65

Measurements of the radiation patterns of the prototype were carried out in a far-field anechoic chamber. Three principal-plane pattern cuts (i.e. zx, zy and xy planes) were taken for three WLAN operating frequencies that cover the whole designated bandwidth. The radiation patterns were measured at 2.45, 5.2 and 5.8 GHz: the measured patterns were normalized and are presented in Fig. 9. The results indicate generally satisfactory agreement between simulated and measured radiation patterns, except at certain points where the differences are noticeable. These differences may be caused either by fabrication errors or during the measurement, which may happen if the antenna under test is slightly misaligned with the reference antenna.

Table II illustrates the measured antenna gain in the broadside direction for frequencies across the 2.4 GHz and 5 GHz bands. The measured antenna gain varied between 1.52 dB and 1.8 dB over the 2.4 GHz band, and 2.65 dB and 2.95 dB over the 5.2 GHz band. For the bandwidths of the three specific operating bands, the variation in the peak antenna gain for both bands is less than 0.3 dB.

Additionally, the Wheeler cap method for measuring radiation efficiency [16,17] was applied to the antenna. Table III presents the measured total efficiency (including mismatch) of the antenna over the 2.4 GHz and 5 GHz bands. As can be seen, the antenna shows good total efficiency in both bands with similar variations, from 0.74 to 0.88.

TABLE III
Measured total radiation efficiency (η).

Lower band									
GHz	2.4	2.41	2.42	2.43	2.44	2.45	2.46	2.47	2.48
η	0.74	0.74	0.77	0.80	0.82	0.85	0.88	0.88	0.87
Upper band									
GHz	5.15	5.2	5.3	5.4	5.5	5.6	5.7	5.8	5.85
η	0.79	0.74	0.76	0.78	0.87	0.86	0.87	0.75	0.74

A. A study of an example application for the antenna

The proposed balanced loop antenna possesses several advantages compared to the prior-to-art antennas designs operating at the same frequency bands. In comparison with the balanced type antennas, the proposed antenna requires no balun in operation [1-5, 18, 19]. In addition, the antenna features low profile design as well as a comparable volume with the ones reported in the literature, including some of the unbalanced type [20]. On the other hand, when compared with the unbalanced type antennas, the proposed balanced antenna is able to operate on its own without requiring a ground plane to be part of the antenna system, unlike the unbalanced type of designs [21]; or it can also be used integrating with the ground plane. In this case, Performance of the proposed design has little variation of the ground plane size, which implies that the same antenna design can potentially be adapted for many other mobile devices with little modification, saving time for antenna customization for the mobile phone industry [4].

An investigation of the effect of handset size (equivalent to the size of the ground plane) on the antenna performance was carried out. The width of the handset, *Gnd_wid*, was kept similar to the width of the antenna whereas the length (equivalent to parameter *Gnd_len*) was varied from 20 mm to 80 mm, as Fig. 10 presents. It is quite clear from Fig. 11 that there is little variation in calculated return loss observed for all design cases. As a result, the antenna resonant frequency is found to have a low degree of sensitivity to the ground plane size. These results indicate that the balanced antenna only induced a little current into the associated ground plane at both bands. The computed current distributions at spot frequencies in the three different operating bands studied (2.45, 5.2 and 5.8 GHz) are shown in Fig. 12, in which it is seen that the induced current in the ground plane is negligible except very close to the antenna. These encouraging results prove the advantage of this balanced loop antenna, in which a stable

IEEE Transactions on Antenna and Propagation, June 2011 (in press.)

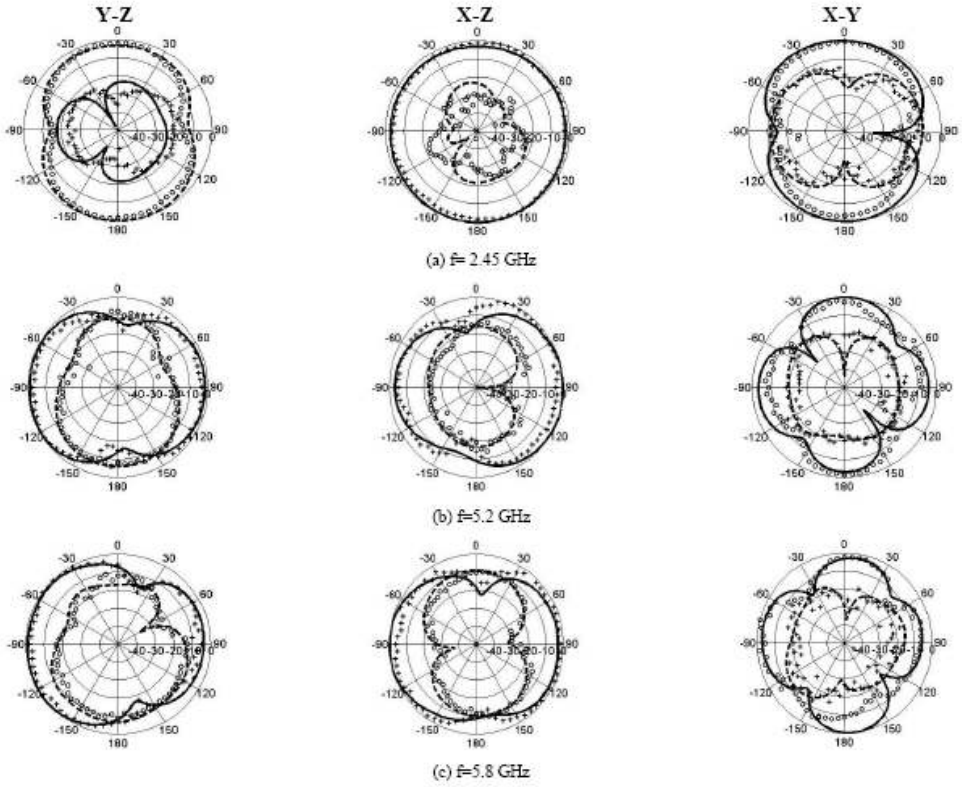

Fig. 9. Radiation patterns of the proposed antenna at 2.45, 5.2 and 5.8 GHz for yz, xz and xy planes. 'ooo' measured E_θ ,' ----' simulated E_θ ,'xxx' measured E_ϕ '——' simulated E_ϕ

performance can be expected when the handheld device is held by a user since the interaction between the antenna and the handset is minimized.

Fig. 10. The final balanced loop antenna in an application with a typical ground plane.

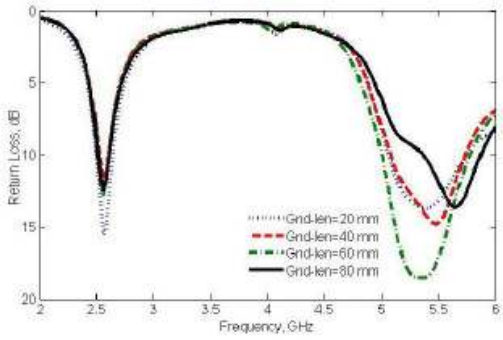

Fig.11. Effect of variation of the ground plane size on the return loss.

IEEE Transactions on Antenna and Propagation, June 2011 (in press.)

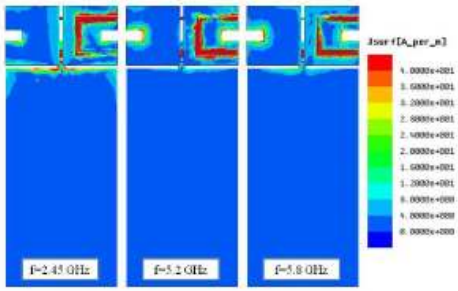

Fig.12. Current distribution on the antenna-groundplane combination in a typical configuration for a handset appliation at three different frequencies.

V. CONCLUSION

A new dual-band balanced antenna using a coplanar waveguide structure to eliminate the balanced feed network has been presented. Several antenna parameters selected with a view to optimizing the antenna's performance have been studied and analyzed. The effect on the antenna performance of bridge wires supporting the coplanar waveguide has also been studied. The best antenna model was fabricated and tested. The characteristics of this balanced antenna design were analyzed in terms of antenna return loss, current distribution, radiation pattern, radiation efficiency and power gain. The simulated and measured results over three license-free frequency bands were in adequately good agreement, confirming the design concept and demonstrating the good impedance bandwidth characteristics and excellent tri-band radiation performance. A study for the proposed antenna in a handset application has demonstrated the advantage of this balanced loop antenna, in that the antenna is insensitive to the associated ground plane and to size variations of the ground plane. These results prove the antenna performance was stable in handheld devices since the interaction between the antenna and the hand would be minimized.

REFERENCES

[1] H. Morishita, H. Furuuchi and K. Fujimoto, "Performance of balance-fed antenna system for handsets in vicinity of a human head or hand", *IEE Proc. Microwaves Antennas & Propagation*, Vol. 149, No, 2, pp. 85-91, April 2002.

[2] A.G. Alhaddad, R.A. Abd-Alhameed, D. Zhou, C.H. See, I.T.E. Elfergani and P.S. Excell, "Low profile dual-band balanced handset antenna with dual-arm structure for WLAN application", *IET Microwaves Antennas and Propagation*, Vol. 5, No. 9, pp. 1045 – 1053, 2011.

[3] H. Morishita, S. Hayashida, J. Ito and K. Fujimoto, "Analysis of built-in antenna for handset using human (head, hand, finger) model", *Electronics and Communications in Japan, Part 1*, Vol. 86, No. 9, pp. 35-45, 2003.

[4] B.S. Collins, S.P. Kingsley, J.M. Ide, S.A. Saario, R.W. Schlub and S.G. O'Keefe, "A Multi-band hybrid balanced antenna", *IEEE 2006 International Workshop on Antenna Technology: small antennas; novel metamaterials*, White Plains, New York, pp.100-103, March 6-8, 2006.

[5] J.J. Arenas, J. Anguera and C. Puente, "Balanced and single-ended handset antennas: free space and human loading comparison", *Microwave and Optical Technology Letters*, Vol. 51, No. 9, pp. 2248-2254, September 2009

[6] R.A. Abd-Alhameed, P.S. Excell, K. Khalil, R. Alias and J. Mustafa, "SAR and radiation performance of balanced and unbalanced mobile antennas using a hybrid formulation", *IEE Proc. Science, Measurement and Technology, special issue on Computational Electromagnetics*, Vol. 151, No. 6, pp. 440-444, November 2004.

[7] G. Ghione and C. U. Naldi, "Coplanar Waveguides for MMIC Applications: Effect of Upper Shielding, Conductor Backing, Finite-Extent Ground Planes, and Line-to-Line Coupling," *IEEE Transactions on Microwave Theory and Techniques*, Vol. 35, pp. 260- 267, Mar 1987.

[8] C. P. Wen, "Coplanar waveguide: A surface strip Transmission line suitable for nonreciprocal gyromagnetic device applications", *IEEE Trans. on Microwave Theory and Techniques*, vol. MTT-17, pp. 1087-1090, Dec. 1969.

[9] S.-M. Deng, M.-D. Wu, and P. Hsu, "Analysis of coplanar waveguide-fed microstrip antennas,", *IEEE Trans. Antennas and Propagation*, Vol. 43, pp. 734-737, Jul 1995.

[10] R. K. Raj, M. Joseph, C. K. Aanandan, K. Vasudevan, and P. Mohanan, "A new compact printed antenna with coplanar configuration," *IEEE Antennas and Propagation Society International Symposium*, vol. 2A, pp. 442 - 445, 2005

[11] Y. Jee and Y.-M. Seo, "Triple-band CPW-fed compact monopole antennas for GSM/PCS/DCS/WCDMA applications," *IET Electronics Letters*, vol. 45, pp. 446 - 448, 2009.

[12] L. L. Libby, "Special Aspects of Balanced Shielded Loops," *Proceedings of the IRE*, Vol. 34, pp. 641- 646, Sept. 1946.

[13] M. N. Z. Abidin, "Measurement of current distribution on wire antennas," Master of Science dissertation in Radio Frequency and Microwave Engineering: University of Bradford, September 1993.

[14] High Frequency Structure Simulator HFSS, Version 13, Ansoft Corporation, USA.

[15] Computer Simulation Technology Corporation, CST Microwave Studio, Version 5.0, Germany.

[16] R. W. Johnston and J. G. McRory, "An improved Small Antenna Radiation-Efficiency Measurement," *IEEE Antennas and Propagation Society Magazine*, Vol. 40, pp. 40-48, 1998.

[17] H. Choo, R. Rogers, and H. Ling, "On the Wheeler Cap Measurement of the Efficiency of Microstrip Antennas," *IEEE Trans. Antennas and Propagation*, Vol. 53, pp. 2328-2332, 2005.

[18] H. Zhang and H Xin, "A Dual-band dipole antenna with integrated-balun," *IEEE Trans. Antennas and Propagation*, Vol. 57, pp. 786-789, 2009.

[19] M.K. Mandal and Z.N. Chen "Compact dual-band and ultrawideband loop antennas", *IEEE Trans. Antennas and Propagation*, Vol. 59, pp. 2774-2779, 2011.

[20] W.-C. Liu and C.-M. Wu, "Broadband dual-frequency CPW-fed planar monopole antenna with rectangular patch", *IET Electronics Letters*, Vol. 40, No. 11, pp. 642-643, 2004.

[21] I. Yeum, J. Park, J. Kim, J. Wee, B. Kim and C. Jung, "Compact and contact quad-band (DVG-H UHF/L WLAN 11a/b) antenna for PMP applications", *IET Electronics Letters*, Vol. 46, No. 1, pp. 11-13, 2010.

www.ietdl.org

Published in IET Microwaves, Antennas & Propagation
Received on 31st May 2010
Revised on 17th January 2011
doi: 10.1049/iet-map.2010.0219

In Special Section on Selected Papers from Mosharaka International Conference on Communications, Propagation and Electronics (MIC-CPE2010)

ISSN 1751-8725

Low profile dual-band-balanced handset antenna with dual-arm structure for WLAN application

A.G. Alhaddad[1] R.A. Abd-Alhameed[1] D. Zhou[2] C.H. See[1] I.T.E. Elfergani[1] P.S. Excell[3]

[1]Mobile and Satellite Communications Research Centre, University of Bradford, Bradford, UK
[2]Surrey Space Centre, University of Surrey, Guildford GU2 7XH, UK
[3]Centre for Applied Internet Research, Glyndwr University, Wrexham, UK
E-mail: r.a.a.abd@bradford.ac.uk

Abstract: In this study, a low profile and dual-band-balanced antenna for mobile handset applications, covering the 2.4 and 5 GHz WLAN frequency bands, is investigated and discussed. The antenna is a thin-strip planar dipole, with folded structure, and a dual-arm on each half of the dipole. The performance of the proposed antenna has been analysed and optimised for the two targeted frequency bands. For validation purposes, an antenna prototype was fabricated and tested. The prototype performance is characterised in terms of the antenna reflection coefficient, radiation pattern, power gain and surface current distribution. The predicted and measured results show relatively good agreement, and confirm good impedance bandwidth characteristics and excellent dual-band performance. In addition, the antenna radiation performance is investigated when the antenna is placed in several locations on the human body, using a hybrid computational electromagnetics technique.

1 Introduction

Many mobile handsets have design constraints on size and weight, partly driven by customer expectations, and partly owing to the increasingly ubiquitous use of location-aware applications. From an antenna design perspective, these constraints may be summarised thus: (i) to reduce the antenna size with unchanged, or improved, performance characteristics; and (ii) to continue to seek reductions in the degradation of antenna performance when in proximity with the operator's body [1].

Balanced antennas offer a genuine choice for the designer in mitigating the effects of the user on the antenna performance [2], since balanced currents only flow on the antenna element, thus dramatically reducing the effect of current flow on the ground plane. As a result, balanced antennas should have good efficiency and, more importantly, should maintain their performance when in use adjacent to the human body [3]. In recent years, several novel mobile antennas designed with the balanced technique have demonstrated the enhanced stability of performance, compared to the unbalanced type, when the handset is in proximity with the human head and/or hand [4–10].

Designing a good balanced mobile antenna is always a challenging task involving the compromise of certain constraints in the design, where small antenna size and multiple frequency bandwidth operation are usually required. Recently, several novel designs of such antenna types have been successfully developed and demonstrated [3–5, 8, 9], most of them being designed and implemented for operations in the current 2 and 3 G mobile frequency bands; however, not much work has been carried out for the potential frequency bands beyond the current mobile frequency ranges, as expected to be used for future mobile communication systems. Therefore, there is motivation to apply this balanced technique to develop antennas for future mobile device applications.

The paper presents and investigates a new design for a built-in dual-frequency balanced antenna for WLAN, and short-range wireless communications allocated frequency bands, that is, 2.4 GHz (2.4–2.484 GHz) and 5 GHz (5.15–5.35 GHz and 5.725–5.825 GHz). The characteristics of this balanced mobile antenna are analysed in terms of input return loss, power gain and radiation pattern, using the HFSS simulation package [11]. In addition, the WLAN-band antenna radiation performance is examined when the antenna is placed in several locations on the human body, simulated using a hybrid computational electromagnetics technique.

2 Antenna design concept

In order to create the balanced antenna with dual-band operation, it was necessary to generate two separate resonant frequencies. This design was approached using a two-tier process. Firstly, each monopole arm of a planar strip dipole was folded. In order to achieve a low-profile folded (i.e. minimised height) balanced antenna, while maintaining sufficient impedance bandwidth to support the targeted WLAN bands, a long slot was introduced into each folded arm of the dipole radiator, as Fig. 1c shows. In this way, the equivalent wavelength of the surface current at 2.4 GHz was increased, compared to the case without the

www.ietdl.org

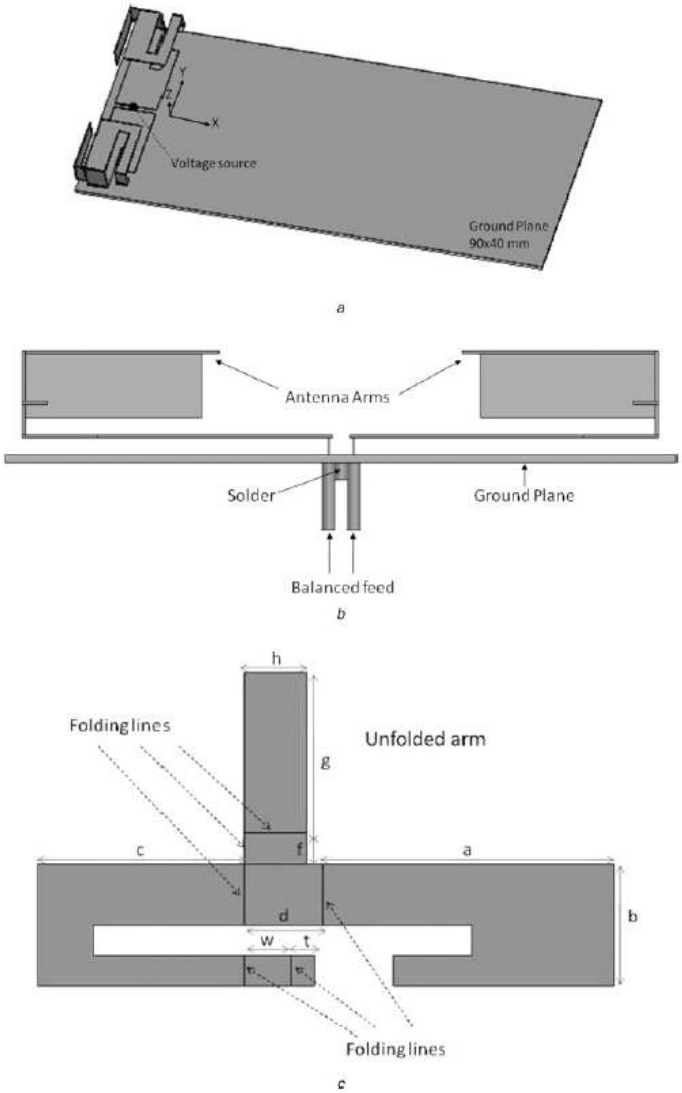

Fig. 1 *Geometry model of the proposed balanced mobile antenna*

a 3D balanced mobile antenna configuration
b Side view of the balanced antenna with connected feed
c Unfolded arm of the balanced mobile antenna configuration studied

long slot. Thus, the folded antenna height (h) can be reduced by 50%, and the low-profile design realised.

Secondly, a technique for introducing another resonant frequency was applied for the proposed antenna after the first tier process. A strip stub with appropriate length and width was inserted into each arm of the planar dipole with folded structure (see Fig. 1*c*). This additional arm was exploited to generate the second resonant frequency for the 5 GHz frequency band [12]. The proper length and width of this added arm was found with the aid of the simulator tool, subject to the input impedance matching required of this antenna design at the 5 GHz frequency band. It was noticed that this added arm for generating antenna resonance at 5 GHz had little effect on the antenna resonant frequency in the 2.4 GHz band. Therefore a dual-frequency operation with low profile of this balanced mobile antenna was achieved with the dual-arm structure, as Fig. 1*a* shows.

The dimensions of this antenna geometry were found to be comparable with practical handset sizes. In order to fully comprehend the influence of these parameters, based on impedance bandwidth, a parametric study was carried out by varying each parameter, while holding the remaining parameter values at the assumed optimum values. The procedure optimises the impedance matching bandwidth for

doi: 10.1049/iet-map.2010.0219

the proposed antenna to achieve the required impedance matching, covering the WLAN frequency bands. The antenna height parameters h and w were considered to be the most sensitive parameters in controlling the impedance bandwidth relative to the target design.

The parameter h was varied from 2 to 5 mm, with a 1 mm step. The optimum value of h was found to be 4 mm, as shown in Fig. 2. Similarly, the parameter w was varied from 1 to 4 mm with a 1 mm step. The optimum value for w was found to be 3 mm, as Fig. 3 shows. As mentioned in the previous section, the purpose of the additional thin strip was to produce the upper resonance of the antenna and it is characterised by the dimensions f and g. This can be established by studying the variation in resonant frequency when they change. Fig. 4 shows that as parameters f and g increase, the

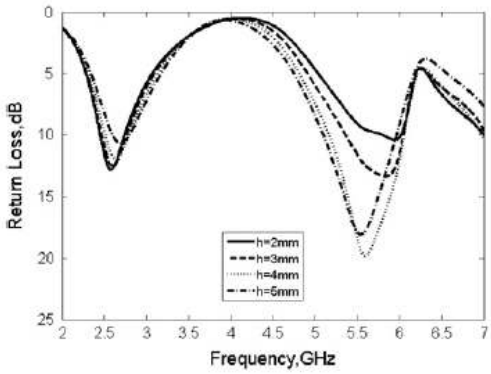

Fig. 2 *Effect of variation of the parameter h on the input return loss*

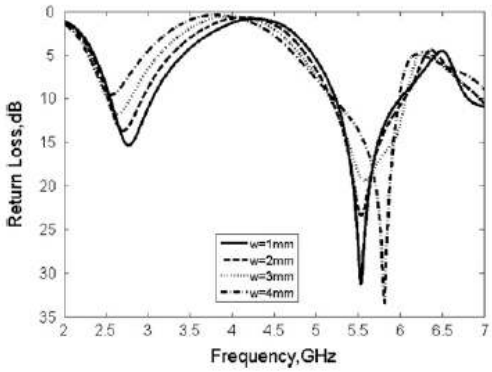

Fig. 3 *Effect of variation of the parameter w on the input return loss*

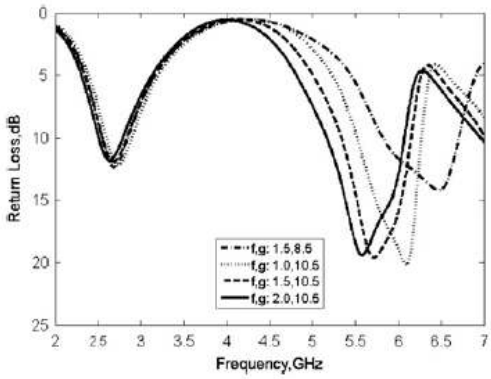

Fig. 4 *Parametric study of parameters f and g (in mm) against operating frequency*

Table 1 Summary of important parameters defining the proposed antenna

Parameters	Value, mm
a	18.5
b	8
c	11.5
d	5
w	3
h	4
t	1.5
f	2
g	10.5

Fig. 5 *Fabricated prototype of the proposed balanced antenna design*

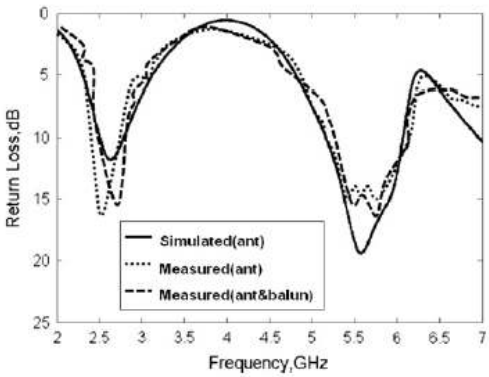

Fig. 6 *Comparison of simulated and measured return losses*

upper resonance decreases and it also slightly affects the lower band.

The optimised dimensions for the model structure to operate at the required frequency bands are summarised in Table 1. The antenna is mounted 1 mm above the ground plane, which has dimensions of 90×40 mm. The model structure has an antenna volume of $38 \times 10 \times 4$ mm. The length and location of each arm were further adjusted, together with second-order effects from other structure parameters, to ensure the best optimisation relative to the WLAN bands, guided by a working return loss better than 10 dB.

3 Simulation and measurement results

For realisation, copper sheet with 0.15 mm thickness was used for fabricating the radiating elements (see Fig. 5). For a balanced antenna system, a balun is usually required as a support feeding network, to provide a balanced feed from an unbalanced source. A commercial balun from ET Industries [13], operating over the frequencies 2–12 GHz, was used as a feeding network to measure the return loss of the proposed design. However, it should be noted that, to model the balun outputs a floating port was used.

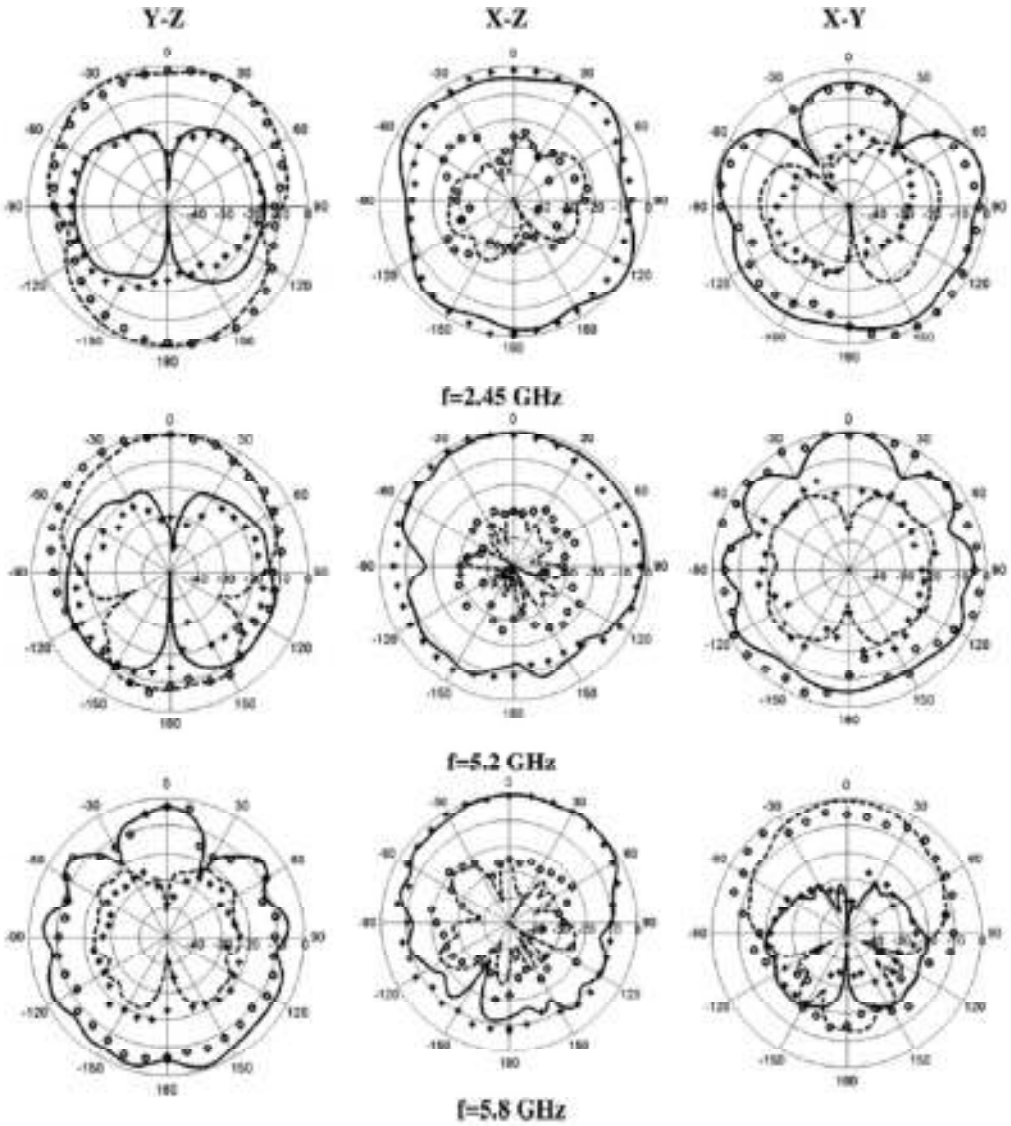

Fig. 7 *Radiation patterns of the proposed antenna at 2.45, 5.2 and 5.8 GHz for yz, xz and xy planes*
'ooo' measured E_θ, '—' simulated E_θ, 'xxx' measured E_ϕ, '———' simulated E_ϕ

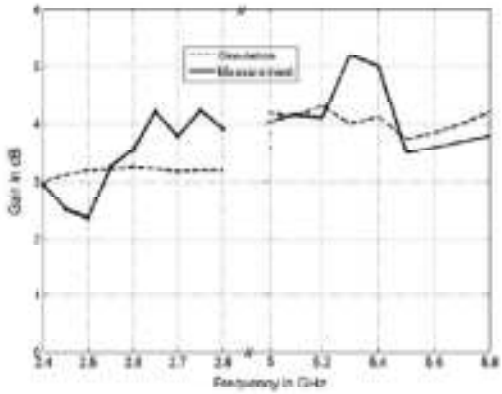

Fig. 8 *Simulated and measured power gains of the proposed antenna*

Input impedance or return loss of the balanced antenna measured in this way is from the antenna as well as the balun, rather than being an actual measurement at the antenna feed point. Therefore in this study another method using S-Parameters [14], which can directly measure the actual impedance at the proposed antenna feed point, was adopted to verify and validate the impedance of the proposed balanced antenna. In this measurement, the balanced antenna is considered as a passive two-port device, and the S-Parameters can be readily measured from a calibrated network analyser, and the differential input impedance (Z_d) of the balanced antenna can be obtained from a simple formula as follows

$$Z_d = 2Z_0 \frac{(1 - S_{11}^2 + S_{21}^2 - 2S_{21})}{(1 - S_{11})^2 - S_{21}^2} \quad (1)$$

where Z_0 is the reference impedance. Fig. 6 shows the measured return loss for the proposed antenna, and proposed antenna with balun compared to the simulated. A good agreement between the simulated and measured return loss [i.e. simulated (ant) and measured (ant) and measured (ant and balun)] can be observed, thus verifying the impedance response of the design.

Measurements of the radiation patterns of the prototype were carried out in a far-field anechoic chamber. Three principal-plane pattern cuts (i.e. *zx*, *zy* and *xy* planes) were taken for three WLAN operating frequencies that cover the whole designated bandwidth. The radiation patterns were measured at selected frequencies of 2.45, 5.2 and 5.8 GHz, respectively; the measured patterns were normalised and presented in Fig. 7. The results indicate a reasonable agreement between simulated and measured radiation pattern. Fig. 8 illustrates the measured antenna gain compared to the simulations in the broadside direction for the frequencies across the 2.4 and 5 GHz bands. It should be noted that the insertion loss of the feed network was subsequently added to the measured power gain at each specific frequency in the measurement plot. As can be seen in Fig. 8, the measured antenna gain varied approximately between 2.3 and 4.3 dB over the 2.5 GHz band, and 3.5 and 5.3 dB over 5.2 GHz band. Generally, these variations in the measured antenna gains were mainly caused by introducing the balun, and from the wire connections between the antenna and the balun. The peak antenna gain variations for the 2.4 and 5 GHz bands are less than 1.0 dB, as compared with the predictions.

In addition, current distribution on the mobile phone ground plane was analysed in simulation at three specific frequencies (including 2.45, 5.2 and 5.8 GHz) of the frequency bands studied in this work, as Fig. 9 presents. As can be observed, the most of the current induced on the antenna system ground plane was concentrated in the area beneath the antenna, and a minimum current distribution appeared on the rest of the ground plane. These results agree well with [15, 16] in which only negligible induced surface currents are shown to exist on the handset structures underneath the antenna. This proves the advantage of using a balanced antenna design in mobile handsets, indicating that the proposed handset antenna design will be insensitive to the hand-loading effect.

Finally, the near- and far-field radiation performances of the proposed antenna mounted in several locations on a human body model at 2.45 and 5.2 GHz were studied and

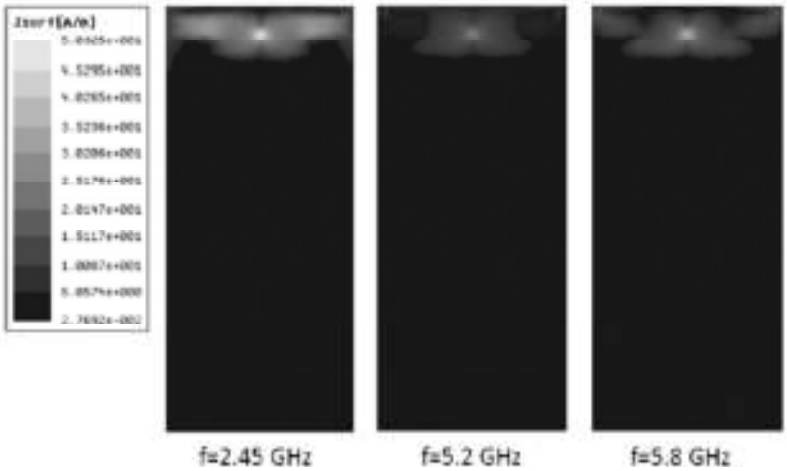

Fig. 9 *Surface current distributions for the proposed balanced antenna at 2.45, 5.2 and 5.8 GHz, respectively*

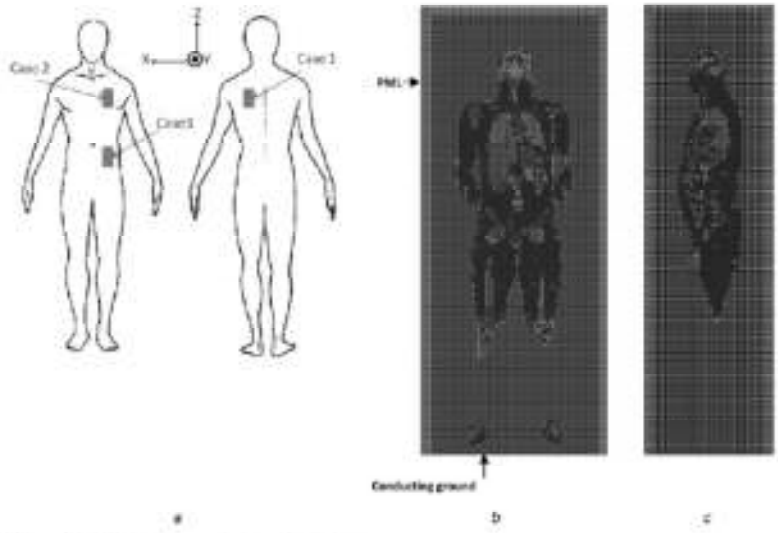

Fig. 10 *Human body model and the proposed antenna locations*
a Antenna locations on human model
b Central geometry slice in the *xz* plane
c Central geometry slice in the *yz* plane

investigated using the hybrid electromagnetic method described in [17]. The human body model used in this study is known as the 'Visible Man', the tissue-classified numerical model for which was developed at Brooks Air Force Base, San Antonio, USA [18]. The model is characterised by 49 types of tissues and has a resolution of 1 mm. However, the finite difference time domain (FDTD) cell size of the present model for both bands considered was 3 mm, for which 42 types of tissues were included in the analysis. This cell size was chosen to speed up the computational time required by the hybrid method, and work within the available memory limits. The positions of the proposed antenna on the human model are shown in Fig. 10. This figure also demonstrates the FDTD domain model, displayed over central slices in the *xz* and *yz* planes. The human body was placed on a perfectly conducting ground plane, and the antenna was replaced by an equivalent Huygens' surface. The physical size of the Huygens' surface was 9 cm × 7.2 cm × 16.2 cm and this is equivalent to 30 × 24 × 54 FDTD cells. The Huygens' surface was carefully placed at the surface of the human model, where the distance between the antenna, handset and human tissues was only two cells. The FDTD problem

Table 2 Radiated and absorbed power distributions of the proposed antenna when it is mounted on the human body over different locations

	2.45 GHz		5.2 GHz	
	P_{rad}/P_{in}	P_{abs}/P_{rad}	P_{rad}/P_{in}	P_{abs}/P_{rad}
location 1: (back)	0.44	1.25	0.76	0.30
location 2: (front)	0.80	0.24	0.94	0.06
location 3: (front)	0.77	0.29	0.92	0.07

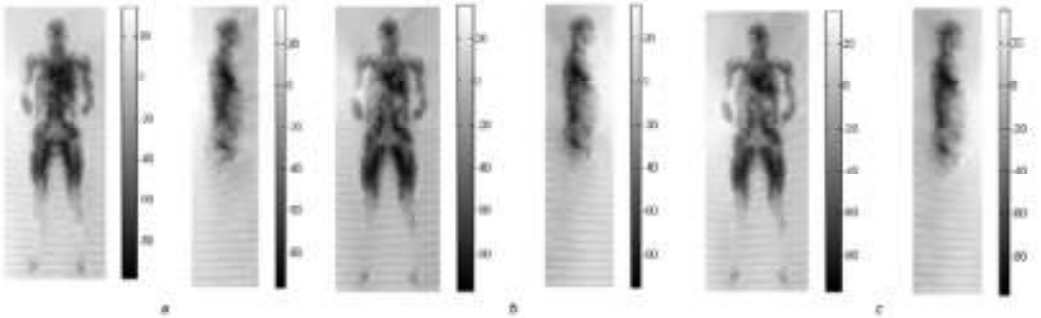

Fig. 11 *Electric field magnitude distributions over the central x = z (left) and y = z (right) slices for 1 W input power at 2.45 GHz band*
a Case 1
b Case 2
c Case 3

www.ietdl.org

space was 180 × 118 × 633 cells, at which it is terminated by a perfectly matched layer (PML) with a thickness of 6 cells. The number of running cycles was set to 40 for both WLAN frequencies. It should be noted that in all cases shown in Fig. 10 the antenna handset was between the antenna and the human tissues.

Radiated and absorbed power distributions of the proposed antenna for the three cases considered are presented in Table 2. The results are in quite reasonable agreement with expectations, except for the poor values achieved at 2.45 and 5.2 GHz when the antenna was placed at the back of the human model. This is believed to be because of the tissue characteristics at this location being quite lossy, compared to other antenna positions.

The total near-field distribution at 2.45 GHz for two central vertical slices is shown in Fig. 11. These fields are normalised to 1 W input power and the scale shown is in dB. It is clear that the distributions within the human tissues, and in their immediate neighbourhood, were not comparable to the fields pointing away from the antenna and the human body. This figure also shows the variations of the standing wave due to the conducting ground. Similarly, the near-field

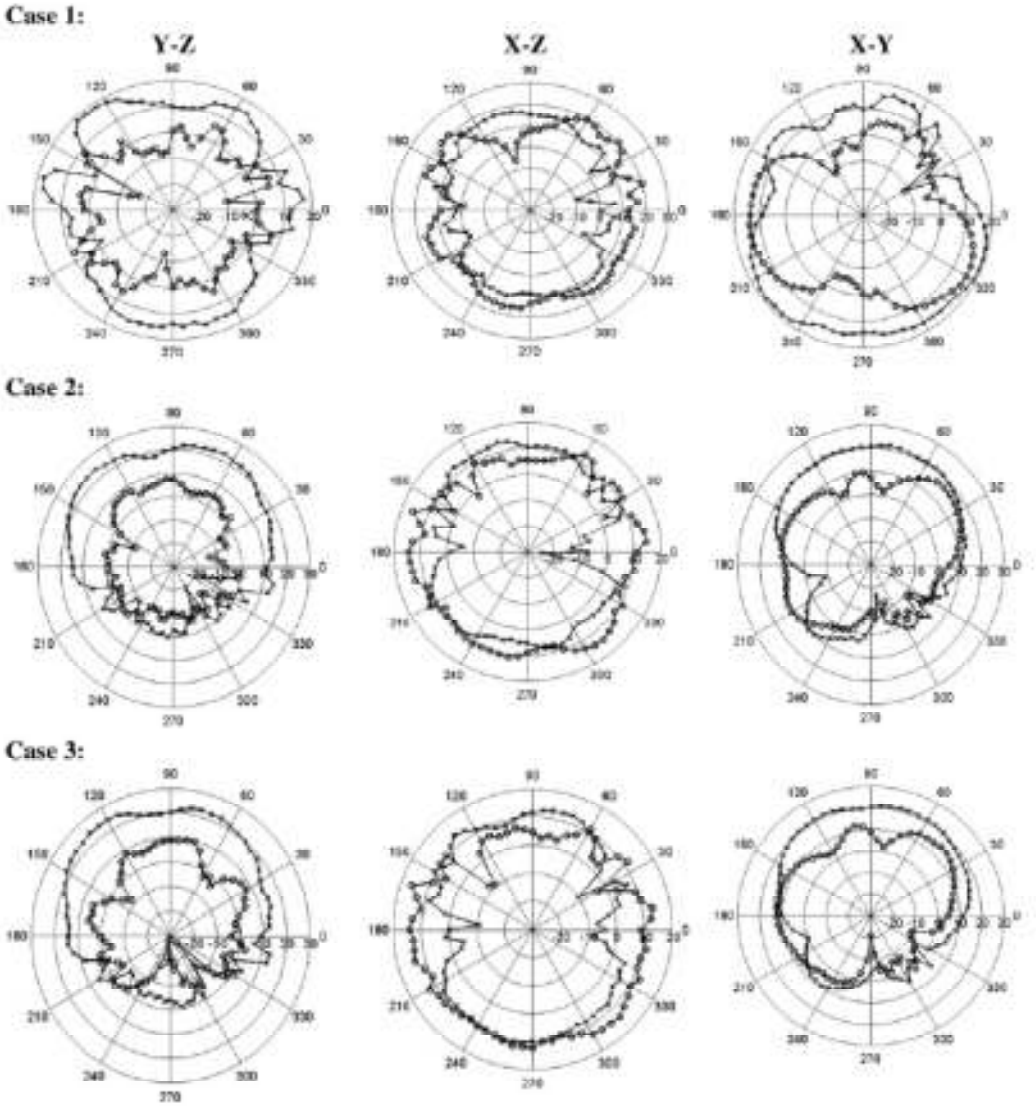

Fig. 12 *Far-field patterns at 2.45 GHz for yz, xz and xy planes*

a Case 1
b Case 2
c Case 3
where 'o-o-o' is computed E_ϕ and '×-×-×' is computed E_θ

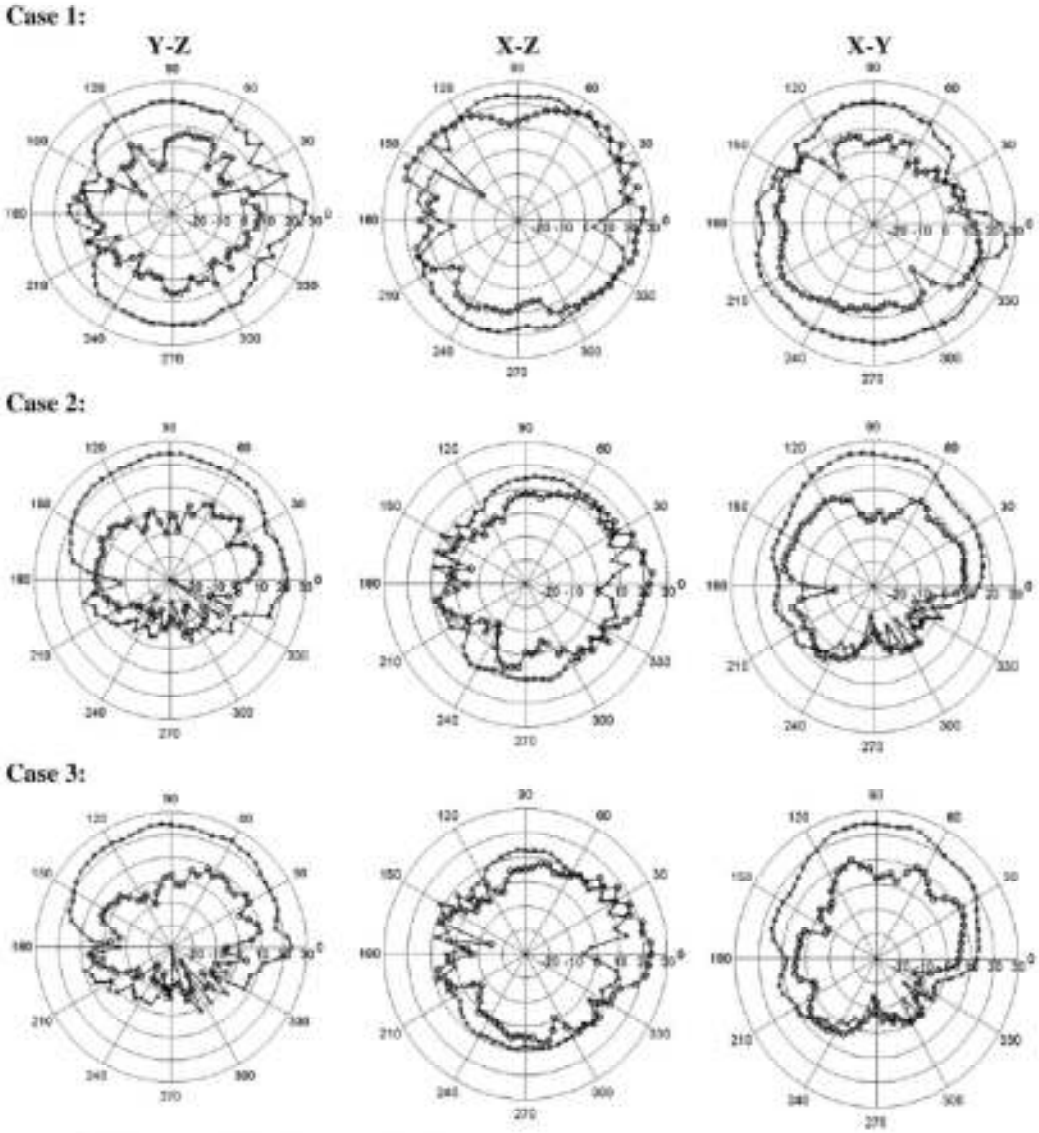

Fig. 13 *Far-field patterns at 5.2 GHz for yz, xz and xy planes*

a Case 1
b Case 2
c Case 3
where 'o-o-o' is computed E_ϕ and 'x-x-x' is computed E_θ

distributions at 5.2 GHz are quite comparable to those shown in Fig. 11, and are thus not presented here.

The far-field components for the three cases mentioned are shown in Figs. 12 and 13. The fields presented are normalised to one 1 W input power for all $y-z$, $x-z$ and $x-y$ planes. The pattern variations in each case show that the fields were stronger in the direction pointing to the normal axis of the handset antenna, and away from the human body. It is clear from the results that the reduced field magnitudes caused by the shadowing effect of the human body fall approximately between 20 and 25 dB.

4 Conclusions

A very-low-profile dual-band balanced handset antenna, with a novel structure, for mobile devices operating over the 2.4 GHz and full 5 GHz WLAN bands has been presented. The proposed antenna model was simulated, fabricated and tested to verify the design concept. The characteristics of this balanced antenna design were analysed in terms of antenna return loss, radiation pattern and power gain. The simulated and measured results over the two frequency bands were in sufficiently good agreement to propose this

IET Microw. Antennas Propag., 2011, Vol. 5, Iss. 9, pp. 1045–1053
doi: 10.1049/iet-map.2010.0219

balanced mobile antenna design as a promising candidate for future mobile WLAN applications.

5 Acknowledgments

The authors gratefully acknowledge the financial support from the UK Engineering and Physical Sciences Research Council (EPSRC) under grant EP/E022936/1.

6 References

1 Morishita, H., Furuuchi, H., Fujimoto, K.: 'Performance of balance-fed antenna system for handsets in vicinity of a human head or hand', *IEE Proc., Microw. Antennas Propag.*, 2002, **149**, (2), pp. 85–91
2 Abd-Alhameed, R.A., Excell, P.S., Khalil, K., Alias, R., Mustafa, J.: 'SAR and radiation performance of balanced and unbalanced mobile antennas using a hybrid formulation', *IEE Proc., Sci. Meas. Technol. Spec. Issue Comput. Electromagn.*, 2004, **151**, (6), pp. 440–444
3 Zhou, D., Abd-Alhameed, R.A., See, C.H., Alhaddad, A.G., Excell, P.S.: 'Compact wideband balanced antenna for mobile handsets', *IET Microw. Antennas Propag.*, 2010, **4**, (5), pp. 600–608
4 Morishita, H., Furuuchi, H., Ide, H., Tanaka, Z., Fujimoto, K.: 'A balance-fed loop antenna system for handset', *IEICE Trans. Fundam.*, 1999, **E82-A**, (7), pp. 1138–1143
5 Morishita, H., Hayashida, S., Ito, I., Fujimoto, K.: 'Analysis of built-in antenna for handset using human (hand,hand,finger) model', *Electron. Commun. Jpn. 1*, 2003, **86**, (9), pp. 35–45
6 Navarrowala, U., Striegel, J.: 'A reduced sized balanced antenna for 2.4 GHz WLAN', IEEE Int. Symp. on Antennas and Propagation, 2003, vol. 2, pp. 6–9
7 Kingsley, S.: 'Advances in handset antenna design', RF Design, 2005, pp. 16–22
8 Collins, B.S., Kingsley, S.P., Ide, J.M., Sauris, S.A., Schlab, R.W., O'Keefe, S.G.: 'A multi-band hybrid balanced antenna', IEEE 2006 Int. Workshop on Antenna Technology: Small Antennas; Novel Metamaterials, White Plains, New York, 6–8 March 2006, pp. 100–103
9 Zhou, D., Abd-Alhameed, R.A., Excell, P.S.: 'Wideband balanced folded dipole antenna for mobile handsets'. The Second European Conf. Antennas and Propagation, Session MoPA, Paper no. 39, Edinburgh, UK, 11–16 November 2007
10 Arenas, J.J., Anguera, J., Puente, C.: 'Balanced and single-ended handset antennas: free space and human loading comparison', *Microw. Opt. Technol. Lett.*, 2009, **51**, (9), pp. 2248–2254
11 High Frequency Structure Simulator HFSS, Version 11, Ansoft Corporation, USA
12 Alhaddad, A.G., Abd-Alhameed, R.A., Zhou, D., *et al.*: 'New design of dual-band balanced handset antenna design for WLAN application'. Proc. Mosharaka Int. Conf. Communications, Propagation and Electronics, Amman, Jordan, 5–7 March 2010, Technical Session 1, pp. 1–4
13 ET Industries, USA, available at http://www.etiworld.com/
14 Meys, R., Janssens, F.: 'Measuring the impedance of balanced antennas by an S-Parameter method', *IEEE Antennas Propag. Mag.*, 1998, **40**, (6), pp. 62–65
15 Kim, Y., Morishita, H., Koyanagi, Y., Fujimoto, K.: 'A folded loop antenna system for handsets developed and based on the advanced design concept', *IEICE Trans. Commun.*, 2001, **E84-B**, (9), pp. 2468–2475
16 Hayashida, S., Morishita, H., Fujimoto, K.: 'Self-balanced wideband folded loop antenna', *IEE Proc. Microw. Antennas Propag.*, 2006, **153**, (1), pp. 7–12
17 Abd-Alhameed, R.A., Excell, P.S., Vaul, J.: 'Currents induced on wired I.T. Networks by randomly distributed phones – a computational study', *IEEE Trans. Electromagn. Compat.*, 2006, **48**, (2), pp. 282–286
18 Mason, P.A., Hurt, W.D., Walters, T.J., *et al.*: 'Effects of frequency, permittivity, and voxel size on predicted specific absorption rate values in biological tissue during electromagnetic-field exposure', *IEEE Trans. Microw. Theory Tech.*, 2000, **48**, pp. 2050–2058

www.ietdl.org

Published in IET Microwaves, Antennas & Propagation
Received on 15th April 2009
Revised on 8th November 2009
doi: 10.1049/iet-map.2009.0153

In Special Issue on Selected Papers from Mosharaka International Conference on Communications, Propagation and Electronics (MIC-CPE 2009)

ISSN 1751-8725

Compact wideband balanced antenna for mobile handsets

D. Zhou[1] R.A. Abd-Alhameed[1] C.H. See[1] A.G. Alhaddad[1] P.S. Excell[2]

[1]Mobile and Satellite Communications Research Centre, University of Bradford, Bradford, West Yorkshire BD7 1DP, UK
[2]School of Computing and Communications Technology, Glyndwr University, Wrexham, LL11 2AW, Wales, UK
E-mail: r.a.a.abd@bradford.ac.uk

Abstract: A novel miniature balanced mobile handset antenna is presented in this study, which covers digital communication system (DCS) (1710–1880 MHz), personal communication system (PCS) (1850–1990 MHz), universal mobile telecommunications system (UMTS) (1920–2170 MHz) and wireless local area network (WLAN) (2400–2484 MHz) frequency bands. The antenna is a built-in planar dipole with folded structure and with the addition of a dual arm on each half of the dipole. The performance of the antenna is analysed and optimised under certain design constraints. The stability performance of the proposed antenna against proximity effects is evaluated. The effects of the phone user's hand on the return loss and radiation patterns have been characterised by simulation with a simple hand model. A prototype of the proposed antenna is fabricated and tested. A wide bandwidth planar balun is used to feed the wideband balanced antenna from an unbalanced source. The calculated and measured results show good agreement and confirm good wideband characteristics with multiband operation. The specific absorption rate (SAR) performance of the antenna is also studied experimentally by measuring near field exposure. The measured results have shown low induced current in the ground plane and thus confirm minimisation of performance variations and SAR.

1 Introduction

Progress towards worldwide wireless communication continues at a remarkable pace, and the antenna element of the technology is crucial to its success. Trends in system evolution indicate the gap between cellular and WLAN technologies is narrowing and developments in software defined radio (SDR) point strongly to the need for new antenna designs to permit user terminals to access several different radio resources at different frequencies according to service requirements. Also, as radio connected services become increasingly commonplace, the possible implications of user exposure to emissions from hand-held terminals are causing increasing concern. Therefore in addition to the traditional design objectives of small size and low cost it is now essential to address the need for (a) wide, or multi-band operation, (b) compliance with international safety guidelines on specific absorption rate (SAR) [1, 2] and (c) weak coupling of the antenna with the handset case in order to achieve a good impedance match that is stable in the presence of a human body.

A good candidate technique is to use balanced antennas to reduce the coupling of the mobile antenna to the handset, since unbalanced antennas drive current into the handset chassis, which interacts strongly with the unpredictable characteristics of the body [3–5]. The maximum SAR values have been shown to be substantially reduced when placed next to the human head, compared with conventional unbalanced antennas, if these antennas are well designed [6].

An antenna with symmetrical structure that is fed with balanced currents to make it electrically symmetrical is said to be a balanced antenna. Dipoles and loops are the most commonly encountered balanced antennas. In addition, balanced antennas may also be realised in meander-line, helix, microstrip forms and so on. A balanced antenna requires a

www.ietdl.org

balanced antenna feeder. In principle, the balanced antenna with balanced feed keeps the ground plane almost free of induced current and studies [7] have confirmed that this is indeed the case. Hence degradation of the antenna performance because of the influence of the human body can be largely eliminated. As a result, balanced antennas should have good efficiency and more importantly should maintain their performance when in use adjacent to the human body.

Balanced antennas may have limitations, such as reduced bandwidth and non-optimal pattern shaping, which can degrade their overall performance. These limitations arise mainly because only the antenna element itself acts as a radiator while the handset is not included in the design. Another issue is that the balun needed to provide balanced currents may itself limit the antennas impedance bandwidth. For commercial exploitation, it is essential to develop novel techniques to improve balanced antenna bandwidth and pattern performance, and to extend the performance of balanced structures to achieve multi-band operation.

In this paper, the design of a compact balanced dipole antenna in folded configuration with a novel dual-arm

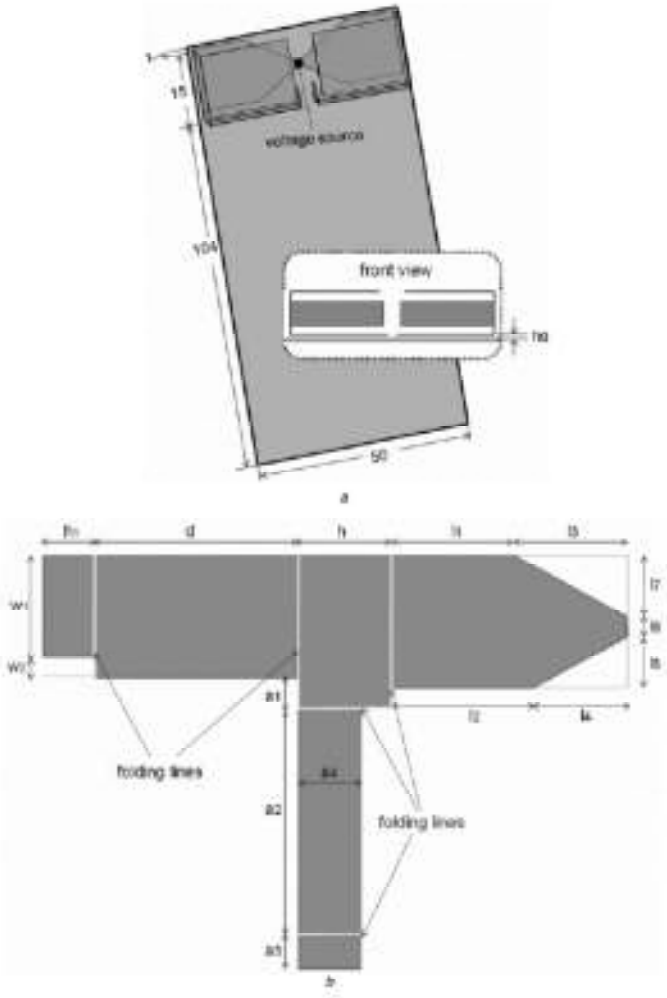

Figure 1 *Antenna configuration studied*

a Balanced antenna with conducting plate
b Important parameters of the proposed antenna

doi: 10.1049/iet-map.2009.0153

www.ietdl.org

structure for mobile handsets is introduced and analysed in order to realise multiple-band operation, including DCS, PCS, UMTS and WLAN (2.4 GHz). A planar balun with corresponding wide bandwidth for feeding the proposed antenna was implemented in a hardware realisation. In the analysis, an electromagnetic simulator based on the finite integration technique was applied to calculate return loss and radiation patterns [8]. The mutual effect of the proposed antenna system in the presence of a human hand phantom is addressed and the SAR performance of the antenna is evaluated by experiment. Finally, the calculated and measured results for the constructed prototype are presented and discussed.

2 Antenna design theory and structure

Planar metal-plate monopole antennas have been investigated previously as good candidates for ultrawideband applications [9, 10]. A pair of such wideband monopole antennas can be integrated together to configure a dipole antenna and still remain a wide bandwidth feature. Following this principle, a wideband planar dipole antenna in free space can be developed. This design concept was applied and implemented in the balanced handset antenna in the authors' previous work [11], in which a simple technique for enhancing impedance bandwidth was employed by symmetrically trimming a triangle at the monopole edge near the feed point, to give a tapered feed. In addition, a slot is introduced in each one of the arms of the planar dipole to mitigate the effects of the ground plane that cause the degradation of antenna performance.

In this work, a further development of this antenna model was carried out to achieve enhanced design features such as a compact size and operation over multiple frequencies bands. In order to compromise between the antenna size and maintaining reduced mutual interaction of the proposed mobile antenna with the handset ground plane, a compact design was achieved, with relative thin strip width, as compared with the design in [11] where the slot on each arm of the folded dipole antenna is removed. Moreover, the technique for generating multiple frequency resonances that was previously applied for folded balanced dipole antennas, as demonstrated in [12], was adapted in this design for further improvement. The discussion includes the impedance bandwidth required to enable multiple-band operation.

Firstly, a single arm balanced dipole antenna with folded structure and tapered feed near the edge of the feeding point, operating at around 2 GHz, was analysed and designed. To achieve a more compact design, the top end of the folded arm was extended and bent down (referring to parameter 'b_1' shown in Fig. 1) to satisfy the required length for each arm to provide the antenna resonances at the desired operating frequencies. Subsequently, an additional thin-strip arm was introduced and inserted in each arm of the planar dipole to generate the additional resonant frequency around the 2.4 GHz band as shown in Fig. 1. Using this technique, the singly resonant antenna was modified and developed as a wideband dual-resonant variant for multi-band operation.

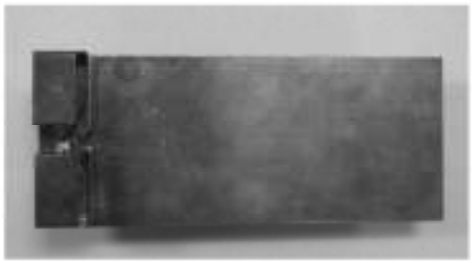

Figure 2 *Photograph of prototype of the proposed balanced antenna design*

The lateral length of the taper feed and its location on the antenna, together with the length and location of the additional arm, and other parameters of the proposed antenna, were adjusted and a further optimisation process was carried out to ensure that the design entirely covered the required frequency bands (1.710–2.485 GHz) at VSWR ≤ 3.

3 Measuring input impedance of balanced antenna

The proposed features of the compact design model were confined within dimensions of 48 (l) × 15 (w) × 9 (h) mm, including the 2 mm gap source for feeding. The optimal antenna configuration studied in terms of return loss, radiation patterns and power gain was found subject to the antenna impedance bandwidth and antenna miniaturisation constraints as follows: $d = 20$, $w_1 = 10$, $w_2 = 2$, $b = 9$, $b_1 = 5$, $b_2 = 1$, $l_1 = 12$, $l_2 = 14$, $l_3 = 11$,

Table 1 Comparison between the present design and the prior art

Item	Frequency range (GHz)	Insertion loss max. (dB)	Relative errors: amplitude (dB)/ phase (deg)	Return loss max. (dB)
prior art in [13]	1.7–3.3	–	±0.3/±5	10
present balun	1.7–3.0	0.9	±0.1/±2	10

doi: 10.1049/iet-map.2009.0153

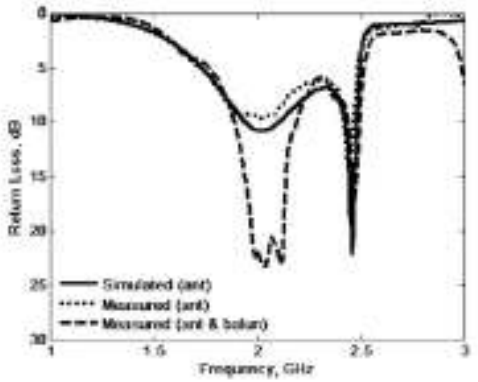

Figure 3 *The simulated and measured return loss against the operating frequency*

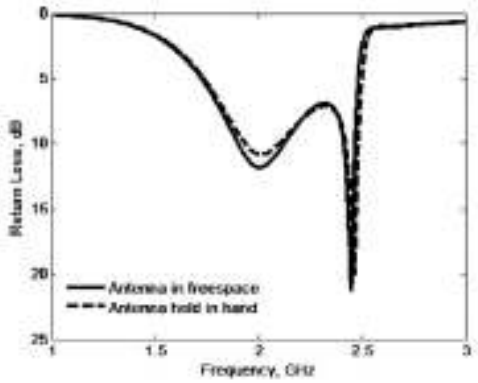

Figure 5 *Comparison of antenna return loss in free space and in presence of hand model*

$l_6 = 9$, $l_5 = 5$, $l_4 = 2$, $l_7 = 6$, $a_1 = 3$, $a_2 = 3$, $a_3 = 22$, $a_5 = 3.5$, $a_4 = 6$; dimensions are in mm. For validation, a prototype of the proposed balanced antenna and its associated ground plane was fabricated using copper sheet of thickness 0.35 mm and 0.5 mm, respectively, as shown in Fig. 2.

For a balanced antenna (e.g. dipole) system, a balun is required as a feeding network, to provide a balanced feed from an unbalanced source. In this study, a wideband planar balun was adapted [13] for the practical measurement. Agilent ADS [14] was used to simulate and analyse the characteristic performance of the balun. Table 1 summarises the measured performance of the planar balun used in this work, compared with the published data in [13]. As can be seen, this balun presents a relatively wideband feature and shows good agreement with the prior art results.

Fig. 3 presents the measured return loss of the prototype antenna against the computed one. As can be seen, a fairly good agreement between the calculated and measured return loss was observed. It should be noted that two different measured impedances were presented here. The first was observed at the input ports of the balanced antenna using the S-parameter method [15] in which the antenna is considered as a two-port device. The second impedance was considered at the input port of the balun.

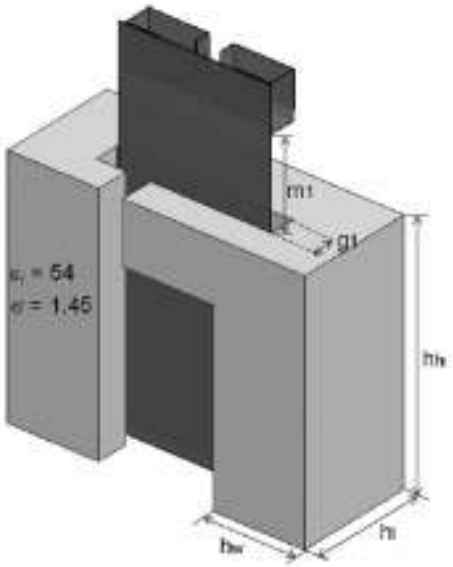

Figure 4 *Hand phantom model with the proposed design*

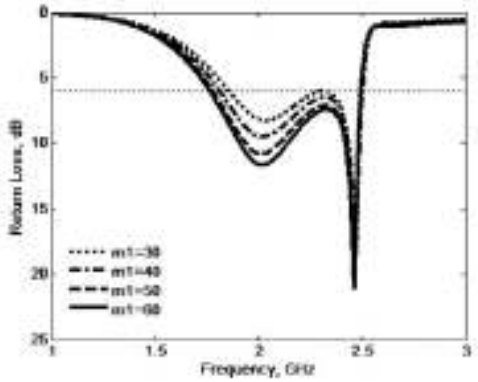

Figure 6 *Parametric study on parameters m1 against operating frequency*

www.ietdl.org

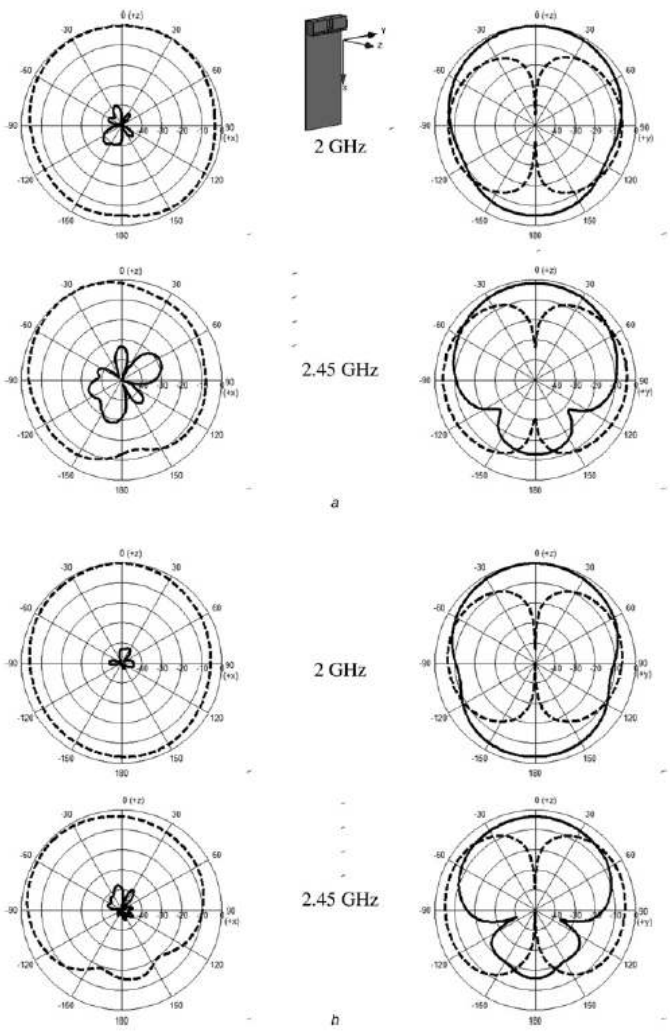

Figure 7 *Comparison of radiation patterns*

a In free space

b In presence of hand model at 2 and 2.45 GHz

'——', calculated E_θ

'---', calculated E_ϕ

4 Analysis stability performance for the antenna and hand model

The mutual effect between the antenna and the human hand model was investigated in order to evaluate the performance dependence of the proposed design. For the electrical properties of the hand model tissue at 2000 MHz, a relative permittivity (ε_r) of 54 and a conductivity (σ) of 1.45 S/m are used. In addition, the dimensions and position of the hand model that holds the phone are illustrated in Fig. 4 and listed as follows: $g1 = 8.5$, $b_h = 80$, $b_1 = 39.5$, $b_w = 30$ and $m1 = 24$ (all dimensions in mm). It is notable that a gap between the hand model and the metallic ground plate is 4 mm in the model.

Antenna performance in presence of human hand model was characterised in terms of the antenna return loss and radiation patterns. Fig. 5 shows the antenna return loss with and without hand model. With the hand model $m1$ was chosen to be 50 mm in the analysis. As can be seen,

IET Microw. Antennas Propag., 2010, Vol. 4, Iss. 5, pp. 600–608
doi: 10.1049/iet-map.2009.0153

the resultant two plots have almost identical variations. The results indicate the proposed design features have low sensitivity of impedance detuning when the phone is held and reduced dependence of the antenna on the ground plane. The effects on various positions of the hand (i.e. 'w1') were also studied. The distance between the antenna and the hand (i.e. parameter 'w1') was varied from 30 to 60 mm in increments of 10 mm. The corresponding return loss results are presented in Fig. 6. As can be observed, there is little variation of the calculated return loss observed for the varied cases. These results agree well with [16, 17] in which they show negligible induced surface currents on the handsets expect underneath the antenna. Similarly, the radiation patterns were examined for the case $w1 = 30$ mm. The calculated patterns of the proposed antenna with and without hand model at frequencies of 2 and 2.45 GHz were presented in Fig. 7. The results found to vary by not more than 2 dB at the maximum when the hand model is included, which suggests that the proposed design induced very little current into the ground plane.

5 Near field measurement

The experimental SAR measurement for the proposed antenna was carried out in an anechoic chamber using the equipment illustrated in Fig. 8, which includes a cubic phantom model and computer controlled three-dimensional

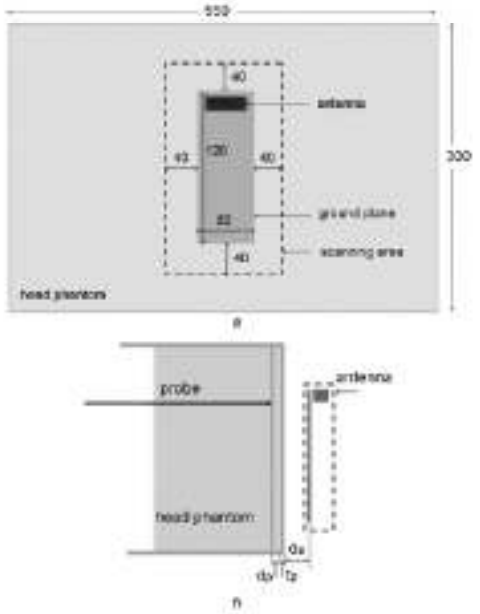

Figure 8 *Diagram of near field measurement set-up for the proposed antenna*

a Bottom view
b Side view

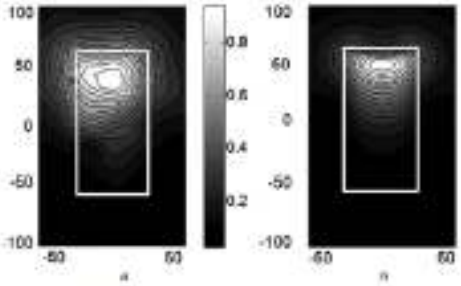

Figure 9 *Normalised SAR distribution at 1.8 GHz*

a Measured SAR
b Computed SAR

(3D) stepper motor system to position the probe. The head model was considered as a single homogenous flat layer, which is good enough compared to a multi-layered spherical head [18].

The cubic phantom, made of plastic 5 mm thick (t_p), has a dimension of 550 (L) × 300 (W), and can be filled with 51 of brain-simulating liquid (lossy tissue-stimulant material) characterised by conductivity $\sigma = 1.3$ S/m and a relative permittivity $\varepsilon_r = 41.8$ at 1.8 GHz. This liquid is composed of 54.90% de-ionised water, 44.92% (2-butoxyethoxy) ethanol or diethylene glycol monobutyl ether and 0.18% NaCl salt as recommended by IEEE Std 1528-200x for the frequency band 1800–1900 MHz [19, 20]. Since the top surface of the phantom is open, the E-field probe can be inserted and positioned to a desired location for measurement. The positioning repeatability of the stepper motor system moving the E-field probe is within ±5 mm. The non-perturbing implantable E-field probe model: EX3DV4 manufactured by SPEAG [21] and connected to EASY4 system is used for near field measurements. The normalised measured and simulated SAR values are shown in Fig. 9. The probe and antenna distances shown in Fig. 8 were considered 2 mm (d_z) and 3 mm (d_x), respectively. A reasonable agreement in SAR distribution between the measured and computed results can be easily noted from Fig. 9. The maximum unaveraged measured and computed SAR values for 1 watt input power are 3.2 and 3.02 W/kg, respectively. These results are much lower than those reported in [20] for a GSM 1800 terrestrial handset, for which the peak SAR in the head was between 10 and 21 W/kg for a head-handset separation of 7.5 mm.

6 Antenna radiation and efficiency results

The measurements of radiation patterns of the prototype were carried out in a far-field anechoic chamber. Two pattern cuts were taken for four selected operating frequencies that cover the designated whole bandwidth in this study. The radiation patterns in the xz- and xy-plane for the balanced folded

www.ietdl.org

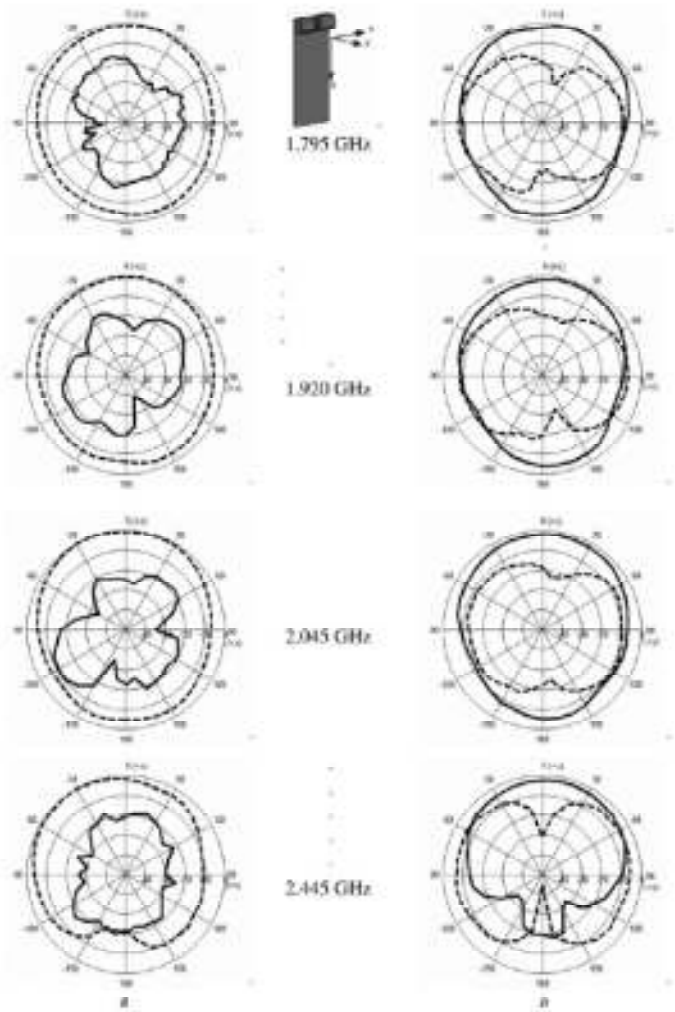

Figure 10 *Measured radiation patterns for the proposed antenna at 1.795, 1.920, 2.045 and 2.445 GHz*

a xz-plane
b yz-plane
'——', measured E_ϕ; '···', measured E_θ

dipole at 1.795, 1.920, 2.045 and 2.445 GHz were measured. The results are presented in Fig. 10, in which the patterns of the prototype antenna are seen to be quite similar to each other. The pattern similarities for the first three selected frequencies (i.e. 1.795, 1.920 and 2.045) were quite reasonable. In addition, the zx-plane presents a nearly omni-directional radiation pattern in all three intended frequency bands; whereas the proposed antenna at 2.445 GHz tends to radiate at the $-x$-direction in the zx-plane cut and at the $+z$-direction in the zy-plane cut, in which the ground plane for this band acts as a good reflector.

Table 2 shows the measured broadside antenna power gain for the frequencies across the DCS, PCS, UMTS and 2.4-GHz WLAN bands. It should be noted that the insertion loss of the feeding network was subsequently compensated for each measured power gain over all bands. As observed, the measured antenna gain varied between 2.7 and 5.4 dB over the entire bandwidth considered.

Radiation efficiency is an important performance parameter that defines antenna power consumption, but sometimes is difficult to measure precisely. A convenient new radiometric technique for measuring radiation

IET Microw. Antennas Propag., 2010, Vol. 4, Iss. 5, pp. 600–608
doi: 10.1049/iet-map.2009.0153

Table 2 Measured antenna gain and antenna efficiency of the proposed design

Frequency (GHz)	1.75	1.8	1.85	1.90	1.95	2.0	2.045	2.1	2.15	2.4	2.445	2.48
antenna gain (dBi)	2.7	3.2	3.6	4.3	4.2	4.2	4.3	4.2	5.4	3.2	3.6	4.1
frequency (GHz)	1.75	1.80	1.845	1.90	1.95	2.01						
antenna efficiency (%)	70.8	76.9	88.5	90.5	95.2	94.4						

efficiency, as previously proposed by the authors [22], was applied to the proposed balanced antenna. This technique is based on the observed dependence of the antenna's noise temperature on its physical temperature, and is presently available for 850 MHz to 2.5 GHz. Measured efficiency results for the present design taking into account the impedance mismatch are presented in Table 2. As can be seen, the antenna has high efficiency over the frequency bands of interests. It was not yet possible to characterise passive intermodulation in this antenna; as in other designs, this can be minimised by care in construction and choice of materials, and in any case is unlikely to be an issue at the power levels used in handsets. The presented results of the antenna efficiency are encouraging and imply the advantage of the present mobile antenna design using a balanced technique.

7 Conclusions

A new compact wideband balanced folded dipole antenna, operating over DCS, PCS, UMTS and 2.4-GHz WLAN bands, has been presented and analysed. The proposed antenna was characterised in terms of the return loss, radiation pattern, power gain and radiation efficiency. Comparison of return loss measurements showed good agreement with the computational predictions. The analysis of the proposed antenna design in the presence of a human hand model confirmed that the antenna induces little current into the ground plane. In addition, the antenna performance was stable since the interaction between the antenna and the hand is minimised. The antenna efficiency has been measured using the radiometric technique and the attained results showed good efficiency performance.

The presented results have proved the design concept for mobile antennas using a balanced technique, which is attractive for practical application in mobile phones. However, the current design has some practical limitations since it does not cover operation in the GSM900 frequency band, which is still in demand at present, or in the 5 GHz band for WLAN, which is increasingly included in new mobile handsets. For the future work, further development of balanced antennas will address this issue of developing new techniques for multi-band realisation.

8 Acknowledgment

The authors would like to gratefully acknowledge the financial support by the Engineering and Physical Sciences Research Council (EPSRC) in the UK under grant EP/E022936/1.

9 References

[1] FCC: 'Evaluating compliance with FCC guidelines for human exposure to radio frequency electromagnetic fields'. OET Bulletin 65, Federal Communication Commission, Washington, DC, August 1997

[2] ICNIRP Guidelines: 'Guidelines for limiting exposure to time-varying electric, magnetic, and electromagnetic fields (up to 300 GHz)', *Health Phys.*, 1998, **74**, (4), pp. 494–522

[3] OGAWA K., IWAI H., KOYANAGI Y.: 'Balance-fed planar built-in antenna', *Electron. Lett.*, 2001, **37**, (8), pp. 476–478

[4] KINGSLEY S.: 'Advances in handset antenna design', *RF Des.*, 2005, pp. 16–22

[5] COLLINS B.S., KINGSLEY S.P., DE J.M., SAARO S.A., SCHLUB R.W., O'KEEFE S.G.: 'A multi-band hybrid balanced antenna'. IEEE 2006 Int. Workshop on Antenna Technology: Small Antennas; Novel Metamaterials, White Plains, New York, 6–8 March 2006, pp. 100–103

[6] ABD-ALHAMEED R.A., EXCELL P.S., KHALIL K., ALIAS R., MUSTAFA J.: 'SAR and radiation performance of balanced and unbalanced mobile antennas using a hybrid formulation', *IEE Proc. Sci. Meas. Technol. (Special Issue on Comput. Electromagn.)*, 2004, **151**, (6), pp. 440–444

[7] MORISHITA H., FURUUCHI H., FUJIMOTO K.: 'Performance of balance-fed antenna system for handsets in vicinity of a human head or hand', *IEE Proc. Microw. Antennas Propag.*, 2002, **149**, (2), pp. 85–91

[8] Computer Simulation Technology Corporation: CST Microwave Studio, Version 5.0, Germany

[9] AMMANN M.J., CHEN Z.N.: 'Wideband monopole antennas for multi-band wireless systems', *IEEE Antennas Propag. Mag.*, 2003, **45**, (2), pp. 146–150

[10] VALDERAS D., LEGARDA J., GUTIERREZ I., SANCHO J.I.: 'Design of UWB folded-plate monopole antennas based on TLM', *IEEE Trans. Antennas Propag.*, 2006, **54**, (6), pp. 1676–1687

[11] ZHOU D., ABD-ALHAMEED R.A., EXCELL P.S.: 'Wideband balanced folded dipole antenna for mobile handsets'. The Second European Conf. on Antennas and Propagation, Session MoPA, Paper No.39, Edinburgh, UK, 11–16 November 2007

[12] ZHOU D., ABD-ALHAMEED R.A., SEE C.H., ALHADDAD A.G., EXCELL P.S.: 'New mobile balanced mobile antenna with wide bandwidth performance'. Proc. European Conf. on Antennas and Propagation, Berlin, Germany, 23–27 March 2009, pp. 549–552

[13] ZHANG Z.Y., GUO Y.X., ONG L.C.: 'A new wideband planar balun on a single-layer PCB', *IEEE Microw. Wirel. Compon. Lett.*, 2005, **15**, (6), pp. 416–418

[14] AGILENT TECHNOLOGIES: version 2005A, 'Advanced design systems', (Santa Rosa, CA)

[15] MEYS R., JANSSENS F.: 'Measuring the impedance of balanced antennas by an S-parameter method', *IEEE Antennas Propag. Mag.*, 1998, **40**, (6), pp. 62–65

[16] KIM Y., MORISHITA H., KOYANAGI Y., FUJIMOTO K.: 'A folded loop antenna system for handsets developed and based on the advanced design concept', *IEICE Trans. Commun.*, 2001, **E84-B**, (9), pp. 2468–2475

[17] HAYASHIDA S., MORISHITA H., FUJIMOTO K.: 'Self-balanced wideband folded loop antenna', *IEE Proc. Microw. Antennas Propag.*, 2006, **153**, (1), pp. 7–12

[18] KIVEKAS O., OLLIKAINEN J., LEHTINIEMI T., VAINIKAINEN P.: 'Bandwidth, SAR, and Efficiency of Internal Mobile Phone Antennas', *IEEE Trans. Electromagn. Compat.*, 2004, **46**, (0), pp. 71–86

[19] MUSTAFA J., ABD-ALHAMEED R.A., EXCELL P.S., MCEWAN N.J.: 'SAR reduction using phased antenna array mobile handset', *Appl. Comput. Electromagn. J. (Spec. Issue on Phased Adapt. Array Antennas)*, 2006, **21**, (3), pp. 196–205

[20] MUSTAFA J.: 'Mobile communication handset antennas with reduced user coupling: design of array and balanced antennas for 1.8 GHz personal communication handset to reduce specific absorption rate'. PhD thesis, Bradford University, 2005

[21] Schmid & Partner Engineering AG: Switzerland, http://www.speag.com/speag/index.php

[22] MCEWAN N.J., ABD-ALHAMEED R.A., ABIDIN M.N.Z.: 'A modified radiometric method for measuring antenna radiation efficiency', *IEEE Trans. Antennas Propag.*, 2003, **51**, (8), pp. 2099–2105

IET Microw. Antennas Propag., 2010, Vol. 4, Iss. 5, pp. 600–608
doi: 10.1049/iet-map.2009.0153

2010 Loughborough Antennas & Propagation Conference 8-9 November 2010, Loughborough, UK

Interaction Between Electromagnetic Field and Human Body for Dual Band Balanced Antenna Using Hybrid Computational Method

A. G. Alhaddad[1], K. N. Ramli[2], R. A. Abd-Alhameed[3], and D. Zhou[4]

Mobile & Satellite Communications Research Centre, School of Engineering, University of Bradford, Bradford, West Yorkshire, United Kingdom, BD7 1DP

***Abstract*—This paper describes a hybrid computational method which efficiently models the interaction between a small antenna placed in proximity with the human body. Results for several test cases of placed in different locations on the body are presented and discussed. The near and far fields were incorporated into the study to provide a full understanding of the impact on human tissue. The cumulative distribution function of the radiation efficiency and absorbed power is also provided. The antennas are assumed to be operating over the 2.4 GHz and 5.2 GHz WLAN frequencies.**

I. Introduction

In wireless communications the finite difference time domain (FDTD) method has become very well established as a both as a design and general analytical tool due to its comparative simplicity, robustness, and capability for handling inhomegeneity within volumetric complexity [1][2]. The introduction, by Taflove, of the total-scattered field formulation provided a major step forward in practical implementation [2], allowing algorithms to be implemented using incident plane waves from arbitrary directions. The computational FDTD domain is discretised into a number of cells which are scaled as a fraction of the wavelength. The associated time step must be kept small during the simulation to satisfy the Courant-Freiderichs stability criterion [2][3]. An absorbing boundary condition (ABC) must be applied to the outer boundary of the FDTD space to obtain the necessary spatial resolution to represent electromagnetic wave interactions in unbounded regions – i.e. to simulate the extension of the finite lattice to infinity. The ABC should be able to absorb the outwardly travelling waves with an extremely low reflection. The perfectly matched layer introduced by Berenger [4] allows boundary reflections better than -80 dB to be realized. FDTD is currently the most widely used method for numerical dosimetry, particularly for the field analysis required to estimate mobile handset radiation effect on the human body [5-9].

This paper presents a hybrid method to model the human body interaction with a dual band balanced antenna structure covering the 2.4 GHz and 5.2 GHz bands. The near and far field performance of the antenna is investigated, with the antenna mounted on several locations of the human body. The radiated and absorbed power distributions are computed for the antenna in the various locations, and with different polarizations. From this we may infer the radiation efficiency of the balanced antenna operating in proximity to the human body; the cumulative distribution function (CDF) of the radiation efficiency for these locations is also evaluated.

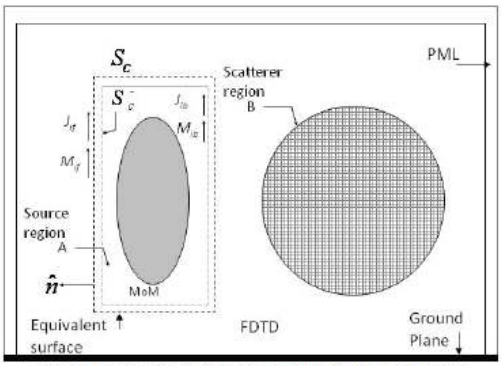

Figure 1: Hybrid MoM/FDTD configuration for the single source and scatterer geometries

II. Theoretical Formulation

Consider the electromagnetic geometry indicated in Fig. 1. This shows two regions, one representing the source region **A**, and the other the scatterer **B**. The source region is bounded by a closed Huygens surface S_c. The method starts by computing the fields due to the real currents of the source region (previously evaluated from the internal excitation) on the surface S_c, excluding the scatterer region **B**. These fields are computed by applying Galerkin's method with set of variable polynomial basis functions [10].

The equivalent surface currents on the surface S_c represent the outward travelling wave-fields from the source to the scatterer, due to the fields of the source region **A**, these may be written as:

$$\boldsymbol{J}_{if} = \boldsymbol{n} \times \boldsymbol{H}_{if} \qquad (1)$$

978-1-4244-7307-6/10/$26.00 ©2010 IEEE

$$\boldsymbol{M}_{if} = \boldsymbol{E}_{if} \times \boldsymbol{n} \quad (2)$$

where $\boldsymbol{n}$ is the outwardly directed unit normal to the surface from the source region. $\boldsymbol{H}_{if}$ and $\boldsymbol{E}_{if}$ are the forward scattered fields from the source region A on the equivalent surface S_c. $\boldsymbol{J}_{if}$ and $\boldsymbol{M}_{if}$ are the equivalent electric and magnetic source currents on the surface S_c. Thus these currents are treated as the source in the FDTD domain, propagating fields to the scatterer by using the $\boldsymbol{E}$ and $\boldsymbol{H}$ curl equations as follows:

$$\nabla \times \boldsymbol{E} = -\partial_t \boldsymbol{B} - \boldsymbol{M}_{if} \quad (3)$$
$$\nabla \times \boldsymbol{H} = \partial_t \boldsymbol{D} + \boldsymbol{J}_{if} \quad (4)$$

The FDTD updating equations for the field components are expanded with a three-dimensional modified total/scattered FDTD formulation for the special components on the Huygens' surface, while the rest of the problem space field components follow the normal updating equations.

The back-scattered fields were computed by FDTD at S_C^- (the closed surface interior to the surface S_c and bounding the region A). This surface is closed in the scattered field region, so that the calculated surface currents are due the scattered field only. The equivalent surface currents due to these fields, representing an additional source to the MoM domain (region A), are given by:

$$\boldsymbol{J}_{ib} = \boldsymbol{H}_{ib} \times \boldsymbol{n} \quad (5)$$
$$\boldsymbol{M}_{ib} = \boldsymbol{n} \times \boldsymbol{E}_{ib} \quad (6)$$

where $\boldsymbol{H}_{ib}$ and $\boldsymbol{E}_{ib}$ are the back-scattered fields computed at S_C^-. Note that $\boldsymbol{n}$ is as above, directed outwards from the source region. $\boldsymbol{J}_{ib}$ and $\boldsymbol{M}_{ib}$ are the electric and magnetic equivalent surface currents at S_C^-. Now, the voltage back scattered (the excitation for the MoM) on the source region can be evaluated using either of the following equations, defined by reciprocity theorem in the same way as in [10]:

$$\begin{aligned} \mathbf{V}_b &= \langle \boldsymbol{J}_{ib} \cdot \boldsymbol{E}_{ms} - \boldsymbol{M}_{ib} \cdot \boldsymbol{H}_{ms}, dS_C^- \rangle \\ &= \iint_{S_C^-} dS_C^- (\boldsymbol{J}_{ib} \cdot \boldsymbol{E}_{ms} - \boldsymbol{M}_{ib} \cdot \boldsymbol{H}_{ms}) \end{aligned} \quad (7)$$

where

$$\boldsymbol{E}_{ib} = -j\omega \boldsymbol{A}(\boldsymbol{r}) - \nabla V(\boldsymbol{r}) - \frac{1}{\epsilon} \nabla \times \boldsymbol{F}(\boldsymbol{r})$$

$$\boldsymbol{A}(\boldsymbol{r}) = \mu \iint_{S_C^-} dS_C^- [\boldsymbol{J}_{ib} G(\boldsymbol{r}, \boldsymbol{r}')]$$

$$V(\boldsymbol{r}) = \frac{-j}{\omega\epsilon} \iint_{S_C^-} dS_C^- [\nabla_s' \cdot \boldsymbol{J}_{ib} G(\boldsymbol{r}, \boldsymbol{r}')]$$

$$\boldsymbol{F}(\boldsymbol{r}) = \epsilon \iint_{S_C^-} dS_C^- [\boldsymbol{M}_{ib} G(\boldsymbol{r}, \boldsymbol{r}')]$$

$G(\boldsymbol{r}, \boldsymbol{r}')$ is the free space green function. The vectors $\boldsymbol{r}$ and $\boldsymbol{r}'$ apply to the source and observation points respectively and S_w is the conducting surface area of the structure within region A. $\boldsymbol{J}_{ms}$ is the electric test function used on the wire. $\boldsymbol{E}_{ms}$ and $\boldsymbol{H}_{ms}$ are the electric and magnetic fields respectively for the test function $\boldsymbol{J}_{ms}$.

Equation (7) explicitly requires a double integral to evaluate $\boldsymbol{E}_{ib}$ and integrate over the surface on the antenna; assuming that the FDTD discretisation is very small compared to the operating wavelength. In this case Equation (7) can be reduced by ignoring the surface integral and evaluating the voltage back-scattered corresponding to the centre of the cell surface, by a summation over grid cell surfaces, to get the following equation for the hybrid MoM/FDTD case:

$$\mathbf{V}_b = \sum_{k=1}^{n_{S_C^-}} \left(\boldsymbol{J}_{ib_k} \cdot \boldsymbol{E}_{ms}(\boldsymbol{r}_k, \boldsymbol{r}') - \boldsymbol{M}_{ib_k} \cdot \boldsymbol{H}_{ms}(\boldsymbol{r}_k, \boldsymbol{r}') \right) a_k \quad (8)$$

where $\boldsymbol{r}_k$ is the position vector of the centre of the cell surface and a_k is the surface area of the cell surface. Therefore $\boldsymbol{J}_{ib_k}$ and $\boldsymbol{M}_{ib_k}$ are considered to be the equivalent surface currents at the centre of the surface cell n. Since the excitation voltages are known, the MoM can be executed to compute the new currents and the procedure can be repeated until the steady state solution is reached.

III. The Antenna

The antenna adopted in this study has been previously described by the authors in [11]. The antenna structure is a compact balanced dual band device, constructed by folding a thin strip planar dipole with an extra arm on each proposed monopole. The balanced design is intended to reduce the current flow on the conducting surface of the user terminal chassis. As a result the antenna has good efficiency, and maintains performance when held in proximity with the human body. This particular device was designed for short range WLAN communications operating in the 2.4 GHz (2.4-2.4835 GHz) and 5 GHz (5.15-5.35 GHz & 5.650-5.925 GHz) bands.

IV. Hybrid Model Method

This process begins by introducing a Huygens' surface around the balanced antenna. The equivalent electric and magnetic source on the Huygens' surface are produced at each time step from the electric and magnetic fields created by the antenna in free space using NEC [12]. This field data is used as an input source for the FDTD code. The Huygens' box is set as shown in Fig. 2, with volume of 30×24×54 FDTD cells. The FDTD method is applied over the entire computational domain. The equivalence principle is carried out in 3D by applying the hybrid electromagnetic method described in [13] with cell size dx=dy=dz= 6.0mm, and time step dt=5ps. A 6 cell PML is used to terminate the FDTD space, and the distance between the antenna and face of the box will be set to 2 cells. The human body model used in this study is known as the "Visible Man", the tissue-classified numerical model for

2010 Loughborough Antennas & Propagation Conference 8-9 November 2010, Loughborough, UK

which was developed at Brooks Air Force Base, San Antonio, TX [14].

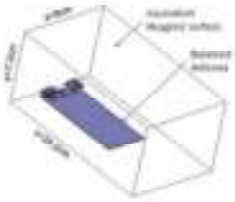

Figure 2: The balanced antenna with the equivalent Huygens box

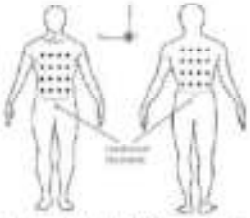

Figure 3: Human body model and the balanced antenna locations

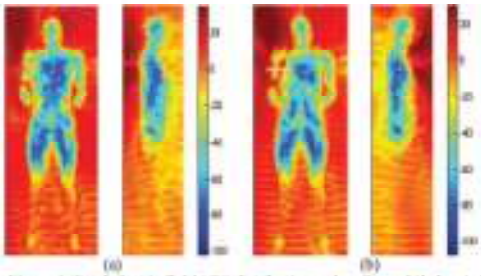

(a) (b)

Figure 4: Total electric field (dB) distributions when the mobile located in horizontal position, (a) Back Location,(b) Front Location

A. *Near field and Far field*

In order to investigate the performance of the antenna in proximity to the human body, the near and far field radiation of the antenna for different locations has been considered, as illustrated in Fig. 3. A total of 32 locations were investigated; 16 locations on the back, and 16 on the front, were taken. Due to the electric field distribution of these points being quite similar to each other, only one position for each case was demonstrated. Fig. 4 illustrates the electric field distribution in the neighborhood, and inside the human body, for the central y-z and x-y planes (dB scale) for the vertically polarized antenna position. Further simulations were performed on the radiation performance using the same antenna locations, but with different polarizations, these were found comparable to the other polarization.

The results of the investigation were conclusive, and made clear that regardless any changes in the polarization, the electric field distribution was almost the same when the mobile positions were changed. Again, as one may expect with the electric field distribution of these points being quite similar to each other, only one position for each case was demonstrated. Fig. 4 clearly illustrates the gulf between the two types of position: i.e. facing the human tissue (and its surrounding area), and that facing away. When the antenna is very close to the human tissue, the surrounded fields are much stronger, and this is clearly indicated in the figures.

Fig. 5 illustrates the far field components of the cases under investigation, the fields for y-z and x-y planes are normalized to one 1 watt input power. From the pattern variations it is clearly evident that the fields were considerably stronger in the direction directly facing the normal axis of the handset antenna, and consequently away from the human tissue.

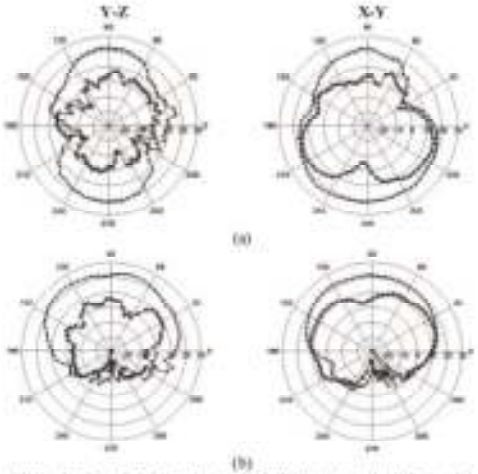

Figure 5: The far field patterns at 2.45 GHz yz, xz and xy planes; for vertical polarization (a) Back Location,(b) Front Location; where 'o-o-o' computed E_θ and 'x-x-x' computed E_ϕ

Consequently, it is no surprise to notice the reduced field magnitudes caused by the tailing effect of the human body falling approximately between 20 dB and 25 dB. However it should be noted that for horizontal polarization the field distribution was quite similar to the vertical one in both manifestation and impact and thus are not presented here.

B. *Cumulative Distribution Function of the Radiation Efficiency*

The absorbed power and radiated power are recorded from the simulation results. The radiation efficiency for the balanced antenna can be calculated using the following formula:

$$\text{efficiency } (\eta) = \frac{P_{\text{radiated}}}{P_{\text{in}} + P_{\text{absorbed}}} \qquad (9)$$

The cumulative distribution function (CDF) is evaluated for each location in order to estimate the probability of the power absorbed and radiation efficiency on the human body. Fig. 7 shows the radiation efficiency, and power absorbed values, and their associated CDF evaluated when the mobile placed on these locations. The CDF of the radiated and absorbed power is difficult to predict from the results collected due to the limited sample size generated through the simulation. Recognising the constraints surrounding memory and simulation time, a total of 32 different locations (in line with the rest of the simulation) have been considered, with a view to extrapolating the necessary data. The data from these

locations was combined to obtain probability of the efficiency, and can be obtained from Fig. 6. The radiation efficiency values increase as the handset moves from the back to the front of the human body. Hence, these figures clearly indicate that the CDF achieves better radiation efficiency (in the neighbourhood of 40% better) when the mobile been placed on the front of the human model compared to the case of the back position. The reasoning for this appears to be due to a loss of characteristics in the tissue at the front, and a greater degree of absorbed power, as can be seen from the figure.

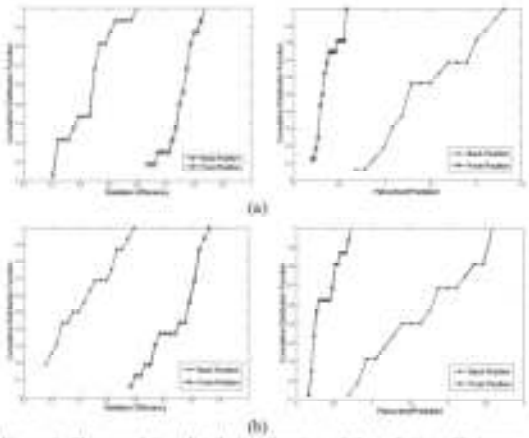

Figure 6: The cumulative distribution function of the radiation efficiency and $P_{absorbed}/P_{radiated}$ when (a) Vertical polarization , (b) Horizontal polarization

In line with our expectations, the figures confirmed that the CDF has similar curves for horizontal and vertical cases for both locations. In addition, it can be reported from Fig. 6 and subsequent calculations, it is evident that standard deviation of the radiation efficiency when the mobile is located in the front is less compared to back location. Taking the previous simulation results into account, we may safely conclude that altering the position of the antenna on the front will not results in a large dispersion in the radiation efficiency. Furthermore the CDF has similar curves for horizontal and vertical cases for both locations.

V. Conclusions

A hybrid MoM/FDTD approach has been adopted for modelling the human body interaction with short range dual band balanced antennas. A total of 32 locations on the human body were investigated, 16 on the back and 16 on the front. In order to ensure the optimal quality of results were achieved through this limited sample, each point was investigated using two polarisations; essentially both horizontal and vertical polarisations. Furthermore, both the far and near fields were incorporated into the study to heighten the understanding of the impact on human tissue both facing the antenna, and not directly facing the antenna. The cumulative distribution function of the radiation efficiency at these locations was also computed. The results support the conclusion that there was a clear improvement in the front compared to the back.

Acknowledgement

The authors would like to thank their colleague Mr.M.B.Child for helpful comments and assistance.

References

[1] K. S. Yee, "Numerical solution of initial boundary value problems involving Maxwell's equations in isotropic media," IEEE Trans on Antennas and Propagation, vol. AP-14, pp. 302-307, 1966.

[2] A. Taflove and S. C. Hagness, Computational electrodynamics: The finite-difference time-domain method, vol. 3rd ed. Boston: MA: Artech House, 2005.

[3] K. S. Kunz and R. J. Luebbers, The finite difference time domain method for electromagnetics, vol. Boca Raton: FL: CRC Press, 1993.

[4] J. P. Berenger, "A perfectly matched layer for the absorption of electromagnetic waves," Journal of Computational Physics, vol. 114, pp. 185-200, 1994.

[5] A. Sani, Y. Zhao, and Y. Hao, "Analysis of on-body propagation channel using a hybrid technique combining the equivalence principle and FDTD," Proceedings of iWAT2008, Chiba, Japan, pp. 502-505, 2008.

[6] M. F. Wong and J. Wiart, "Modelling of electromagnetic wave interactions with the human body," Comptes Rendus Physique, vol. 6, pp. 585-594, 2005.

[7] J. Wang, O. Fujiwara, S. Watanabe, and Y. Yamanaka, "Computation with a parallel FDTD system of human-body effect on electromagnetic absorption for portable telephones," IEEE Transactions on Microwave Theory and Techniques, vol. 52, pp. 53-58, 2004.

[8] O. P. Gandhi and J. Chen, "Numerical dosimetry at power-line frequencies using anatomically based models," Bioelectromagnetics, vol. 13, pp. 43-60, 1992.

[9] K. Fujii, M. Takahashi, K. Ito, and N. Inagaki, "Study on the electric field distributions around whole body model with a wearable device using the human body as a transmission channel," First European Conference on Antennas and Propagation. EuCAP pp. 1 - 4, 6-10 Nov. 2006

[10] M. A.-A. Mangoud, "Hybrid Computational Electromagnetics Methods for Personal Communications Applications," in Department of Electronic and Electrical Engineering, vol. PhD Thesis: University of Bradford, 2001.

[11] A. G. Alhaddad, R. A. Abd-Alhameed, D. Zhou, C. H. See, E. Elfergani, M. Bin-Melha, and P. S. Excell, "New Design of Dual-band Balanced Handset Antenna Design for WLAN Application," In proceeding of Mosharaka International Conference on Communications, Propagation and Electronics (ISBN: 978-9957-486-06-8), vol. Technical Session 1, pp. 1-4, Amman, Jordon, 5-7 March 2010.

[12] NEC-Win Professional V1.1,@1997 Nittany Scientific Inc.,USA.

[13] R. A. Abd-Alhameed, P. S. Excell, and J. Vaul, "Currents Induced on wired LT. Networks by Randomly distributed phones –A Computational study," IEEE Trans on Electromagnetics and Compatibility, vol. 48, pp. 282-286, May 2006.

[14] P. A. Mason, W. D. Hurt, T. J. Walters, J. A. D'Andrea, K. L. R. P. R. Gajsek, K. I. S. D. A. Nelson, and J. M. Ziriax, "Effects of frequency, permittivity, and voxel size on predicted specific absorption rate values in biological tissue during electromagnetic-field exposure," IEEE Transactions on Microwave Theory and Techniques, vol. 48, pp. 2050 - 2058, Nov 11, 2000.

2009 Loughborough Antennas & Propagation Conference 16-17 November 2009, Loughborough, UK

Dual-band Balanced Handset Antenna for WLAN Application

A. G. Alhaddad[#1], R. A. Abd-Alhameed[#2], D. Zhou[#3], C. H. See[#4], M. Usman[#5], Z. Zainal Abidin[#6], P. S. Excell[*7]

[#] *Mobile and Satellite Communications Research Centre*
University of Bradford, Bradford, West Yorkshire, BD7 1DP, UK
[1]A.G.Alhaddad@bradford.ac.uk; [2]r.a.a.abd@bradford.ac.uk; [3]d.zhou2@bradford.ac.uk
[4]c.h.see2@bradford.ac.uk; [5]musman3@brad.ac.uk; [6]z.b.zainalabidin@brad.ac.uk
[*] *Glyndwr University, Wrexham, LL11 2AW, Wales, UK*
[7]p.excell@glyndwr.ac.uk

***Abstract*— A built-in planar metal plate antenna for mobile handsets with balanced operation is presented. The antenna was designed by folding a thin strip planar dipole with extra arm on each monopole. The antenna features balanced operation, is to reduce the current flow on the conducting surface of the handset body. The antenna design model intends to cover 2.4-GHz and the 5.2-GHz WLAN applications. For practical validation, the antenna prototype was fabricated. The measured return loss, radiation pattern and power gain of the prototype antenna are presented to verify the antenna performance. The measured results are found in good agreement with the calculated results.**

I. INTRODUCTION

Wireless communication has been gained popularity over last decade; this advances the mobile electronic equipments. In order to cater this high demand and increase competiveness from the commercial market, it is imperative to manufacturers to make mobile handsets as small and light as possible; without compromising functionality. Small antenna design has been a challenge for small handsets. These challenges include keeping the antenna performance unchanged or improved, even though the antenna size becomes small and reduce the degradation of antenna performance caused by the operator's adjacent effect [1].

Unbalanced antennas such as Planar Inverted–F antenna (PIFAs) have been used extensively in mobile communication systems and have attracted much attention from researchers and engineers because of their advantage of compact, low profile and easy to manufacture. However, it has a narrow bandwidth and needs a height from substrate to ground for matching [2-3]. Moreover, these antennas exhibit inferior performance when it is held by users. This can be attributed to the user holding the mobile phone, which largely covers the ground plane since the ground plane is used as part of the radiator in these antennas. Therefore, radiating currents are induced on both the ground plane and the antenna element resulting in currents flowing on the human body, which degrade the performance of the antenna's radiation characteristics and introduce losses and uncertainty in its matching [4].

As a symmetric structure is fed by balanced lines and has two conductors carrying currents of equal magnitude but 180 degree out of phase, a balanced structure is a genuine alternative to avoid the aforementioned degradation of the antenna performance. As these currents cancel the effect of each other, the current flows only on the antenna element and not on the ground plane. So if the mobile phone is held by a human, no coupling takes place between the antenna and the human body thus the performance of the antenna is not affected [5]. A major drawback of balanced antennas is that they have a narrow bandwidth; nevertheless this bandwidth can be improved by certain techniques like using genetic algorithms [6]. A balun is one key component to excite a balanced antenna, as it is a device which enables compatibility between systems and is used for converting signals between an unbalanced circuit structure and a balanced circuit structure.

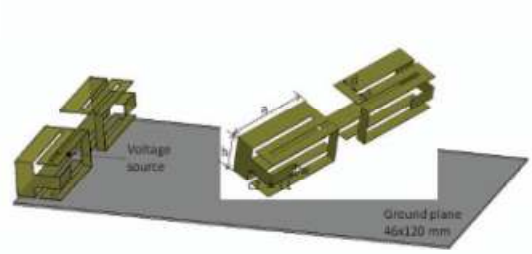

Fig. 1. The new proposed antenna design model.

Recently, several antennas for mobile handsets to cover dual band operation (2.4 and 5.2GHz) have been reported [7-8]. In these papers, characteristics of a built-in wideband planar metal plate antenna are introduced and analyzed in order to achieve dual-band operation. In this paper, a new designed dual band balanced handset antenna for 2.4 and 5.2GHz applications is presented. Simulation and measurement results are given to illustrate the characteristics of the proposed antenna. An electromagnetic field simulator Ansoft HFSS [9] was employed to predict the return loss and radiation pattern.

978-1-4244-2721-5/09/$25.00 ©2009 IEEE

2009 Loughborough Antennas & Propagation Conference 16-17 November 2009, Loughborough, UK

II. Antenna Design Concept

Through multiple simulated attempts, by conducting several modification of the antennas in [10] to move toward the desired outcome of developing highly compact and multi-application antenna for WLAN and Short range communication systems. The simulation process yielded a design where the antenna is mounted above a rectangular shaped metal plate of 46 × 120 mm, which acts as the mobile handset chassis or what today we would identify as the ground plane of a practical mobile phone handset, as seen in Figure 1.

The proposed dual-band balanced mobile antenna was achieved to generate another resonant frequency by using a two tier process. Firstly, it was started by folding the monopole arm into a zig-zag shape that was folded into itself, as shown figure 1. Secondly, an additional thin-strip arm was inserted into each arm of the planar dipole [11]. This folded element of the proposed antenna is designed to operate at 2.4 GHz with a single arm to generate the second resonant frequency for 5.2 GHz. This enabled the development of a wideband dual-resonant variant for multi-band operation, through the modifications of the single resonant antenna.

The proposed antenna design and simulation studied in terms of return loss and radiation patterns was performed using Ansoft HFSS (High Frequency Structure Simulator), which uses a 3D full-wave finite element Method (FEM). The dimensions of the antenna geometry are given in Fig. 1, whereas a = 18 mm, d = 4 mm, w = 3 mm, h = 8 mm, s = 2 mm, c1=c2= 6 mm. There are two identified variable parameters h and w, which is considered to be the most sensitive geometry parameter for meeting the design goals. Both H and W control the individual length of each one of the folded arms. Therefore it is desired to fully understand the performance of this proposed antenna by tuning these two parameters to achieve the required 2.4 GHz and 5.2 GHz for WLAN and Short range communication systems.

Parametric study has been carried out to optimize the impedance matching bandwidth for the proposed antenna at 2.4 GHz and 5.2 GHz bands, the optimum value of h and w were found to be 8 mm and 3 mm respectively, and this can be described in figures 2 and 3 respectively. Moreover, by modifying the length and location of the additional arm of the proposed antenna, this ensures the antenna can cover the required two frequency bands (i.e. 2400-2485 MHz & 5150-5350 MHz) at return loss ≤ -10dB.

III. Simulation And Measurement Results

In order to effectively characterize the proposed antenna, two antenna properties were measured; return Loss and radiation pattern. In regards to return loss, two methods were undertaken for this measurement exercise, which includes using a balun and implementing the S-Parameter method. By using the first method, a commercially hybrid junction from ET Industries [12] that operates from 2 to 12 GHz has been utilized in this measurement exercise, as a balanced feeding network. In this case, this balun is required as a support

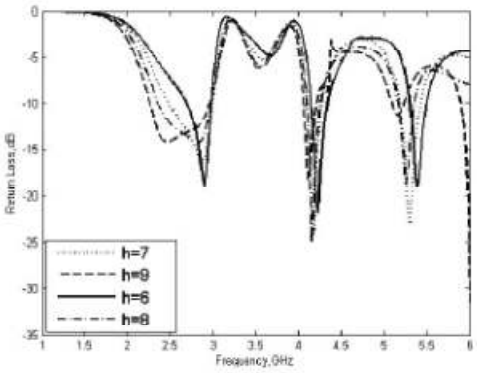

Fig. 2. Variation of the parameter h on the effect of return loss.

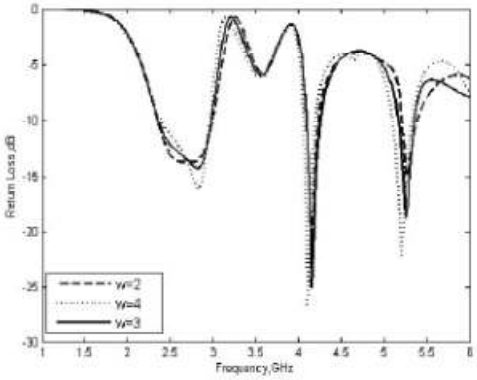

Fig. 3. Variation of the parameter w on the effect of return loss.

feeding network, to provide a balanced feed from an unbalanced source.

Figure 5 illustrates the measured return loss of the prototype antenna. With consideration to the errors caused by manufacturing the proposed antenna, this measured result shows fairly good agreement with simulated result. Using the S-Parameter method for measuring input impedance for the balanced antennas [13] was the second method to verify the impedance of the proposed antenna. As for this methodology; balanced antennas are considered as two-port devices and the S-Parameters can be obtained from a well-calibrated Network Analyzer. By employing some mathematical operation formula used by [13] the differential input impedance of the balanced antenna can be obtained.

The results from this exercise also gave much confidence to the measurement carried out, as the measured return loss in this method was relatively correlated with the first. Furthermore there was also fairly good agreement between this and the previous method, and the whole simulation

Fig. 4. Photograph of prototype of the proposed balanced antenna design.

exercise too, as can be seen in Figure 5. From this measurement exercise it was found, this result verifies the actual impedance of the proposed antenna and the effectiveness of proposed antenna system with integrated balun, for which both of them confirm the validation. Besides, it also supports the evaluation of the radiation performance of the prototype antenna.

In regards to measuring the radiation pattern, this was done from taking two pattern cuts for two WLAN operating frequencies in which it covers the designated whole bandwidth in this study; the measurements of the radiation patterns of the prototype were carried out in a far-field anechoic chamber. As illustrated in Figure 6, the radiation patterns in the xz plane and yz plane for the balanced folded dipole at 2450 MHz, 3000 MHz and 5200 MHz were measured. The measured radiation patterns showed asymmetrical radiation, and this would be attributed essentially to the asymmetrical antenna structure in fabrication and imbalanced outputs from the balun device in testing. By investigating the impact of the operator's hand and head on the antenna performance, it was found there was very little effect, which explains that the antenna has a perfect balanced structure.

Measured broadside antenna power gain for the frequencies across the 2.4 GHz and 5.2 GHz WLAN bands were also investigated. It was found that the maximum measured antenna gain at lower and upper WLAN bands were 3.5 dBi and 3.4 dBi, respectively.

In addition, current distribution on the mobile phone ground plane was analyzed using the EM simulator, as can be seen in the Figure 7 a high proportion of the current induced on the ground plane and the currents were concentrated in the area beneath the antenna. Moreover, a minimum current distribution appeared on the rest of the ground plane. Therefore this investigation clearly illustrates the advantage of using balanced antenna design for future mobile handsets.

IV. Conclusions

A new dual-band balanced dipole antenna with a 'zig zag' structure for mobile devices operated at 2.4 GHz and 5.2 GHz WLAN bands has been presented. This study has sought to verify the characteristics of the proposed antenna in terms of antenna return loss and radiation pattern. The simulation and

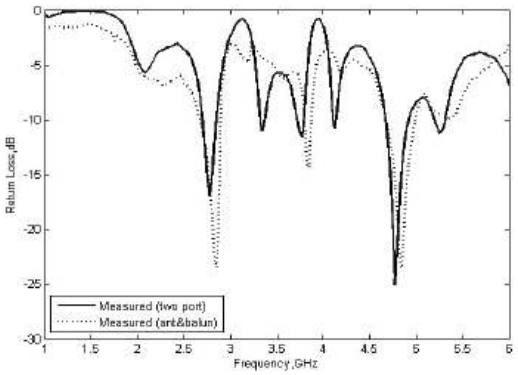

Fig. 5. Comparison of measured return loss.

measured results over the two operating frequency bands showed reasonable agreement, and therefore indicate this antenna can be able to be implemented in mobile phone.

References

[1] H. Morishita, H. Furuuchi and K. Fujimoto, "Performance of balance-fed antenna system for handsets in vicinity of a human head or hand", IEE Proc.-Microw. Antennas Propag., Vol. 149, No, 2, pp. 85-91, April 2002.

[2] Z. Li and Y. Rahmat-Sammii, "Optimization of PIFA-IFA combination in handset antenna designs", IEEE Trans. On Antennas and Propagation, Vol. 53, No. 5, pp. 1770-1778, May 2005.

[3] Y-S. Wang, M-C. Lee and S-J. Chung, "Two PIFA-related miniaturized dual-band antennas", IEEE Trans. On Antennas and Propagation, Vol. 55, No.3, pp. 805-811, March 2007.

[4] R.A. Abd-Alhameed, P.S. Excell, K. Khalil, R. Alias and J. Mustafa, "SAR and radiation performance of balanced and unbalanced mobile antennas using a hybrid formulation", Invited paper, IEE Proceedings-Science, Measurement and Technology special issue on Computational Electromagnetics, vol. 151, No. 6, pp. 440-444, November 2004.

[5] H. Morishita, S. Hayashida, J. Ito and K. Fujimoto, "Analysis of built-in antenna for handset using human (heand,hand,finger) model", Electronics and communications in Japan, Part 1, Vol. 86, No. 9, pp. 35-45, 2003.

[6] D. Zhou, R.A. Abd-Alhameed and P.S. Excell, "Bandwidth enhancement of balanced folded loop antenna design for mobile handsets using genetic algorithms", PIERS Online, Vol. 4, No. 1, pp.136-139, 2008.

[7] J. Janapsatya, K.P. Esselle and T.S. Bird, "A dual-band and wideband planar inverted-F antenna for WLAN applications", Microwave and Optical Technology Letters, Vol. 50, pp.138-141, January 2008.

[8] C.H. See, R.A. Abd-Alhameed, D. Zhou and P.S. Excell, "Dual-frequency planar inverted F-L-antenna (PIFLA) for WLAN and short range communication systems", IEEE Transactions on Antennas and Propagation, Vol.56, No 10, pp.3318-3320, October 2008.

[9] High Frequency Structure Simulator, Version 11, Ansoft Corporation, USA.

[10] D. Zhou, R.A. Abd-Alhameed and P.S. Excell, "Wideband balanced folded dipole antenna for mobile handsets", In proceedings of The European Conference on Antennas and Propagation: EuCAP 2007, Paper no. MoPA.012, Edinburgh, UK, 11-16 November 2007.

[11] D Zhou, RA Abd-Alhameed, CH See and PS Excell, "Design of multiband balanced folded dipole antenna based on a dual-arm structure for mobile handsets", In proceeding of Progress In Electromagnetics Research Symposium, pp. 318-321, July 2-6, Cambridge, USA, 2008.

[12] ET Industries, USA, http://www.etiworld.com/

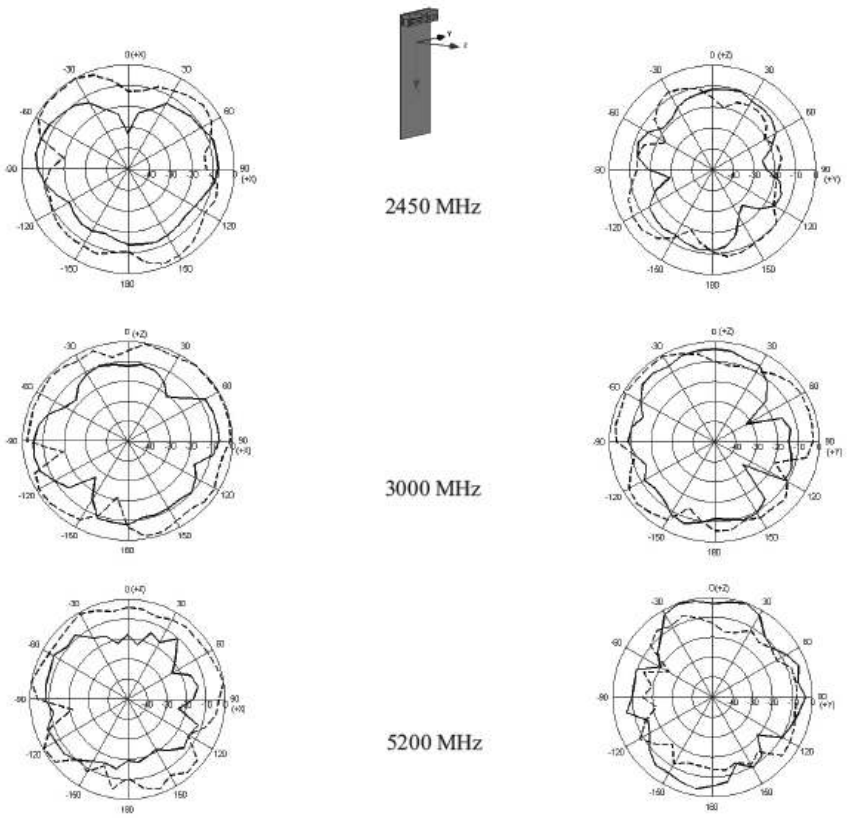

Fig. 6. Radiation patterns of the proposed antenna for 2450 MHz, 3000 MHz and 5200 MHz at: (left) xz plane; (right) yz plane, where '——' measured E_θ and '- - -' measured E_ϕ.

[13] R. Meys and F. Janssens, "Measuring the impedance of balanced antennas by an S-Parameter method", IEEE antennas and propagation magazine, vol. 40, no. 6, pp. 62-65, December 1998.

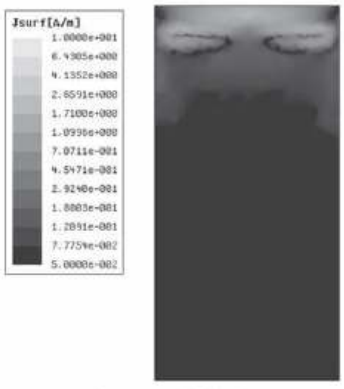

Fig.7.Current distribution.

New Balanced Mobile Antenna with Wide Bandwidth Performance

D. Zhou[#1], R. A. Abd-Alhameed[#2], C. H. See[#3], A. G Alhaddad[#4], P. S. Excell[*5]

[#] *Mobile and Satellite Communications Research Centre*
University of Bradford, Bradford, West Yorkshire, BD7 1DP, UK
[1]d.zhou2@bradford.ac.uk, [2]r.a.a.abd@bradford.ac.uk,[3]c.h.see2@bradford.ac.uk,
[4]a.g.alhaddad@bradford.ac.uk,

[*] *Glyndwr University, Wrexham, LL11 2AW, Wales, UK*
[6]p.excell@glyndwr.ac.uk

Abstract— **In this paper, a balanced antenna for mobile handset applications with broad bandwidth performance, covering frequencies from 2.6 GHz to 5.8 GHz, is investigated and discussed. The antenna is a variant of folded dipole antenna and a dual-arm on each monopole. The performance of the proposed antenna was analysed and optimised under certain size constrain. For validation, the antenna prototype was fabricated and tested. The performance of this balanced antenna was characterised in terms of the antenna return loss, radiation pattern and power gain. The calculated and measured results in terms of return loss show good agreement and the results also show good wideband characteristics.**

I. INTRODUCTION

Over recent years, balanced antenna systems have become of interest to mobile phone antenna designers due to their stable performance when held adjacent to the human body by mobile phone users [1-4], compared with that of the unbalanced designs (e.g. PIFAs) [5-8]. In this type of antenna, balanced currents only flow on the antenna element, thus dramatically reducing the effect of current flow on the ground plane (i.e. phone chassis). The implementation of antenna designs using balanced technique causing minimised coupling with the human head/hand and hence minimised SAR would be attractive to many consumers, thus increasing the market acceptance of mobile devices using such antennas.

Dipoles and loops are the most commonly types of balanced antennas used in the handset applications. Designing a good balanced mobile antenna is always a challenging task in order to be able to compromise certain constrains in the design, where small antenna size and multiple frequency bandwidth operation are usually required. Recently, several novel designs of such antenna type have been successfully developed and demonstrated [9-11], in which most of them were designed and implemented for operations in the current 2G and 3G frequency bands; however, not much of work has been done for the frequency band beyond 3G for the future mobile communication systems. Therefore, there is motivation to apply this balanced technique and develop antennas for future mobile devices applications.

This paper presents and investigates a new design of a built-in, small size and low profile folded balanced-dipole antenna with wideband impedance bandwidth. The characteristics of this balanced folded dipole antenna with a novel dual-arm structure integrated on the variant of folded loop for mobile handsets are analysed. For the analysis, an electromagnetic simulator based on the finite integration technique [12] was used to calculate the return loss and the radiation patterns for comparisons.

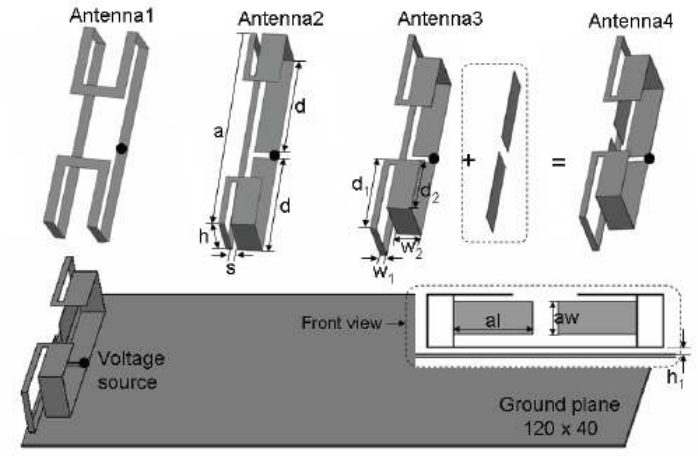

Fig.1 Antenna configuration studied.

II. ANTENNA DESIGN CONCEPT AND STRUCTURE

Basically, a wideband folded dipole antenna, developed on the basis of the 'Antenna1' as illustrated in Fig. 1, was first attempted and then several modifications were introduced to achieve an enhanced wideband feature for mobile handset applications. The antenna, as shown in Fig. 1, is mounted on the top of a rectangular conductor plate (dimension: 120×40 mm), which can be regarded as the mobile handset chassis or ground plane of a practical mobile phone.

In the previous work, a single band folded loop antenna (see 'Antenna1' in Fig. 1) [13], operating at GSM1800 mobile phone frequencies, was designed and optimized using genetic algorithm with the aim of improving the impedance bandwidth. Moreover, a variant of the folded loop antenna system (see 'Antenna2' in Fig. 1) was investigated at higher resonant frequency 2680 MHz in [14], where wider bandwidth was obtained by performing a parametric study on the width (w_2) of strip lines for such an antenna. This reported design was analysed in this study and the calculated return loss was shown in Fig. 2. Then it was found that the actual resonant frequencies of the antenna can be easily controlled with tuning the parameter d while keeping the main parameter a constant. An example of such a design was illustrated as 'Antenna3' in Fig. 1, where the important dimensions in mm are a=35.8, d=13.5, h=8, s=1, w_1=1, w_2=4, d_1=13 and d_2=9, and the corresponding return loss was presented in Fig. 2.

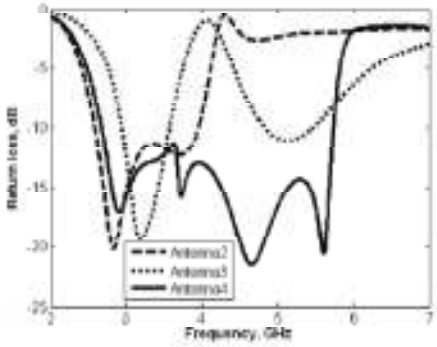

Fig. 2 Calculated return loss of the antennas presented in Fig. 1.

Furthermore, a design concept for generating another resonant frequency for balanced mobile antenna with folded structure was employed. This technique was applied by inserting an additional thin-strip arm in each arm of the planar dipole (see 'Antenna 4' in Fig. 1 and resultant return loss in Fig. 2); as a result, the single resonant antenna was modified and developed as a wideband dual-resonant variant for multi-band operation. Finally, this new proposed antenna was successfully developed and achieved with very large impedance bandwidth operation over the frequencies.

The optimal antenna configuration studied in terms of return loss, radiation patterns and power gain was observed with aid of CST simulator (a=35.8, d=13.5, h=8, s=1, w_1=1, w_2=4, d_1=13, d_2=9, al=12.5, aw=5 and h_1=1). As can be seen from Fig. 1, there are two variable parameters d and al, which control the overall length of the proposed folded loop and the length of the added arms, and hence subsequently have the effect on tuning the resonant frequencies for this wideband design. In order to fully comprehend, the influence of these parameters based on its impedance bandwidth, the parametric study is carried out here by varying each parameter, while holding the remaining parameter values at the assumed optimum values. From the observation of Figs 3 and 4, the optimum value of d and al was found to be 13.5 mm and 12.5 mm respectively, for the best performance of the proposed antenna on the frequency bandwidth with small size as possible.

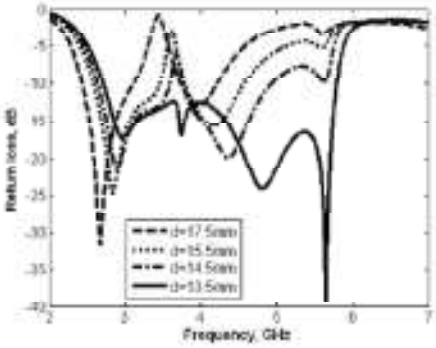

Fig. 3 Variation of the parameter d on the effect of return loss.

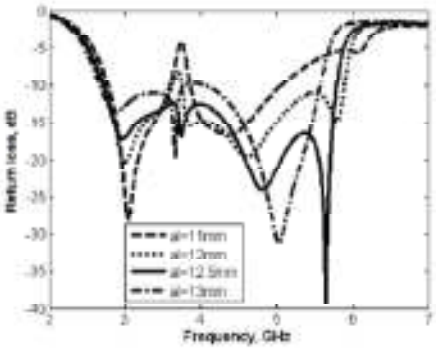

Fig. 4 Variation of the parameter al on the effect of return loss.

The proposed antenna features of the compact design, has used the size dimensions of (l × w × h) of 36 × 6 × 8 mm, which in fact possess the same overall dimension as the design demonstrated in work [14]. The length and location of the additional arm, including other parameters of the proposed antenna, were adjusted and further optimised to ensure that the design covered wide frequency bandwidth (i.e. 2.6-5.8 GHz) at suitable working VSWR ≤ 2.

III. SIMULATION AND MEASUREMENT RESULTS

For the hardware realisation, copper sheet with 0.35 mm and 0.5 mm thickness were used for fabricating the proposed balanced antenna and the associated ground plane (see Fig. 5). For a balanced antenna (e.g. dipole) system, a balun is usually required as a support feeding network, to provide a balanced

feed from an unbalanced source. A commercially hybrid junction from ET Industries [15] that operates from 2 to 12 GHz has been utilized in this work. Fig. 6 presents the measured and simulated return loss of the prototype antenna. As can be seen, taking into account the errors caused in the antenna fabrication and assembly, a close agreement between the calculated and measured return loss was observed.

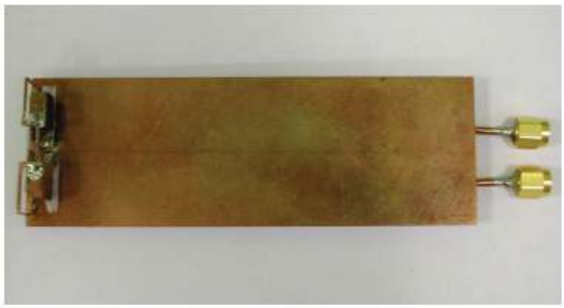

Fig. 5 Photograph of the prototype antenna.

The calculated radiation patterns of the prototype were normalized and shown in Fig. 7, where two pattern cuts (i.e. xz plane and yz plane) were taken for the whole frequency bandwidth covered. Five specific frequencies of the radiation patterns in the xz plane and yz plane of the prototype anten were selected in this study. These are 2.9 GHz, 3.5 GHz, 4 GHz, 5.2 GHz and 5.8 GHz. It can also be seen from Fig. 7 similar radiation patterns were observed at yz plane except t one at 2.9 GHz; the proposed antenna tends to radiate at t +z direction. The calculated peak gain for this antenna, w found to vary between 4.5 dBi to 6.6 dBi over all operat frequency bands.

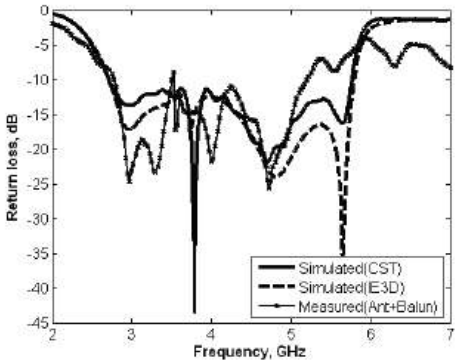

Fig. 6 Comparison of Simulated and measured return loss.

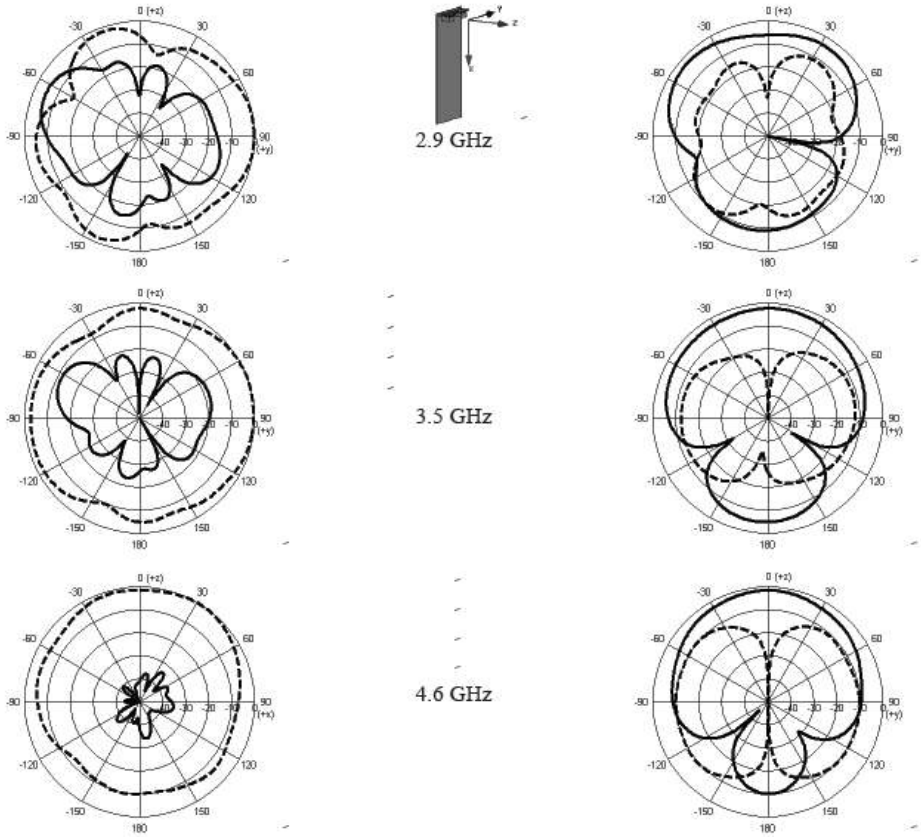

Fig. 7 Radiation patterns of the proposed antenna for 2.9 GHz, 3.5 GHz, 4.6 GHz, 5.2 GHz and 5.8 GHz at: (left) xz plane; (right) yz plane; ('—' measured E_θ, and '- - -' measured E_ϕ).

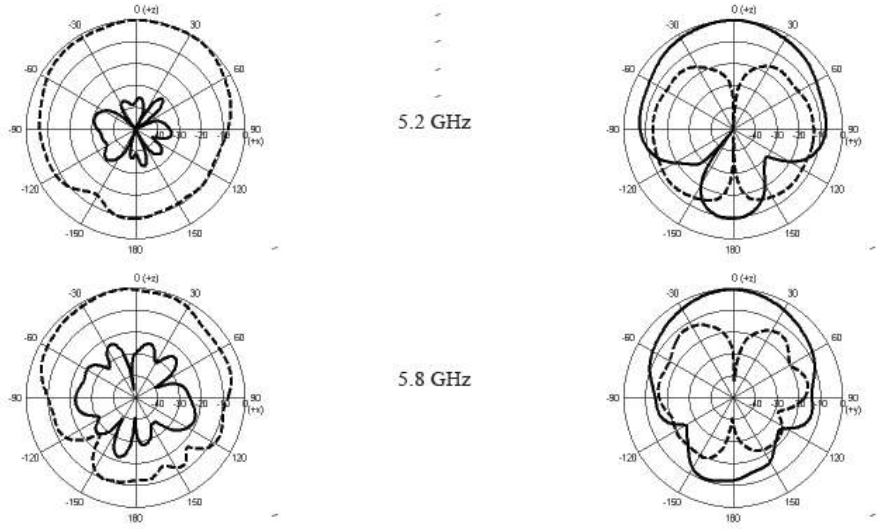

Fig. 7 (continued) Radiation patterns of the proposed antenna for 2.9 GHz, 3.5 GHz, 4.6 GHz, 5.2 GHz and 5.8 GHz at: (left) xz plane; (right) yz plane; ('—' measured E_θ, and '- - -' measured E_ϕ).

In addition, current distribution on the mobile phone ground plane was analyzed using the EM simulator: it was observed that most of the current induced on the ground plane were high in the area beneath the antenna and minimum current distribution appeared on the rest of the ground plane, as theoretically expected. This proves the model advantage of using a balanced antenna designs for future mobile handsets.

IV. CONCLUSIONS

A new wideband balanced folded dipole antenna operating over wide frequency bands, has been presented and analysed. Hardware realisation was applied to evaluate and validate the design theory. Comparison of return loss measurements showed good agreement with the computational predictions. The results are encouraging for further practical investigation of this antenna in finding the human effect with the phone, including performance of radiation and SAR of this new development.

ACKNOWLEDGMENT

The authors would like to gratefully acknowledge the support by the Engineering and Physical Sciences Research Council (EPSRC) in the UK under grant EP/E022936/1.

In addition, the authors express their deep appreciation to their colleague Dr. N.J. McEwan, from University of Bradford, for his support in the antenna simulation.

REFERENCES

[1] H. Morishita, H. Furuuchi and K. Fujimoto, "Performance of balance-fed antenna system for handsets in vicinity of a human head or hand", IEE Proc.-Microw. Antennas Propag., Vol. 149, No, 2, pp. 85-91, April 2002.

[2] R.A. Abd-Alhameed, P.S. Excell, K. Khalil, R. Alias and J. Mustafa, "SAR and radiation performance of balanced and unbalanced mobile antennas using a hybrid formulation", IEE Proceedings-Science, Measurement and Technology special issue on Computational Electromagnetics, vol. 151, No. 6, pp. 440-444, November 2004.

[3] S. Kingsley, "Advances in handset antenna design", RF Design, pp. 16-22, May 2005.

[4] B.S. Collins, S.P. Kingsley, J.M. Ide, S.A. Saario, R.W. Schlub and S.G. O'Keefe, "A Multi-band hybrid balanced antenna", IEEE 2006 International Workshop on Antenna Technology: small antennas; novel metamaterials, White Plains, New York, pp.100-103, March 6-8, 2006.

[5] M. Ali, G.J. Hayes, H-S. Hwang, and R.A. Sadler, "Design of a Multiband Internal Antenna for Third Generation Mobile Phone Handsets,", IEEE Transactions on Antennas and Propagation, Vol. 51, pp. 1452-1461, July 2003.

[6] P. Ciais, R. Stara, G. Kossiavas, and C. Luxey, "Compact internal multiband antenna for mobile phone and WLAN standards", Electronic Letters, Vol. 40, pp. 920-921, July 2004.

[7] R.A. Bhatti and Seong Ook Park, "Hepta-band internal antenna for personal communication handsets", IEEE Transactions on antennas and propagation, Vo. 55, Issue 12, pp. 3398-3403, December 2007.

[8] C.H. See, R.A. Abd-Alhameed, P.S. Excell, N.J. McEwan and J.G. Gardiner, "Internal triple-band folded planar antenna design for third generation mobile handsets", IET Microwaves, Antennas & Prapagation, Vol. 2, Issue 7, pp. 718-724, October 2008.

[9] H. Morishita, H. Furuuchi, H. Ide, Z. Tanaka and K. Fujimoto, "A balance-fed loop antenna system for handset", IEICE Trans. Fundamentals, Vol. E82-A, no. 7, pp. 1138-1143, 1999.

[10] U. Navsariwala and J. Svigelj, "A reduced sized balanced antenna for 2.4GHz WLAN", IEEE international symposium on antennas and propagation, Vol. 2, pp. 6-9, June 2003.

[11] D. Zhou, R.A. Abd-Alhameed and P.S. Excell, "Wideband balanced folded dipole antenna for mobile handsets", The 2nd European Conference on Antennas and Propagation, Session MoPA, Paper no.39, Edinburgh, UK, 11-16 November 2007.

[12] Computer Simulation Technology Corporation, CST Microwave Studio, Version 5.0, Germany.

[13] D. Zhou, R.A. Abd-Alhameed and P.S. Excell, "Bandwidth enhancement of balanced folded loop antenna design for mobile handsets using genetic algorithms", PIERS Proceedings, pp. 727-730, Hangzhou, China, March 24-28, 2008.

[14] S. Hayashida, H. Morishita, Y. KIM, Y. Koyanagi and K. Fujimoto, "Wideband folded loop antenna for handsets", IEEE AP-S Proc., Vol. 3, pp. 2-5, Jun., 2002.

[15] ET Industries, USA, http://www.etiworld.com/.

1264 PIERS Proceedings, Beijing, China, March 23–27, 2009

Dual-frequency Balanced Mobile Antenna for WLAN and Short Range Communication Systems

D. Zhou[1], R. A. Abd-Alhameed[1], C. H. See[1],
S. W. J. Chung[1], A. G. Alhaddad[1], and P. S. Excell[2]

[1]Mobile and Satellite Communications Research Centre
University of Bradford, Bradford, West Yorkshire, BD7 1DP, UK
[2]Glyndwr University, Wrexham, LL11 2AW, Wales, UK

Abstract— In this paper, a balanced antenna for mobile handset applications with dual-frequency performance, that covers 2.4-GHz and 5.2-GHz WLAN bands, is investigated. The antenna is a thin-strip planar dipole with folded structure and a dual-arm on each monopole. Performance of the proposed antenna was analysed and optimised against the targeted two frequency bands. For validation, a prototype of the antenna was fabricated and tested. The performance of this balanced antenna was verified and characterised in terms of the antenna return loss, radiation pattern and power gain. The predicted and measured results show fairly good agreement and the results also confirm good impedance bandwidth characteristics for the proposed balanced antenna with dual-band operation.

1. INTRODUCTION

The need to expand the bandwidth of antennas in mobile handheld devices follows from the ever-increasing data rates, and hence spectrum requirements, of mobile devices. Antennas are a major part of the complete design in mobile device design. Conventionally, the unbalanced planar inverted F antenna (PIFA) is one of the most popular candidates for compact built-in antennas for mobile handsets. PIFAs use the ground plane as a part of the radiator, which enables very small antennas to achieve sufficient gain and bandwidth [1–4]. In almost all cases, radiating currents are induced on both the ground plane and the antenna element. In use, however, these antennas exhibit poor performance when held by users. This is mainly because the user holding the mobile phone largely takes the place of the ground plane resulting in currents flowing on the human body, which degrade the performance of the antenna's radiation properties and introduce losses and uncertainty in its matching.

Balanced antenna is a good alternative candidate since balanced currents only flow on the antenna element in this type of antenna, thus dramatically reducing the effect of current flow on the ground plane. As a result, balanced antennas should have good efficiency and more important to maintain their performance when in use adjacent to the human body [5]. In recent years, several novel mobile antennas designed with the balanced technique have demonstrated the enhanced stability of antenna performance, compared to the unbalanced type, when the handset is approximately placed next to the human head and/or hand [6–8].

This paper presents and analyses a new design of a built-in dual-frequency balanced-dipole antenna for WLAN and short range wireless communications. The characteristics of this balanced folded dipole antenna with a novel dual-arm structure for mobile handsets are analysed. In the analysis, an electromagnetic simulator based on the finite integration technique was applied to calculate return loss and radiation patterns [9].

2. ANTENNA DESIGN CONCEPT

Basically, the first antenna design attempted was designed in free space and then several modifications were introduced to achieve a dual-band feature for mobile handset applications. The antenna, as shown in Fig. 1, is mounted on the top of a rectangular conductor plate (45×100 mm), which can be regarded as the mobile handset chassis or ground plane of a practical mobile phone.

The design concept for producing dual-band balanced mobile antennas was applied and implemented in the authors' previous work, as illustrated in [10], where a technique to generate another resonant frequency was employed by inserting an additional thin-strip arm in one of the arms of the planar dipole; as a result, the single resonant antenna was modified and developed as a wide-band dual-resonant variant for multi-band operation. In this study, the new proposed antenna was developed using the same design principle, but designed with simpler configuration for different

Progress In Electromagnetics Research Symposium, Beijing, China, March 23–27, 2009 1265

applications in WLAN and short range communication systems. Initially, a folded antenna with single arm, operating at around 2.4 GHz, was designed and optimized using the EM simulator. Subsequently, a new technique was applied by inserting an additional thin-strip arm (see Fig. 1) that will be used to obtain the resonant frequency for 5.2 GHz band.

The proposed antenna features a compact design, with dimension ($l \times w \times h$) of $38 \times 8 \times 8$ mm. The length and location of the additional arm, including other parameters of the proposed antenna, were adjusted and further optimised to ensure that the design entirely covered the required two frequency bands (i.e., 2400–2485 MHz & 5150–5350 MHz) at VSWR ≤ 2.5.

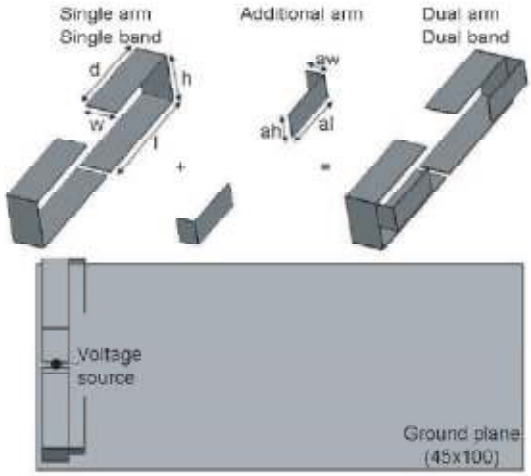

Figure 1: Balanced mobile antenna configuration studied.

3. SIMULATION AND MEASUREMENT RESULTS

The optimal antenna configuration studied in terms of return loss, radiation patterns and power gain was found with aid of CST simulator ($l = 18.5$, $d = 14.5$, $w = 5$, $h = 8$, $al = 10$, $aw = 3$, $ah = 4$; dimensions are in mm). For the hardware realisation, copper sheet with 0.15 mm thickness was used for fabricating the proposed balanced antenna (see Fig. 2). For a balanced antenna (e.g., dipole) system, a balun is usually required as a support feeding network, to provide a balanced feed from an unbalanced source. A commercially hybrid junction from ET Industries [11] that operates from 2 to 12 GHz has been utilized in this work. Fig. 3 presents the measured and simulated return loss of the prototype antenna. As can be seen, taking into account the errors caused by

Figure 2: Photograph of prototype of the proposed balanced antenna design.

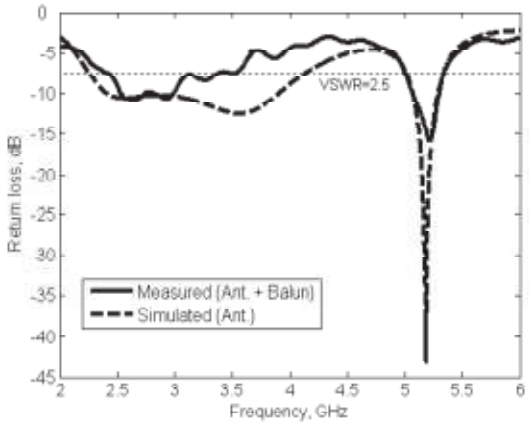

Figure 3: Comparison of simulated and measured return loss.

manufacturing the proposed antenna, a fairly good agreement between the calculated and measured return loss was observed.

Measurements of the radiation patterns of the prototype were carried out in a far-field anechoic chamber. Two pattern cuts were taken for two selected operating frequencies that cover the designated whole bandwidth in this study. The radiation patterns in the xz plane and yz plane for the balanced folded dipole at 2450 MIIz and 5200 MIIz were measured, as presented in Fig. 4. The measured patterns at the lower band shown asymmetrical radiation, which is mainly due to the asymmetrical antenna structure in fabrication and imbalanced outputs from the balun device in testing. It is worth mentioning that the measured patterns of the prototype at higher frequencies in the lower band (e.g., 2600 MHz, 3000 MHz and 3200 MHz) are similar to the ones at 2450 MHz presented in Fig. 4, as observed. This is because antenna impedance matching at those frequencies were all generated and controlled by the single-arm folded dipole containing; whereas, the proposed antenna at 5200 MHz tends to radiate at the $+z$ direction in both plane cuts. In this case, the ground plane in this band acts as a good reflector.

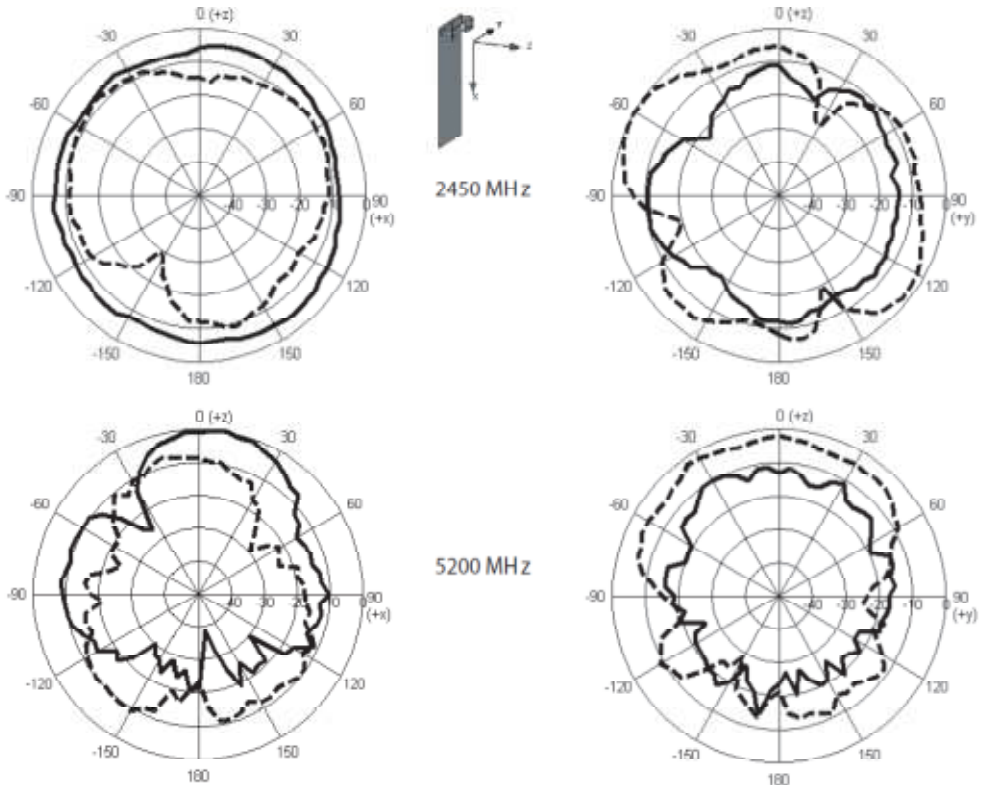

Figure 4: Radiation patterns of the proposed antenna for 2450 MHz and 5200 MHz at: (left) xz plane; (right) yz plane, where '—' measured E_θ and '- - -' measured E_ϕ.

Measured broadside antenna power gain for the frequencies across the 2.4 GHz and 5.2 GHz WLAN bands were also investigated. It is notable that the insertion loss of the feeding network was subsequently compensated for each measured power gain over all bands. It was found that the maximum measured antenna gain at lower and upper WLAN bands were 2.3 dBi and 6.2 dBi, respectively.

In addition, current distribution on the mobile phone ground plane was analyzed using the EM simulator: it was observed that most of the current induced on the ground plane concentrated in the area beneath the antenna and minimum current distribution appeared on the rest of the ground plane, as expected. This proves the model advantage of using a balanced antenna in designs for mobile handsets. The results are encouraging for practical investigation of this antenna in finding the performance of radiation and SAR of this new development.

4. CONCULSIONS

A dual-band balanced folded dipole antenna with novel structure for mobile devices operated over 2.4 GHz and 5.2 GHz WLAN bands has been presented. The proposed antenna model was experimentally verified in terms of antenna return loss, radiation pattern and power gain. The simulated and measured results over all frequency bands considered, show a good agreement and this made the proposed antenna an attractive candidate for mobile handset applications.

ACKNOWLEDGMENT

The authors would like to gratefully acknowledge the support by the Engineering and Physical Sciences Research Council (EPSRC) under grant EP/E022936/1.

REFERENCES

1. Li, Z. and Y. Rahmat-Sammii, "Optimization of PIFA-IFA combination in handset antenna designs," *IEEE Trans. on Antennas and Propagation*, Vol. 53, No. 5, 1770–1778, May 2005.
2. Wang, Y.-S., M.-C. Lee, and S.-J. Chung, "Two PIFA-related miniaturized dual-band antennas," *IEEE Trans. on Antennas and Propagation*, Vol. 55, No. 3, 805–811, March 2007.
3. Janapsatya, J., K. P. Esselle, and T. S. Bird, "A dual-band and wideband planar inverted-F antenna for WLAN applications," *Microwave and Optical Technology Letters*, Vol. 50, 138–141, January 2008.
4. Huynh, M.-C. and W. Stutzman, "Ground plane effects on planar inverted-F antenna (PIFA) performance," *IEE Proc.-Microw. Antennas Propag.*, Vol. 150, 209–213, August 2003.
5. Zhou, D., R. A. Abd-Alhameed, and P. S. Excell, "Wideband balanced folded dipole antenna for mobile handsets," *Proceedings of The European Conference on Antennas and Propagation: EuCAP 2007*, Paper No. MoPA.012, Edinburgh, UK, November 11–16, 2007.
6. Morishita, H., H. Furuuchi, and K. Fujimoto, "Performance of balance-fed antenna system for handsets in vicinity of a human head or hand," *IEE Proc.-Microw. Antennas Propag.*, Vol. 149, No, 2, 85–91, April 2002.
7. Morishita, H., S. Hayashida, J. Ito, and K. Fujimoto, "Analysis of built-in antenna for handset using human (hcand,hand,finger) model," *Electronics and communications in Japan*, Part 1, Vol. 86, No. 9, 35–45, 2003.
8. Abd-Alhameed, R. A., P. S. Excell, K. Khalil, R. Alias, and J. Mustafa, "SAR and radiation performance of balanced and unbalanced mobile antennas using a hybrid formulation," Invited paper, *IEE Proceedings-Science, Measurement and Technology special issue on Computational Electromagnetics*, Vol. 151, No. 6, 440-444, November 2004.
9. Computer Simulation Technology Corporation, CST Microwave Studio, Version 5.0, Germany.
10. Zhou, D., R. A. Abd-Alhameed, C. H. See, and P. S. Excell, "Design of multiband balanced folded dipole antenna based on a dual-arm structure for mobile handsets," *PIERS Online*, Vol. 4, No. 8, 821–824, 2008.
11. ET Industries, USA, http://www.etiworld.com/.

Proceedings of

Mosharaka International Conference on Communications, Propagation and Electronics

(MIC-CPE 2009)

6-8 February 2009, Holiday Inn, Amman, Jordan

Organized by

MOSHARAKA FOR RESEARCHES AND STUDIES

Hands On Jordan

Conference General Chairman

MOHAMMAD M. BANAT, JORDAN UNIVERSITY OF SCIENCE AND TECHNOLOGY, JORDAN

Conference Organizer and Editor

JASER MAHASNEH, MOSHARAKA FOR RESEARCHES AND STUDIES, JORDAN

ISBN: 978- 9957- 486- 06- 8

Wideband Reduced-Size Balanced Antenna Design for Mobile Handsets

D. Zhou[#1], R. A. Abd-Alhameed[#2], C. H. See[#3], A. G. Alhaddad[#4], P. S. Excell[*5]

[#] *Mobile and Satellite Communications Research Centre*
University of Bradford, Bradford, West Yorkshire, BD7 1DP, UK
[1] d.zhou2@bradford.ac.uk
[2] r.a.a.abd@bradford.ac.uk
[3] c.h.see2@bradford.ac.uk
[4] A.G.Alhaddad@bradford.ac.uk

[*] *Glyndwr University, Wrexham, LL11 2AW, Wales, UK*
[5] p.excell@glyndwr.ac.uk

Abstract— **A compact balanced antenna for mobile handset applications with enhanced bandwidth performance, covering four bands (GSM1800, GSM1900, UMTS and 2.4-GHz), is investigated. The antenna is a built-in planar dipole with folded structure and with additional of a dual-arm on each monopole. A wide bandwidth planar balun is used to feed the wideband balanced antenna from an unbalanced source. A prototype of the proposed antenna is fabricated and tested. The performance of the antenna is verified and characterized in terms of return loss, radiation patterns and power gain. The calculated and measured results show good agreement and also the antenna confirms good wideband characteristics with multiband operation.**

I. Introduction

Over several years, the need to expand the operated bandwidth of antennas in mobile handheld devices follows from the ever-increasing data rates, and hence spectrum requirements, of mobile devices. The implementation of antenna designs causing minimised coupling with the human head and hand and hence minimised SAR would be attractive to many consumers, thus increasing the market acceptance of devices using such antennas.

A good candidate is a balanced antenna [1, 2]. An antenna with symmetrical structure that is fed with balanced currents to make it electrically symmetrical is said to be a balanced antenna. Dipoles and loops are the most commonly encountered balanced antennas [3-5]. In this type of antenna, balanced currents only flow on the antenna element, thus dramatically reducing the effect of current flow on the ground plane. As a result, balanced antennas should have good efficiency and more importantly to maintain their performance when in use adjacent to the human body [6].

In this paper, characteristics of a built-in balanced folded dipole antenna with a novel dual-arm structure for mobile handsets are introduced and analysed in order to realise multiple-band operation, including GSM1800, GSM1900, UMTS and WLAN (2.4 GHz). A planar balun with corresponding wide bandwidth for feeding the proposed antenna was implemented in a hardware realization. In the analysis, an electromagnetic simulator based on the finite integration technique was applied to calculate return loss and radiation patterns [7].

II. Antenna Design Concept and Structure

Planar metal-plate monopole antennas have been investigated in the past as good candidates for ultrawide-band applications [8, 9]. A pair of such wideband monopole antennas can be integrated together to configure a dipole and still remain a wide bandwidth feature. Following this principle, a wideband planar dipole antenna in free space can be developed. This design concept of balanced antennas was applied and implemented in the authors' previous work, as illustrated in [10], in which a simple technique for enhancing antenna impedance bandwidth was employed by symmetrically trimming a triangle at the monopole edge near the feed point, to give a tapered feed. In addition, a slot is introduced in each one of the arms of the planar dipole to mitigate the effects of the ground plane that causes the degradation of antenna performance.

In this work, a further development of this antenna model was carried out for the purpose to achieve the design features such as, a compact small size and operating over multiple frequencies bands. In order to compromise the antenna size and maintaining the less mutual effect on the proposed mobile antenna with the handset ground plane, a compact design was achieved, with relative thin strip width (compared with the design in [10]) in which, the slot on each arm of the folded dipole antenna is removed (see Fig. 1). Moreover, the technique for generating multiple frequency resonances that was previously applied for folded balanced dipole antennas, as demonstrated in [11], was also adapted in this design for further improvement. This also discusses the impedance bandwidth to enable multiple-band operation.

Initially, a single arm balanced dipole antenna with folded structure and taper feed near edge of the feeding point operating at around 2 GHz, was designed and optimized using the EM simulation package. In order to achieve compact design, the top end of the folded arm was extended and bent down (referring to parameter 'h_1') to satisfy the required length for each arm to meet the antenna resonances at the desired operating frequencies. Subsequently, an additional thin-strip arm was introduced and inserted in one of the arms of the planar dipole to generate the additional resonant

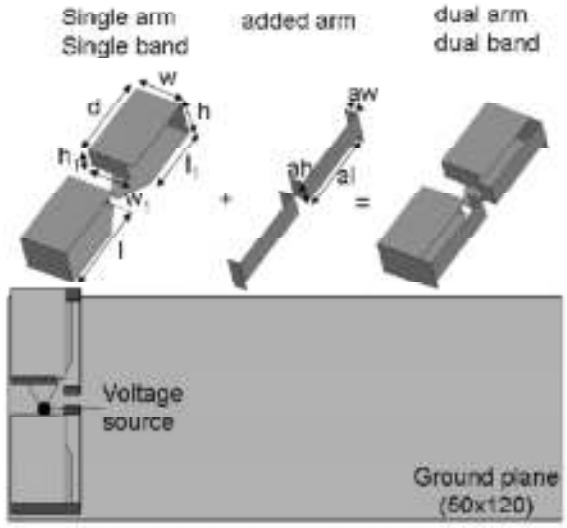

Fig. 1 Antenna configuration studied. (a) balanced folded dipole antenna with conducting plate; (b) front view of the antenna model; (c) unfolded structure of the proposed antenna.

frequency around 2.4 GHz band. Using this technique, the single resonant antenna was modified and developed as a wideband dual-resonant variant for multi-band operation.

The proposed antenna features of the compact design model, was established with dimension of 48 (l) × 14 (w) × 9 (h) mm. The lateral length of taper feed and location on the antenna, together with the length and location of the additional arm, including other parameters of the proposed antenna, were adjusted and further optimization process carried out to ensure that the design entirely covered the required frequency bands (1710-2485 MHz) at VSWR ≤ 3.

III. Results and Discussion

For a balanced antenna (e.g. dipole) system, a balun is required as a support feeding network, to provide a balanced feed from an unbalanced source. In this study, a wideband planar balun was adapted [12] and further modifications were applied by rearrangement of the element locations for the purpose of the practical measurement. Agilent ADS [13] was used to simulate and analyse the characteristic performance of this modified balun. The balun structure was mounted on Duroid material (ε_r = 3.48, h = 0.8 mm, and tanδ = 0.0019). Table 1 summarizes the measured performance of the planar balun used in this work, compared with the published data as reported in [12]. As can be seen, this balun presents a relatively wideband feature and show good agreement with the prior art results.

The optimal antenna configuration studied in terms of return loss, radiation patterns and power gain was found with aid of CST simulator (d=20, w=12, w1=10, h=9, h_1=5, l=23, l1=12, aw=3.5, ah=6, al=22; dimensions are in mm). For the hardware realisation, copper sheet of thickness 0.35 mm was used for fabricating the proposed balanced antenna (see Fig. 2). The ground plane of the proposed antenna was printed on one side of the dielectric substrate and planar balun was placed on the other side of the substrate. The non-conductive material was used to suspend the antenna from the ground plane with 1mm distance. The associated planar balun location was carefully arranged to feed the proposed antenna and the position in details for it was described in authors' previous work [11]. In this way, the prototype balanced antenna and its feeding network virtually share the same ground plane as one whole system with close integration.

Table 1: Comparison between the present design and the prior art.

Item	Frequency range (GHz)	Insertion loss max. (dB)	Relative Errors: Amplitude (dB)/ Phase (degrees)	Return loss max. (dB)
Prior art in [12]	1.7-3.3	-	± 0.3 / ± 5	10
Present Balun	1.7-3.0	0.9	± 0.1 / ± 2	10

Fig. 3 presents the measured and simulated return loss of the prototype antenna. As can be seen, taking into the account the errors caused by manufacturing the proposed antenna, a

fairly good agreement between the calculated and measured return loss was observed.

Fig. 2 Photograph of prototype of the proposed balanced antenna design.

Moreover, an S-Parameter method for measuring input impedance for the balanced antennas [14] was also adopted in order to verify the impedance of the proposed antenna. In this case, balanced antennas are considered as two-port devices and the S-Parameters can be obtained from a well-calibrated Network Analyzer. Subsequently, a simple formula is employed to derive the differential input impedance of the balanced antenna. The measured return loss in this method was also presented in Fig. 3, in which a fairly good agreement between the simulated and measured return loss (i.e. simulated (ant) and measured (ant)) was observed. This result verifies the actual impedance of the proposed antenna, in addition, the effectiveness of proposed antenna system with integrated balun, confirms the validation. It also supports the evaluation of the radiation performance of the prototype antenna.

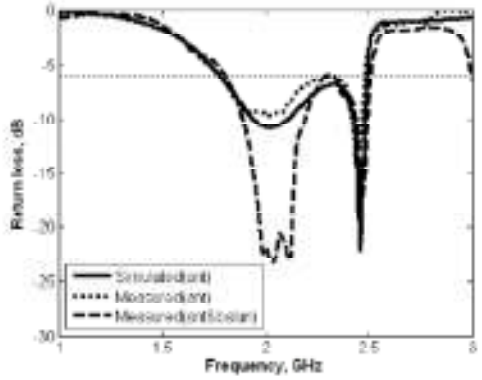

Fig. 3 The simulated and measured return loss versus the operating frequency.

The measured radiation patterns of the prototype were carried out in a far-field anechoic chamber. Two pattern cuts were taken for four selected operating frequencies that cover the designated whole bandwidth in this study. The radiation patterns in the zx plane and zy plane for the balanced folded dipole at 1795, 1920, 2045 and 2445 MHz were measured. The results were verified and plotted against the prediction in Fig. 4, in which the patterns of the prototype antenna are seen to be quite similar to each other for the first three cases. Moreover, the zx plane presents a nearly omni-directional radiation pattern in all intended three frequency bands; whereas, the proposed antenna at 2445 MHz tends to radiate at the -x direction in zx plane cut and at the +z direction in zy plane cut. In this case, the ground plane in this band acts as a good reflector.

Fig. 5 illustrates the measured broadside antenna power gain for the frequencies across the GSM1800, GSM1900, UMTS and 2.4-GHz WLAN bands. It is notable that the insertion loss of the feeding network was subsequently compensated for each measured power gain over all bands. As observed, the measured antenna gain was varied between 2.7 dB and 5.4 dB over the entire bandwidth considered.

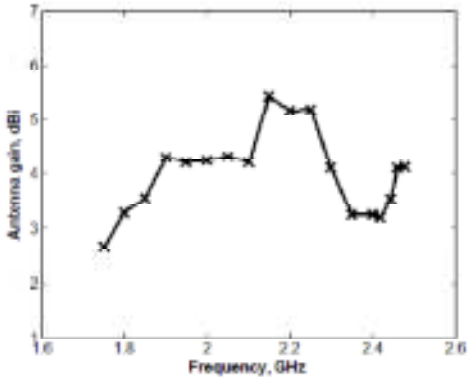

Fig. 5 Measured antenna gain for the proposed folded balanced antenna.

IV. Conclusions

A new compact wideband balanced folded dipole antenna, together with its feeding network, operated over GSM1800, GSM 1900, UMTS and 2.4-GHz WLAN bands, has been presented. The proposed antenna was experimentally verified in terms the input impedance, radiation pattern and power gain. The simulated and measured results over all frequency bands considered, show a good agreement and this made the proposed antenna an attractive candidate for mobile handset applications.

Acknowledgment

The authors would like to gratefully acknowledge the support by the Engineering and Physical Sciences Research Council (EPSRC) in the UK under grant EP/E022936/1.

In addition, the authors express their deep appreciation to their colleague Dr. N. J. McEwan, from University of Bradford, for his support in the antenna simulation.

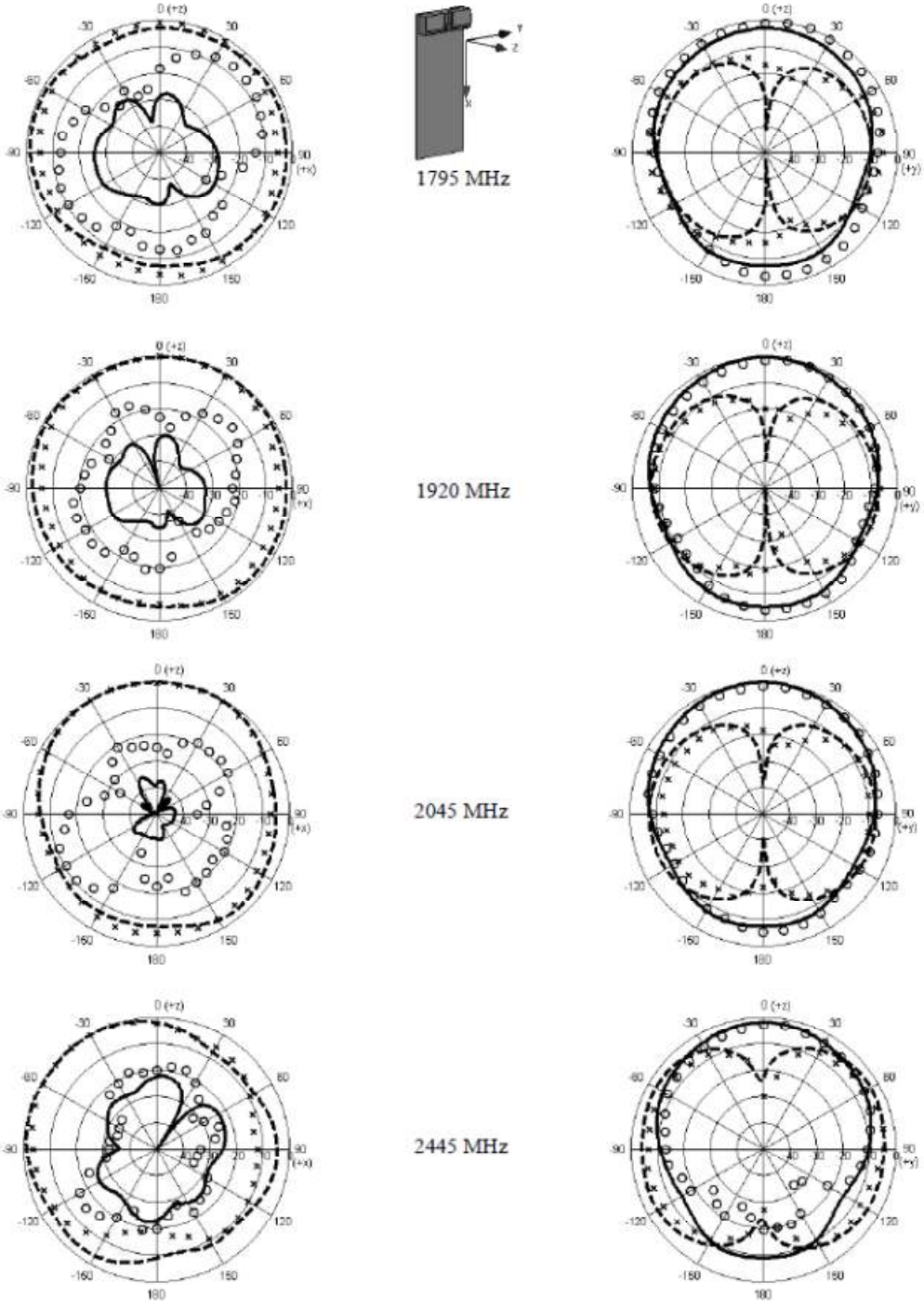

Fig. 4 Radiation patterns of the proposed antenna for 1795 MHz, 1920 MHz, 2045 MHz and 2445 MHz at: (left) zx plane; (right) zy plane; ('ooo' measured E_θ, '——' simulated E_θ, '+++' measured E_ϕ, and '------' simulated E_ϕ).

REFERENCES

[1] H. Morishita, H. Furuuchi and K. Fujimoto, "Performance of balance-fed antenna system for handsets in vicinity of a human head or hand", *IEE Proc.-Microw. Antennas Propag.*, Vol. 149, No. 2, pp. 85-91, April 2002.

[2] S. Kingsley, "Advances in handset antenna design", RF Design, pp. 16-22, May 2005.

[3] R.A. Abd-Alhameed, P.S. Excell, K. Khalil, R. Alias and J. Mustafa, "SAR and radiation performance of balanced and unbalanced mobile antennas using a hybrid formulation", Invited paper, *IEE Proceedings Science, Measurement and Technology special issue on Computational Electromagnetics*, vol. 151, No. 6, November 2004, pp. 440-444.

[4] S. Hayashida, H. Morishita, Y. Kim, Y. Koyanagi and K. Fujimoto, "Wideband folded loop antenna for handsets", *IEEE AP-S Proc.*, vol. 3, pp. 2-5, Jun., 2002.

[5] D. Zhou, R.A. Abd-Alhameed and P.S. Excell, "Bandwidth enhancement of balanced folded loop antenna design for mobile handsets using genetic algorithms", PIERS Proceedings, pp. 727-730, March 24-28, Hangzhou, China, 2008.

[6] B.S. Collins, S.P. Kingsley, J.M. Ide, S.A. Saario, R.W. Schlub and S.G. O'Keefe, "A Multi-band hybrid balanced antenna", IEEE 2006 International Workshop on Antenna Technology: small antennas; novel metamaterials, White Plains, New York, pp.100-103, March 6-8, 2006.

[7] Computer Simulation Technology Corporation, CST Microwave Studio, Version 5.0, Germany.

[8] M.J. Ammann and Z.N. Chen, "Wideband Monopole Antennas for Multi-Band Wireless Systems", *IEEE Antennas and Propagation Magazine*, Vol. 45, No. 2, pp. 146-150, April 2003.

[9] K.-L. Wong, C.-H. Wu and S.-W. Su, "Ultrawide-band square planar metal-plate monopole antenna with a trident-shaped feeding strip", *IEEE Transaction on antennas and propagation*, Vol. 53, No. 4, pp. 1262-1269, April 2005.

[10] D. Zhou, R.A. Abd-Alhameed and P.S. Excell, "Wideband balanced folded dipole antenna for mobile handsets", *The 2nd European Conference on Antennas and Propagation*, Session MoPA, Paper no.39, Edinburgh, UK, 11-16 November 2007.

[11] D. Zhou, R.A. Abd-Alhameed, C.H. See and P.S. Excell, "Design of multiband balanced folded dipole antenna based on a dual-arm structure for mobile handsets", In proceeding of Progress In Electromagnetics Research Symposium, pp. 318-321, July 2-6, Cambridge, USA, 2008.

[12] Z.Y. Zhang, Y.X. Guo and L.C. Ong, "A new wideband planar balun on a single-layer PCB", *IEEE Microwave and wireless components letters*, Vol. 15, no. 6, pp. 416-418, June 2005.

[13] Agilent Technologies, Santa Rosa, CA, Advanced Design Systems, Version 2005A.

[14] R. Meys and F. Janssens, "Measuring the impedance of balanced antennas by an S-Parameter method", IEEE antennas and propagation magazine, vol. 40, no. 6, pp. 62-65, December 1998.

Ninth Informatics Workshop for Research Students Bradford UK ISBN 978 1 85143 251 6

Ultra-Wideband Balanced Antenna for Mobile Handsets

A G Alhaddad, D Zhou, R A Abd-Alhameed and C H See

Abstract-- **A built-in planar metal plate Ultra-Wideband antenna for mobile handsets with balanced operation is proposed. The antenna exhibits balanced operation, to reduce the current flow on the conducting surface of the handset body. The antenna performance is also examined and tested with the existence of the operator's hand. The measured results show good promising of wideband converges of most of the wireless frequency bands.**

Keywords: **Balanced Antennas, Planar Antennas, Ultra-Wide bandwidth.**

I. Introduction

One of the trends observed in the mobile telephone technologies in the last ten years is to dramatically reduce the size and the weight of the handset. Antennas used for such handsets must also follow down-sizing of the handset unit. Problems considered here on the design of antenna systems for small handsets are firstly, on how to keep the antenna performance unchanged or improved, even though the antenna size becomes small, and secondly, how to reduce the degradation of antenna performance caused by the operator's adjacent effect.

An unbalanced antenna such as Planar Inverted-F antenna (PIFAs) is among the most used radiating elements for mobile terminals. An advantage of PIFA is compact, low profile and easy to manufacture. However, it has a narrow bandwidth and needs a height from substrate to ground for matching [1-4]. Furthermore these antennas exhibit poor performance when held by users. This is mainly because the user holding the mobile phone largely takes the place of the ground plane since the ground plane is used as part of the radiator in these antennas therefore radiating currents are induced on both the ground plane and the antenna element resulting in currents flowing on the human body, which degrade the performance of the antenna's radiation properties and introduce losses and uncertainty in its matching [5].

The alternative strategy is to use a balanced antenna, as it has a symmetric structure and is fed by balanced lines one that has two conductors carrying currents of equal magnitude but 180 degree out of phase. These currents cancel the effect of each other and hence the current flows only on the antenna element and not on the ground plane. So if the mobile phone is held by a human, no coupling takes place between the antenna and the human body thus the performance of the antenna is not affected. A major drawback of balanced antennas is that they have a narrow bandwidth; however this bandwidth can be increased by certain techniques like using genetic algorithms. The most common encountered balanced antennas are dipole and loops. In addition, because a balanced antenna requires a balanced feed, a balun is needed. It is a device used for converting signals between an unbalanced circuit structure and a balanced circuit structure. A balun provides compatibility between systems [6]. Through a balun an unbalanced coaxial wire is connected to a two conductor balanced lines.

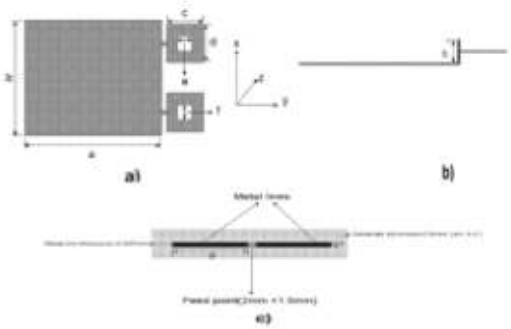

Fig. 1 Antenna configuration, a) Top view, b) Side view, c) Substrate and metal lines, a=75mm, b=60mm, c=20mm, d=20mm, e=8mm, f=8mm, g=18mm, h=10mm, t=1.5mm

Recently, many conventional balanced antennas have been successfully designed to cover operation in the 1.7 – 2.2 GHz and 1.7 - 2.5GHz bands for mobile handsets [7-8]. In these papers, characteristics of a built-in ultra wideband balanced planar metal plate antenna are introduced and analyzed in order to achieve multiple-band operation from 3.1 to 10.6 GHz.

In this paper, a newly developed planar metal plate ultra-wideband balanced antenna is presented (see Fig. 1). The antenna exhibits a balanced operation which leads to a significant reduction of current on the handset body and as a result of which the antenna's performance is not affected by the human operator's hand.

The authors are with the Mobile and Satellite Communications Research Centre, University of Bradford, Bradford, BD7 1DP, UK. a.g.alhddad@brad.ac.uk, R.A.A.Abd@Bradford.ac.uk, dzhou1@brad.ac.uk, chsee2@brad.ac.uk.

Ninth Informatics Workshop for Research Students Bradford UK ISBN 978 1 85143 251 6

II. ANTENNA DESIGN AND EXPERIMENTAL RESULTS

The proposed antenna design and simulation was carried out using Ansoft HFSS (High Frequency Structure Simulator), which uses a 3D full-wave finite element Method (FEM). The details of the antenna geometry are shown in Fig. 1, in which two metals ground planes are used for this particular antenna design. The vertical ground plane of the proposed antenna is made up of copper with thickness of 0.5mm and dimensions of a × b (see Fig 1a). The horizontal ground plane is also made up of copper with thickness of 0.035mm, height h and it lies below the substrate (see Fig 1b and 1c). The substrate used is FR-4 and its thickness is 0.8mm. It should also be noted that printed feed lines of thickness 0.035mm, length g and width t (see Fig 1c), are used on the horizontal ground plane to feed the antenna radiating patches.

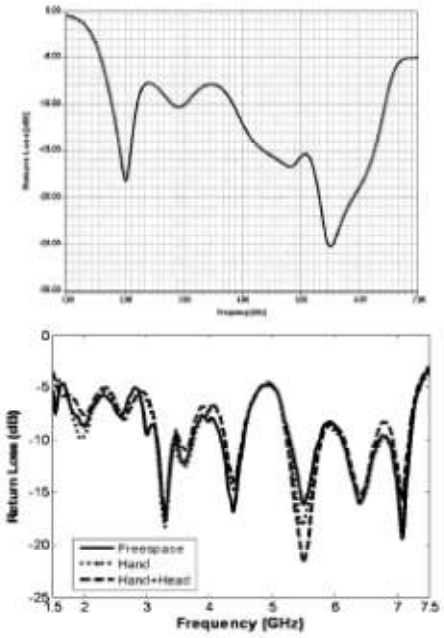

Fig 2 Input return loss of the antenna; (top) simulated return loss, (bottom) measured returns loss.

The antenna is fed at the centre. The radiating patches are made up of copper with thickness of 0.5mm and have square shapes of e×f as shown in Fig 1a. Furthermore, the antenna is fed by balanced network which provide equal magnitude but 180 degree out of phase current for the two arms of the antenna. The input impedance of the antenna is 100Ω. The conversion from the normal 50Ω to 100Ω impedance is provided by balun.

The proposed antenna structure has been simulated and tested for studying the characteristics of the antenna. The measurement of the return loss and radiation pattern is carried out using the anechoic chamber of the mobile and satellite communications research centre.

Fig 2 shows the response of the return losses of the antenna for a wide frequency range from 1 to 7 GHz range. Fig 2b shows the measured returns loss of the antenna in free space, in operator's hand and in talk position. The simulated bandwidth for return loss of 8dBs is around 4.6 GHz ranging from 1.7 to 6.3 GHz (i.e., relative bandwidth is 115%). The measured return loss for the measured bandwidth of -6 dB is found from 1.6 to 7.3 GHz. By inspecting Fig 2b, it can be revealed that the effect of the operator's hand and head on the antenna performance is very small which explains that the antenna has a perfect balanced structure.

III CONCLUSIONS

A new ultra-wideband balanced antenna, together with its feeding network been presented and analyzed. Hardware realization was applied to evaluate and validate the design theory. The simulated and measured input return loss of the antenna showed a reasonable agreement. The relative antenna bandwidth achieved was around 115% that made the antenna an attractive candidate for mobile handset applications.

References

1. H. Morishita, H. Furuuchi and K. Fujimoto, Performance of balance-fed antenna system for handsets in vicinity of a human head or hand, *IEE Proc.-Microw. Antennas Propag.*, Vol. 149, No, 2, pp. 85-91, April 2002.
2. S. Hayashida, H. Morishita, Y. Kim, Y. Koyanagi and K. Fujimoto, Wideband folded loop antenna for handsets, *IEEE AP-S Proc.*, vol. 3, pp. 2-5, Jun., 2002.
3. M.J. Ammann and Z.N. Chen, Wideband Monopole Antennas for Multi-Band Wireless Systems, *IEEE Antennas and Propagation Magazine*, Vol. 45, No. 2, pp. 146-150, April 2003.
4. K.-L. Wong, C.-H. Wu and S.-W. Su, "Ultrawide-band square planar metal-plate monopole antenna with a trident-shaped feeding strip", *IEEE Transaction on antennas and propagation*, Vol. 53, No. 4, pp. 1262-1269, April 2005.
5. R.A. Abd-Alhameed, P.S. Excell, K. Khalil, R. Alias and J. Mustafa, SAR and radiation performance of balanced and unbalanced mobile antennas using a hybrid formulation, *IEE Proceedings-Science, Measurement and Technology special issue on Computational Electromagnetics*, vol. 151, No. 6, November 2004, pp. 440-444.
6. Z.Y. Zhang, Y.X. Guo and L.C. Ong, "A new wideband planar balun on a single-layer PCB", *IEEE Microwave and wireless components letters*, Vol. 15, no. 6, pp. 416-418, June 2005.
7. D. Zhou, R.A. Abd-Alhameed and P.S. Excell, "Wideband balanced folded dipole antenna for mobile handsets", *In proceedings of The European Conference on Antennas and Propagation: EuCAP 2007*, Paper no. MoPA.012, Edinburgh, UK, 11-16 November 2007.
8. D. Zhou, R.A. Abd-Alhameed, C.H. See and P.S. Excell, "Design of multiband balanced folded dipole antenna based on a dual-arm structure for mobile handsets", *PIERS Proceedings*, Cambridge, USA, 2-6 July 2008 (accepted for publication).